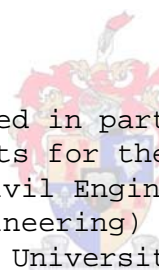


Scale Model Validation of QUAYSIM and WAVESCAT Numerical Models of Ship Motions

By
Lerika Susan Eigelaar



Thesis presented in partial fulfilment of
the requirements for the degree Master of
Science in Civil Engineering (Port and
Coastal Engineering) at Stellenbosch
University.

Supervisor: Mr. Geoff Toms
Faculty of Engineering

March 2015

Declaration

By submitting this thesis electronically, I declare that the entirety of the work contained therein is my own, original work, that I am the sole author thereof (save to the extent explicitly otherwise stated), that reproduction and publication thereof by Stellenbosch University will not infringe any third party rights and that I have not previously in its entirety or in part submitted it for obtaining any qualification.

March 2015

Copyright © 2015 Stellenbosch University

All rights reserved

Abstract

Various numerical modelling software packages are available for predicting moored ship motions and forces. The focus of this study was to validate the numerical models QUAYSIM and WAVESCAT and how these models together form a procedure for predicting moored ship motions and forces under the impact of high and low frequency waves.

The validation procedure applied in the study involved numerical modelling of a given physical model situation in which moored ship motions and forces were measured under both high and low frequency wave conditions. A physical model with built-in bathymetry was provided by the Council for Scientific and Industrial Research (CSIR) Hydraulics Laboratory in Stellenbosch. The model consisted of a moored container vessel at a jetty, with various mooring lines and fenders. A JONSWAP spectrum, which combines high and low frequency wave components, was used to simulate wave conditions for the modelling of ship motions. The wave periods and wave heights were measured at observation stations located at specific points in the basin. Other measurements such as those of the forces in the fenders and mooring lines were also determined.

A multi-step approach was used to numerically predict the ship motions and forces. Firstly, the coastal processes occurring within the basin, which was set up to simulate the physical model wave behaviour, were measured to calibrate the SWAN Delft3D-WAVE model. The wave heights and periods for the respective observation stations were obtained and compared to the physical model measurements. The Delft3D-FLOW SURFBEAT model was used to calculate the low frequency waves in the coastal area. Low frequency waves are the main cause of larger ship motions and forces, therefore it is important to investigate them as part of the ship motion prediction procedure.

After the waves had been computed, wave forces acting on the vessel needed to be determined for both high and low frequency waves. These wave forces were modelled with the combinations SURFBEAT/LF-STRIP (low frequency waves) and SWAN/WAVESCAT (high frequency waves). LF-STRIP provided the link between low frequency wave models and ship motion models, converting the low frequency waves into long wave forces acting on the vessel. WAVESCAT converted the high frequency waves to short wave forces. The calculated long wave forces and short wave forces served as the input required to run the ship motion model QUAYSIM to determine the movements of the moored ship as well as the restraining forces in the lines and fenders. The ship motions and forces were compared to the physical model, with the intention of possibly validating the QUAYSIM/WAVESCAT approach for predicting moored ship motions.

The study provides an overview of both the setup and results of the physical and numerical model. A description of each of the numerical models SWAN, SURFBEAT, LF-STRIP, WAVESCAT and

QUAYSIM is provided, along with a comparison between the physical and numerical models for each procedure. The validation procedure provided useful documentation of the quality of these numerical modelling approaches, already in use in some design projects.

The numerical models WAVESCAT and QUAYSIM models of ship motion have shown to provide a good correlation between the physical model and the numerical approach. However, improvements are still required. Good comparisons were obtained for the long wave motions (horizontal movements - surge, sway and yaw). The surge and sway motions were slightly overestimated by QUAYSIM. The magnitude of the yaw was comparable but the not well represented in spectral plots.

Opsomming

Daar is verskeie numeriese modelleringsagtewareprogramme beskikbaar waarmee skipbewegings en -kragte voorspel kan word. Die fokus van hierdie studie was om die numeriese modelle QUAYSIM en WAVESCAT te valideer. Saam vorm hierdie twee modelle 'n prosedure om vasgemaakte skipbewegings en -kragte veroorsaak deur lang- en kortgolfaksie te bepaal.

Die validasieprosedure wat in hierdie studie gebruik is, behels 'n numeriese modelering van 'n fisiese situasie waar 'n vasgemaakte skip se bewegings en kragte onder kort- en langgolfkondisies gemeet is. 'n Fisiese model met ingeboude batimetrie is voorsien deur die Council for Scientific and Industrial Research (CSIR) se hidroliese laboratorium in Stellenbosch. Die model bestaan uit 'n vasgemaakte houer by 'n pier met verskeie ankerlyne en bootbuffers. 'n JONSWAP-spektrum, wat kort- en langgolfkomponente kombineer, is gebruik om golfomstandighede vir die modellering van skipbewegings te simuleer. Golfperiodes en golfhoogtes is by spesifieke waarnemingstasies in die gesimuleerde hawe-area gemeet. Verdere opmetings, soos dié van die kragte in die bootbuffers en ankerlyne, is ook gedoen.

'n Stap-vir-stap benadering is gevolg om die skipbewegings numeries te voorspel. Eerstens is die kusprosesse wat in die gesimuleerde hawe plaasvind, gekalibreer met die numeriese pakket SWAN Delft3D-WAVE. Die golfhoogtes en golfperiodes vir elke waarnemingstasie is bereken en vergelyk met die fisiese model se opmetings. Die SURFBEAT-module van Delft3D-FLOW is gebruik om die lae-frekwensie golwe in die kusarea te bereken. Lae-frekwensie golwe is die hooforsaak van skipbewegings en daarom is dit belangrik om dit te ondersoek gedurende die voorspellingsprosedure van skipbewegings.

Na die golwe bereken is, moes die kragte wat beide kort en lang golwe op die skip uitoefen ook bereken word. Hierdie golfkragte is gemodelleer deur middel van die kombinasies SURFBEAT/LF-STRIP (langgolwe) en SWAN/WAVESCAT (kortgolwe). LF-STRIP het die skakel tussen golfmodelle en skipbewegingsmodelle verskaf en die lae-frekwensie golwe omgeskakel in langgolfkragte wat op die skip uitgeoefen is. WAVESCAT het die hoë-frekwensiegolwe omgeskakel in kortgolfkragte wat op die skip uitgeoefen is. Die berekende langgolf- en kortgolfkragte is ingevoer op die skipbewegingsmodel QUAYSIM om die skipbewegings en inperkingskragte in die bootbuffers en ankerlyne te bepaal sodat dit vergelyk kon word met die fisiese model, met die doel om moontlik die QUAYSIM/WAVESCAT-prosedure om gemaakte skipbewegings te voorspel te valideer.

Die studie verskaf 'n oorsig van die opstel en resultate van die fisiese en numeriese modelle. Elk van die numeriese modelle SWAN, SURFBEAT, LF-STRIP, WAVESCAT en QUAYSIM word beskryf en vergelykings word getref tussen die numeriese en fisiese modelle vir elke prosedure.

Die validasieprosedure verskaf nuttige dokumentasie van die kwaliteit van hierdie numeriese modeleringsprosedures wat reeds in sekere ontwerpprojekte gebruik word.

Die numeriese WAVESCAT en QUAYSIM modelle van skipbewegings het 'n goeie korrelasie tussen die fisiese model en die numeriese benadering gelewer. Verbeteringe is wel steeds nodig. Goeie vergelykings is verkry vir langgolfbewegings (horisontale bewegings – stuwing (“surge”), swaai (“sway”) en gier (“yaw”)). Die stu- en swaai bewegings was effens oorskat met QUAYSIM. Die grootte van die gier was wel vergelykbaar maar is nie grafies goed uitgebeeld nie.

Acknowledgements

The thesis involved validating a numerical model of moored ship motions with the use of physical model tests. The research was done by a masters student in the Port and Coastal Engineering field at the University of Stellenbosch. The physical model tests were carried out at the CSIR Hydraulics Laboratory in Stellenbosch. The thesis provided me with the opportunity to experience various concepts relating to the field of Port and Coastal Engineering, such as ship hydrodynamics, coastal processes, numerical modelling, and physical modelling. Throughout this journey, many people contributed towards the development of my understanding of these coastal engineering concepts. There are people whose contributions are central to this thesis and it would give me great pleasure to acknowledge them for their time, enthusiasm, availability, and exceptional advice.

Firstly, I would like to thank Geoff Toms for his encouragement and passion for the Coastal Engineering field. It has been wonderful learning from you in class (which greatly increased my knowledge before attempting this thesis) and also throughout the thesis process, during which you introduced me to the CSIR staff and guided me in the right direction. You are someone whom many can learn from, with your patience and ability to absorb bits of everything in the Coastal Engineering field. I would like to thank you for giving me more than what is expected of you and for going the extra mile.

Secondly, I would like to acknowledge Luther Terblanche for guiding and advising me. I am profoundly grateful for all the time you have taken to assist me throughout this process. Thank you for all the assistance with the numerical software and directing me and preparing me for the physical model process. Thank you for all the time you have invested in me and thank you for all your patience. Our discussions and conversations over the last two years definitely helped me reach my goals.

Thank you to Wim van der Molen for all your suggestions and advice. Thank you for the fact that I could always count on you when something went wrong or when I did not understand a concept entirely.

Thank you to all the CSIR staff for their help, being either physical help with the equipment or even the helpful advice concerning the physical model test runs. There are too many people at the CSIR to mention. Thank you for all the time, the patience, the advice, the show of interest, and the all the help. I could not have done it without you.

Thank you to Mr. Hibbert for taking the time to read through my thesis. Your comments were very helpful. Thank you for the fast feedback and for your availability.

Lastly, I would like to thank my family and friends for their support. They always listened when I spoke about my thesis progress. Thank you for taking the time and reading through the rough drafts before the final project was handed in. Without your encouragement and support, I am not sure how I would have made it.

Lerika Eigelaar

Dedications

Physical Modelling Team

August, Mario
Jappie, Rafick
Prins, William
Solomons, Reagan
Kieviet, Johan
Roux, Pierre
Thesnaar, Eldré

Numerical Modelling Team

Henning, Hermanus
Terblanche, Luther
Harribhai, Jatin

Supervisor

Toms, Geoff

In co-operation with:



University of Stellenbosch

Faculty of Civil Engineering

Department of Coastal Engineering



Council for Scientific and

Industrial Research

Table of Contents

Declaration	i
Abstract	Error! Bookmark not defined.
Opsomming	Error! Bookmark not defined.
Acknowledgements	vi
Dedications	viii
Table of Contents	ix
List of Figures	xii
List of Tables	xviii
List of Symbols	xx
Chapter 1: Introduction	1
<i>1.1 Background</i>	<i>1</i>
<i>1.2 Objective</i>	<i>2</i>
<i>1.3 Thesis Approach</i>	<i>2</i>
<i>1.4 Thesis Outline</i>	<i>3</i>
Chapter 2: Numerical Modelling of Long waves and Ship Motions	5
<i>2.1 Background</i>	<i>5</i>
<i>2.2 Overview of Past Numerical Models</i>	<i>7</i>
<i>2.3 Computational Approach</i>	<i>9</i>
<i>2.4 Overview of Current Models</i>	<i>12</i>
2.4.1 SWAN (Delft3D–WAVE).....	<i>12</i>
2.4.2 SURFBEAT (Delft3D-FLOW)	<i>13</i>
2.4.3 LF-STRIP (Low Frequency Wave Forces)	<i>14</i>
2.4.4 QUAYSIM (Ship Motion Model)	<i>15</i>
Chapter 3: Physical Modelling	18
<i>3.1. Background</i>	<i>18</i>
<i>3.2 Overview</i>	<i>18</i>

3.3 Model Facility and Equipment.....	19
3.3.1 Keogram System	20
3.3.2 Basin Layout	23
3.3.3 Wave Generators	27
3.3.4 Bollards, Fenders and Mooring lines.....	28
3.3.5 Calibrating a Ship	30
3.4 Test Procedure.....	31
3.4.1 Objectives	31
3.4.2 Procedure.....	31
3.5 Scaling Effects.....	32
3.6 Output and Analyses	35
Chapter 4: Validation by Numerical Modelling	39
4.1 Overview.....	39
4.2 SWAN.....	40
4.3 SURFBEAT.....	43
4.3.1 Model Dependence.....	54
4.4 Results	56
4.4.1 QUAYSIM Approach	56
4.4.2 Ship Motions	60
4.4.1.1 Test 1	62
4.4.1.2 Test 2	63
4.4.1.3 Test 3	64
4.4.1.4 Test 4	65
4.4.3 Fender and mooring Line Forces.....	67
Chapter 5: Summary and Conclusion.....	69
5.1 Summary	69
5.2 Conclusion	69
References	71
Appendix A: Physical Modelling Procedure	74
Appendix B: Calibrating a Ship	78
Appendix C: Physical Modelling, Fender and Mooring Line Force Correlation.....	81

<i>C1: Test 01</i>	81
<i>C2: Test 02</i>	84
<i>C3: Test 03</i>	87
<i>C4: Test 04</i>	90
Appendix D: Practical Realities of the Physical Modelling Process	93
Appendix E: Swan Computation Results	95
<i>E1: Test 01</i>	95
<i>E2: Test 02</i>	96
<i>E3: Test 03</i>	97
<i>E4: Test 04</i>	98
Appendix F: SURFBEAT Correlation	99
<i>F1: Test 01</i>	99
<i>F2: Test 02</i>	103
<i>F3: Test 03</i>	107
<i>F4: Test 04</i>	111
Appendix G: Grid Dependency and Time Dependency checks	115
Appendix H: Numerical Modelling Procedure	117
<i>H1: Hull Form Data</i>	117
<i>H2: Mesh Generation</i>	118
<i>H3: WAVESCAT</i>	121
<i>H4: LF-STRIP</i>	122
<i>H5: QUAYSIM</i>	123
Appendix I: QUAYSIM Results	125
<i>I1: Test 01</i>	125
<i>I2: Test 02</i>	127
<i>I3: Test 03</i>	129
<i>I4: Test 04</i>	131

List of Figures

Figure 1: Bound long wave in high frequency wave groups (Stuart, 2013).....	6
Figure 2: Ship motions (van der Molen W. , 2006 (a))	7
Figure 3a: Outline of study approach	10
Figure 4: Wave propagation in Delft3D-FLOW (SURFBEAT) where curved lines represent wave rays (orthogonals) (Delft3D-FLOW, 2011).....	14
Figure 5: Input files for QUAYSIM	16
Figure 6: Ship-bound and Earth-fixed coordinate systems (cross-sectional view)	17
Figure 7: Ship-bound and Earth-fixed coordinate systems (top view).....	17
Figure 8: Equipment fixed to the jetty	20
Figure 9: Keogram system	21
Figure 10: Example of a Keogram result.....	22
Figure 11: Movement plotted with Matlab	22
Figure 12: Full basin layout	24
Figure 13: Basin layout (half-filled).....	24
Figure 14: Probe positions.....	25
Figure 15: Single capacitance probe, P2-P10 (left), directional probe, D1 (right).....	26
Figure 16: Cross-section of mid-ships	26
Figure 17: Cross-section of basin layout at mid-ships.....	27
Figure 18: Cross-section of vessel	28
Figure 19: Bollard dimensions	29
Figure 20: Fender dimensions.....	29
Figure 21: Test 03, Strain gauge vs keogram force measurements, mooring lines.....	36

Figure 22: Test 03, graphical representation of mooring line force correlation	37
Figure 23: Test 03, graphical representation of fender force correlation	37
Figure 24: Test 03, strain gauge vs keogram force measurements, fenders	38
Figure 25: Procedure steps indicating how the numerical modelling calculations compared to the physical modelling measurements	39
Figure 26: Numerical set-up of SWAN – bathymetry of model domain	40
Figure 27: Test 03, high frequency wave height comparison	42
Figure 28: SURFBEAT simulation domain	46
Figure 29: Test 04, long wave and short wave spectra correlation between the physical model, SWAN, and SURFBEAT	49
Figure 30: Test 04, long wave and short wave spectra correlation between the physical model, SWAN, and SURFBEAT (contd.)	50
Figure 31: Test 04, long wave and short wave spectra correlation between the physical model, SWAN, and SURFBEAT (contd.)	51
Figure 32: Test 04, long wave and short wave spectra correlation between the physical model, SWAN, and SURFBEAT (contd.)	52
Figure 33: Surface profiles for oscillating waves (Scheffner, 2006)	52
Figure 34: Dependency test results	55
Figure 35: Dependency test results (contd.)	56
Figure 36: Calibration and validation	57
Figure 37: Different approaches to validating QUAYSIM	58
Figure 38: Ship motion spectra calculated for different methods	59
Figure 39: Viscous effects	61
Figure 40: Ship motion spectra for Test 01	62
Figure 41: Ship motion spectra for Test 02	63

Figure 42: Ship motion spectra for Test 03	64
Figure 43: Ship motion spectra for Test 04	65
Figure 44: Regular wave result.....	66
Figure 45: Mooring system.....	74
Figure 46: Testing spring stiffness.....	75
Figure 47: Bollard-pulley-mooring-line system	75
Figure 48: Generic performance curve of a super cone fender	76
Figure 49: Fender calibration.....	77
Figure 50: Cradle used for calibration procedures	78
Figure 51: Levelling of the cradle	78
Figure 52: Displacement test.....	79
Figure 53: Swinging test	79
Figure 54: Lifting the centre of gravity	80
Figure 55: Test 01, graphical representation of fender-force correlation	81
Figure 56: Test 01, strain gauge vs Keogram force measurements, fenders	82
Figure 57: Test 01, graphical representation of mooring-line-force correlation.....	82
Figure 58: Test 01, strain gauge vs Keogram force measurements, mooring lines.....	83
Figure 59: Test 02, graphical representation of fender-force correlation	84
Figure 60: Test 02, strain gauge vs Keogram force measurements, fenders	85
Figure 61: Test 02, graphical representation of mooring-line-force correlation.....	85
Figure 62: Test 02, strain gauge vs Keogram force measurements, mooring lines.....	86
Figure 63: Test 03, graphical representation of fender-force correlation	87
Figure 64: Test 03, strain gauge vs Keogram force measurements, fenders	88

Figure 65: Test 03, graphical representation of mooring-line-force correlation.....	88
Figure 66: Test 03, strain gauge vs Keogram force measurements, mooring lines.....	89
Figure 67: Test 03, graphical representation of fender-force correlation	90
Figure 68: Test 04, strain gauge vs Keogram force measurements, fenders	91
Figure 69: Test 04, graphical representation of mooring-line-force correlation.....	91
Figure 70: Test 04, strain gauge vs Keogram force measurements, mooring lines.....	92
Figure 71: Test 01, physical model high frequency wave heights vs numerical model high frequency wave heights.....	95
Figure 72: Test 03, physical model high frequency wave heights vs numerical model high frequency wave heights.....	96
Figure 73: Test 03, physical model high frequency wave heights vs numerical model high frequency wave heights.....	97
Figure 74: Test 04, physical model high frequency wave heights vs numerical model high frequency wave heights.....	98
Figure 75: Test 01, long wave and short wave spectra correlation between the physical model, SWAN, and SURFBEAT	99
Figure 76: Test 01, long wave and short wave spectra correlation between the physical model, SWAN, and SURFBEAT (contd.).....	100
Figure 77: Test 01, long wave and short wave spectra correlation between the physical model, SWAN, and SURFBEAT (contd.).....	101
Figure 78: Test 01, long wave and short wave spectra correlation between the physical model, SWAN, and SURFBEAT (contd.).....	102
Figure 79: Test 02, long wave and short wave spectra correlation between the physical model, SWAN, and SURFBEAT	103
Figure 80: Test 02, long wave and short wave spectra correlation between the physical model, SWAN, and SURFBEAT (contd.).....	104
Figure 81: Test 02, long wave and short wave spectra correlation between the physical model, SWAN, and SURFBEAT (contd.).....	105

Figure 82: Test 02, long wave and short wave spectra correlation between the physical model, SWAN, and SURFBEAT (contd.).....	106
Figure 83: Test 03, long wave and short wave spectra correlation between the physical model, SWAN, and SURFBEAT	107
Figure 84: Test 03, long wave and short wave spectra correlation between the physical model, SWAN, and SURFBEAT (contd.).....	108
Figure 85: Test 03, long wave and short wave spectra correlation between the physical model, SWAN, and SURFBEAT (contd.).....	109
Figure 86: Test 03, long wave and short wave spectra correlation between the physical model, SWAN, and SURFBEAT (contd.).....	110
Figure 87: Test 04, long wave and short wave spectra correlation between the physical model, SWAN, and SURFBEAT	111
Figure 88: Test 04, long wave and short wave spectra correlation between the physical model, SWAN, and SURFBEAT (contd.).....	112
Figure 89: Test 04, long wave and short wave spectra correlation between the physical model, SWAN, and SURFBEAT (contd.).....	113
Figure 90: Test 04, long wave and short wave spectra correlation between the physical model, SWAN, and SURFBEAT (contd.).....	114
Figure 91: Dependency test results.....	115
Figure 92: Dependency test results (contd.).....	116
Figure 93: Hull form panels	117
Figure 94: Top view of panel allocation	118
Figure 95: Mesh of the B300 vessel.....	119
Figure 96: Vessel mesh and quay wall mesh.....	120
Figure 97: Description for heading of LF-STRIP	123
Figure 98: Ship motion spectra for Test 01	125
Figure 99: Ship motion spectra for Test 02	127

Figure 100: Ship motion spectra for Test 03	129
Figure 101: Ship motion spectra for Test 04	131

List of Tables

Table 1: Vessel calibration results.....	30
Table 2: Test conditions.....	32
Table 3: Test 03, mooring line and fender force correlation.....	35
Table 4: Wave conditions at the input boundary for physical model and SWAN model	41
Table 5: Probe depths	43
Table 6: Roller parameters	45
Table 7: standing wave period present in the basin	53
Table 8: Ship motion values calculated for different methods.....	58
Table 9: Comparable results	60
Table 10: Ship motion values for Test 01	62
Table 11: Ship motion values for Test 02.....	63
Table 12: Ship motion values for Test 03.....	64
Table 13: Ship motion values for Test 04	65
Table 14: Fender and mooring line correlation between physical model and QUAYSIM, Test 01	67
Table 15: Fender and mooring line correlation between physical model and QUAYSIM, Test 02	68
Table 16: Fender and mooring line correlation between physical model and QUAYSIM, Test 03	68
Table 17: Fender and mooring line correlation between physical model and QUAYSIM, Test 04	68
Table 18: Test 01, mooring line- and fender-force correlation	81
Table 19: Test 02, mooring line- and fender-force correlation	84
Table 20: Test 03, mooring line- and fender-force correlation	87
Table 21: Test 04, mooring line- and fender-force correlation	90
Table 22: Mesh file structure for vessel (van der Molen W. , 2011 (b))	118

Table 23: Mesh file structure for quay wall (van der Molen W. , 2011 (b)).....	120
Table 24: WAVESCAT file structure (van der Molen W. , 2011 (b))	121
Table 25: LF-STRIP input file structure (van der Molen W. , 2011 (c)).....	122
Table 26: Input file structure for WAVEFORCES	123
Table 27: Ship motion values for Test 01	125
Table 28: Fender and mooring line correlation between physical model and QUAYSIM, Test 01	126
Table 29: Ship motion values for Test 02	127
Table 30: Fender and mooring line correlation between physical model and QUAYSIM, Test 02	128
Table 31: Ship motion values for Test 03	129
Table 32: Fender and mooring line correlation between physical model and QUAYSIM, Test 03	130
Table 33: Ship motion values for Test 04	131
Table 34: Fender and mooring line correlation between physical model and QUAYSIM, Test 04	132

List of Symbols

B	beam
CD	chart datum
CSIR	Council for Scientific and Industrial Research
C _g	short wave group celerity [m/s]
C	celerity [m/s] (wave speed)
Cr	courant number
D	draught
DirM	mean wave direction
f	frequency
F _{max}	maximum force
F _s	significant force calculated from average 1/3 greatest trough-crest values
F _x	force in horizontal direction
g	acceleration of gravity
h	water depth [m]
H _{m0}	significant wave height calculated from the spectral domain to be four times the standard deviation of the water surface deviation from the mean
H _{max}	maximum trough-crest or crest-trough value of the highest eight wave in a wave record
H _s	significant wave height calculated in the time domain as the average 1/3 greatest trough-crest values
KG	height of centre of gravity (CG)
K _{xx}	transverse radius of gyration
K _{yy}	longitudinal radius of gyration
LCG	distance of CG aft of mid-ship
l_B	natural length of the basin
Loa	length overall
L _{pp}	length between perpendiculars
M	mass
m	metre
m_0	moments of the wave spectrum
n	number of nodes along the axis of a basin
s	second in time
S(f)	frequency as a function of the spectral energy
Spr	wave spreading

SWL	still water level
T_n	natural free oscillating period of a basin
T_p	peak wave period for entire spectrum
T_s	mean interval of the 1/3 greatest trough-crest values
Δt	change in time
Δx	size of the grid cell in the x-direction
Δy	size of the grid cell in the y-direction

Chapter 1: Introduction

1.1 Background

Understanding ship motions has always been important for port development. Large ship motions of moored ships can discontinue the loading/unloading process and cause line breaking accidents. Line-breaking causes damage to both the ship and the quay wall. More importantly, line breaking compromises the safety of the workers on the port or the ship itself. Down-time or inefficient loading/unloading of container vessels at modern ports is not often tolerated. Shipping lines that compete with one another require port terminals with uninterrupted service.

When a specific ship motion criterion has been surpassed, loading/unloading is not always stopped immediately, but gradually slowed down. The productivity of the loading/unloading process is strongly dependant on the motions of the moored ship. Large roll motions may cause damage to the container slot. Whenever surge or sway movements occur, the crane operator has difficulty unloading/loading. Down-time depends on the vessel type. Roll-on/roll-off (“ro-ro”) vessels and container ships are more sensitive to ship motions; ore carriers, LNG carriers and tankers allow larger movements (van der Molen W. , Behaviour of Moored Ships in Harbours, 2006 (a)).

Large ship motions, however, do occur in sheltered ports. Specifically, container vessels are impacted most as large ships are easily affected by low frequency harbour oscillations. The ship motions are caused by low frequency waves penetrating into the harbour and exciting harbour oscillations. To accommodate larger vessels, entrance channels are dredged deeper and wider, and container terminals are relocated closer to the seaward side of the port, causing them to be affected more severely by ocean waves (Van der Molen, 2006). Recent developments in container ship design and terminal development have highlighted the importance of ship motion problems (Headland & Poon, 1998).

In order to understand ship motions, it is necessary to understand the causes thereof. High frequency waves are typically kept out of the harbour by means of a breakwater structure, but low frequency waves are much more difficult to keep out. Low frequency waves created in oceanic storms are amplified if the wave frequency reaches the same resonant frequency as that of the basin. Low frequency waves can also diffract from breakwater heads, thereby penetrating into the harbour and generating an amplified wave pattern (Van der Molen, 2006). Bound long waves are known to be underlying low frequency waves found within groups of high frequency waves. A bound long wave is released at the basin entrance, thereafter behaving like a free wave. If its frequency approaches that of the resonant frequency of the basin, this wave amplifies as it

propagates through the basin. Bound long waves significantly contribute to low frequency drift forces. “Drift forces” refer to forces which cause a vessel to naturally drift in the direction of the oncoming wave. This is typically seen in anchored ships which rotate until they are faced head-on towards the oncoming wave. Drift forces vary with the periods of the passing waves, but together with the bound long waves, contribute to low frequency forces. These low frequency drift forces are able to excite large, long wave ship motions (Van der Molen, 2006).

Research done in the 1970s and early 1980s has led to the development of several numerical models for calculating wave forces acting on ships, as well as moored ship motions. One of these models is TERMSIM, a predecessor of MOORSIM (Ligteringen, van der Molen, van der Lem, & de Waal, 2003). During berth and jetty design, such six degrees of freedom (6DOF) models are used to determine the forces generated in mooring lines and fenders, as well as the ship motions at berth. Examples of these models are QUAYSIM and TERMSIM. These models are called 6DOF models because the forces and motions obtained are calculated in the 6DOF, consisting of three translation (i.e. surge, sway and heave) and three rotation (i.e. roll, pitch and yaw) components (Ligteringen, van der Molen, van der Lem, & de Waal, 2003). Numerical model software packages with 6DOF simulation programmes have been used for over twenty years. The validation of physical model outcomes, however, are still lacking within these software packages (Ligteringen, van der Molen, van der Lem, & de Waal, 2003). Some models have been validated, but not yet published due to confidentiality agreements. If numerical models are validated and published more frequently, an engineer may more confidently use these numerical models and interpret the results. Also, it is important to determine the ship motions in the preliminary design stage of a port or new port extensions, as well as during the operational stage. Should the models be validated, it would be economically viable to predict ship motions more often (Van der Molen, 2006).

1.2 Objective

The objective of this study was to measure ship motions, forces in fenders and mooring lines in a physical model, and compare these measurements with predicted values using numerical models to simulate the physical model geometry, inputs and results. The ultimate goal was to use a multi-step approach to validate the numerical models QUAYSIM and WAVESCAT.

1.3 Thesis Approach

The physical model has a built-in bathymetry provided by the CSIR Hydraulics Laboratory in Stellenbosch. The focus was to avoid uncertainties and keep the physical model simple. This meant keeping the provided scale allocated to the model, having a straight beach and having no breakwaters/obstacles in the basin. The physical model consisted of a jetty with fenders, bollards

and mooring lines used to moor a container carrier vessel to it. The tests were done with two scenarios:

1. The jetty being a pile supported jetty
2. The jetty being a solid quay wall

Probes were placed in the basin to measure the wave height and wave periods at certain locations. The wave runs were carried out and the wave heights, wave periods, fender forces, mooring line forces, and ship motions were measured. The measurements were used as reference data for the numerical calibration and validation procedure. Calibration of a model implies adjusting the model by means of prototype measurements, in such a way that the model data correlates well to the prototype data. The model is then reproducing a specific situation in the prototype. Validation of the model implies simulation and comparison using another known situation, without adjusting the model any further. Calibration alone is not a sufficient guarantee of reliability. Both calibration and validation stress the need of prototype data.

This thesis involved investigating the ship motions of a scale model of a moored ship that has been subjected to low frequency waves, in order to validate the ship motion models WAVESCAT/QUAYSIM. In an Attempt to validate this method, a multi-step approach of calibrating a series of numerical models was used. The numerical models used the exact replica of the built-in basin. The physical model was not subjected to a specific scenario, but was used for the purpose of validating the numerical models WAVESCAT/QUAYSIM. The SWAN module from Delft3D-WAVE was calibrated using the measured wave conditions obtained inside the basin. Once these wave conditions had been calibrated, the SURFBEAT module from Delft3D-FLOW was used to resolve the low frequency waves occurring in the basin. WAVECAT, WAVEFORCES, and LF-STRIP are the models used to transfer the waves into forces acting on a vessel (QUAYSIM requires forces acting on a vessel to calculate the ship motions). Consequently, the ship motions calculated by QUAYSIM were inflicted by the calibrated long/short wave forces. In this way, the numerical modelling procedure WAVESCAT/QUAYSIM could be validated.

This specific approach has been used before, but could not be published because of confidentiality agreements. This study is a documentation of the validation of the WAVESCAT/QUAYSIM procedure, with the purpose of using this method for future projects.

1.4 Thesis Outline

Chapter 2 deals with the literature review covering relevant topics of the physical modelling process as well as a description of the numerical models used. The numerical models used for this project are discussed in more detail to gain a proper understanding how they operate and what their limitations are. Chapter 3 discusses a detailed description of the physical modelling process

and the procedures thereof. The numerical modelling methodology and results are explained in Chapter 4. The results of the physical model are explained step by step in parallel to the numerical modelling chapter for comparison purposes. Chapter 5 provides a summary and conclusion of the study. The appendices are referred to in text and should be viewed respectively.

Chapter 2: Numerical Modelling of Long waves and Ship Motions

2.1 Background

Large ships are easily affected by low frequency waves which can generate large ship motions (van der Molen W. , 2006 (a)). Munk (1949) and Tucker (1950) originally examined and analysed the presence of low frequency waves related to high frequency wave groups in the coastal zone (J. A. Battjes, 2004), (Tucker, 1950), (Munk, 1949). They proposed that low frequency waves are generated in the surf zone because of the beat phenomenon produced by wave grouping within incident wind generated waves. Consequently, the low frequency waves were named “surf beat”. The interaction of incident/primary waves causing second order (group) bound long waves was found (J. A. Battjes, 2004). The high frequency wave group propagates from deep water, over the sloping ocean floor, towards the breaking zone and is so heightened. As the high frequency wave group breaks, an underlying bound long wave, known as a free long wave, reflects off the shore. Another coastal process discovered was the generation of free long waves as a result of a moving breaking point (J. A. Battjes, 2004). Since the presence of low frequency or long waves was discovered, more investigations were carried out to understand the physics and the origin of low frequency waves.

Van der Molen (2006) provided a good description of the origin and existence of long waves inside and ports. Long waves, also known as low frequency waves, are formed in more than one way. In oceanic storms, low frequency waves near to harbour resonance are generated. The low frequency waves shoal in shallow water, therefore becoming of significant importance in coastal areas and ports. These waves are also the set-down beneath wave groups. High frequency wave groups are represented by varying heights and lengths. Therefore, water is ejected from the wave group and a low frequency wave is formed in the length scale of the wave group length. This is called a bound long wave, as it is bounded by a high frequency wave group. The celerity of the bound long wave is equal to the group velocity. The height of the bound long wave increases as the wave propagates in shallower water. This is often where harbours and mooring facilities are situated. A bound long wave may cause excitations in an open basin even if the length of the bound long wave does not match the length of the resonant wave length of the basin.

Figure 1 shows an underlying bound long wave present in short wave groups. The red line represents the present long wave. The blue line represents the short wave groups. The bound wave forms a low frequency wave at the harbour entrance, consequently behaving like a free long wave. This generated wave is enhanced in the basin, if the frequency is close to the resonant frequency of the basin (van der Molen W. , 2006 (a)).

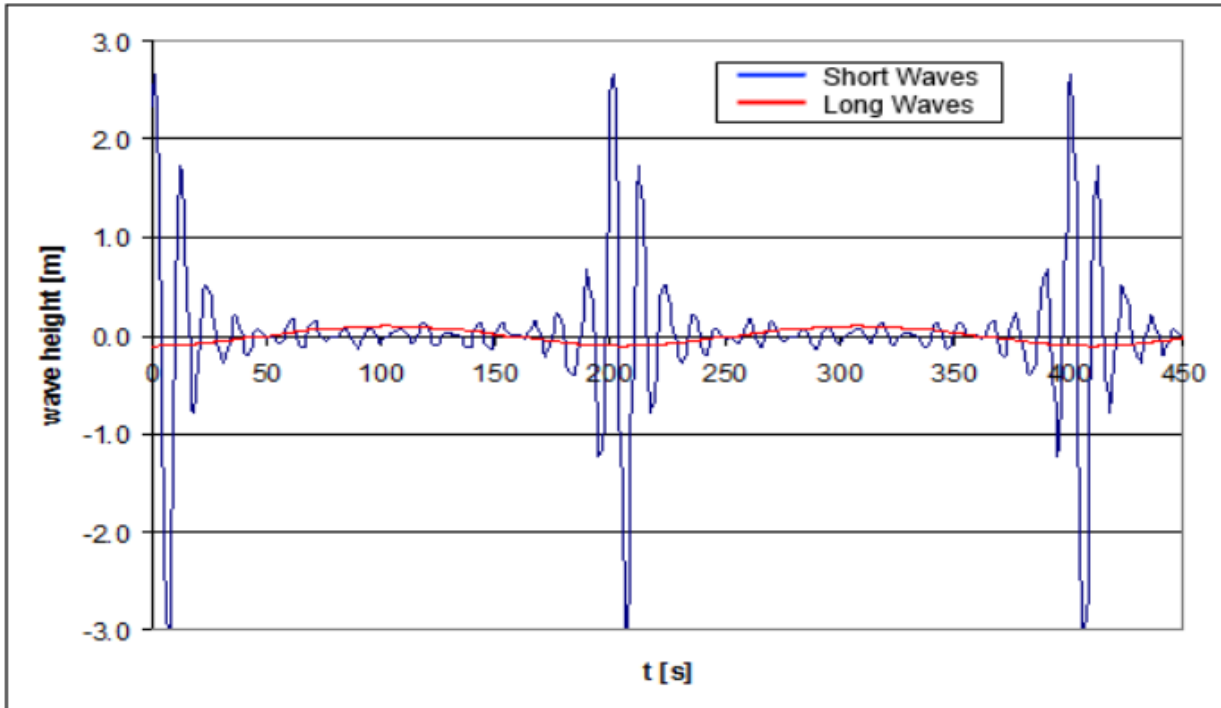


Figure 1: Bound long wave in high frequency wave groups (Stuart, 2013)

Another challenge is to protect the vessels from low frequency induced motions. The ‘Harbour Paradox’ by Miles and Munk (1961) states that one might expect a narrowing harbour entrance to lead to the reduction of harbour surging, but it can lead to enhancements instead (Miles & Munk, 1961). Therefore, the solution for protection against low frequency motions is contradictory. Having a narrow harbour entrance prevents the oscillations from leaving the harbour, thus remaining in the harbour basin (van der Molen W. , 2006 (a)).

Knowing that low frequency waves cause ship oscillations, it is important to understand how a vessel can oscillate. A vessel can displace in six movements. Figure 2 illustrates the various ship motions and their directions. The “surge” movement is a longitudinal displacement in x-direction along the bow and stern. “Sway” is displacement measured in the transverse (y-direction). “Heave” is the vertical displacement in the z-direction. “Roll” (φ) is a moment rotating around the x-axis, displacing vertically at the starboard and port side of the vessel. “Pitch” (θ) is a moment rotating around the y-axis, displacing vertically at the bow and stern. “Yaw” (ψ) is defined as the moment rotating the z-axis, displacing laterally at the bow and stern.

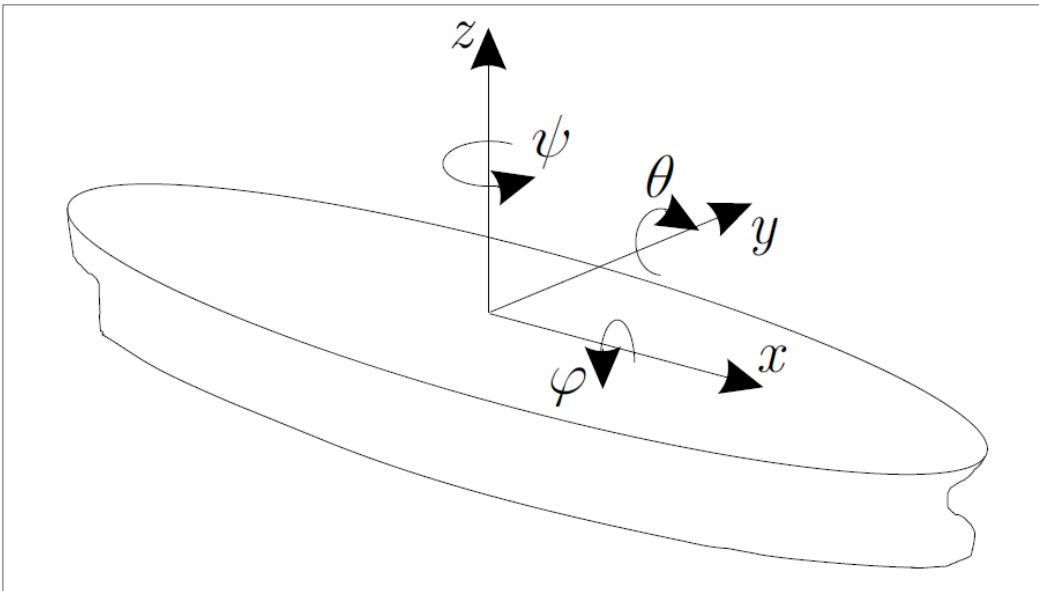


Figure 2: Ship motions (van der Molen W. , 2006 (a))

Research on low frequency waves and moored ship motions has led to the development of numerical modelling packages. Early numerical modelling packages involved a ship moored to a quay wall/pile supported jetty (van Oortmerssen, 1976) or a single point moored tanker (Wichers, 1988). These models calculated a ship's response up to the second order. However, these models make use of an irregular uni-directional wave train (van der Molen W. , 2006 (a)). Inside a harbour (where the vessels are located), other coastal processes such as refraction, diffraction and reflection occur. The aforementioned models do not account for these processes, thus extensions to these models are required for modelling ship motions in an arbitrary wave field (van der Molen W. , 2006 (a)).

2.2 Overview of Past Numerical Models

In 1971, Remery and Hermans reported results for excitations and ship motions of a barge moored to a single point in wave groups (Remery & Hermans, 1971). The focus was placed on the surge motion which showed that the amplitude in the low frequency motion was caused by a low frequency drift force. At the time, they used an unrealistic large damping coefficient in their model to calculate the low frequency surge motion (Hermans & Huijsmans, 1987). In 1980, Pinkster published a pressure integration technique to calculate the low frequency drift force (Pinkster, 1980). This involves integrating the wave elevation over the water line and integrating the particle velocities over the submerged hull. This technique is able to consider the low frequency second order drift force in a wave group directly (van der Molen W. , 2006 (a)). It is however, difficult to evaluate the derivative of the water velocity over the floating body correctly (Hermans & Huijsmans, 1987), and the technique is only applicable to vessels without forward speed.

More recent numerical models on the behaviour of ship motions in irregular waves are time domain approaches. Most of these models were designed in the Netherlands and examples of them

include TERMSIM (developed at MARIN), BAS (developed at WL Delft Hydraulics) and SHIPMOORINGS (developed at Alkyon). These models integrate the equations of motion in time only. The hydrodynamic coefficients, first order and second order wave force transfer functions need to be calculated beforehand with other numerical models which consider the wave-body interaction of the moving body in still water and of the fixed body in waves (van der Molen W. , 2006 (a)).

Some of these models involve the strip theory (Ursell, 1949). Ursell (1949) developed formulations to compute forces on an oscillating circular cylinder. These formulations were used by Korvin-Kroukovsky and Jacobs (1957) to develop a quasi-three-dimensional method to determine ship motions (Korvin-Kroukovsky & Jacobs, 1957). This method is called the “strip theory”. The strip theory divides the wetted hull of a vessel into a number of cross-sectional strips. Each cross-sectional strip is considered to be part of an infinitely long cylinder. The fluid flow is treated as if it is completely underneath the body and fluid flow along the ends of the vessel is neglected (van der Molen W. , 2006 (a)). As a result, this theory can only be applied to slender bodies, or to situations where the wave lengths are short compared to the ship’s length for the determination of the hydrodynamic coefficients (van der Molen W. , 2006 (a)). The theory considers forward speed by approximating, which is theoretically insufficient. Nonetheless, the strip theory corresponds well to physical model experiments and is still currently incorporated into numerical models, even though far more advanced three-dimensional methods have since been established. The strip theory may still be effectively used, particularly in early vessel design stages (van der Molen W. , 2006 (a)).

More common than the strip theory method is the three-dimensional panel method. The panel method is used more extensively and is a great deal more popular. Faltinsen (1990) and Lee & Newman (2005) gave proper theoretical summaries of force calculations by making use of the panel method (van der Molen W. , 2006 (a)), (Faltinsen, 1990), (Lee & Newman, 2005). Most panel method models make use of linear frequency-domain methods, in which the wetted hull is divided into a certain number of quadrilateral panels. Hence, the so-called “panel method” originated. The founder of the numerical model DIFFRAC, Van Oortmerssen (1976), was the first to successfully develop a feasible model. DIFFRAC is able to determine the moored ship response of a tanker vessel. By using the method of images, Van Oortmerssen succeeded in including the effect of a quay wall on the ship motions. The most widespread frequency-domain model, Wave Analysis at MIT (WAMIT), was created at MIT (Massachusetts Institute of Technology). This model has been extended and revised with different modules making it suitable for various wave-structure interactions and offshore engineering (van der Molen W. , 2006 (a)).

Recently, a new process-based numerical model for nearshore and coast called “XBEACH” was developed by Roelvink, Reniers, van Dongeren, van Thiel de Vries, McCall, & Lescinski, (2009). XBEACH is still a young model based on Delft 3D (McCall, Plant, & van Thiel de Vries). The model

resolves coupled 2D horizontal equations for wave propagation, flow, sediment transport and seabed changes, for spectral (varying) wave and flow boundary conditions. The model takes into consideration changes in wave height over time, which enables it to solve the low frequency wave motions caused by this variation (Roelvink, Reniers, van Dongeren, van Thiel de Vries, McCall, & Lescinski, 2009). XBEACH can sufficiently calculate the high frequency wave and low frequency wave propagation. By obtaining the same wave heights in the numerical model as in the physical model, XBEACH is calibrated.

From here the following procedure will apply:

XBEACH =>> WAVESCAT =>> LF – STRIP =>> WAVEFORCES =>> QUAYSIM

With this approach, modelling with SWAN and SURFBEAT becomes unnecessary. SWAN and SURFBEAT however, are more user friendly as they have a graphical user interface (GUI). For this reason, the Delft3D-FLOW/WAVE packages were used in this study.

2.3 Computational Approach

Figure 3a and 3b illustrates the computational approach carried out to reach the objectives of this study. This approach involved following a chain of numerical modelling procedures. The computational approach in consideration makes use of the strength of each numerical model to ultimately calculate the ship motion. Figure 3a provides an outline of the modelling approach where Figure 3b provides a more detailed description of the procedure. In Figure 3b the main heading on the left indicates the specific procedure, and the descriptive text on the right details the nature of that procedure.

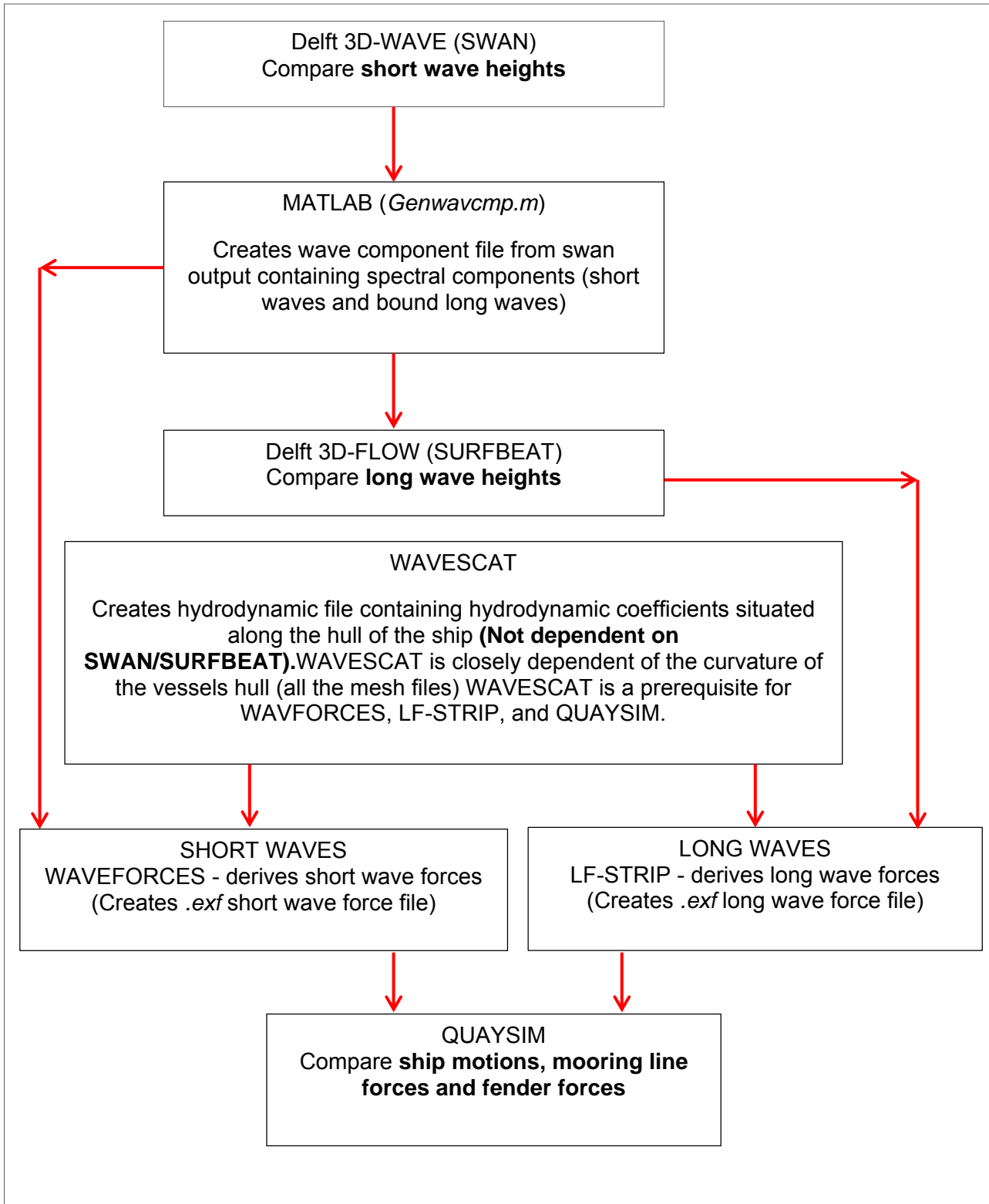


Figure 3a: Outline of study approach



Figure 3b: Detailed description of the computational approach

2.4 Overview of Current Models

2.4.1 SWAN (Delft3D-WAVE)

SWAN (Simulating WAVes Nearshore) was developed mainly at Delft University of Technology in the Netherlands. SWAN is known to be the standard model for modelling nearshore wave propagation. For this reason, Deltares (the Netherlands) have integrated the SWAN modelling package into the Delft-3D model suite.

The SWAN model is fully spectral in all directions and all frequencies. As a result, random wave fields can simultaneously be modelled from various wave directions. For example; extreme cases such as wind sea along with a large swell can be modelled. SWAN determines the progression of random high frequency waves in coastal areas as the waves propagate from deep water to shallow water including the effect of currents. This model offers an effective way to model high frequency wave propagation as it takes into account refraction processes that occur when the waves change direction due to a sloping bathymetry. Other processes modelled by SWAN include wave generation caused by wind, wave dissipation due to white capping, wave dissipation due to bottom friction, wave dissipation due to depth-induced breaking, and non-linear wave-wave interactions (Delft3D-WAVE, 2011). The ability to model such a wide range of coastal processes in one model increases the likelihood of a model being able to closely replicate real-life coastal wave situations.

A normal computation for the prediction of nearshore wave propagation can be carried out by SWAN (Delft3D-WAVE) to provide the wave directions and input wave spectrum for SURFBEAT (Delf3D-FLOW). The domain required for the SWAN computation should contain the full flow grid used for SURFBEAT. This is necessary for the wave directions and peak periods to be calculated at each grid point of the flow grid. The output locations should be points near to the open boundary of the flow grid.

The domain for SWAN may even be larger than the grid used for SURFBEAT. However, the SWAN bathymetry should be identical to the bathymetry used for the SURFBEAT model. Should the grid be extended for the SWAN calculations, the refraction process is included in the calculations, as the waves propagate from deep water to shallow water. As mentioned above, the SWAN grid may be coarser than the flow grid used for SURFBEAT. Note, however, that the coarser the grid, the less accurate the results may be, depending on the presence or absence of coastal structures. Coastal structures will cause diffraction patterns which will not be picked up by the model if the grid is too coarse. The diffraction effects should be modelled in SWAN if the domain contains coastal structures such as breakwaters or small islands. The diffraction patterns behind these structures are computed with the respective wave pattern directions (van der Molen W. , 2011 (c)).

2.4.2 SURFBEAT (Delft3D-FLOW)

SURFBEAT computations are carried out with Delft3D-FLOW. Delft3D-FLOW is a multi-dimensional hydrodynamic replication model, determining non-steady flow and transport situations that may be caused by tidal and meteorological forces. Delft3D-FLOW can be computed on a rectilinear boundary-fitted grid or a curvilinear boundary-fitted grid. Output consists among other forms of time series water level elevations, at locations in the domain at which the low frequency wave heights can be calculated. For this reason, Delft3D-FLOW is an effective way to calculate the low frequency wave heights occurring in the basin.

All grid and hydrodynamic options possible for FLOW are possible for SURFBEAT. Similarly, the restrictions for FLOW also hold for SURFBEAT. A uniform water level at the open boundary is recommended as inaccuracies in the water levels at the boundary slowly decay to the specified mean water level with this boundary condition. With the water levels specified at the boundaries, the decay effect disappears after a few wave periods (van der Molen W. , 2011 (c)). The non-linear wave-wave interactions which lead to double frequency peaks in the wave spectrum may be neglected in such a case of FLOW computation. The non-linear wave-wave interactions occur near the surf zone and in most cases are not significant near the boundary of the FLOW grid, where the wave components are generated. The non-linear interactions barely affect the mean wave directions and the peak period (van der Molen W. , 2011 (c)).

Figure 4 illustrates a typical situation modelled in Delft3D-FLOW (SURFBEAT) in which the wave rays or orthogonals represent wave propagation. Boundary A indicates the oceanic boundary. The depth at this boundary should be sufficient, meaning that the waves entering through this boundary should qualify as low frequency waves to satisfy the shallow water approximation. Boundary C indicates the coastline. Care should be taken to ensure that the coastline boundary is assigned a shallow depth. Boundaries B and D are adjacent boundaries closing off the domain (modelling area).

Suppose that the bound long wave enters the domain at point 'a'. Refraction occurs because of the seabed changes as the wave propagates to shallower water. The high frequency wave group, which drives the bound long wave, refracts as it approaches point 'b'. Wave breaking dissipates the wave energy and the high frequency wave group disappears, thereby releasing the bound long wave. Here, the wave energy is transformed to roller energy through the process of wave breaking. Spatial variations in the roller energy create forces on the water. It is not clear how roller energy travels, but it is modelled by using celerity twice that of the group celerity of the high frequency wave groups. The roller energy quickly dissipates in the shallower areas. This is a steady process occurring along trajectory 'a-b' as the high frequency wave group approaches the shallower areas. The free (released) bound long wave easily reflects at the coastline and propagates along

trajectory 'b-c'. The waves must be able to exit the oceanic boundary after being reflected from point 'b'.

The same process described above occurs closer to boundary B, starting at point 'd'. A high frequency wave group enters at point 'd' and propagates along trajectory 'd-e'. The high frequency wave group dissipates along the coastline and the free bound long wave is reflected from the coastline. The free bound long wave should be able to exit the computational domain at the adjacent boundary B (curve 'e-f'). The same process holds for bound long waves entering at point 'g' and travelling along trajectory 'g-f': the bound long wave should be able to exit the adjacent boundary B (Delft3D-FLOW, 2011).

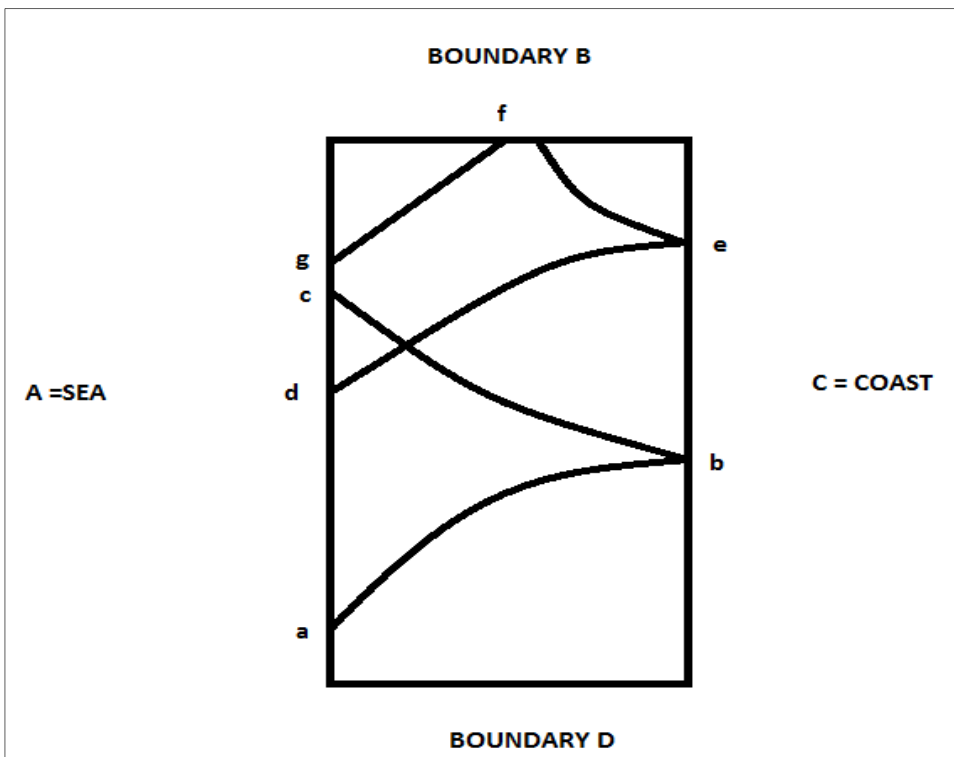


Figure 4: Wave propagation in Delft3D-FLOW (SURFBEAT) where curved lines represent wave rays (orthogonals) (Delft3D-FLOW, 2011)

2.4.3 LF-STRIP (Low Frequency Wave Forces)

When a vessel is moored at a jetty in shallow water, it is relevant to focus on low frequency waves because the long wave forces serve as exciting forces in the dynamic mooring simulation. The low frequency forces imposed on the vessel can be calculated using a combination of numerical models, i.e. SURFBEAT/LF-STRIP. The SURFBEAT module from Delft3D-FLOW is used to calculate low frequency waves in a coastal area, a sheltered bay or a harbour facing the ocean. LF-STRIP provides the link between the low frequency wave model and the ship motion model. LF-STRIP is a strip model used to convert the calculated low frequency wave surface elevations and

fluid velocities to wave forces acting on a moored ship. In this way, the ship motions caused by low frequency waves may be investigated (van der Molen W. , 2011 (c))

2.4.4 QUAYSIM (Ship Motion Model)

QUAYSIM is a program developed by the CSIR to investigate and determine the behaviour of a moored ship in the time domain. Such results can contribute to the downtime analysis of new harbours or port extensions. One of the main input data files required for QUAYSIM is the low and high frequency wave forces acting on a vessel. The software WAVEFORCES generates the forces imposed on a vessel from a standard wave spectrum or from the output from SWAN. The interaction with current and wind is only modelled using current and wind coefficients. The time series of gusting wind can be generated with a model called WINDSPEED, but will not be used for the purpose of this study (van der Molen W. , 2011 (d)).

Figure 5 illustrates the main input files required for QUAYSIM. Each sub-heading represents a data set required for the relevant main input file. For instance, the environmental data set consists of the wave force files, wind and current velocity data, and the water levels data. As mentioned above, the wave force files are calculated with numerical models such as LF-STRIP (low frequency waves) and WAVEFORCES (high frequency waves) from a standard wave spectrum. These force files are text files made up of a single time column with wave forces with 6DOF. The wave forces are represented as surge, sway and heave (kN), and the moments as roll, pitch and yaw (kNm).

The ship data set is made up of the ship's dimensions called the 'shipmain.dat' file, current and wind force coefficients in separate files, and viscous damping coefficients in a damping file. For each current direction; surge, sway, and yaw coefficients are specified. Wind force coefficients are provided for different loading conditions. The viscous damping coefficients are intended to represent the viscous effects in the fluid, while damping can include viscous effects in the mooring system (van der Molen W. , 2011 (d)).

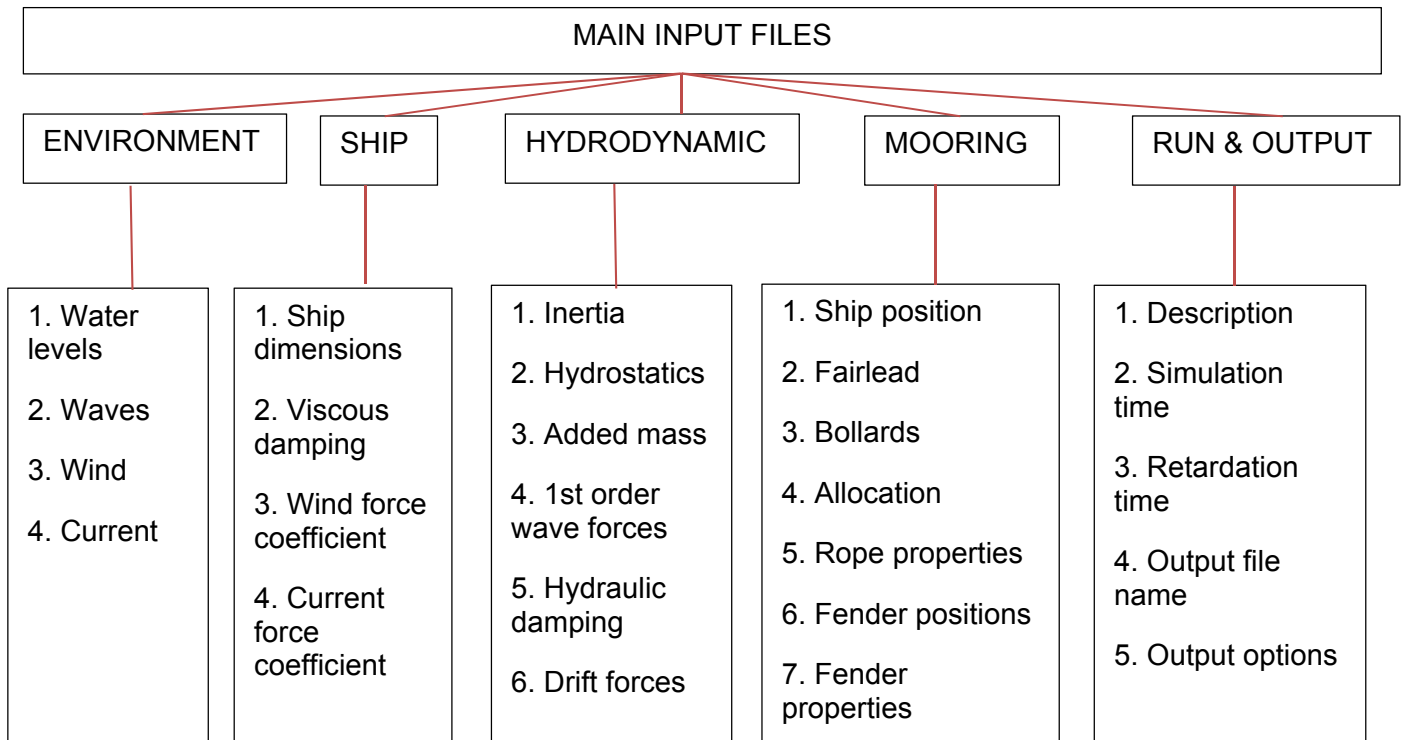


Figure 5: Input files for QUAYSIM

The hydrodynamic data set is created by WAVESCAT and needs to be imported for use in QUAYSIM. This data set is a '.hyd' file containing information about the moment of inertia of the vessel, the added mass, the first order wave forces, the drift forces, and the hydraulic damping coefficients.

The mooring data set is specified in a file called the 'moorsys.dat' file. The mooring file is used to define the location of the fenders, mooring lines, and bollards. The position of the ship is defined as the shift of the ship-bound coordinate system from the earth-fixed coordinate system. Figures 6 and 7 show a top and cross-sectional view of the jetty and the vessel to better illustrate these coordinate systems. The origin of the earth-fixed coordinate system is located at 'mid-ships'(x-direction), jetty deck level (z-direction), and fender edge (y-direction). The origin of the ship-bound coordinate system is located at 'mid-ships' (x- and y-direction) and vessel deck level (z-direction).

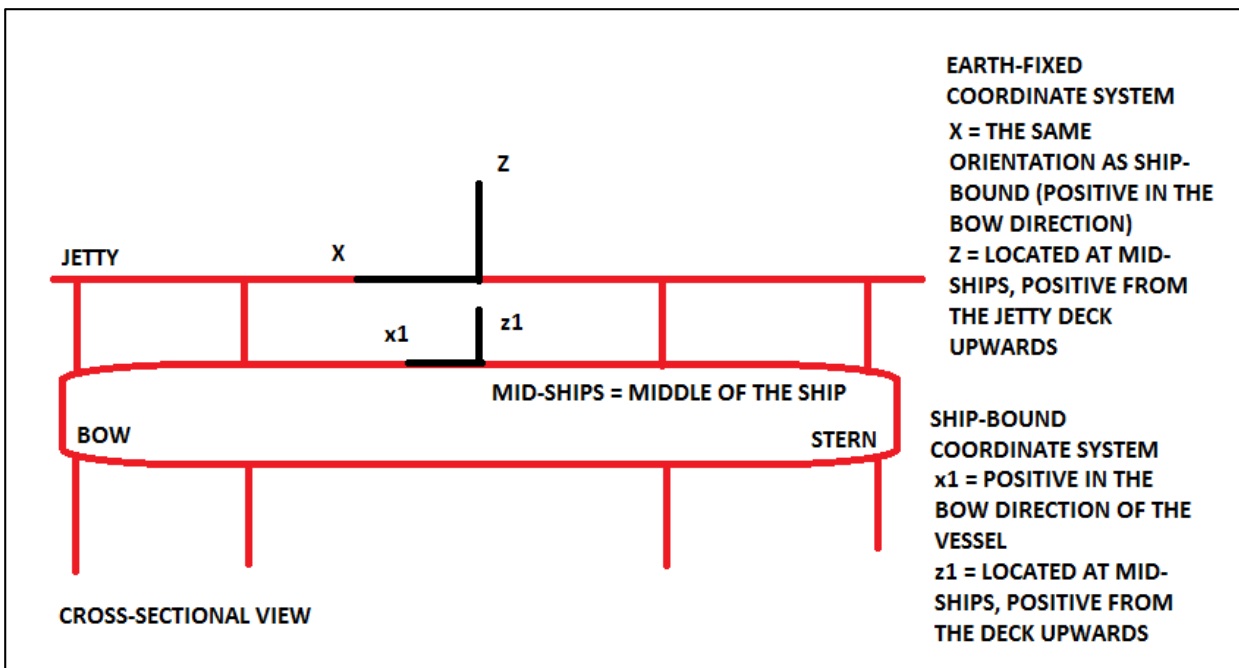


Figure 6: Ship-bound and Earth-fixed coordinate systems (cross-sectional view)

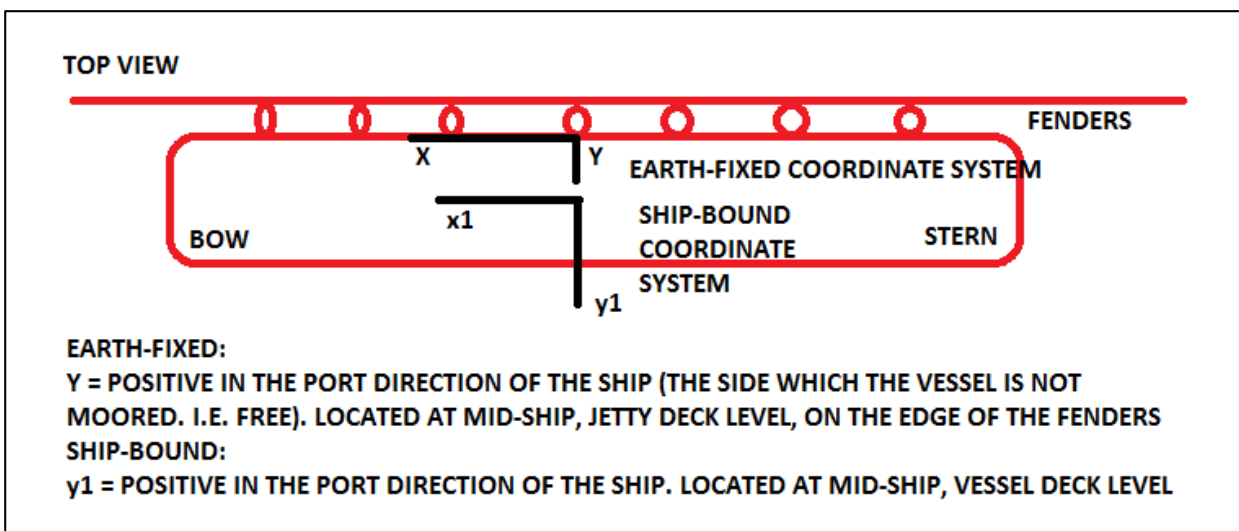


Figure 7: Ship-bound and Earth-fixed coordinate systems (top view)

Four output files are generated and stored in the output folder. An OUT file consists of a summary of the input conditions and an estimate of the natural periods. Natural periods are highly dependent on motion amplitude, therefore these are only indicative. These periods include periods for heave, roll and pitch in the case of free floating vessels, as well as for surge, sway and yaw in the case of moored vessels. A DEF file is created including the names of the output results for which the time series is specified. The standard output results are time, ship motions, mooring line forces, fender compressions, and fender forces. A RES and a SEQ files are generated containing the time series of these quantities (the SEQ file is a text file and the RES file is a binary file). The RES and SEQ files can be analysed with the Matlab function 'plotres.m'. The time series of the ship motions, mooring forces, and the excursions of certain points on the ship can be plotted in this way.

Chapter 3: Physical Modelling

3.1. Background

Physical modelling contributes towards understanding coastal processes and the effects thereof. It provides the link between real life situations and theoretical understanding. Through the use of physical modelling, a real life situation can be replicated and observed. Institutions such as the CSIR (South Africa), Deltares (The Netherlands), and MARIN (The Netherlands) make use of physical modelling to investigate and unravel processes occurring in a model space for a specific problem.

The physical modelling process makes use of laboratory equipment to replicate a real life problem to a calculated or given scale. The calibrated physical model should replicate the boundaries and restrictions of the problem under investigation, whether it is a real life situation, a case study, or even a situation to understand processes. In this chapter, the physical modelling process and the equipment used is discussed in more detail to outline the situation of the proposed problem.

3.2 Overview

The physical model testing was carried out in the Coastal & Hydraulics Laboratory at the CSIR, Stellenbosch. A model size design vessel of 300 000 DWT and a 3D-modelling area of 24 x 33 m at a scale of 1:100 was provided by the CSIR. The given physical model measurements were primarily focused on:

1. vessel motions
2. fender forces
3. mooring line forces
4. water levels at allocated locations
5. waves

As ship motions are of most importance to this study, wave conditions providing significant ship motions were selected for model testing. The ship motions were for a fully laden 300 000 DWT vessel calibrated to a 1:100 scale for two different berthing conditions, namely:

1. jetty supported by piles
2. solid quay wall

These two berthing conditions were chosen because one expects to find different ship motions in the case of each. The waves are expected to casually pass through a jetty supported by piles but

reflect off a solid quay wall, causing two different types of ship motions. Both phenomena were investigated in this study.

All wave conditions were tested for the same jetty supported by piles/quay wall layout. The mooring arrangement used consisted of 8 mooring lines. Three lines were fixed to the bow, another three to the stern and two offset from the centre of the vessel. The same bollards and fenders were used for all the tests carried out.

The model bathymetry (sea-bed depths) consisted of the current built-in bathymetry gently sloping towards an absorption beach, as well as being enclosed with absorption beaches. The bathymetry can be shaped and built for specific situations, but for this project the current built-in bathymetry was kept because it is an expensive procedure to reshape it and was not necessary for this specific study.

3.3 Model Facility and Equipment

The following section deals with the modelling equipment, software and details of the facility used for this study. This includes all modelling equipment such as wave generators, wave probes, cameras, vessel, fenders, mooring lines, and the keogram system. Details regarding the basin layout are also provided. The equipment required for the physical model is explained in detail in the various sections below, the following list serving as a summary:

- For the keograms:
 - 2 cameras monitoring ship motions
 - 2 mirrors
 - 2 movement tracking plates attached below the mirrors
 - 2 movement tracking plates fixed to the vessel
- 3D basin (24 x 33 x 3 m)
- 10 wave probes and probe boxes
- 3 cameras recording movements
- jetty with quay wall
- jetty supported by piles
- 8 fenders + network interface
- 8 mooring lines
- 8 bollards + network interface
- 1 calibrated 300 000 DWT vessel
- equipment used to calibrate vessel

Figure 8 provides an overview of how the previously mentioned equipment is fixed to the jetty (each feature being described later in this chapter). The fenders are represented by the white Teflon buds fixed below the jetty. The bollards work together with a spring-pulley mooring line system and were positioned at 8 locations. The bollards and fenders were fixed to a network interface located more or less at mid-ships, labelled 'bollard/fender box'. 'Mid-ships' refers to a location on the jetty that aligns with the middle of a moored vessel. The keogram system measures ship motions and is explained in detail below.

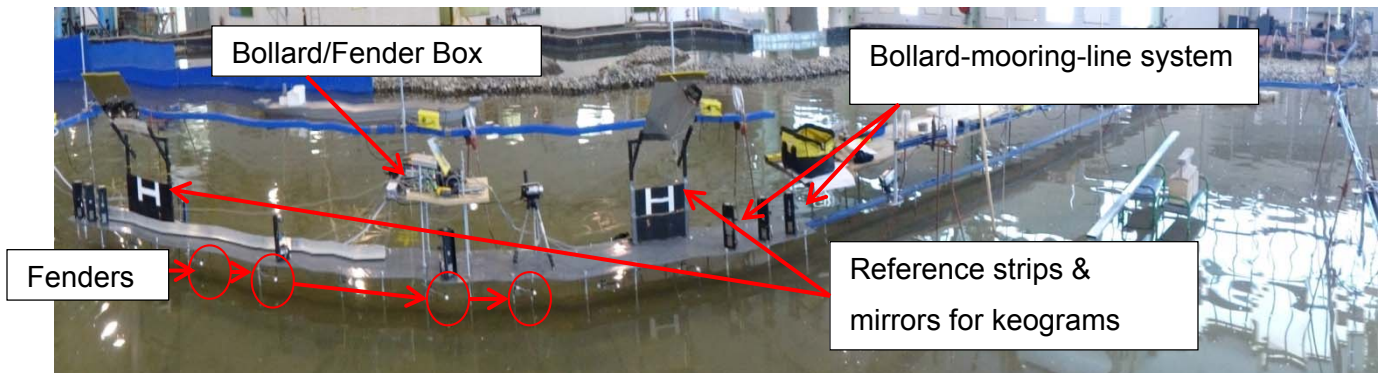


Figure 8: Equipment fixed to the jetty

3.3.1 Keogram System

The keogram system is used to record mooring line forces, fender forces, and ship motions. A brief description of this system is provided below (for a more detailed account, cf. Van der Molen & Hough, 2009).

Figure 9 shows the keogram set-up. The keogram measuring system makes use of steel reference plates fixed to the bow and the stern of the vessel. Above each reference plate, a mirror is fixed at a 45 degree angle. Reference strips are located below each mirror. Cameras are placed perpendicular to the vessel, but further away from the vessel at the bow and the stern. Each camera records the reflection of the reference plate and the movement of the black and white reference strip during testing. The reference strips below the mirrors record the heave, roll and pitch, whereas the reflection of the keogram plates record the surge, sway and yaw movements.

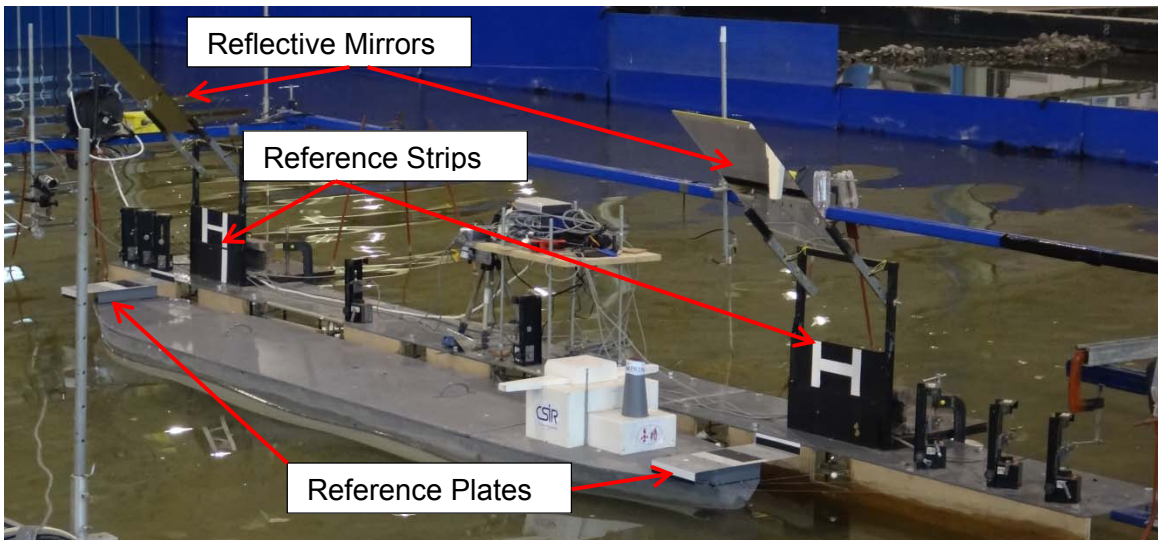


Figure 9: Keogram system

By means of wiring, the two cameras are connected to a computer on which both recordings (bow and stern) are recorded live and are processed. During a test, the keogram recorder programme creates rows of pixels for each sampling line monitored by the cameras. The sampling lines are taken from the reference plates and reference strips. These rows are placed above one another in an image known as a “keogram”. An example of a keogram is displayed in Figure 10.

In a description of the reference lines recorded, one needs to follow the ‘white over black’ movement as these lines progress to the bottom. Referring to the first white line from the top, the surge movement is recorded (below the red sampling line). The sway is recorded below the green line. The two lines below the yellow line represent the heave movement on the port and starboard side, respectively. Lastly, the two strips below the orange line are used for scaling. The movements of the stern are represented in the same order. All movements are then digitised and converted using a Matlab function in order to obtain values for motion in all six directions. Figure 11 shows the output obtained from Matlab. The ship motions for all DOF are plotted against prototype time.

The fender and mooring line forces can also be calculated from the ship motions. The mooring line forces were calculated via a Matlab script provided by the CSIR, making use of; the measured ship motions in six degrees of freedom, the position of the attachment between the mooring line and the ship, and the mooring line stiffness in the springs. In the same way the fender forces were calculated making use of the fender stiffness, measured ship motions, and the contact points of the fenders to the ship’s hull (van der Molen & Hough, 2009).

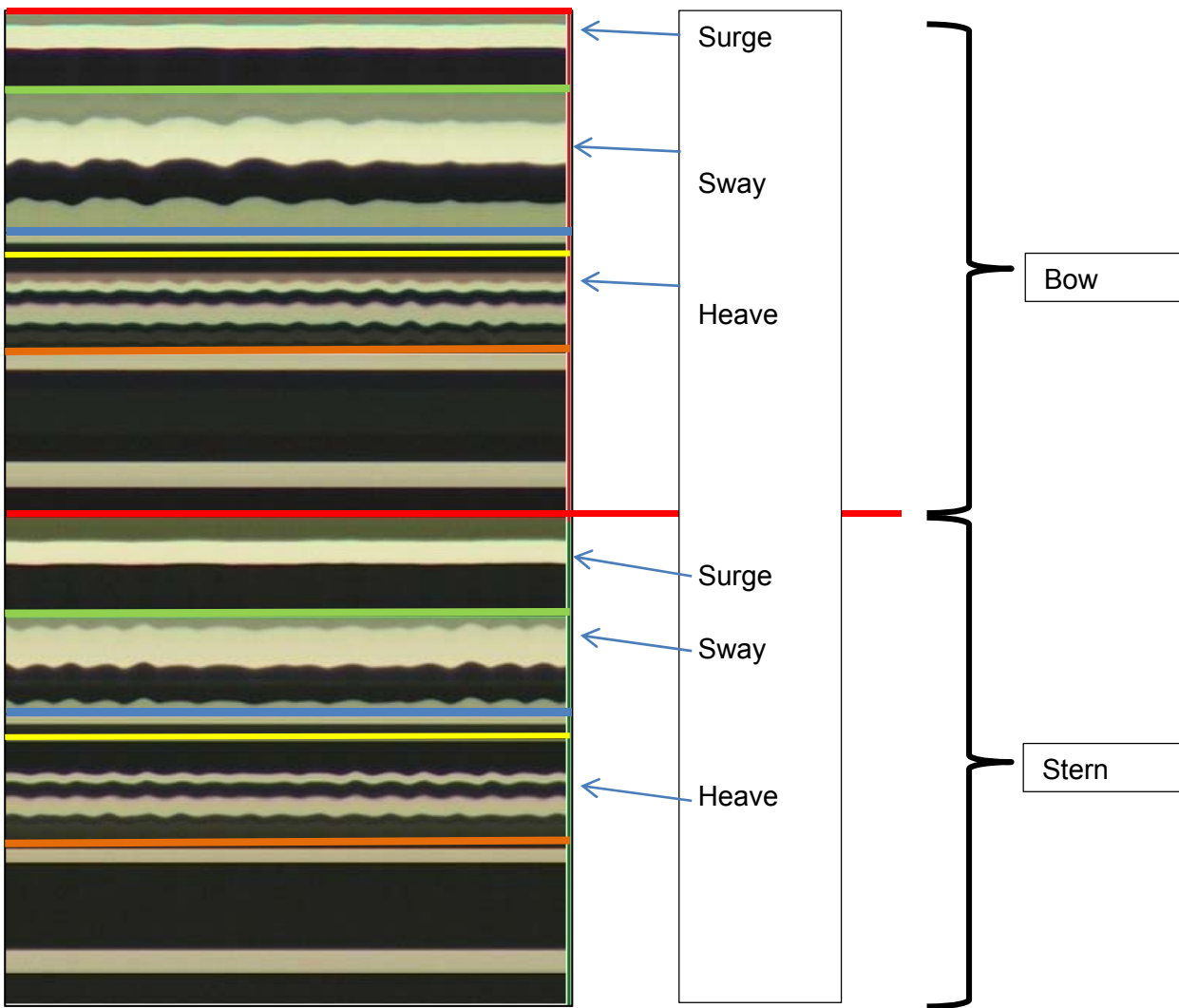


Figure 10: Example of a Keogram result

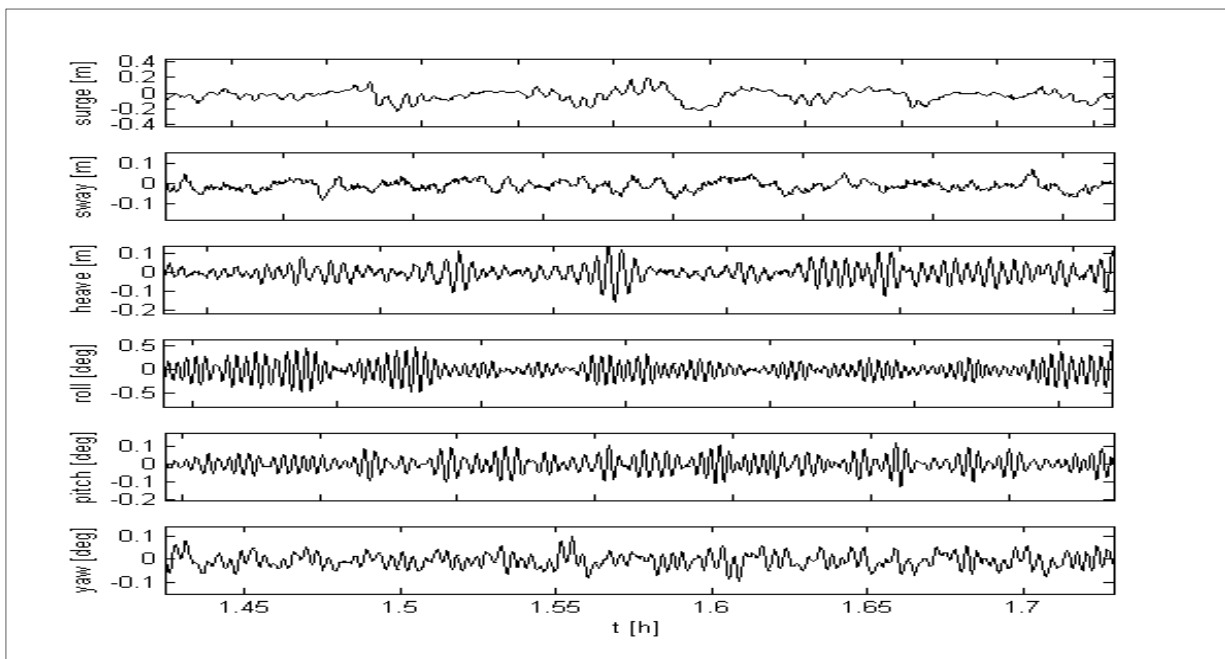


Figure 11: Movement plotted with Matlab

3.3.2 Basin Layout

Figure 12 shows the physical modelling area used to carry out the tests. The provided modelling area was 24 x 33 x 3 m. The basin had the current built-in bathymetry, i.e. it is 65 m deep at the wave generators (southern boundary) and gradually becomes shallower towards the northern beach. The model has no structures except for the jetty and beaches. No additional headlands or breakwaters were modelled here. Thus, the vessel is moored along a pile supported jetty exposed to the ocean. A physical model with a basic layout was chosen with the purpose of avoiding complications during the numerical modelling process. Also, 3D effects are minimised with a gentle slope. Only equipment required for model testing was used and no additional features were added to the model.

As illustrated in Figure 12, wave guides were placed at the borders of the wave generators extending in the y-direction (16.5 m). Absorption beaches continue from where the wave guides end. The model boundary was 'enclosed' with absorption beaches on the western, eastern, and northern boundaries. These beaches account for reflection, ensuring that as few waves as possible reflect from the model boundaries. As the waves approach the beaches, the gravel dissipates the wave energy and few or no waves reflect off the gravel. The wave guides, however, do cause reflection if directional waves are made in the basin. In this case, the wave guides should be moved and placed in the direction of the on-going wave, thereby guiding the wave in the correct direction.

The jetty runs perpendicular to the wave generators. The wave generators were situated at the southern boundary of Figure 12. The quay wall was modelled by attaching a solid wooden 'wall' to the jetty on the starboard side of the vessel. The vessel was orientated stern to bow facing the oncoming waves and moored on the starboard side.

All water levels are referenced to chart datum (CD). Mean sea level was taken as CD. A calibrated model vessel draft and freeboard were known. Knowing these dimensions, a water level was chosen accordingly. The allocated water depth is 31 m from CD at mid-ships and 65 m at the wave generators, the vessel yielding a draft of 10 m.

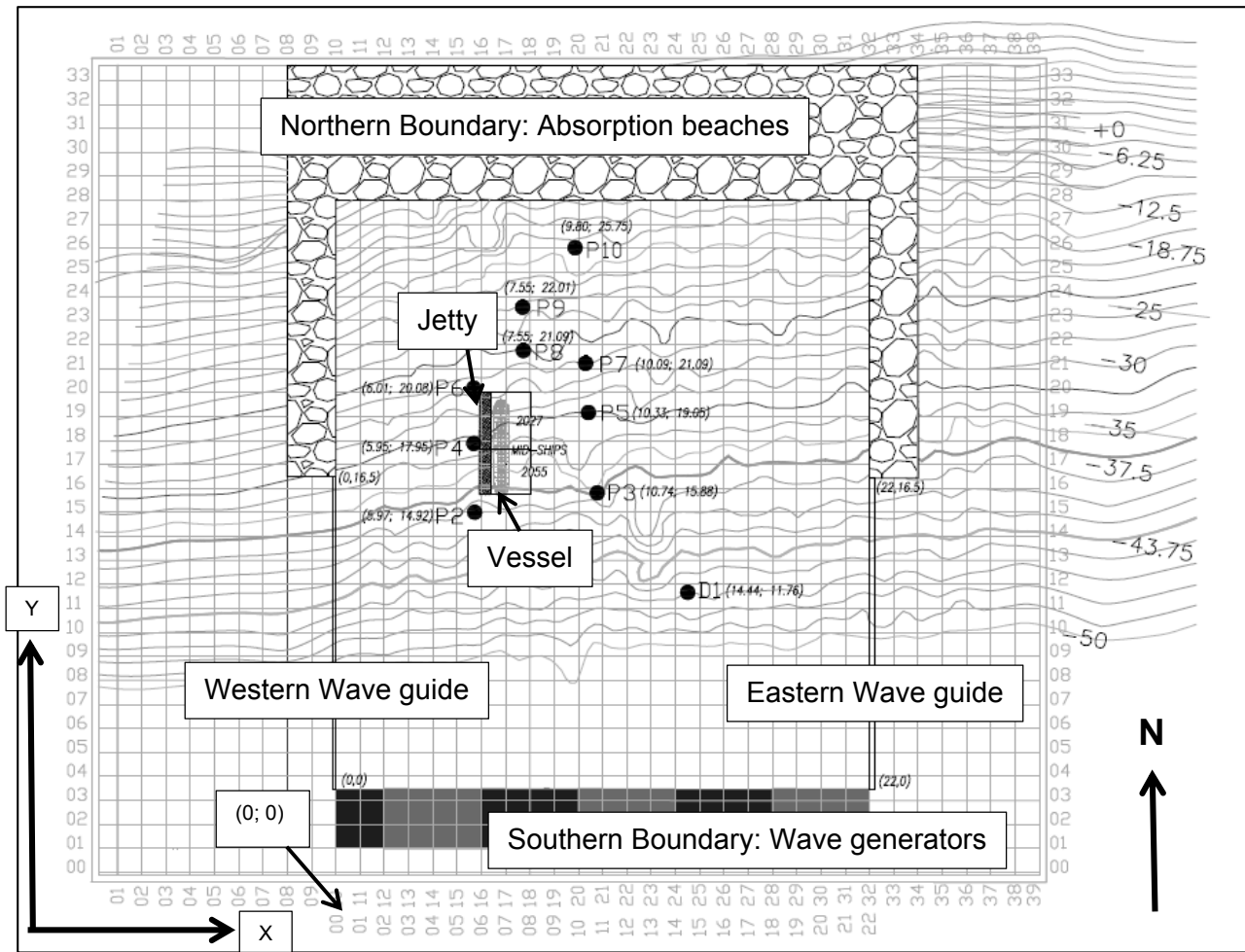


Figure 12: Full basin layout

Figure 13 shows the positioning of the jetty with respect to the wave generators. The wave generators are situated at the southern boundary, with wave guides on the eastern and western boundaries. Notice the absorption beach starting where the wave guides end.

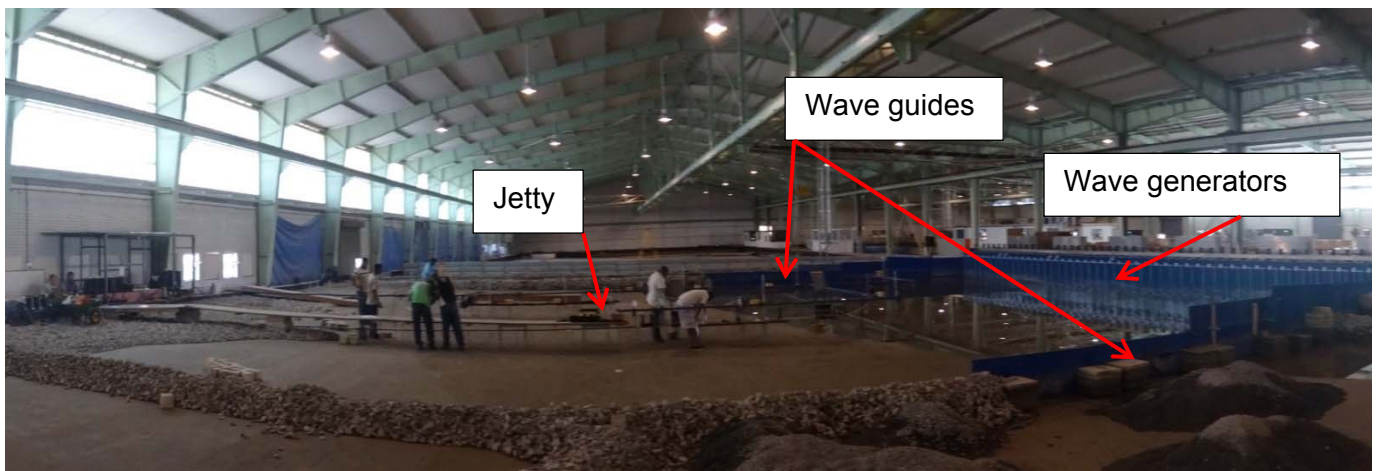


Figure 13: Basin layout (half-filled)

Figure 14 provides an enlarged view of a section of Figure 12. Here, the probe positions are more clearly indicated. Alongside each probe, the coordinates (as they relate to the basin coordinates) are indicated. Because the full basin was not used as the model space, the x-axis was re-numbered, which is later of significance to the numerical modelling process. This is clearly seen on Figure 12 (full basin layout). Probe D1 was a directional probe, whereas probes P2-P10 were single capacitance probes. All the probes measured water elevations and wave periods. Probe D1, additionally, measured wave direction and spreading.

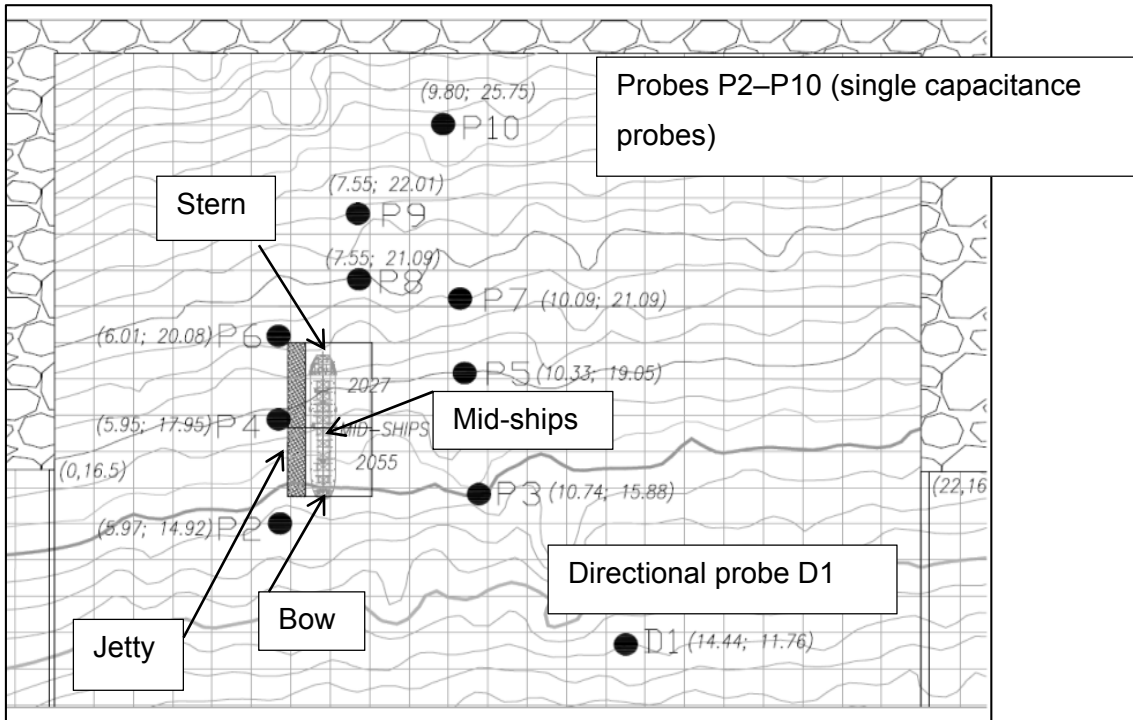


Figure 14: Probe positions

Figure 15 shows what the probes look like: on the left, a single capacitance probe (probes P2-P10) and on the right, a directional probe (probe D1). These probes consist of twin-wire gauges connected to an amplifier (probe box). The capacitance difference measured by the wires changes as the water level around the probe rises or falls. The probe measurement output consists of a time series water surface elevation. The wave parameters were then calculated from this.

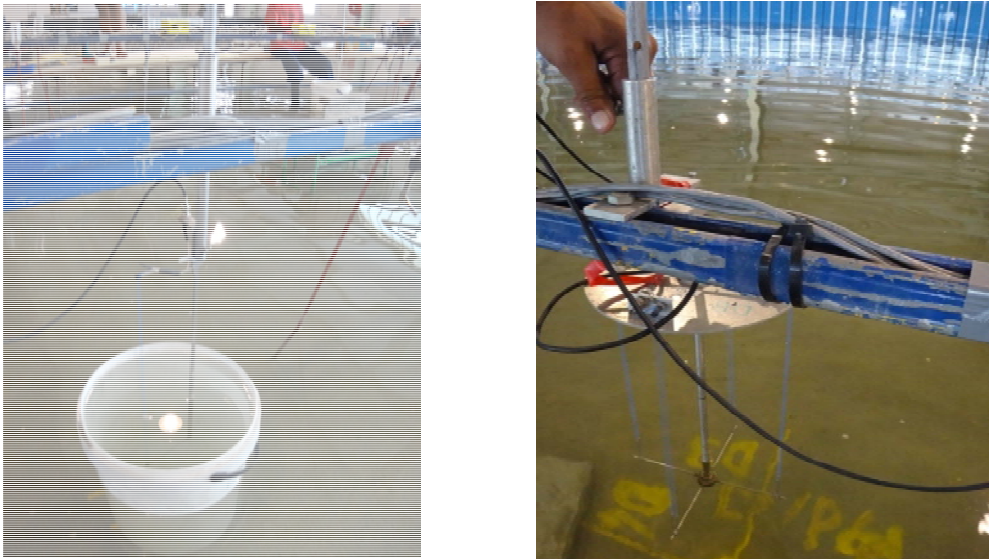


Figure 15: Single capacitance probe, P2-P10 (left), directional probe, D1 (right)

The probes were calibrated by taking three measurements in still water for each probe. Each probe can be shifted upwards or downwards. In this way, three measurements were taken, representing three different water levels. These three measurements covered the range of wave heights (in the length of the wires) expected to be measured at the probe. A calibration constant was calculated from the available range. The calibration constant was used to convert the measured wave heights into prototype wave height measurements. The probes used at the CSIR were accurate to 0.5 mm model scale. In this specific case (1:100 scale), the probes were accurate to 0.05 m prototype (50 mm prototype).

Figures 16 and 17 show the levels at mid-ships (recall that this is the location at the jetty where the moored vessel is at mid-point). The fenders are situated at +3 m CD and the jetty deck at +12 m CD. These dimensions were provided as a fully constructed jetty was already available.

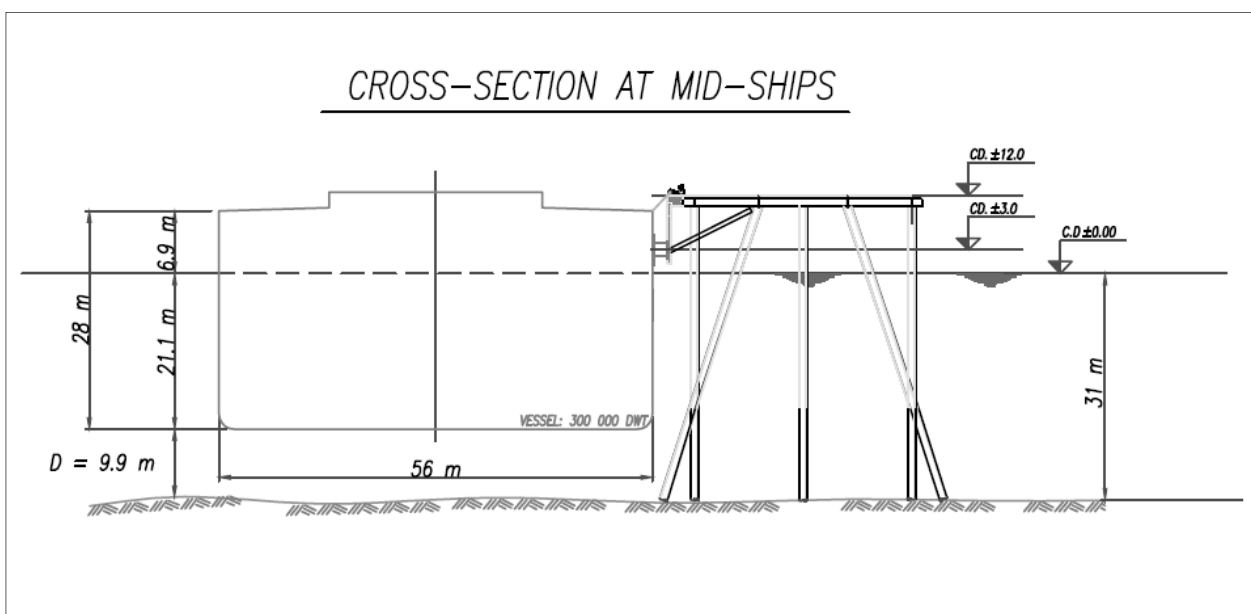


Figure 16: Cross-section of mid-ships

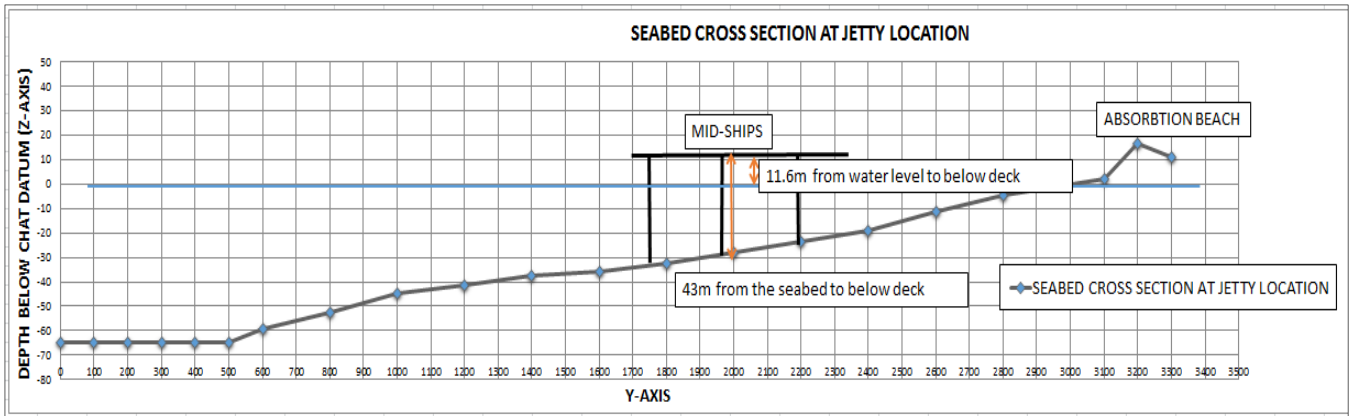


Figure 17: Cross-section of basin layout at mid-ships

During the vessel calibration process (which ensures that a fully laden vessel obtains the correct response to a 1:100 scale), the freeboard was determined. The vessel should have sufficient draft during the physical model process. Fortunately, the given jetty dimensions provide an appropriate water depth at mid-ships. Having the jetty height at approximately +12 m CD a water depth of 31 m is obtained. This yields a sufficient under-keel clearance of 9.9 m. This jetty will not be able to accommodate vessels with larger under-keel clearances. The largest container vessel to date is the Maersk Triple E class, having a draft of 14.5 m (MAERSK, 2013). The first generation container vessels have a draft of 9.0 m (Ligteringen H., 2012). The design vessel used for the current study had a length of 337 m, a beam of 54 m and a draft of 21.1 m

Important factors to take note of when designing the fender positioning and jetty height, and determining the design water level are mentioned below.

1. Fender positioning: The fender should be in contact with the vessel at the correct location to ensure correct force measurements during a test run. Should the fender be submerged or placed in such a manner that the rim of the deck touches it, incorrect force measurements will follow.
2. Water level: The water level should be deep enough to ensure sufficient draft for the fully laden vessel. The jetty should be high enough that the fenders are not submerged.
3. Freeboard: The freeboard of a fully laden vessel relates to the draft of the vessel.

3.3.3 Wave Generators

The wave generators were manufactured by HR Wallingford and consist of multi-element segments which in total acquire a length of 24 m. There are 48 individual paddles, each 0.5 m in length (Beresford, 2007). These paddles are placed parallel to the basin boundary wall. The parameters for the wave generators are set for each test, depending on the test conditions. The parameters required for test runs vary depending on the type of wave. For calibration procedures,

a desired wave height is required at a certain location in the basin. A dominant probe is chosen to monitor the wave heights occurring at that point in order to adjust the wave conditions fed to the wave generators. This is achieved by altering the gain factor. The gain factor of the wave generator controls the output wave height by which the desired wave height at the dominant wave probe is achieved.

Furthermore, each paddle has a dynamic wave absorption feature. This feature was not employed due to the large 3D basin. If switched on, the feature would generate false waves instead of absorbing the reflected waves. Rock beaches surrounding the model act as absorption beaches to reduce the effect of reflecting waves.

The paddles are moved by signal generation software able to generate the wave at a specified angle. A Jonswap spectrum was used. The wave test conditions in section 3.4 illustrate the different test runs and different parameters used.

3.3.4 Bollards, Fenders and Mooring lines

A moored ship makes use of terminal equipment (such as bollards, fenders and mooring lines) to be securely fixed to a quay wall or jetty. The terminal equipment needs to be properly represented in the physical model process in order to obtain reliable results. The equipment used to replicate the proposed situation should be calibrated to ensure that the results from the physical model are modelled correctly.

The second measuring system is referred to as the strain gauge measuring system (keogram measuring system in section 3.3.1 being the other system). The strain gauge measuring system makes use of mooring lines, bollards and fenders which are connected to strain gauges which physically measure the forces. The details of the procedure for setting up the bollards, fenders and mooring lines in the physical model are given in Appendix A.

Figure 18 shows the cross-section of the vessel. It also displays the simplified mooring arrangement and bollard allocations.

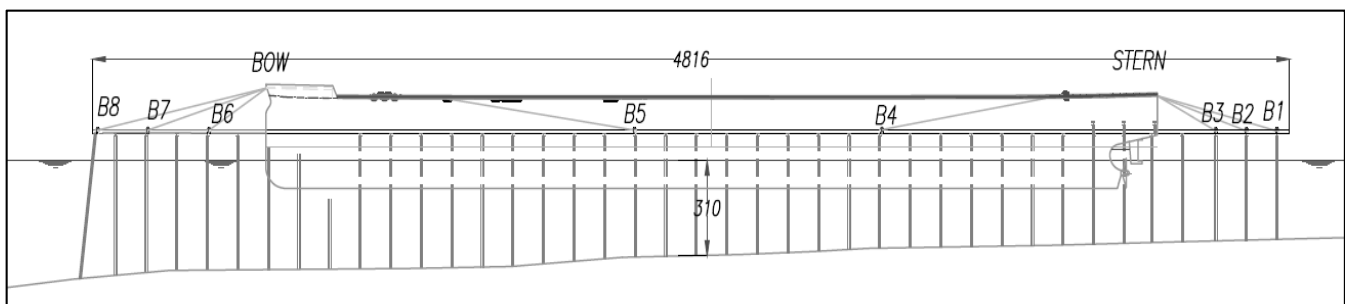


Figure 18: Cross-section of vessel

Figures 19 and 20 represent the bollard and fender dimensions along the jetty. These dimensions are of great significance for the analysis and numerical modelling process. The dimensions represented here indicate the distance of the bollards/fenders from mid-ships. In Figure 19 below, B6 and B7's mooring lines attached to the same fairlead located at the bow. B2 and B3's mooring lines attached to the same fairlead connected at the stern.

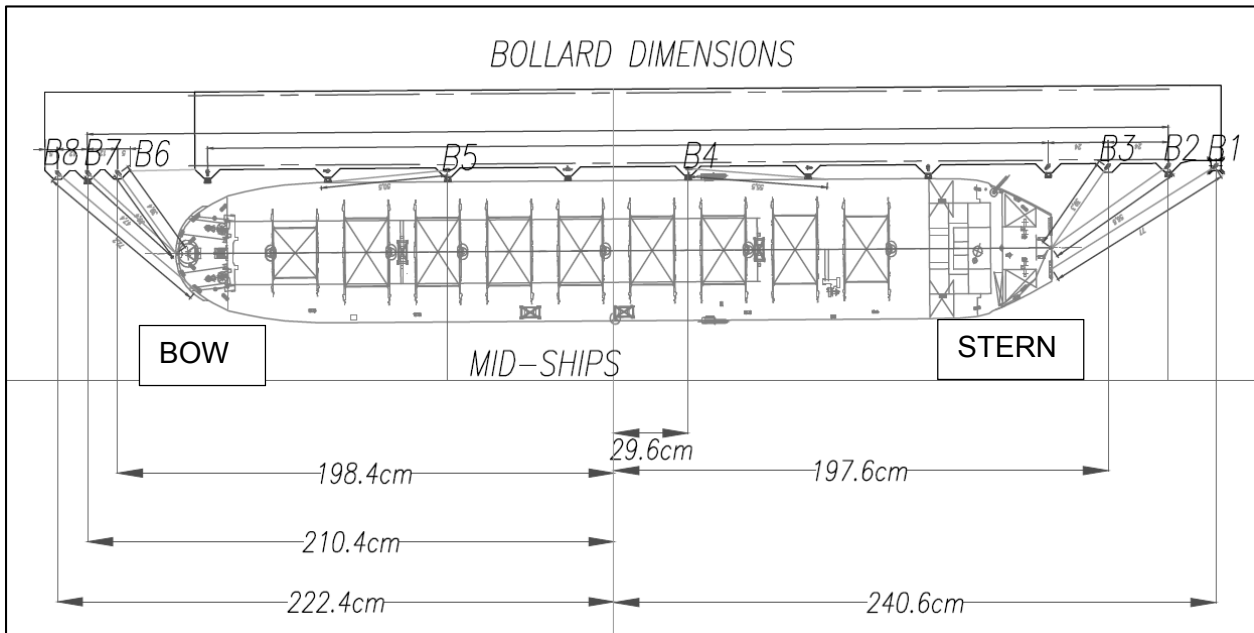


Figure 19: Bollard dimensions

Figure 20 illustrates the fender dimensioning measured from mid-ships. F1, F2, and F8 did not touch the vessel because of the curvature of the hull form.

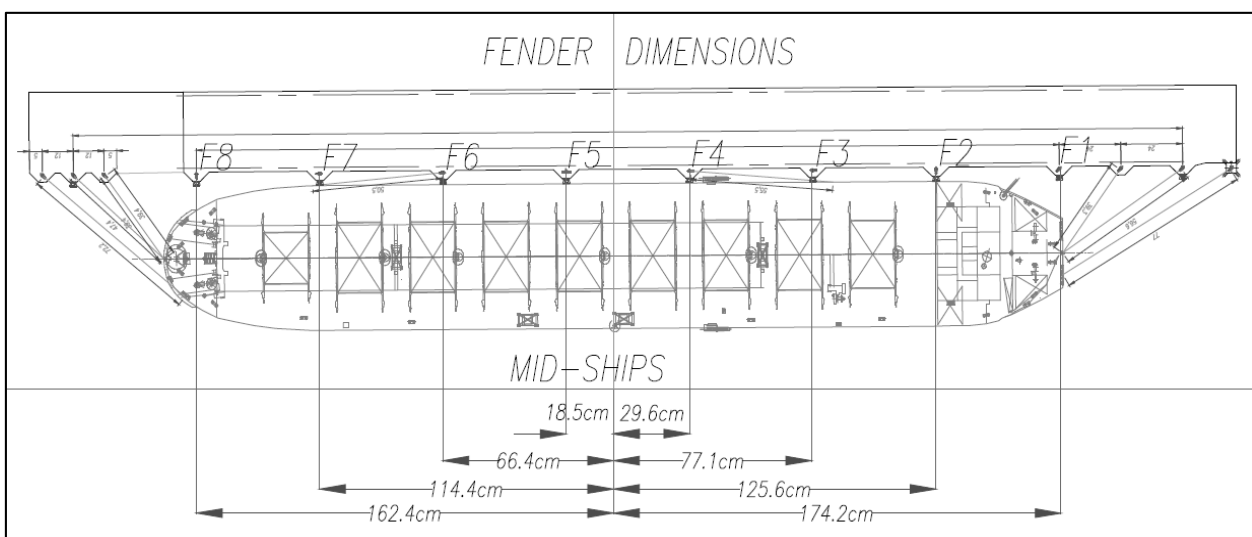


Figure 20: Fender dimensions

3.3.5 Calibrating a Ship

To ensure that the prototype ship and the model ship exhibit the same behaviour, the model ship needs to be calibrated to fit the properties of the prototype ship. The model ship calibration process consists of four tests, of which three are done in the cradle swing and the other one in a filled basin. The vessel needs to be calibrated for a fully laden 300 000 DWT vessel. The prototype values were provided by the CSIR. The details of the calibration procedure of the ship are given in Appendix B.

The primary values to check during the calibration process are:

1. The height of the centre of gravity above the keel (KG) (displacement test)
2. The transverse radius of gyration (K_{xx}) (roll in water, period measurement)
3. Longitudinal radius of gyration (K_{yy}) (pitch in cradle, swinging test)

The vessel calibration procedure ensures that the fully laden model vessel has the same behavioural characteristics as the prototype vessel. Table 1 shows the results obtained for the calibration procedure. These values are also used in the numerical modelling procedure. All physical modelling is carried out in a 1:100 scale. The analyses of the physical model measurements, however, are carried out in prototype, because the numerical modelling procedure is carried out using prototype values.

Table 1: Vessel calibration results

Description	Symbol	Target Value	B300 prototype	B300 model
Length over all	L_{oa}	350 m	337 m	3.37 m
Length between perpendiculars	L_{pp}	332.5 m	326 m	3.26 m
Beam	B	56 m	54 m	0.54 m
Draught	T	21.8 m	21.1 m	0.21 m
Displacement volume	∇	Not Specified	302577.32 m ³	0.30257732 m ³
Displaced weight in salt water	Δ	300 000 t	299 983 t	299.983 kg
Block coefficient		0.815	0.815	0.815
Cargo tonnage	DWT	300 000 t	299 983 t	299.983 kg
Height of centre of gravity (CG)	KG	13.3m	14 m	0.14 m
Distance of CG forward of mid-ships	LCG	10 m	10 m	0.1 m
Transverse radius of gyration	K_{xx}	19.04 m	19.8 m	0.198 m
Longitudinal radius of gyration	K_{yy}	87.5 m	88.98 m	0.889 m

3.4 Test Procedure

3.4.1 Objectives

The objective of the physical model tests was to obtain measurements which should be comparable to the numerical modelling procedure for the purpose of validation of these numerical models. The results required from the physical model testing include:

1. Wave Heights (short and long wave)
2. Fender Forces
3. Mooring Line Forces
4. Ship Motions

3.4.2 Procedure

A testing schedule was used to ensure that all necessary tests were carried out under the same conditions. Firstly, before each test run, the water level was checked to ensure that the same water level was used throughout testing. Repeatability tests are often carried out to ensure that the same water levels are obtained at the probes for the same test conditions. Changing the water levels could result in inaccurate results when carrying out repeatability tests.

Secondly, the probes had to be cleaned to ensure that no dust particles were attached to the wires. Particles can easily attach to the probe wires, potentially causing the probe to take faulty readings. On each testing day, the probes are reset to zero. In doing so, the probes are set to have the same reference point from which to measure the changing water levels.

Next, the fenders and the bollards had to be reset to zero for the same reason, i.e. to ensure that the same reference point is used. The 'zero-ing' of the bollards and fenders can be done more than once throughout the testing day. The bollards and fenders have target readings which need to be obtained before testing. For instance, all mooring lines (attached to the bollards) need to measure a target reading between 210-310 kN. If these values are not obtained for all mooring lines, the mooring lines need to be adjusted as they are not representing the correct stiffness. As for the fenders, these need to be aligned in such a manner that they touch the hull's curvature. If all the fenders are touching the hull, readings may be recorded. If not, all the fenders need to be re-aligned simultaneously to ensure that the full weight of the vessel is not allocated to one fender, but evenly distributed along the fenders.

After all checks had been carried out, the model was ready for testing. A 10 minute waiting period was required for the water to settle and to become completely still before activating the wave generators. At this point, all systems were recording. Each test run lasted 31 minutes, yielding a

prototype time of 5 hours (three hours of prototype time being the minimum time required for analytical reasons).

Table 2 illustrates the test conditions carried out, a Jonswap spectrum having been chosen for all these conditions. The focus was to investigate ship motions with a quay wall and ship motions without such a wall. Therefore, the test conditions of tests 01 and 02 (with a quay wall) were replicated in tests 03 and 04, this time without a quay wall.

Table 2: Test conditions

Test No.	Wave Type in Wave Generator	Spectrum	Angle (deg)	Gain	Spreading	Wave Generator Time (s)	Analysis Time (s)	Mooring Type	Water Level (Midships)	Tp (s)	Hm0 at wave Generator (m)
1	White Noise Set Down	Jonswap	Head on Waves (180 deg)	1.2	20, n=7	1600	1860	Quay Wall	31	12	2.5
2	White Noise Set Down	Jonswap	Head on Waves (180 deg)	1	25, n=4	1600	1860	Quay Wall	31	12	1.5
3	White Noise Set Down	Jonswap	Head on Waves (180 deg)	1.2	20, n=7	1600	1860	Jetty	31	12	2.5
4	White Noise Set Down	Jonswap	Head on Waves (180 deg)	1	25, n=4	1600	1860	Jetty	31	12	1.5

The wave conditions were based on observing the vessel movement. A few test runs were carried out to inspect the severity of the vessel movement. Considering the physical model investigates ship motions, wave heights were chosen accordingly.

Throughout the testing procedure, a daily record of all happenings was kept. If unexpected results were to occur during the numerical modelling procedure, the record notes may be used to determine possible inaccuracies that may have caused these results.

3.5 Scaling Effects

All physical models are scaled because of practical reasons and also to accommodate the restrictions of the working environment. Consequently, the coastal processes being modelled need to be scaled as well. In this model, Froude's Law of scaling was applied. The physical model was created by scaling all lengths. To reduce scale effects, models are constructed and scaled to be as large as possible. Not all physical processes can be scaled, therefore scaling effects are a factor to contend with. Most scaling effects occur due to properties of water which cannot be scaled to the same scale as the rest of the model. These properties include density, viscosity, and surface tension.

The waves generated by the wave generators were, by nature, rotational free gravity surface waves. Viscosity does not contribute significantly to these types of waves. Because viscosity could

be neglected, Reynold's law of scaling was not appropriate for the purposes of the physical model employed in the present study. Other factors such as bottom friction are also considered. As a wave propagates in the ocean, it dissipates due to bottom friction. The waves in the model basin travel over such a small distance that dissipation due to bottom friction does not contribute significantly to the physical model. Surface tension, however, is applicable to small waves as it influences their celerity. "Small waves" include waves moving over depths of 2 cm only, and waves of 0.35 s periods (Hughes, 1995). These are very small values and are not significant in the present physical model study, therefore surface tension could also be neglected.

Gravitational and inertia forces, however, are the main forces contributing to wave propagation. For this reason, Froude's Law of scaling was selected to scale the physical model. Equations 1-5 below show Froude's Law of scaling equations used to scale the model.

$$F_N = \frac{V_p}{\sqrt{gL_p}} = \frac{V_m}{\sqrt{gL_m}} \quad (1)$$

$$\frac{V_p}{V_m} = \frac{\sqrt{gL_p}}{\sqrt{gL_m}} = \sqrt{\frac{L_p}{L_m}} \quad (2)$$

$$\frac{V_p}{V_m} = \frac{\frac{L_p}{T_p}}{\frac{L_m}{T_m}} = \frac{L_p}{L_m} * \frac{T_m}{T_p} \quad (3)$$

$$\frac{V_p}{V_m} = \sqrt{\frac{L_p}{L_m}} = \frac{L_p}{L_m} * \frac{T_m}{T_p} \quad (4)$$

$$\frac{T_p}{T_m} = \sqrt{\frac{L_p}{L_m}} \quad (5)$$

$$\frac{W_p}{W_m} = \frac{\gamma_p}{\gamma_m} * \frac{Vol_p}{Vol_m} = \frac{\gamma_p}{\gamma_m} * \frac{L_p^3}{L_m^3} \quad (6)$$

$$\frac{F_p}{F_m} = \frac{W_p}{W_m} * \frac{g}{g} \quad (7)$$

F_N

Froude number

L_m

length in model scale

L_p	prototype Length
T_m	time in model scale
T_p	time in prototype
V_p	prototype velocity
V_m	velocity in model scale
W_p	weight in prototype
W_m	weight in model scale
γ_p	unit weight in prototype
γ_m	unit weight in model scale
Vol_p	volume in prototype
Vol_m	volume in model scale
F_p	force in prototype
F_m	force in model scale

3.6 Output and Analyses

As previously described, there were various measuring systems in place to obtain the desired measurements during the physical modelling process. In summary, the capacitance probes firstly measured the water levels. This output was processed by means of a compiled data acquisition program called 'GoAnalysis' and stored in a '.dac' file format. Secondly, the keogram system measured the ship motions, mooring line forces and fender forces. The output was digitised with data acquisition software called 'ShipWatcher' and was stored as a '.txt' file. The strain gauge system measures the mooring line forces and the fender forces. Next, the strain gauge system is analysed with data acquisition software called 'Catman' and stored as an '.ASCII' file. The output file from each measuring system was collected and was used together with the mathematical software Matlab to convert the data from raw data files to useful figures and relevant values.

On grounds of the physical model results, the fender forces and mooring line forces were investigated throughout the physical modelling process. The fender and mooring line forces are strongly connected to the behaviour of the vessel. When larger forces are measured in the fenders and mooring lines, larger movements follow. As mentioned above, the mooring line and fender forces were measured with two measuring systems, namely the keogram and strain gauge measuring system (cf. Section 3.3.1 and Section 3.3.4). The keogram measuring system measured the ship motions and derives the forces from the measured ship motions. The strain gauge measuring system measured the forces and derived the ship motions from the forces. The mooring line and fender forces measured were plotted on one another to investigate whether the output forces had similar trends/good correlations between the different measuring systems. When a good relationship was achieved, it was used as an indicator of whether things had gone well in the physical model. Receiving measurements indicating the same forces to exist in both systems implies that the same ship motions were measured, and that the test was well performed.

Table 3 shows the forces measured in the fenders and mooring lines. A comparison between the two measuring systems was carried out to evaluate the quality of the physical model test run.

Table 3: Test 03, mooring line and fender force correlation

Mooring Lines	Fender Forces
---------------	---------------

	Strain Gauge Output	Keogram Output		Strain Gauge Output	Keogram Output
M1	529	507	F1	-	-
M2	520	523	F2	-	-
M3	700	647	F3	2209	1922
M4	660	639	F4	1535	1269
M5	470	473	F5	2063	1586
M6	627	606	F6	1922	1528
M7	626	604	F7	1730	1403
M8	437	460	F8	-	-

Figure 21 shows the time series mooring line forces obtained by the strain gauge measuring system (blue) and the keogram measuring system (red). From this graphical representation it is clear that a good correlation was obtained. This pattern followed for all mooring line forces in all tests and can be viewed in Appendix C.

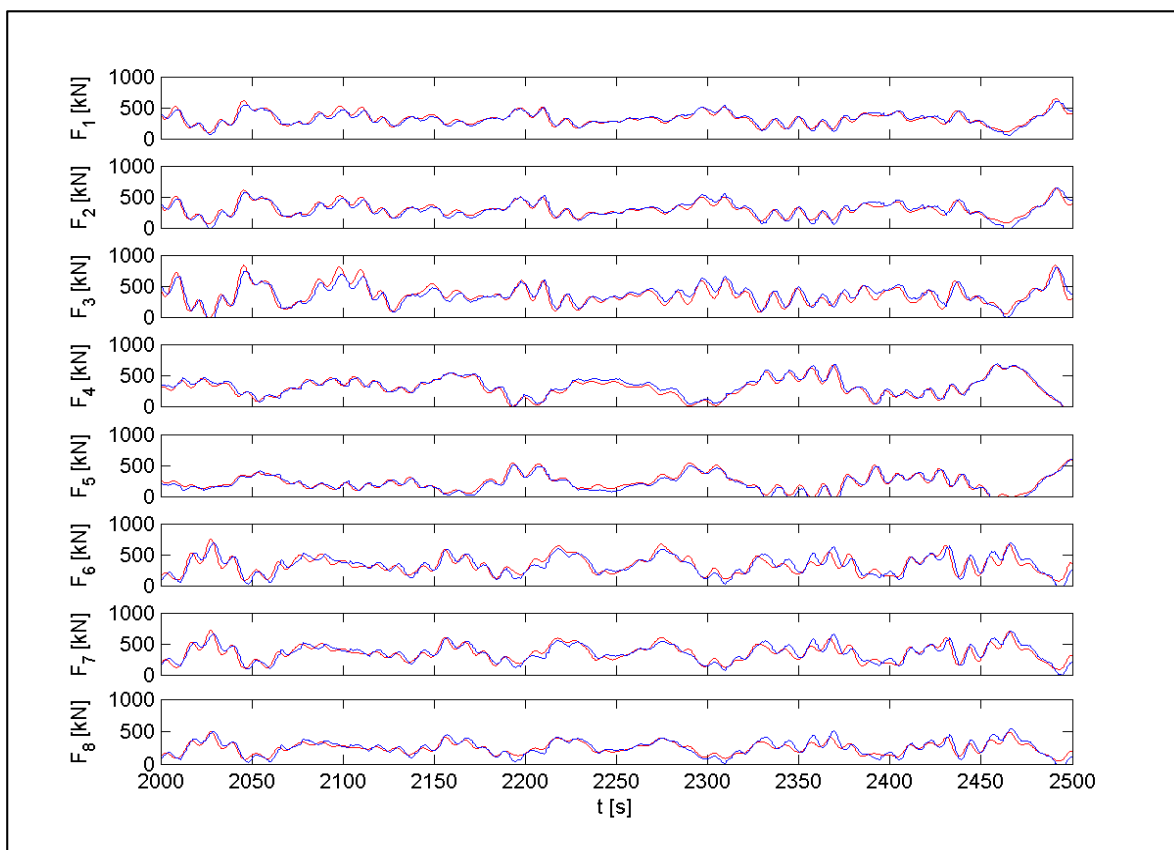


Figure 21: Test 03, Strain gauge vs keogram force measurements, mooring lines

Figure 22 shows the comparison obtained between the strain gauge and keogram measuring systems. A good correlation was obtained for all mooring-line-forces. Appendix C contains an overview for each test conducted. All tests showed a good relationship between the different measuring systems.

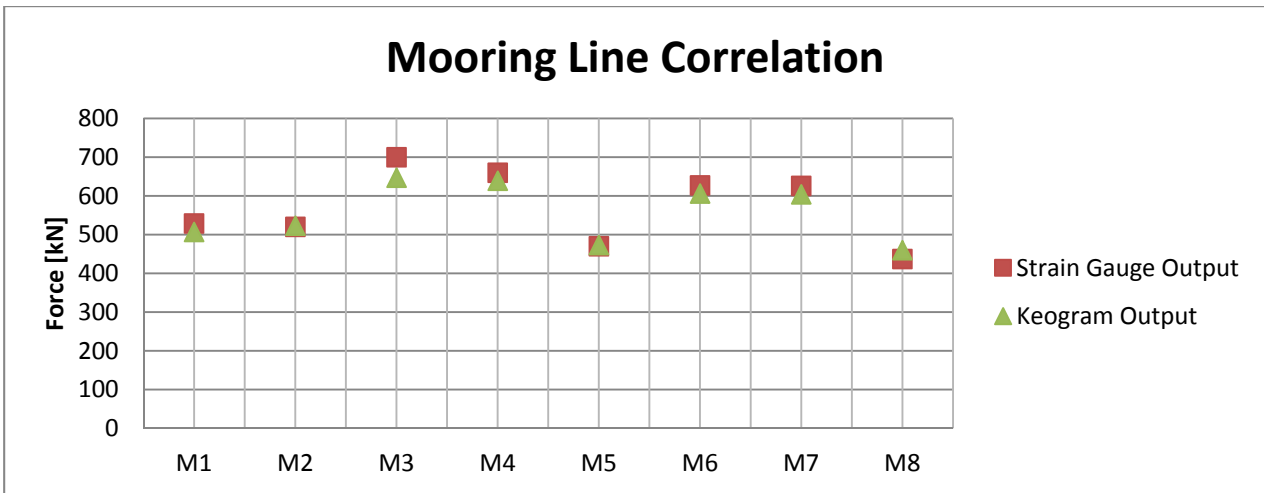


Figure 22: Test 03, graphical representation of mooring line force correlation

Figure 23 shows the individual fender force values for each measuring system. As is visually evident, a less desirable correlation was achieved for fenders 5 and 7. This pattern was seen throughout the tests. The process of positioning the fender in the physical model is quite tedious. During still water conditions, the fender should touch the hull’s curvature just enough to register a reading and at the same time not press excessively on the hull. In other words, the force exerted on the fenders by the vessel should be distributed equally amongst the fenders. The fenders, however, should also be aligned in a straight line. This means that, at some locations along the jetty, a fender might not touch the hull due to the curvature of the hull curving away from the fender. Fender positioning can be sensitive even to the millimetre. This problem is increased by the fact that, when the final positioning is achieved, the fender sometimes shifts whilst being fixed.

Because of the sensitivity of the fenders in the physical model, the strain gauge measurements may differ from the keogram measurements, as seen on Figure 23 below. Appendix C shows the physical modelling results/correlation obtained for the fender and mooring line forces between the measuring systems.

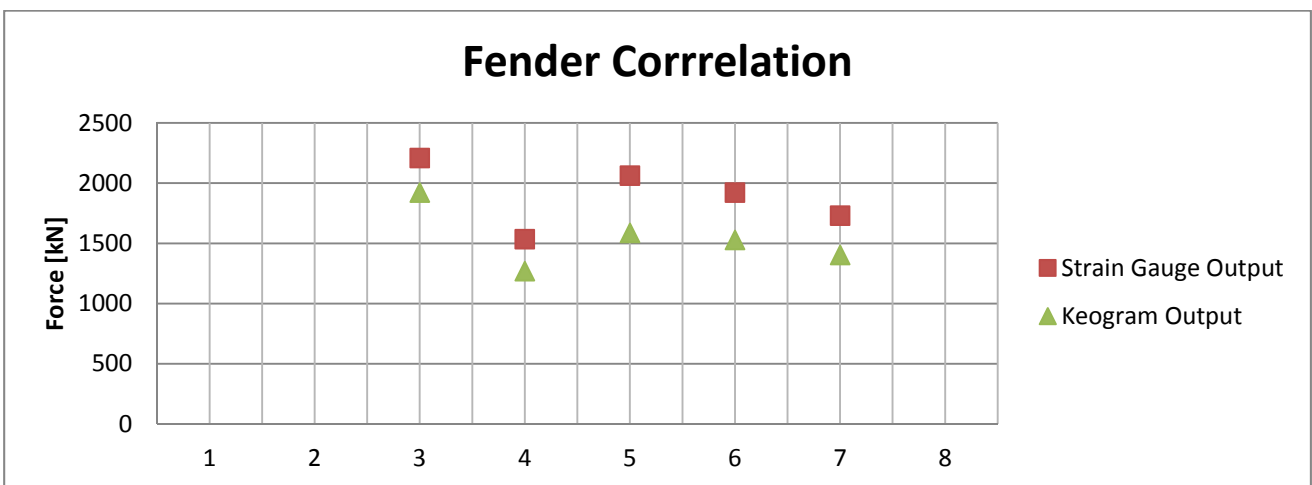


Figure 23: Test 03, graphical representation of fender force correlation

Figure 24 shows the fender forces measured by the strain gauge measuring system (blue) and the fender forces measured by the keogram system (red). Fenders 1, 2 and 8 were 'dummy' fenders which did not touch the hull's curvature. The vessel did not press against these fenders as they were out of range. Graphically, when plotted on a time series, a good correlation is seen in Figure 24. When the fender force values are plotted individually, as in Figure 23, the correlation is not as good as expected. The physical model measurements were now ready to be compared with the numerical modelling process.

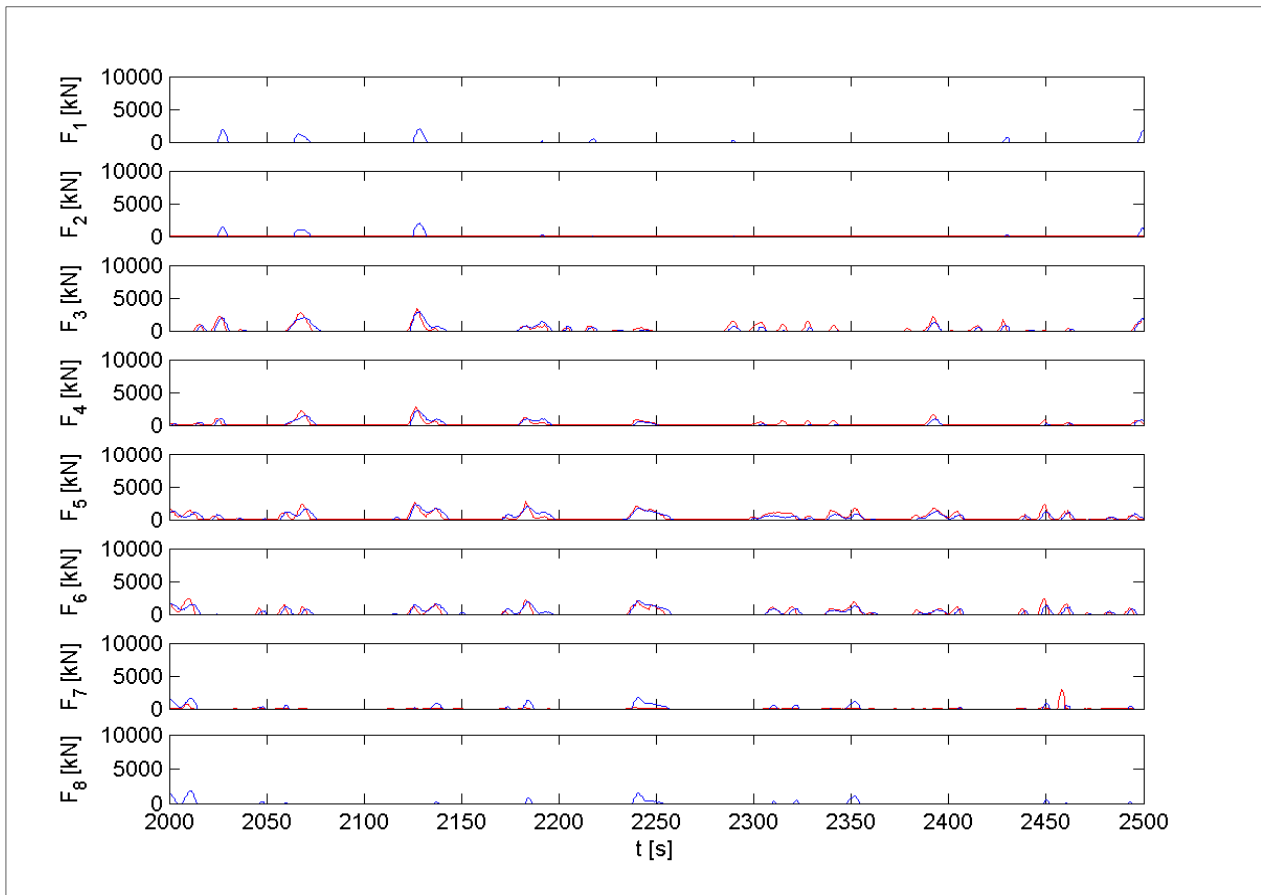


Figure 24: Test 03, strain gauge vs keogram force measurements, fenders

Chapter 4: Validation by Numerical Modelling

4.1 Overview

The physical modelling results are discussed together with the numerical modelling process as each step is reached. Figure 25 explains the numerical modelling process and the comparison procedure that follows.

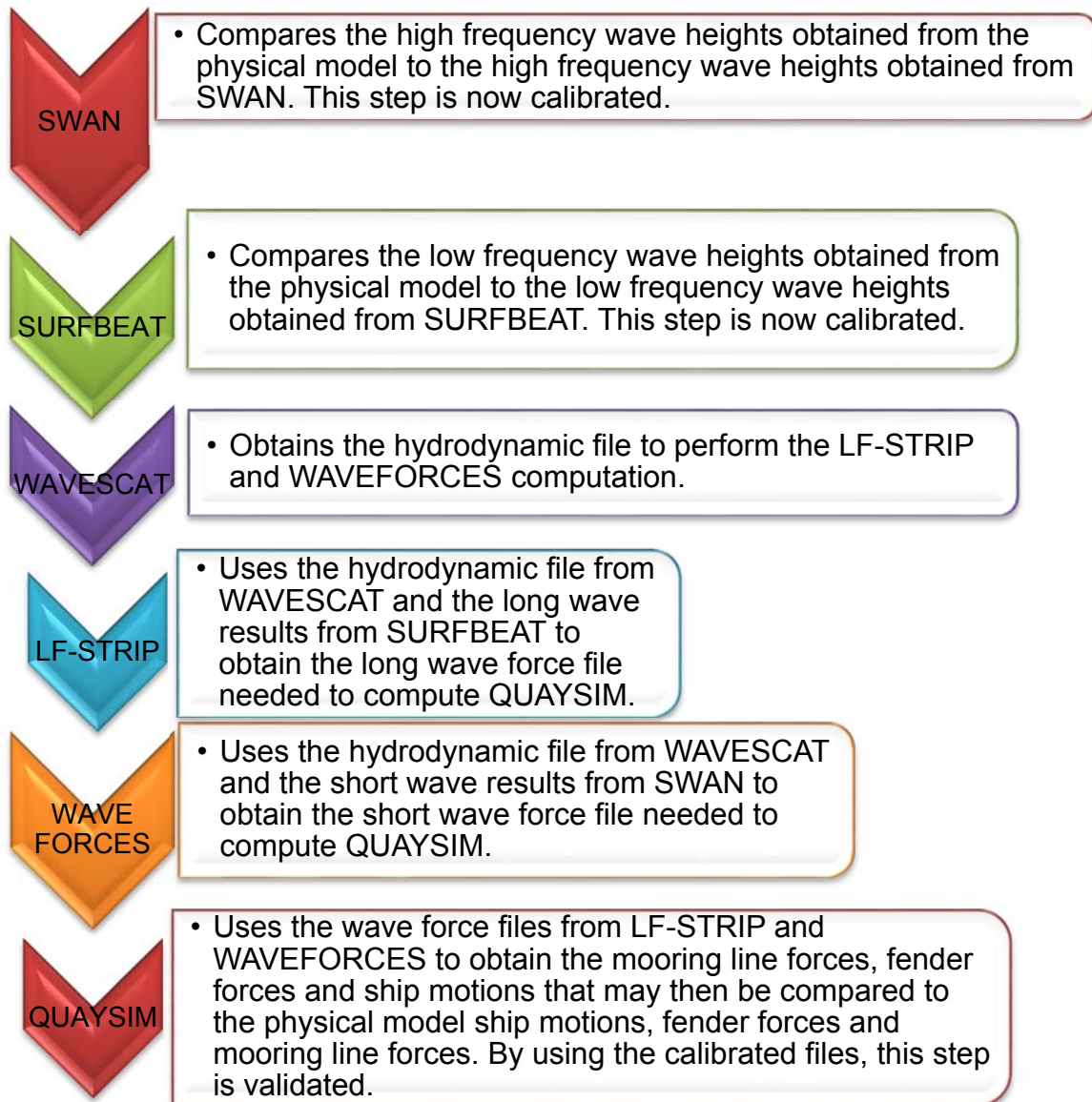


Figure 25: Procedure steps indicating how the numerical modelling calculations were compared to the physical modelling measurements

4.2 SWAN

A stand-alone SWAN run was carried out to model the high frequency wave heights measured by the probes in the physical model basin. For this run to be successful the numerical model space was the same as that of the physical model.

Figure 26 illustrates the SWAN set-up for the high frequency wave height calibration procedure. The SWAN domain was created with the Delft3D-RGFGRID module. The southern boundary represents the location of the wave generators. The wave guides were indicated on the eastern and western boundaries, respectively. The quay wall was situated in the centre of the model domain. Absorption beaches were located at the eastern and western borders where the wave guides end. This domain set-up represents a replica of the current built-in bathymetry of the physical model. Notice the change in colour as the depth of the basin changes.

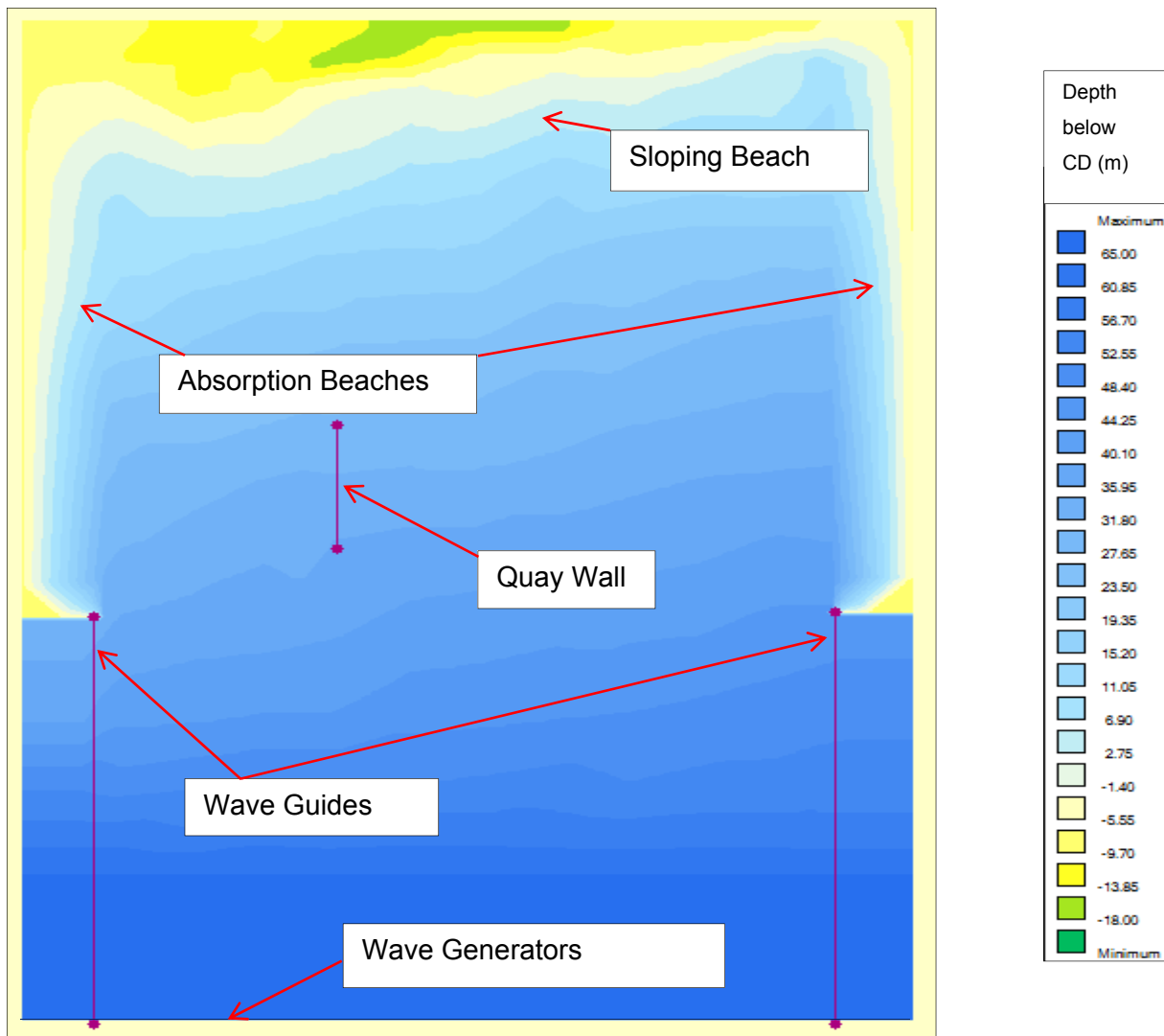


Figure 26: Numerical set-up of SWAN – bathymetry of model domain

A series of numerical runs were carried out to calibrate the SWAN model. By using the same basin layout and applying different input wave heights to the model, the ultimate wave condition was numerically obtained. The input wave heights of the numerical model, was adjusted to obtain good comparison with the physical model wave heights. Table 4 illustrates the difference in wave input conditions for the physical model at the input boundary, as opposed to the numerical model. The probes were placed at the same locations as in the physical model.

Table 4: Wave conditions at the input boundary for physical model and SWAN model

	Physical Model	Swan Model
Test 01	Quay Wall: T =12 s, Hs = 2.5 m Spreading = 20 deg	Quay Wall: T =12 s, Hs = 2.05 m Spreading = 20 deg
Test 02	Quay Wall: T =12 s, Hs = 1.5 m Spreading = 25 deg	Quay Wall: T =12 s, Hs = 1.2 m Spreading = 30 deg
Test 03	Pile Supported Jetty: T =12 s, Hs = 2.5 m Spreading = 20 deg	Pile Supported Jetty : T =12 s, Hs = 2.70 m Spreading = 20 deg
Test 04	Pile Supported Jetty : T =12 s, Hs = 1.5 m Spreading = 25 deg	Pile Supported Jetty : T =12 s, Hs = 1.2 m Spreading = 30 deg

The probe locations refer to output locations. These output locations were analysed during the SWAN computations to ensure that the same wave heights as in the physical model were obtained numerically by adjusting the SWAN input wave heights. The error difference was kept as small as possible. Figure 27 represents a comparison between the high frequency wave heights of the physical model and that of the numerical model for Test 03. For a good comparison, less than 10% difference in wave height was expected between SWAN and the physical model.

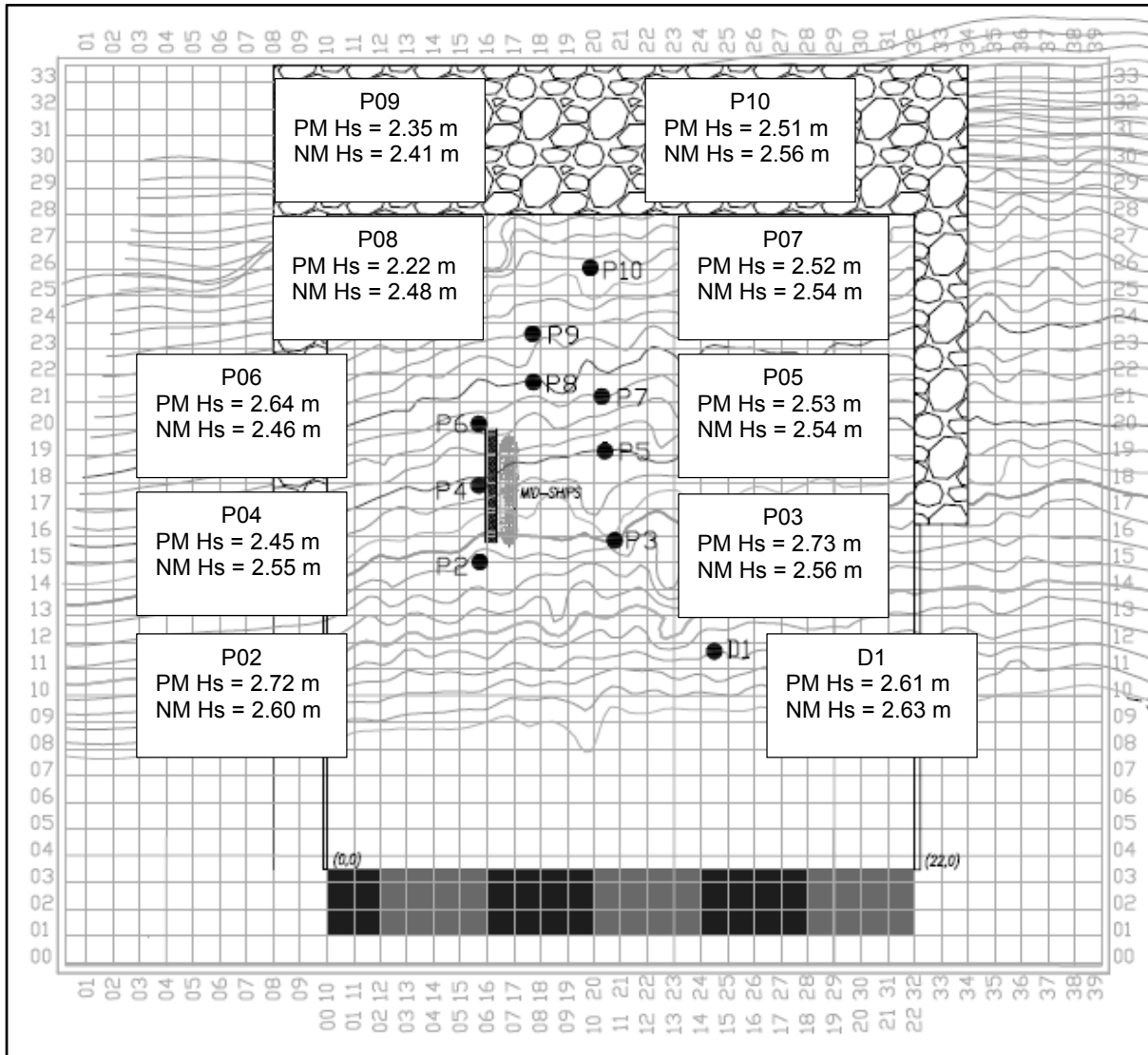


Figure 27: Test 03, high frequency wave height comparison

To investigate the coastal processes both numerically and physically, the output locations were plotted on the basin layout as shown in Figure 27. In this figure, PM denotes physical model and NM denotes numerical model. Wave heights are expected to decrease from probe 1 to 3 to 5 to 7, and from probe 2 to 4 to 6. Recall that a wave propagates in the ocean, wave energy is dissipated as a result of bottom friction and refraction, causing a decrease in wave height. As the wave approaches the coastline, the water depth reduces, where shoaling occurs. Therefore, the wave heights are expected to increase again slightly from probes 7 to 8 to 9 to 10.

In the physical model, the wave height increases from probe 1 to 3 and 1 to 2, contrary to expectation. The waves decrease in height as they approach probes 3 to 5 to 7, and from probe 2 to 4, but increase at probe 6. Shoaling occurs from probe 8 to 9 to 10. Probe 6's depth is close to the depth of probe 7 to 8, therefore the increase in wave height at probe 6 could be caused by shoaling. Table 5 shows the depths allocated at each probe.

Table 5: Probe depths

	Depth
Probe No:	[m]
PDA	45.40
WP2	35.60
WP3	37.10
WP4	32.60
WP5	29.90
WP6	27.90
WP7	26.00
WP8	25.20
WP9	20.20
WP10	14.90

In the numerical model, the wave heights have a more consistent behaviour. The wave heights decrease from probes 1 to 3 to 5 and from 2 to 4 to 6 due to refraction and energy dissipation. The wave height further decreases from probes 5 to 7 to 8 to 9. Shoaling occurs from probe 9 to 10. This behaviour in both the numerical model and physical model is evident when plotted in the manner shown in Figure 27. Appendix E contains all plots for wave height comparisons.

SWAN was calibrated by analysing the comparison between the physical model output and the SWAN output. The calibration procedure is a repetitive process in which the input parameters are manipulated to a limited extent in order to obtain suitable results.

In general, a good correlation was obtained between the physical model and the SWAN model. Section 4.3 continues with the next numerical approach, SURFBEAT. Here, the SWAN model results were used to generate a wave component file. This file was used as input at the boundary to determine the bound long waves released into the model.

4.3 SURFBEAT

SURFBEAT is an extension to the Delft3D-FLOW module which permits the programme to model the effects of high frequency wave groups on low frequency waves. These low frequency waves are caused by differences in the radiation stresses in the high frequency wave groups that enable a low frequency wave to propagate with the group of high frequency waves. High frequency wave groups are also referred to as carrier waves, because they 'carry' underlying low frequency waves with them. In the literature, these low frequency waves are known as "bound long waves". A bound long wave's celerity is equal to the group celerity of the high frequency wave groups (C_g).

The high frequency wave energy is a component modelled by the Delft3D-WAVE (SWAN) package. The high frequency wave energy propagates into the model space with group celerity,

based on the peak frequency. To summarise, the mean wave direction field and wave energy are not calculated with the SURFBEAT module but imported from the Delft3D-WAVE (SWAN) package (Delft3D-FLOW, 2011).

A SWAN module was pre-run to simulate the high frequency wave heights at locations in the basin (Delft3D-FLOW, 2011). To enable the SURFBEAT module, the roller parameters in Delft3D-FLOW were activated. The main purpose of the SURFBEAT/roller module was to include roller equations. The boundary conditions, however, were taken from a wave components '.wcm' file containing all the spectral components of the surface elevation at a specific point with an assigned depth. These spectral components were converted into high frequency wave energy at the boundary. The wave component file was generated using the output from the SWAN module and a Matlab script provided by the CSIR. The wave components file describes the Fourier components of the incoming high frequency waves (Delft3D-FLOW, 2011).

The roller parameters are defined in Table 6. These parameters were set to 'yes' and the "Filwcm" parameter assigned to the wave component file. Various validations have been done on the roller parameters; the default values can be used or defined otherwise by referring to past papers on these validations. "Alpharo" should remain as the assigned default value in most situations. "Betaro" is related to the breaker steepness and has the default value of 0.1 Roelvink (1993). According to Boers (2005) "Betaro" can have a smaller value of 0.44 (Boers, 2005). Smaller values result in larger low frequency waves. "Gamdis" is the breaker parameter, which is defined as the relation of the wave height to water depth. The breaker parameter is defined as the relation of the wave height to water depth. The default value recommended by Roelvink (1993) is 0.55 (Roelvink J. A., 1993 (a)). Battjes & Stive, 1985 (1985), however, recommend values between 0.5 and 0.8 (Battjes & Stive, 1985). The "Ndis" parameter considers the randomness of the wave height in a broken wave and the amount of energy transferred before wave breaking (Roelvink J. A., 1993 (a)). Roelvink (1993) recommends a relatively high value (between 10-20) for regular cases on a steep slope. This may result in an overestimation of the wave height at a location before breaking. The reason for this is that, bottom friction is not accounted for in the high frequency wave energy balance equation used in SURFBEAT. Bottom friction can, however, be replicated by assigning a smaller value of "Ndis". A value of 2 is recommended if bottom friction is included. (van der Molen W. , 2011 (c)).

Table 6: Roller parameters

Roller	#yes#
Filwcm	#runid.wcm#
Alpharo	1.0
Betaro	0.4
Gamdis	0.55
Ndis	6

The same computational grid used for SWAN was also used for SURFBEAT. However, in SURFBEAT the courant number (being depth related to ensure numerical stability) should preferably not be larger than 10 in the entire domain and less than 2 in most of the domain. The courant number is calculated by Equation 6 (Delft3D-WAVE, 2011), where Δx should be smaller than 1/10 of the shortest wave length in the domain. The time step was chosen so that the courant number is generally smaller than 10. The SURFBEAT model was tested to check whether the model was grid dependent and whether it was affected by the time step. These checks should always be done. Results for these checks can be found in Appendix G.

$$C_r = \frac{\Delta t}{\Delta x} \sqrt{gh} \quad (6)$$

C_r	courant number
g	acceleration of gravity (m/s^2)
h	water depth (m)
Δt	change in time (s)
Δx	size of the grid cell in the x-direction (m)
Δy	size of the grid cell in the y-direction (m)

Figure 28 represents the modelling area and the components assigned in the basin. The southern boundary is represented by the red line. This boundary was allocated to be uniform water levels with a time series forcing type (uniform water level boundaries are suggested as default). Absorption beaches were inserted in the bathymetry to replicate the absorption beaches in the physical model. The same output locations were assigned with respect to the probe locations in the physical model and the SWAN model. In the SURFBEAT simulation, extra observation points along the quay wall (where the vessel was placed) were assigned. The low frequency wave elevations at those points were used in the LF-STRIP simulation to calculate the low frequency wave forces at the relevant locations.

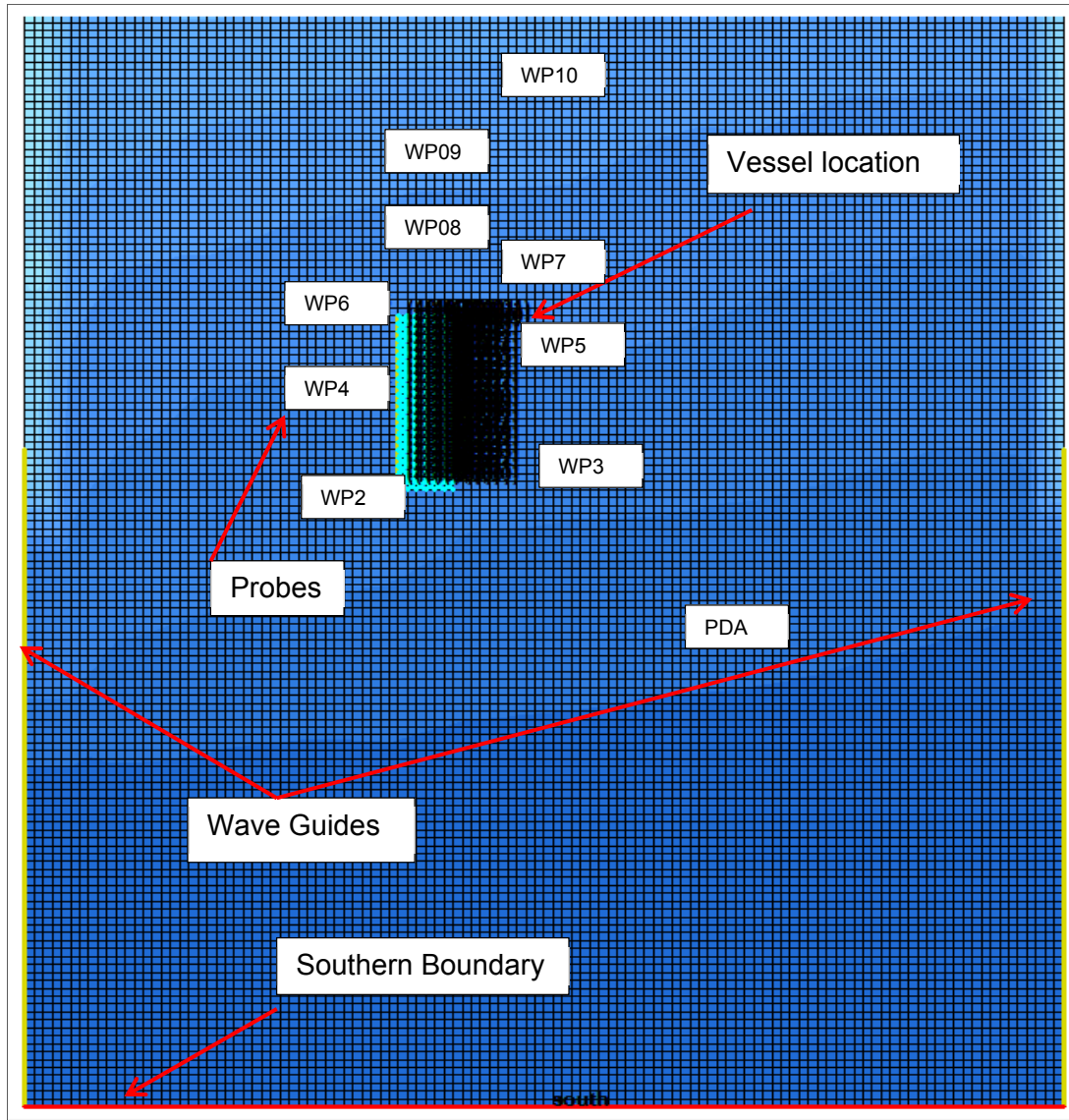


Figure 28: SURFBEAT simulation domain

The calibration procedure was carried out by using the output files from SWAN and activating the roller parameter for SURFBEAT. The resulting low frequency wave energy frequency spectrum of each probe was used to calculate the low frequency wave height (Equations 7 and 8) by integrating the area below the graph using standard spectral analysis:

$$m_0 = \int S(f) f^0 df \quad (7)$$

$$Hm_0 = 4\sqrt{m_0} \quad (8)$$

m_0	moments of the wave spectrum
Hm_0	significant wave height calculated from the spectral domain to be four times the standard deviation from the mean
$S(f)$	spectral energy as a function of the frequency
df	change in frequency
f^0	frequency

(Demirbilek & Linwood Vincent, 2006)

Figures 29 to 32 show the results obtained for Test 04 (12 s, 1.2 m, pile supported jetty). For each probe the low-frequency spectra is plotted next to the high-frequency spectrum. The red lines represent the physical model results as the SURFBEAT results are plotted blue, and the SWAN results black. Here, the low-frequency wave heights of SURFBEAT were compared to the low-frequency wave heights obtained in the physical model. The results for all the tests can be found in Appendix C. In general, there is a good correlation between the SWAN model and the physical model for both short and long waves.

The probes in the basin are accurate to 0.5mm model scale, yielding an accuracy 0.05m prototype. The low frequency waves obtained numerically range between 0.03m to 0.15m prototype. Having such small low frequency waves may influence the accuracy measured in the basin during physical modelling. The low frequency waves calculated are within 15% error difference to the physical model results in most cases.

The difference in accuracy between the two models may explain the peaked results. There were of course a few outliers. It is difficult to get the exact same result for all the probes. Reasons for the outliers could be a number of aspects. The wave generation in the physical model may introduce differences in the propagated wave spectrum compared to the numerical model. The absorption beaches in the numerical model were modelled with a gentler slope as opposed to the absorption beach in the physical model which made use of steeper slopes and coarser rocks. The physical model measurements are dependent on the events occurring on a specific day. For instance, on a specific day, a particular probe might have been faulty to a certain measure and not noticed. The next day the probes are 'zeroed' again with the purpose of improving accuracy but on the contrary, if 'zeroed' incorrectly, faulty readings are measured. Another reason might be the accuracy of the

probes. When very small wave heights are chosen for the testing procedure even smaller low frequency waves were measured. The smaller low frequency waves are measured, the more chance of faulty readings. It is very difficult to work with very small readings in a physical model. That being said, the smaller the waves modelled in the physical model, the larger the chance of scaling effects. The surface tension in smaller waves is a lot more than in larger waves. This might also be a reason for the low frequency wave outliers as seen on Figures 29 to 32.

However, there is general good correlation between the low-frequency wave heights obtained at the probes. The low frequency H_{m0} wave height difference between the physical model and the numerical model has a better agreement compared to that of the graphical representation in Figures 29 to 32.

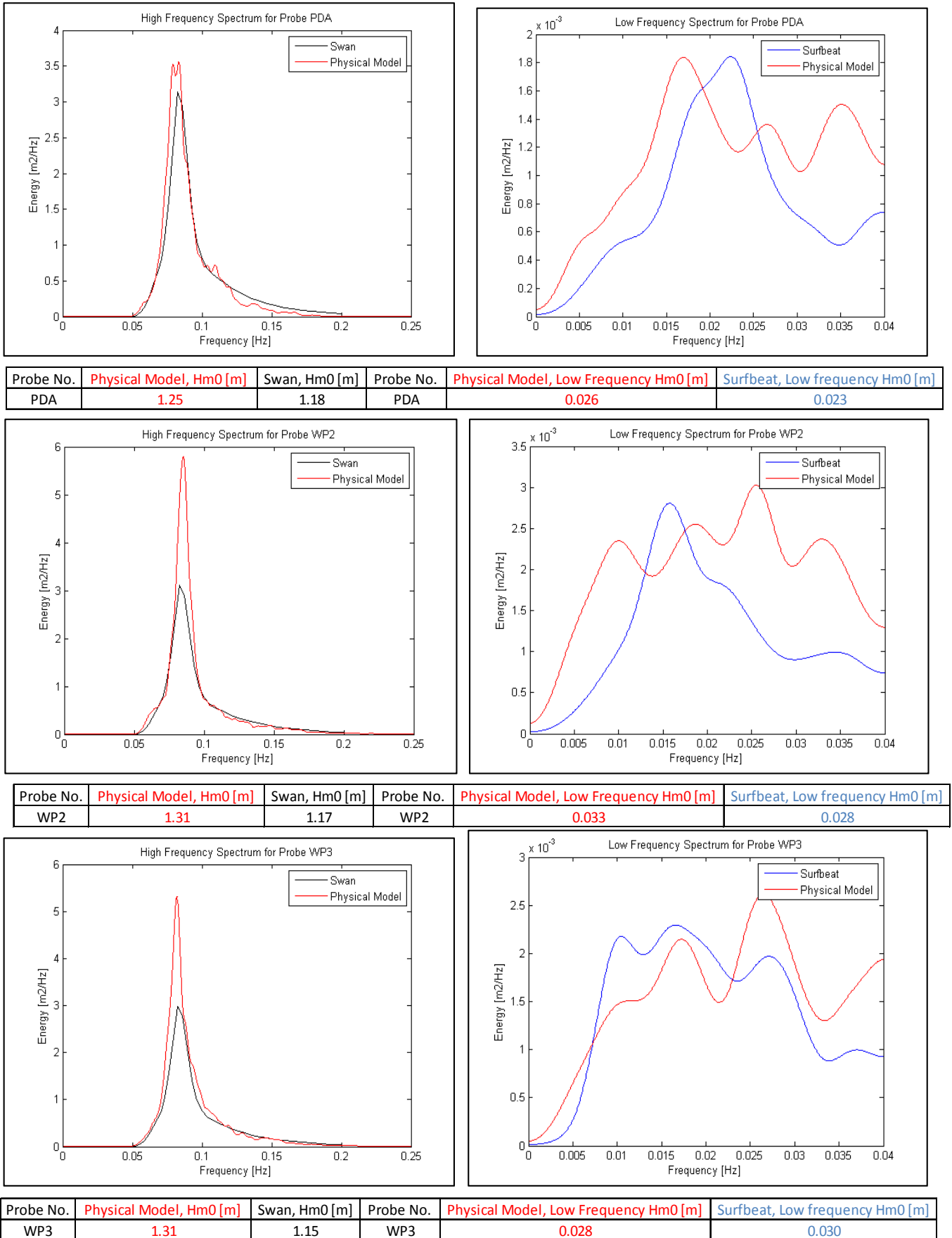


Figure 29: Test 04, long wave and short wave spectra correlation between the physical model, SWAN, and SURFBEAT

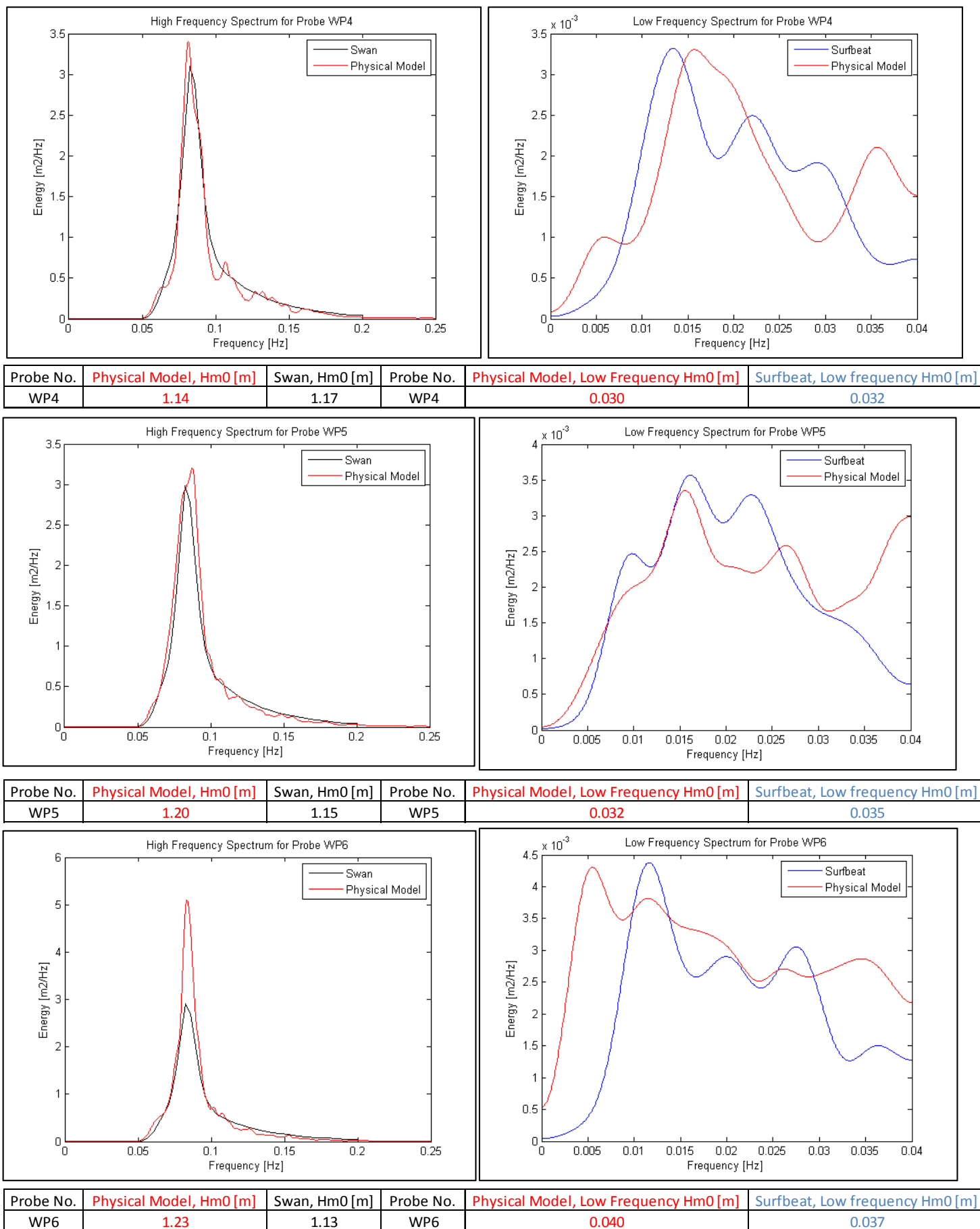
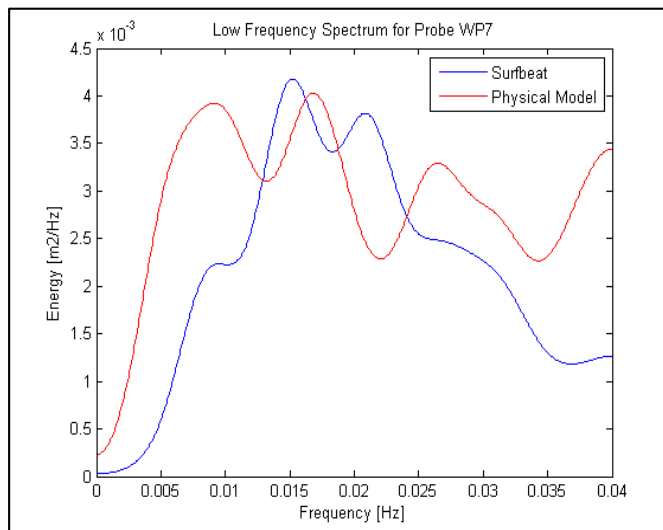
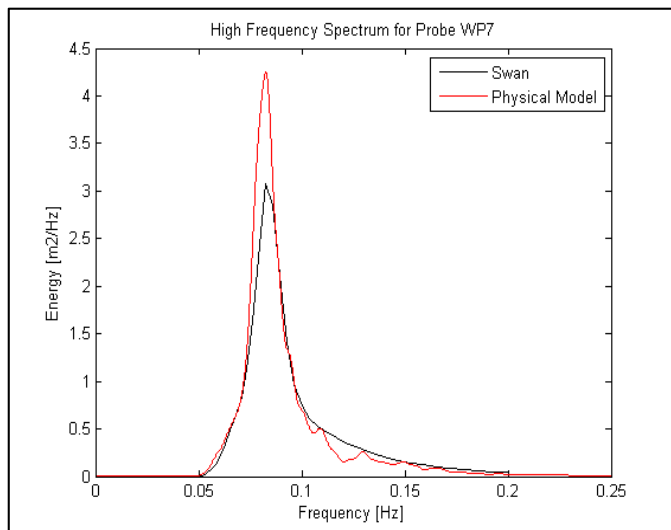
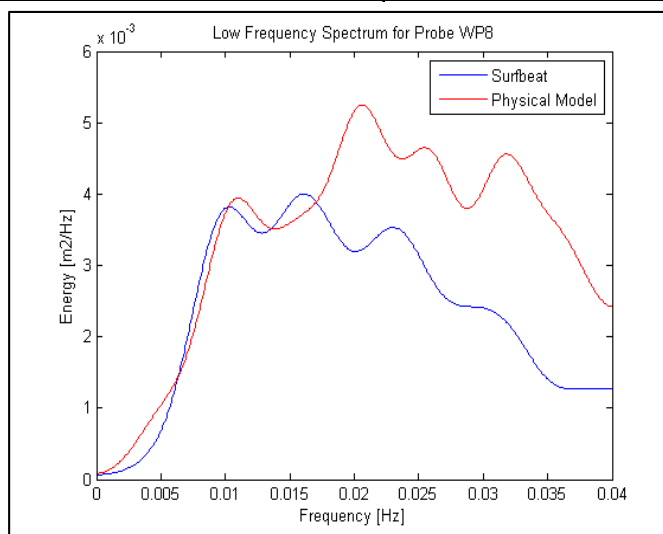
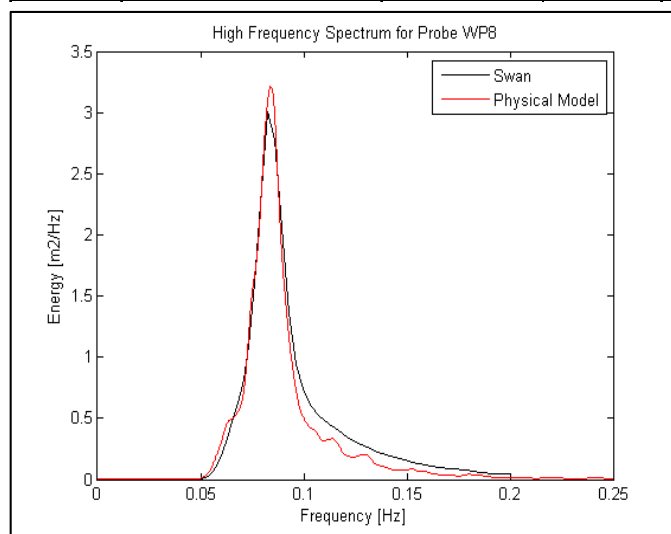


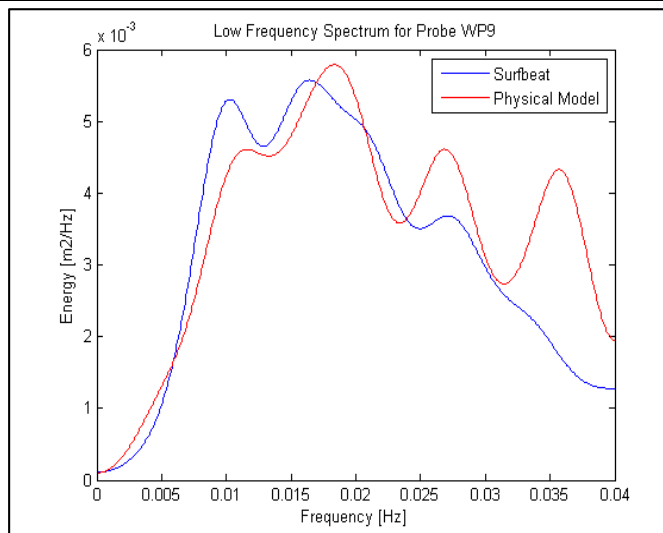
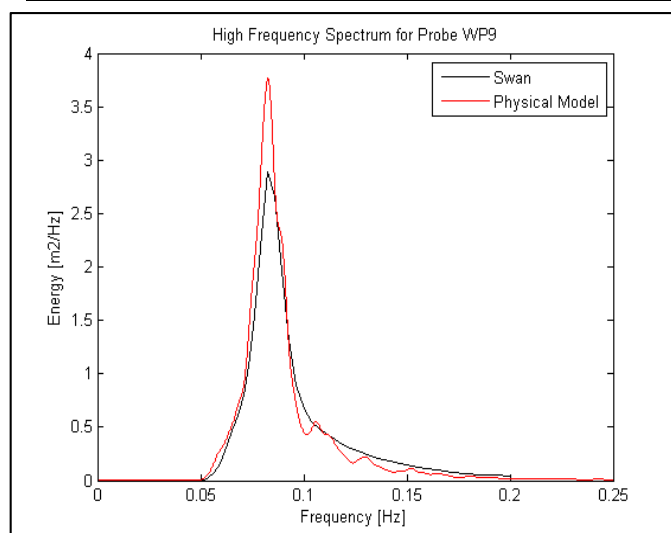
Figure 30: Test 04, long wave and short wave spectra correlation between the physical model, SWAN, and SURFBEAT (contd.)



Probe No.	Physical Model, Hm0 [m]	Swan, Hm0 [m]	Probe No.	Physical Model, Low Frequency Hm0 [m]	Surfbeat, Low frequency Hm0 [m]
WP7	1.20	1.16	WP7	0.039	0.037



Probe No.	Physical Model, Hm0 [m]	Swan, Hm0 [m]	Probe No.	Physical Model, Low Frequency Hm0 [m]	Surfbeat, Low frequency Hm0 [m]
WP8	1.07	1.14	WP8	0.042	0.039



Probe No.	Physical Model, Hm0 [m]	Swan, Hm0 [m]	Probe No.	Physical Model, Low Frequency Hm0 [m]	Surfbeat, Low frequency Hm0 [m]
WP9	1.15	1.12	WP9	0.043	0.045

Figure 31: Test 04, long wave and short wave spectra correlation between the physical model, SWAN, and SURFBEAT (contd.)

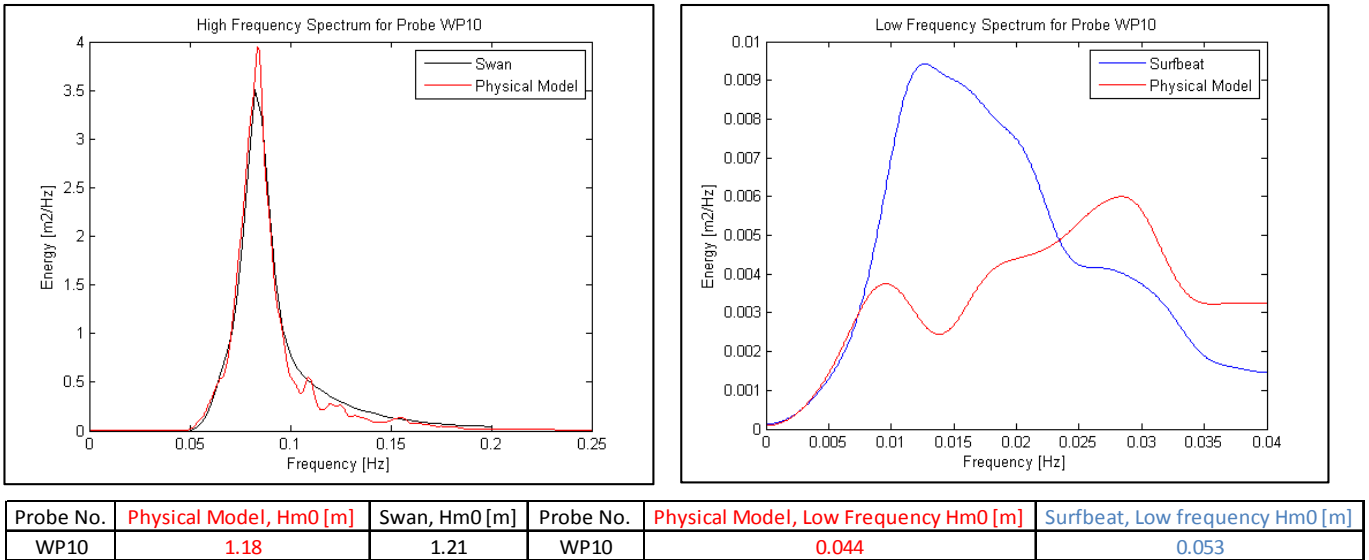


Figure 32: Test 04, long wave and short wave spectra correlation between the physical model, SWAN, and SURFBEAT (contd.)

In order to explain the sudden peaks occurring in the SURFBEAT model, seiches were investigated. Seiches are defined as standing waves or oscillations of the free surface of a body of water. In short, seiches are low frequency waves penetrating a harbour basin. The basin can be closed or semi-closed basin. The frequency of the wave is a function of the forcing, geometry and bathymetry of the basin (Scheffner, 2006). The modes of oscillation, however, are strongly related to the geometry of the basin. Figure 33 shows the different modes of oscillations for different geometric settings.

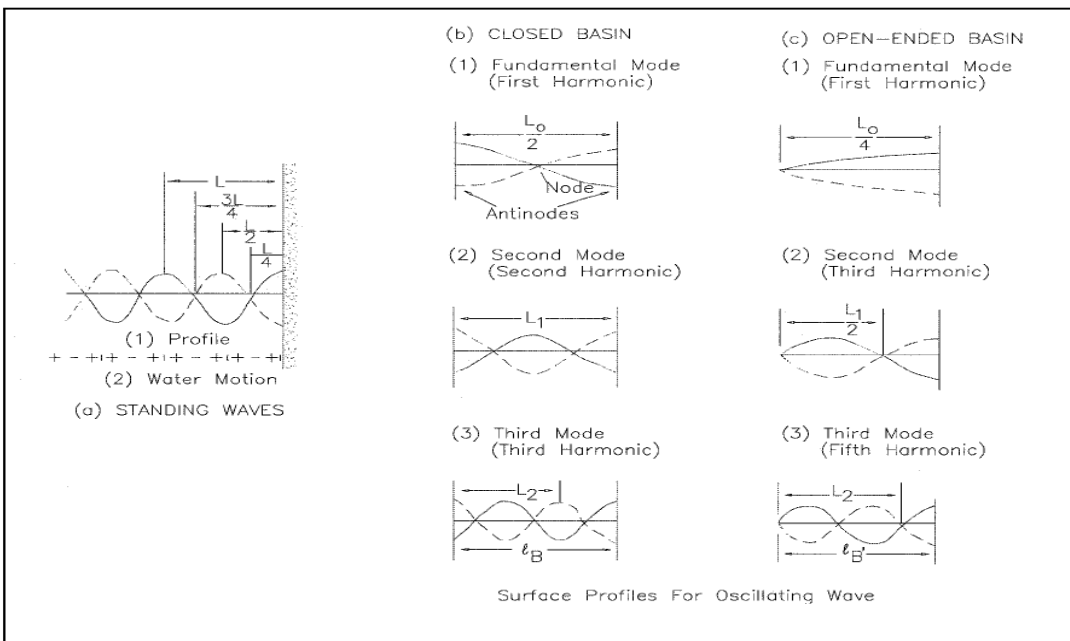


Figure 33: Surface profiles for oscillating waves (Scheffner, 2006).

Equation 9 calculates the standing wave period in a closed basin assuming a uniform depth, whereas Equation 10 calculates the longest standing wave period in an open basin. Fundamental mode corresponds to $n=0$.

$$T_n = \frac{l_B}{n\sqrt{gh}} \quad (9)$$

$$T_n = \frac{4l_B}{(1 + 2n)\sqrt{gh}} \quad (10)$$

l_B	natural length of the basin
T_n	natural free oscillating period of a basin
n	number of nodes along the axis of a basin
g	acceleration of gravity (m/s ²)
h	water depth (m)

Equation 9 was used to calculate the standing wave period in the basin. For a closed basin, the first fundamental mode was used to calculate the standing waves in the length and in the width of the basin. The calculated standing wave period, however, is only a rough approximation because the formula is dependent on the basin depth. The current built-in bathymetry did not have a uniform depth, but a sloping bathymetry, therefore the standing wave period for an average depth was calculated. Table 7 shows the calculated standing wave in the basin for each test.

Table 7: standing wave period present in the basin

Average Depth [m]	Low frequency Tp, Length of Basin [s]	Low frequency Tp, Width of Basin [s]	Test 01, SURFBEAT, Low frequency Tp	Test 02, SURFBEAT, Low frequency Tp	Test 03, SURFBEAT, Low frequency Tp	Test 04, SURFBEAT, Low frequency Tp
29.48	65.2	53	66.10	64.12	67.79	64.59

Notice how the standing wave period occurring in the basin is close to the standing wave period calculated by SURFBEAT. If the peak frequency of the basin was close to the applied peak frequency (of the low frequency waves), it may be one of the reasons for the sudden peaks in the SURFBEAT model.

Reasons why the standing waves might not be picked up in the physical model refer back to the accuracy of the probes. The SURBEAT model has a different level of accuracy as opposed to the level of accuracy measured in the physical model. Another reason might be the modelling of the absorption beaches. The absorption beaches are modelled differently in the numerical model as in the physical model. In the physical model the absorption beaches were built using a 7mm size rock and were much steeper than could be represented in the numerical model. The beaches were therefore extremely permeable allowing energy to dissipate into the beaches.

4.3.1 Model Dependence

In SURFBEAT it is recommended practice to carry out a grid dependence check and a time step check. Any SURFBEAT model should be time independent and no longer influenced by the time step. For instance; should the time step change, the same wave heights should be obtained, otherwise the model suggests the initial time step was too large resulting in a less accurate model. Figure 34 and 35 shows the comparison between the time dependency check and grid dependency check, compared back to the original SURFBEAT run. By applying different time steps to the same model, the same results should be obtained, for the initial time step to pass the time step check.

The grid dependence check requires smaller grid cell sizes with the same conditions and bathymetry. As the grid cell sizes change so do the courant numbers and the time step for the model. Models with finer grids produce finer meshes which subsequently yields more accurate results. Instead of analysing a 15x15m grid a 10x10m grid was used. Figure 34 and 35 shows the comparison for the grid dependency check. Having a finer grid enables SURFBEAT to analyse smaller areas thus processing more detail and thereby yielding a more accurate result compared to a coarser mesh. The grid dependency check however, should yield more or less the same results as the design grid proving that the results are not grid dependent therefore correct results. The model should ultimately be grid independent and time step independent.

Both time and grid dependency checks were carried out. The results for the time dependency and grid dependency checks are presented in Appendix G. Upon inspection, both dependency checks were deemed to be sufficient.

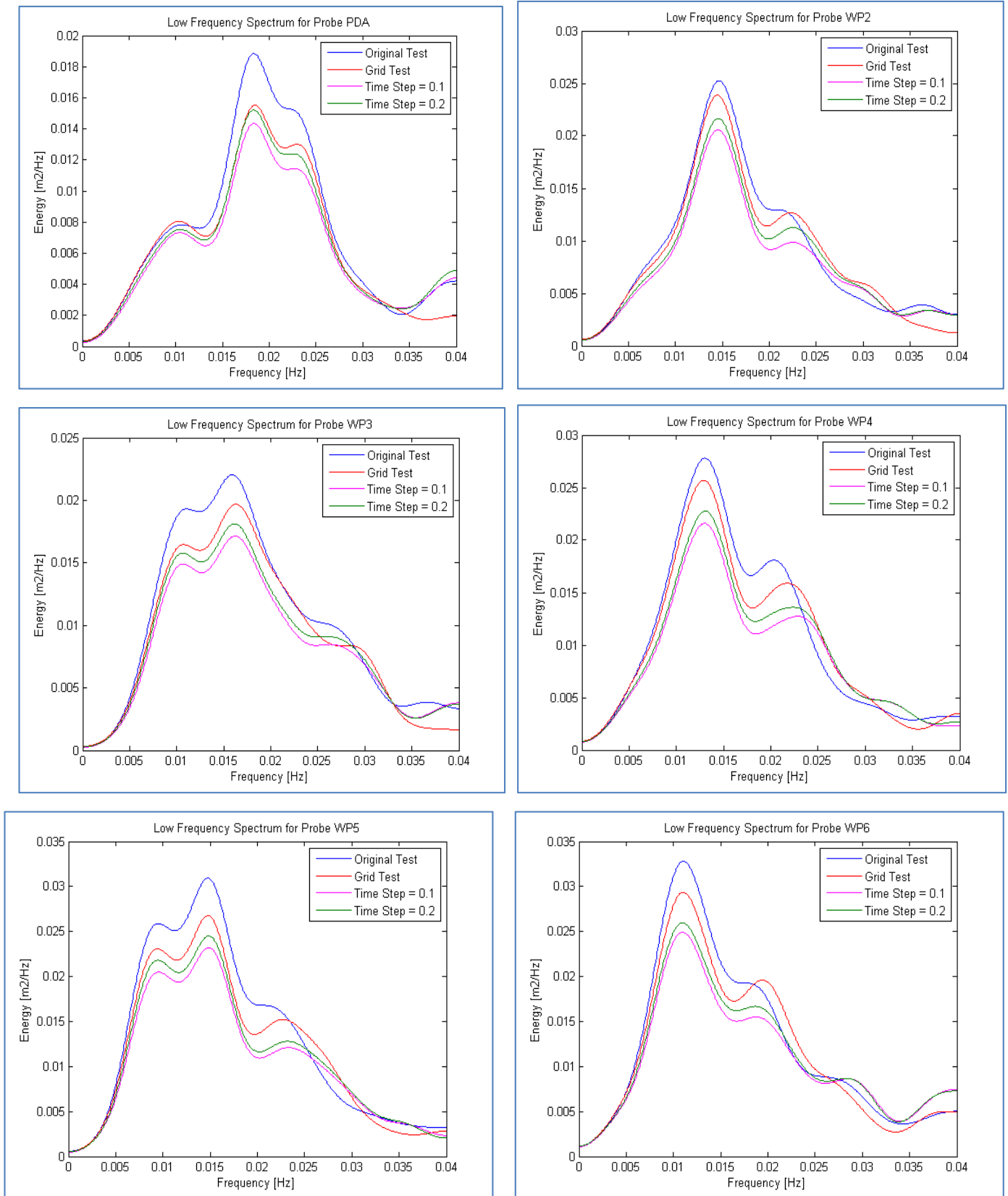


Figure 34: Dependency test results

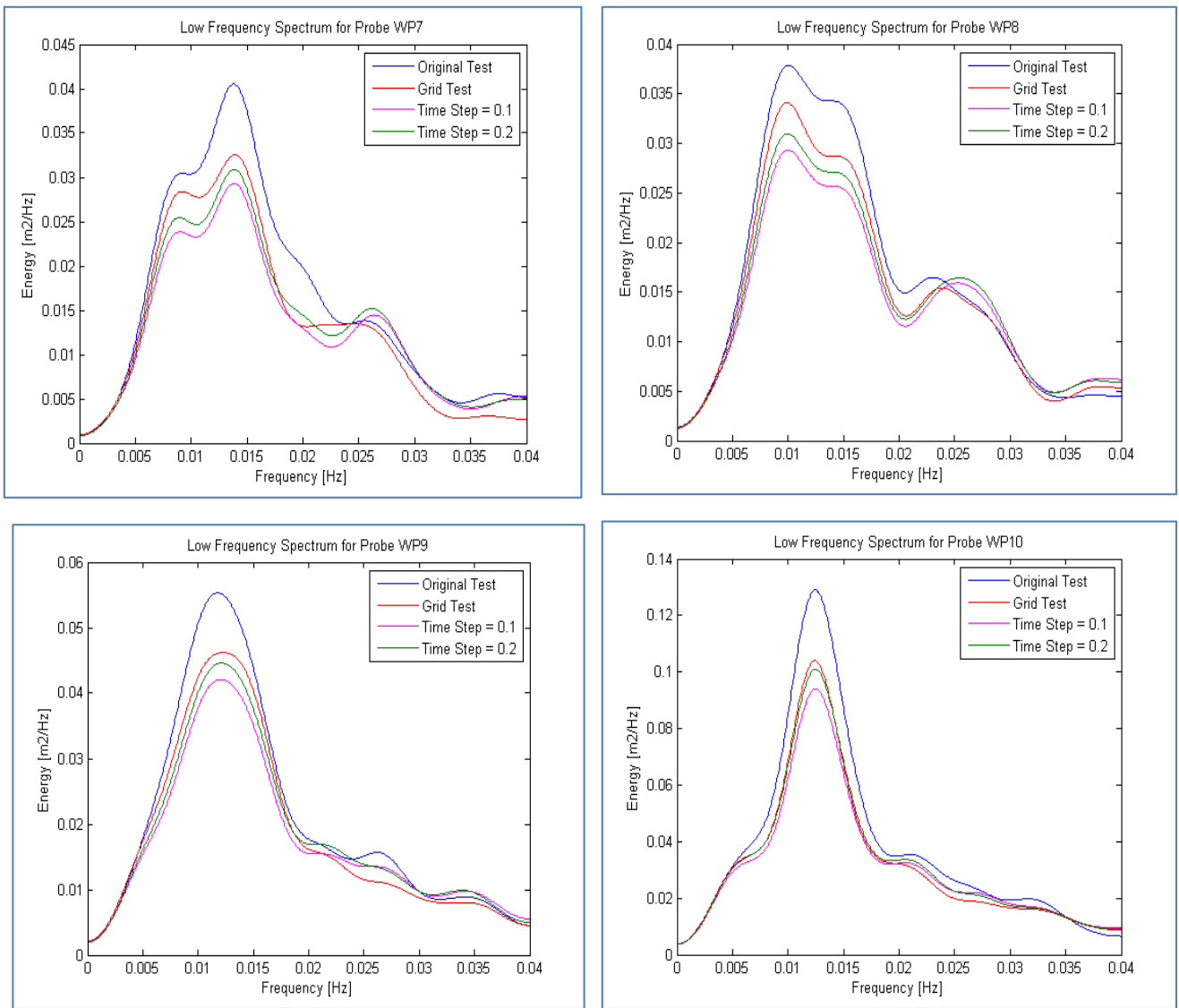


Figure 35: Dependency test results (contd.)

4.4 Results

4.4.1 QUAYSIM Approach

Figure 36 represents the calibration and validation procedure. For SWAN and SURFBEAT to be calibrated, a good comparison should be obtained between the physical and numerical model by adjusting the calibration parameters. The calibrated results are used as input for the numerical model chain of procedures. The exact step-by-step procedure is explained in Appendix H which explains the input files required for each step required for QUAYSIM.

SWAN	SURFBEAT	Hull-	Mesh-	WAVE-	LF-	WAVE-	QUAYSIM
------	----------	-------	-------	-------	-----	-------	---------

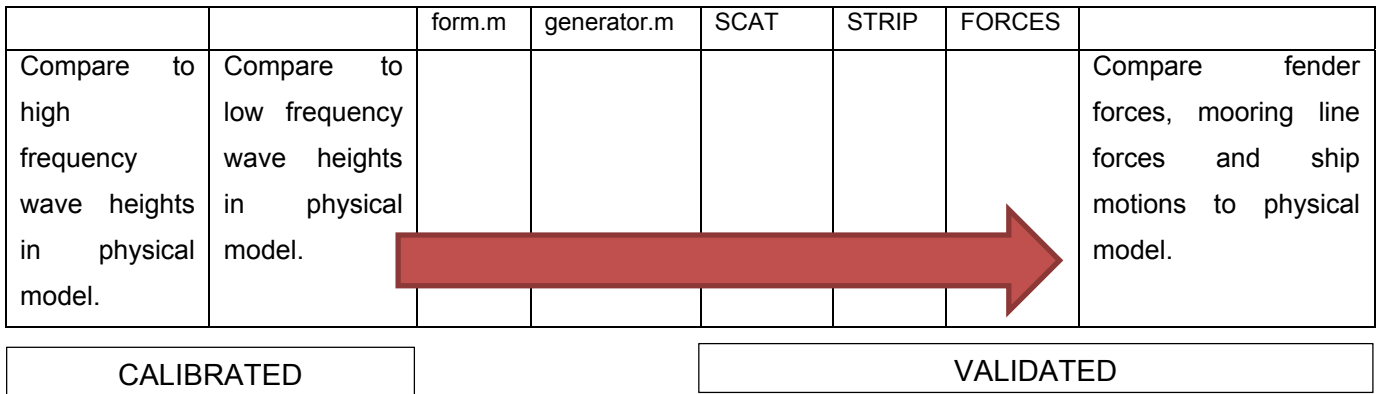


Figure 36: Calibration and validation

Finally, the results from the numerical models were used to validate QUAYSIM. QUAYSIM calculates moored ship motions due to wave forcing. In this study, four different wave force inputs were generated: long wave forces from SURFBEAT/LFSTRIP; long wave forces from WAVEFORCES/WAVESCAT (theoretical set-down computation); short wave forces from SWAN/WAVESCAT/WAVEFORCES and; short wave forces from WAVEFORCES/WAVESCAT (theoretical computation). Figure 37 below show the possible approaches. All the methods were investigated to fully inspect which one yields the most desirable result. Each method analyses ship motion values, ship motion spectra, fender forces, and mooring line forces. The following methods are represented by coloured arrows to ease the analysis investigation and discussion (Figure 37). The methods are explained and numbered below.

1. Method **BLUE** – Long wave forces (SURFBEAT/LF-STRIP) used, short wave forces (WAVEFORCES/WAVESCAT) used
2. Method **RED** – Long wave forces (SURFBEAT/LF-STRIP) used, short wave forces (SWAN/WAVESCAT/WAVEFORCES) used
3. Method **GREEN** – Long wave forces (WAVEFORCES/WAVESCAT) used, short wave forces (SWAN/WAVESCAT/WAVEFORCES) used
4. Method **PURPLE** - Long wave forces (WAVEFORCES/WAVESCAT) used, short wave forces (WAVEFORCES/WAVESCAT) used

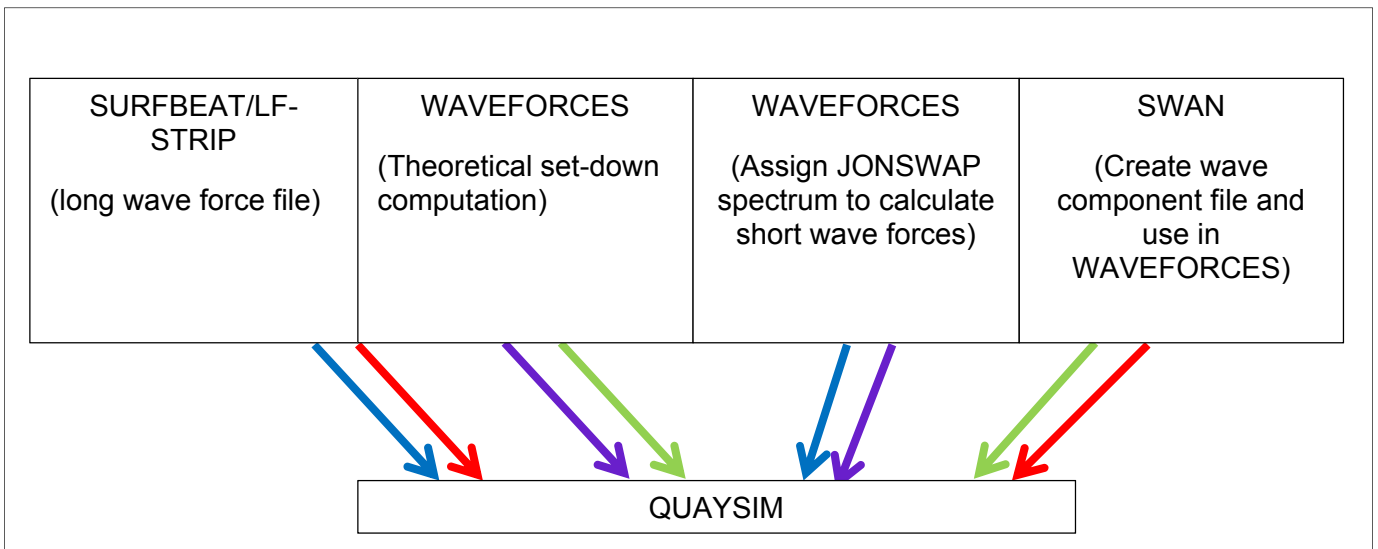


Figure 37: Different approaches to validating QUAYSIM

Table 8 shows the ship motion values calculated for the different methods. Figure 38 shows how the ship motion spectra corresponds to the physical model. Method 1 (blue) calculates the best values and compares the best to the physical model graphically in Figure 38.

Table 8: Ship motion values calculated for different methods

SHIP MOTIONS					
	PM	1	2	3	4
surge [m]	1.2	1.1	1.3	1.0	1.5
sway [m]	0.5	0.7	1.6	1.6	0.1
heave [m]	0.4	0.3	0.4	0.4	0.3
roll [deg]	1.2	0.3	0.3	0.3	0.2
pitch [deg]	0.3	0.3	0.3	0.3	0.3
yaw [deg]	0.3	0.2	0.4	0.3	0.1

For method 1, the LF-STRIP force file and the WAVEFORCES short wave force was used. The long wave ship motions (horizontal motions - surge, sway, and yaw) compare well. The roll however, was very difficult to replicate. The same frequency was obtained, but the magnitude of the roll was not achieved

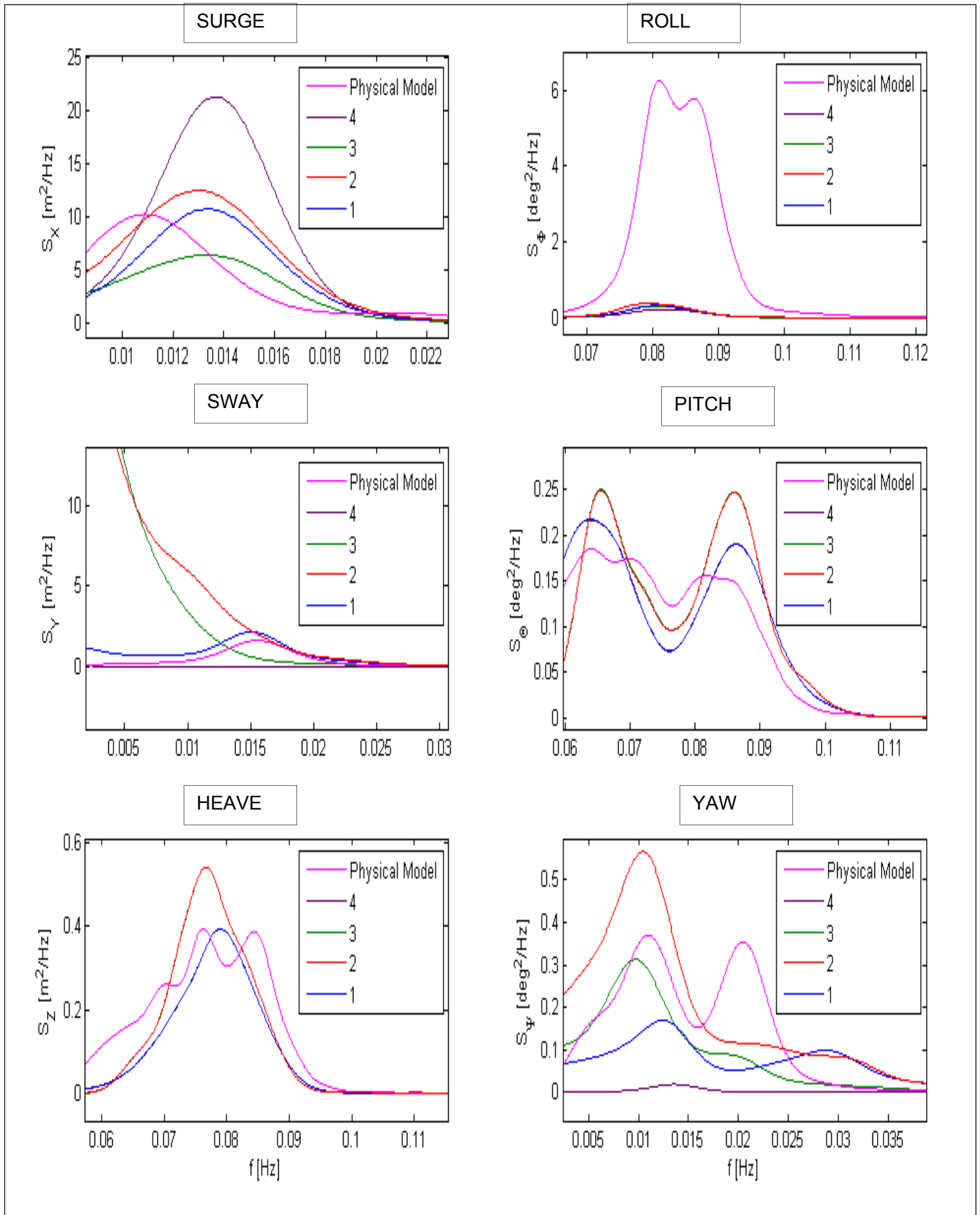


Figure 38: Ship motion spectra calculated for different methods

It is clear that the data suggests by making use of the SWAN wave component file for WAVEFORCES, larger motions are calculated (Method 2 and 3). A reason for this could possibly be that the spreading assigned in SWAN was larger than what the physical model measured/experienced at the time. Accurate measurement of spreading using a four probe array is still challenging for irregular waves at model scale. The vessel motions in sway are sensitive to the direction of the approaching wave, which may explain some of the differences in the measured and modelled sway motions.

Method 4 also suggests an overestimation in surge movement and an underestimation in sway. Generally the values for Method 4 do not correspond well, in comparison with the other methods and will not be considered further. QUAYSIM is a potential flow model which does not consider viscous effects. This might be one of the reasons for these results. However, this test should not be eliminated completely. In comparison to the other methods, method 4 deems less desirable. Further testing with this method might yield improvements.

4.4.2 Ship Motions

Figures 40 to 43 show comparison of the ship motion spectra for all tests while Tables 10-13 illustrates the ship motion values obtained for each movement. The red curves represent the physical model results whereas the black curves represent the QUAYSIM results. For all tests the results can be found in Appendix I. The same pattern, however, occurs within tests. Good correlation was achieved for surge, sway heave, pitch, and yaw motions. From the tests carried out, the data suggest that QUAYSIM seems to underestimate the roll movement.

Table 9 illustrates how the tests were compared. The tests carried out with a quay wall behaved similarly; just as the tests carried out with a pile supported jetty behaved similarly. The tests with the same test conditions were compared to investigate the effect of the presence of a quay wall. Referring to Table 9 and following the horizontal arrow, tests with different test conditions were compared with the same pile supported jetty. The vertical arrow shows tests with the same test conditions, being compared having a quay wall and without.

Table 9: Comparable results

	Same Test Conditions	Same Test Conditions
With Quay Wall	Test 01	Test 02
Pile Supported Jetty	Test 03	Test 04



From Test 01 and 02 (different test conditions, quay wall present) the data suggests larger sway motions were measured numerically. Subsequently, a better relationship was obtained for the roll

(magnitude). The same spectral pattern was achieved for the pitch (QUAYSIM measures slightly less).

QUAYSIM is a potential flow model in which viscous effects are not considered. The volume of water between the vessel and the quay wall (about 3cm model scale, or 3m prototype in QUAYSIM) is compressed and decompressed whilst the vessel moves. Figure 39 illustrates the viscous effect referred to occurring between the vessel and the quay wall. This might be one of the reasons for the over prediction in surge whilst modelling with a quay wall.

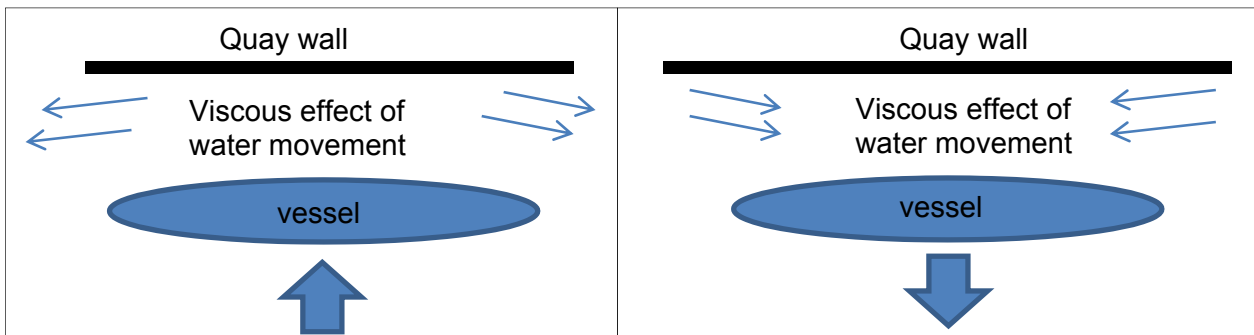


Figure 39: Viscous effects

Whilst comparing Test 01, Test 03 (with and without quay wall) and Test 02, Test 04 (with and without quay wall) numerically many interesting things are noticed. The same pattern is seen between numerical comparisons. Larger sway and surge was measured with the presence of a quay wall. Heave compared well in all tests. The roll measured without a quay wall is significantly smaller than the roll measured with a quay wall. With a quay wall a better relationship is obtained for the yaw as opposed to without a quay wall. Without a quay wall better pitch values were measured. The pitch values decreased with the quay wall present.

4.4.1.1 Test 1

Table 10: Ship motion values for Test 01

	XHmo PM	QUAYSIM
surge [m]	0.86	0.94
sway [m]	0.24	0.59
heave [m]	0.24	0.2
roll [deg]	1.73	0.78
pitch [deg]	0.23	0.15
yaw [deg]	0.19	0.23

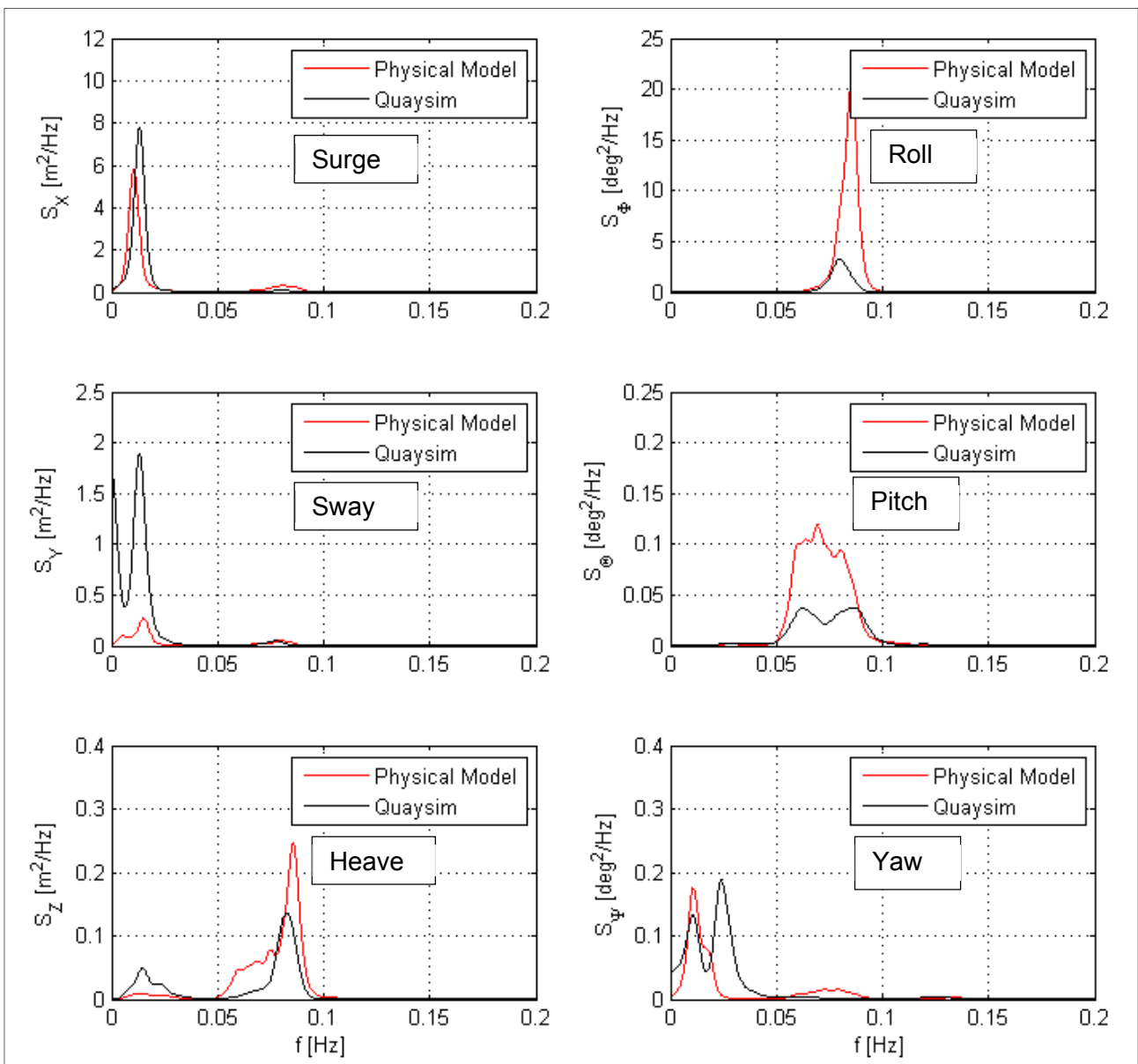


Figure 40: Ship motion spectra for Test 01

4.4.1.2 Test 2

Table 11: Ship motion values for Test 02

	XHmo PM	Quaysim
surge [m]	0.39	0.46
sway [m]	0.11	0.26
heave [m]	0.14	0.12
roll [deg]	0.94	0.55
pitch [deg]	0.15	0.1
yaw [deg]	0.09	0.12

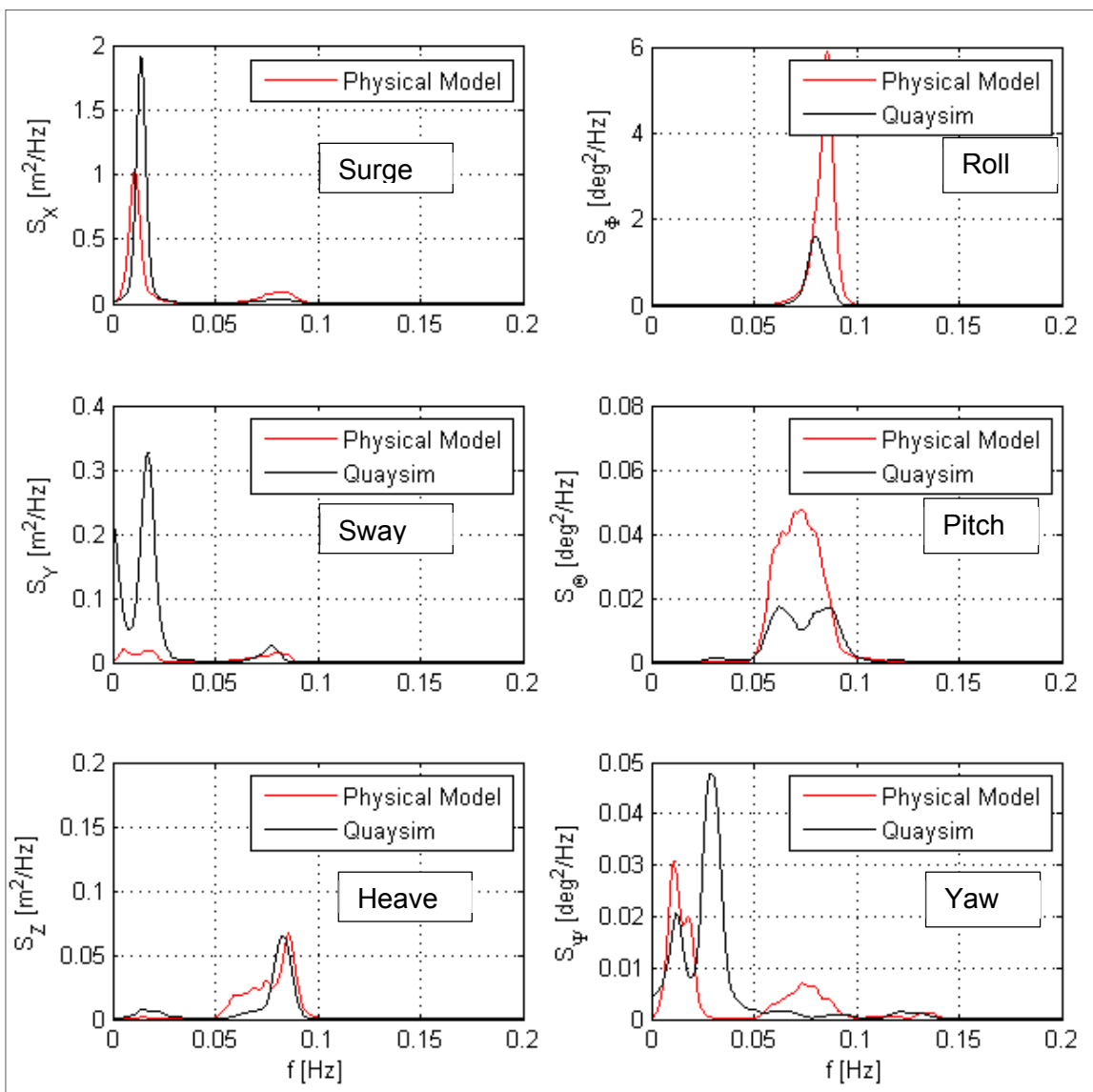


Figure 41: Ship motion spectra for Test 02

4.4.1.3 Test 3

Table 12: Ship motion values for Test 03

	XHmo PM	QUAYSIM
surge [m]	1.15	1.16
sway [m]	0.49	0.64
heave [m]	0.38	0.33
roll [deg]	1.20	0.28
pitch [deg]	0.30	0.31
yaw [deg]	0.34	0.23

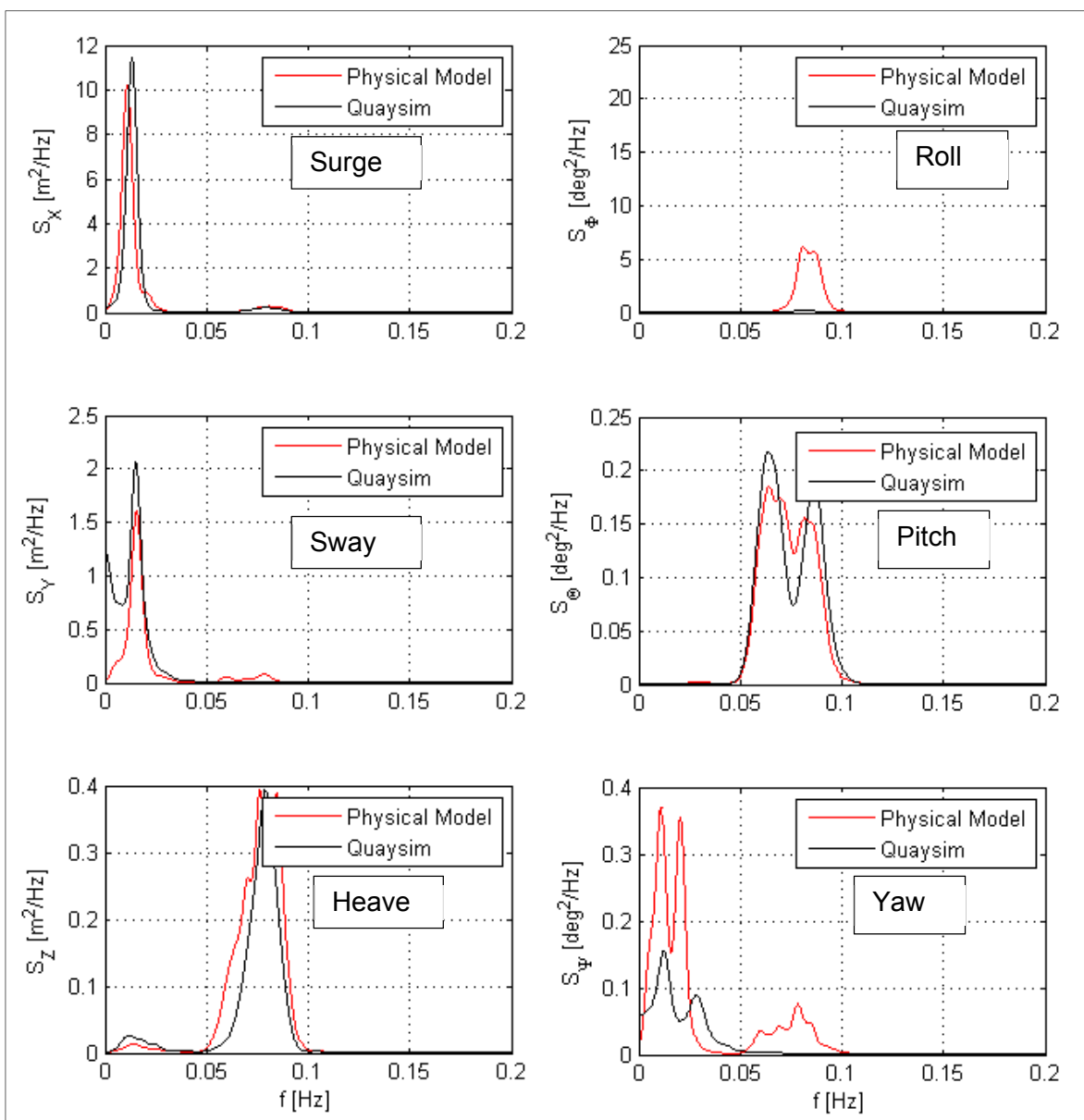


Figure 42: Ship motion spectra for Test 03

4.4.1.4 Test 4

Table 13: Ship motion values for Test 04

	XHmo PM	QUAYSIM
surge [m]	0.31	0.41
sway [m]	0.12	0.12
heave [m]	0.17	0.19
roll [deg]	0.59	0.13
pitch [deg]	0.16	0.19
yaw [deg]	0.13	0.05

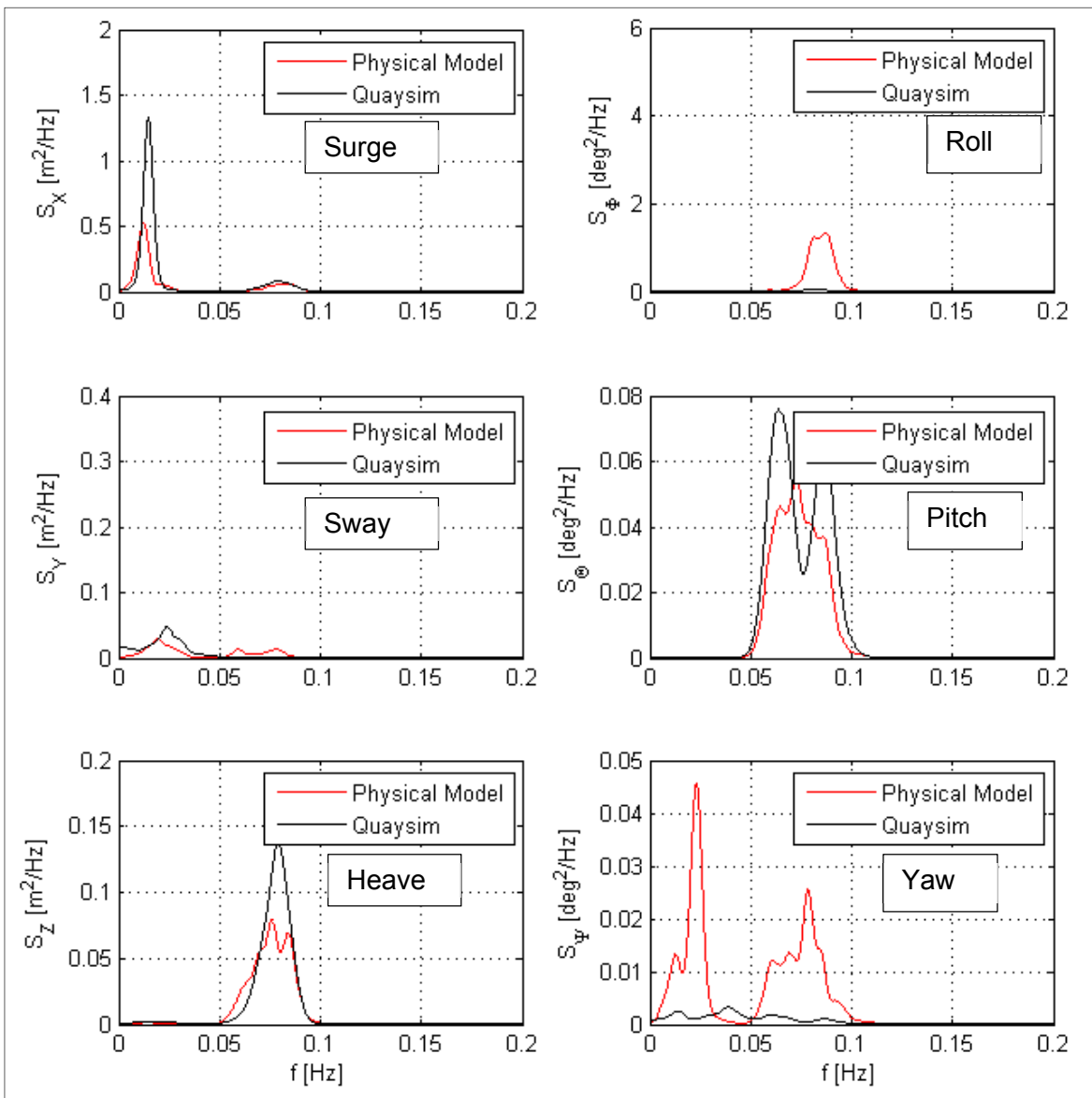


Figure 43: Ship motion spectra for Test 04

In all tests, an extra long wave component was present in the sway. A regular wave test was carried out to investigate whether QUAYSIM calculates regular waves and the natural period correctly. Figure 44 illustrates the result obtained. No extra long wave components was present in these tests. The long wave component present in the sway in Test 01 – 04, could be either due to viscous effects or either due to associated method used (Diffraction calculations using the LF-STRIP long wave force file or relying on QUAYSIM to resolve the long wave forces).

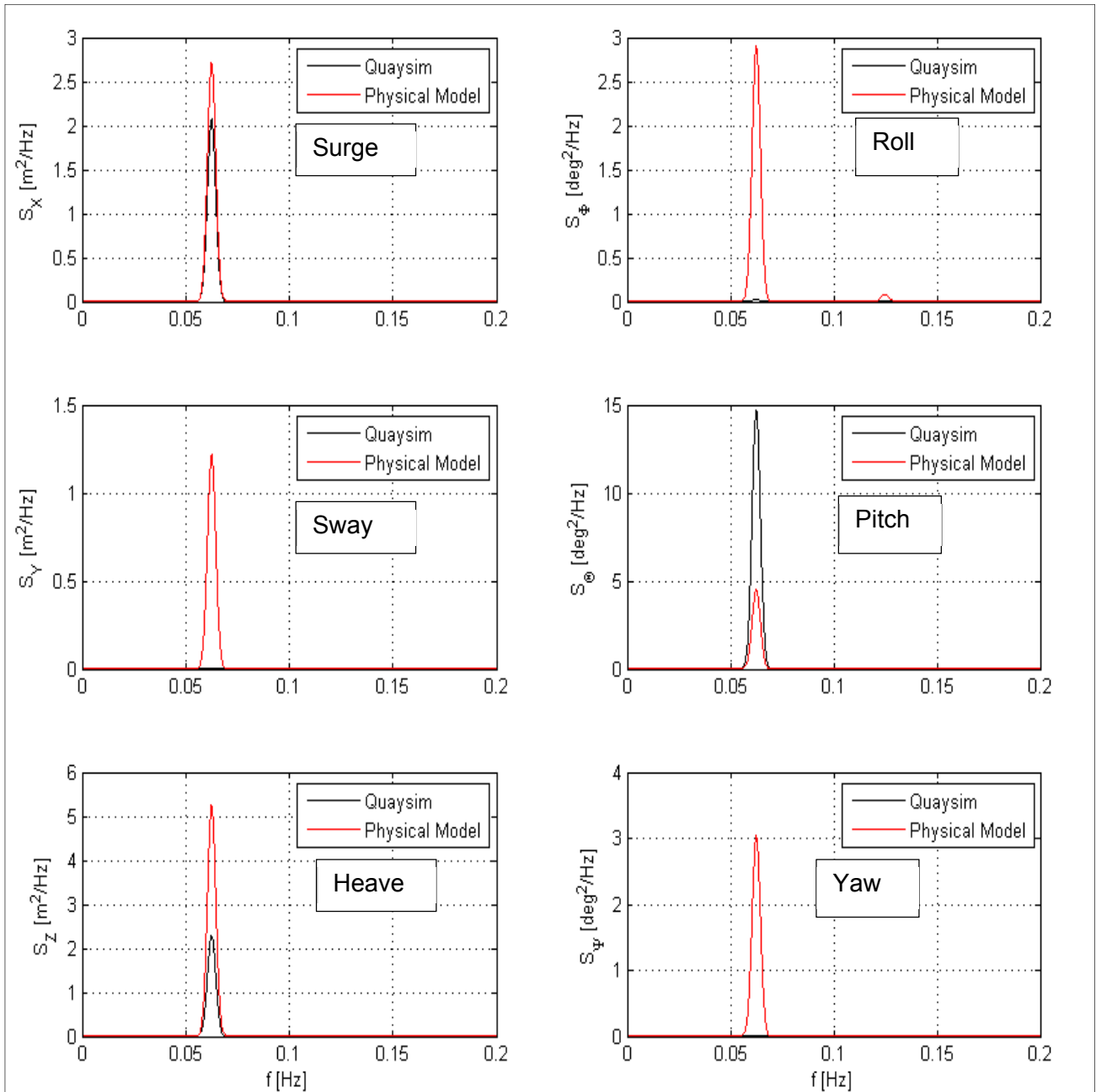


Figure 44: Regular wave result

4.4.3 Fender and mooring Line Forces

Tables 14 to 16 show the fender and mooring line forces calculated by QUAYSIM compared to the forces measured in the physical model. Agreements within 15% were achieved for mooring lines and 30% for fenders having a few outliers in some cases.

Reasons for the outliers will now be discussed. As mentioned previously, physical model fender measurements involved a tedious process because of the sensitivity of the fender positions. The stiffness of the fenders and mooring lines modelled in the physical model might decrease over time, as the physical model is run over a two-month period. The fenders and mooring lines are exposed to water all the time. Therefore the stiffness recorded initially might not be the stiffness when the last tests are run. The initial stiffness was used to carry out the QUAYSIM run. The material used to model the fenders, was Teflon buds. The surface of the Teflon buds has a significantly smooth surface, in which little to no friction occurs. This is not entirely true for prototype fenders, which usually have a rubber surface. The friction factor in the numerical model needed some adjustment, but this might also be a reason for the outliers from fender forces.

Table 14: Fender and mooring line correlation between physical model and QUAYSIM, Test 01

	Physical Model Fender Forces [kN]	QUAYSIM Fender Forces [kN]	Physical Model Mooring Line Forces [kN]	QUAYSIM Mooring Line Forces [kN]
F1			407	433
F2			423	482
F3	1157	946	449	545
F4	827	850	566	561
F5	1360	872	425	525
F6	1331	1031	514	518
F7	1274	1338	498	506
F8			436	436

Table 15: Fender and mooring line correlation between physical model and QUAYSIM, Test 02

	Physical Model Fender Forces [kN]	QUAYSIM Fender Forces [kN]	Physical Model Mooring Line Forces [kN]	QUAYSIM Mooring Line Forces [kN]
F1			355	339
F2			351	369
F3	624	658	367	396
F4	452	584	416	408
F5	898	602	348	378
F6	726	707	356	384
F7	523	915	333	390
F8			336	334

Table 16: Fender and mooring line correlation between physical model and QUAYSIM, Test 03

	Physical Model Fender Forces [kN]	QUAYSIM Fender Forces [kN]	Physical Model Mooring Line Forces [kN]	QUAYSIM Mooring Line Forces [kN]
F1			507	436
F2			523	484
F3	1922	1031	647	554
F4	1269	880	639	645
F5	1586	855	473	554
F6	1528	970	606	543
F7	1403	1237	604	545
F8			460	468

Table 17: Fender and mooring line correlation between physical model and QUAYSIM, Test 04

	Physical Model Fender Forces [kN]	QUAYSIM Fender Forces [kN]	Physical Model Mooring Line Forces [kN]	QUAYSIM Mooring Line Forces [kN]
F1			348	313
F2			362	338
F3	837	406	401	341
F4	499	387	370	391
F5	877	412	305	373
F6	619	473	374	333
F7	475	563	387	353
F8			319	304

Chapter 5: Summary and Conclusion

5.1 Summary

QUAYSIM and WAVESCAT are two numerical ship motion models created by the CSIR that needed to be validated for publication purposes. Such validation would enable the CSIR to refer clients to the relevant research as proof of the workability of the software. Although the software has been tested in the past, it could not be published due to confidentiality agreements. The ultimate objective of this thesis was therefore to validate the two numerical ship motion models WAVESCAT and QUAYSIM. Because of the magnitude of the thesis scope, the objective of the project was split into two phases:

1. Physical modelling

The first objective was to obtain physical model measurements of high frequency wave heights, low frequency wave heights, fender forces, mooring line forces, and ship motions. A simple set-up was used without any obstacles in the basin. The current built-in bathymetry was used with a jetty positioned perpendicular to the wave generators. The test runs carried out for a pile supported jetty were reproduced for a solid quay wall. The physical model measurements were carried out for calibration and validation purposes.

2. Numerical modelling

The numerical modelling was carried out by calibrating the high frequency wave model SWAN and the low frequency wave model SURFBEAT. A good correlation existed between the wave heights obtained in the physical model, SWAN and SURFBEAT. These were well calibrated. The high frequency wave output was used to determine the short wave forces by means of WAVEFORCES. The low frequency wave output was used to determine the low frequency wave forces by means of LF-STRIP. The calibrated results were used to calculate the hydrodynamic coefficients of an oscillating ship, using WAVESCAT. QUAYSIM makes use of the hydrodynamic output provided by WAVESCAT, the high frequency wave force file from WAVEFORCES (calibrated) and the low frequency wave force file from LF-STRIP (calibrated). This approach is adequate, as it uses the strength of each numerical model independently.

5.2 Conclusion

The numerical models WAVESCAT and QUAYSIM, models of ship motion, have shown to provide a good correlation between the physical model and the numerical approach. Improvements however, are still required.

To validate QUAYSIM/WAVESCAT completely, more test runs are required to explain the underestimation in roll and the presence of the long wave component in the sway. Small values were measured in the physical model. Should larger values be measured (i.e. test with larger wave conditions), the results would probably be more comparable. It is often tedious working with small measurements between numerical and physical models. Due to difference in accuracy between the two models, the chances of incorrect interpretations are more likely. It is recommended that more tests with larger wave conditions should be carried out.

To investigate the degree of accuracy of the validation, bi-directional waves should also be investigated where waves are applied at a few angles. Waves no longer approach the jetty head-on but at an angle. Different ship motions are expected in this way. Sufficient comparison between the two models would strengthen the validation.

Generally, from inspection, good comparisons were obtained for the long wave motions (horizontal movements - surge, sway and yaw). The motions do not deviate far from each other. There are however, a few concerns. From these tests, graphically an extra long wave component was present in the sway in all tests. This is the reason for the slight over prediction in sway measurements in all tests. To investigate the extra long wave component generated in the sway with QUAYSIM, tests with a range of regular waves should be tested in the physical model. It is still unclear from where the extra long wave component originates.

The surge is better presented in all tests but QUAYSIM also seems to calculate a slightly larger surge in all situations. Even though the yaw is well comparable, graphically it is not well represented. Moreover, in all tests the same frequency was obtained for the roll but the magnitude of the roll calculated in QUAYSIM was severely underestimated from tests carried out. For future tests it is important that the numerical modelling procedure should also run where possible in parallel to the physical modelling procedure, this way mistakes can easily be noticed and eliminated.

References

- Delft3D-FLOW. (2011). *Manual*. The Netherlands: Deltares ©.
- Delft3D-WAVE. (2011). *Manual*. Delft, The Netherlands: Deltares ©.
- MAERSK. (2013, December 10). Retrieved August 18, 2014, from World Largest Ship: <http://www.worldslargestship.com/>
- Battjes, J., & Stive, M. (1985). Calibration and Verification of a Dissipation Model for Random Breaking Waves. *Journal of Geophysical Research*, 90, 9159 - 9167.
- Benedict, K., Baldauf, M., & Kirchhoff, M. (2004). *Estimating potential danger of roll resonance for ship operation*. Schiffahrtskolleg.
- Beresford, P. (2007). *HR WaveMaker Wave Generation Control Program*. Wallingford: HR Wallingford.
- Boers, M. (2005). *Surf Zone Turbulence*. Delft: Delft University of Technology.
- Demirbilek, Z., & Linwood Vincent, C. (2006). Coastal Engineering Manual. In *Water Wave Mechanics, Part II, Coastal Hydrodynamics, Chapter II-2*. Washington DC: U.S Army Corps of Engineers.
- Faltinsen, O. M. (1990). *Sea Loads on Ships and Offshore Structures*. Cambridge: Cambridge University Press.
- Headland, J., & Poon, Y.-K. (1998). Numerical Modeling of Long Wave Ship Motions. *Journal of Coastal Engineering*.
- Hermans, A. J., & Huijsmans, R. H. (1987). The Effect of Moderate Speed on the Motion of Floating Bodies. *Journal of Ship Technology Research / SCHIFFSTECHNIK*.
- Hughes, S. A. (1995). Physical Models and Laboratory Techniques in Coastal Engineering. In S. A. Hughes, *Advanced Series on Ocean Engineering* (Vol. 7). London: World Scientific Publishing.
- J. A. Battjes, H. J. (2004). *Shoaling of Subharmonic Gravity Waves*. American Geophysical Union.
- Journée, J. (2001). *User Manual of Seaway*. Delft: Delft University of Technology.
- Korvin-Kroukovsky, B. V., & Jacobs, W. R. (1957). *Pitching and Heaving Motions of a Ship in Regular Waves*.

- Lee, C. H., & Newman, J. N. (2005). *Computation of Wave Effects using the Panel Method*. USA: MIT.
- Ligteringen H., V. H. (2012). *Ports and Terminals*. Delft, The Netherlands: VSSD.
- Ligteringen, H., van der Molen, W., van der Lem, J., & de Waal, J. (2003). Behaviour of a Moored LNG Ship in Swell Waves. *Journal of Waterway, Port, Coastal and Ocean Engineering*.
- Lopez, M., & Iglesias, G. (2013). *On the long waves disturbing ship operations in Ferrol (Spain)*. EGU General Assembly 2013.
- Miles, J., & Munk, W. (1961). Harbor paradox. *Journal of the Waterways and Harbors Division*, 111-130.
- Munk, W. H. (1949). Surf beats. In W. H. Munk, *Surf beats* (pp. 849– 854). Eos Trans AGU.
- Pinkster, J. (1980). *Low Frequency second order wave exciting forces on floating structures*. Marin.
- Remery, G., & Hermans, A. (1971). The Slow Drift Oscillations of a Moored Object in Random Seas. In *Offshore Technology in Civil Engineering* (Vol. 3, pp. 47-56). ASCE.
- Roelvink, D., Reniers, A., van Dongeren, A., van Thiel de Vries, J., McCall, R., & Lescinski, J. (2009). Modelling Storm Impacts on Beaches, Dunes and Barrier Island. *Journal of Coastal Engineering*.
- Roelvink, J. A. (1993 (a)). *Surfbeat and its Effect on Cross-Shore Profiles*. Delft: Delft University of Technology.
- Scheffner, N. (2006). Coastal Engineering Manual. In *Water Levels and Long Waves, Part II, Coastal Hydrodynamics, Chapter II-5*. Washington DC: U.S. Army Corps of Engineers.
- Stuart, D. (2013). *Characterizing long wave agitation in the Port of Ngqura using a Boussineq Wave Model*. Stellenbosch: University of Stellenbosch.
- Tucker, M. J. (1950). Surf beats: Sea waves of 1 to 5 min. . In M. J. Tucker, *Surf beats* (pp. 202, 565– 573.). London: Proc. R. Soc.
- Ursell. (1949). *On the Heaving Motion of a Circular Cylinder on the Surface of a Fluid*. Manchester: The University of Manchester.
- van der Molen, W. (2006 (a)). *Behaviour of Moored Ships in Harbours*. Delft: Delft University of Technology.
- van der Molen, W. (2011 (b)). *Boundary Element Model: WAVESCAT*. Stellenbosch, South Africa: CSIR.

- van der Molen, W. (2011 (c)). *Low-Frequency wave force program: LF-STRIP/SURFBEAT*. Delft: Delft University of Technology.
- van der Molen, W. (2011 (d)). *Moored Ship Response Program: QUAYSIM*. Stellenbosch: CSIR.
- van der Molen, W., & Hough, G. (2009). *Highly accurate measurement of small-scale vessel motions*. Wellington, New Zealand.
- van der Molen, W., Rossouw, M., Phelp, D., Tulsi, K., & Terblanche, L. (2010). *Innovative technologies to accurately model waves and moored ship motions*. Stellenbosch: CSIR.
- van Oortmerssen. (1976). *The Motions of a Moored Ship in Waves*. Wageningen: Netherlands Ship Model Basin.
- Wichers, J. (1988). *Simulation Model for a Single Point Moored Tanker*. Delft: Delft University of Technology.

Appendix A: Physical Modelling Procedure

The stiffness of the mooring system has a significant effect on the resulting ship motions. The vessel, together with the mooring lines, behaves like a mass-spring system, which resonates if the system frequency reaches the natural frequency. The natural surge period of a moored vessel ranges from 30 seconds to a few minutes. This range is almost the same for natural periods

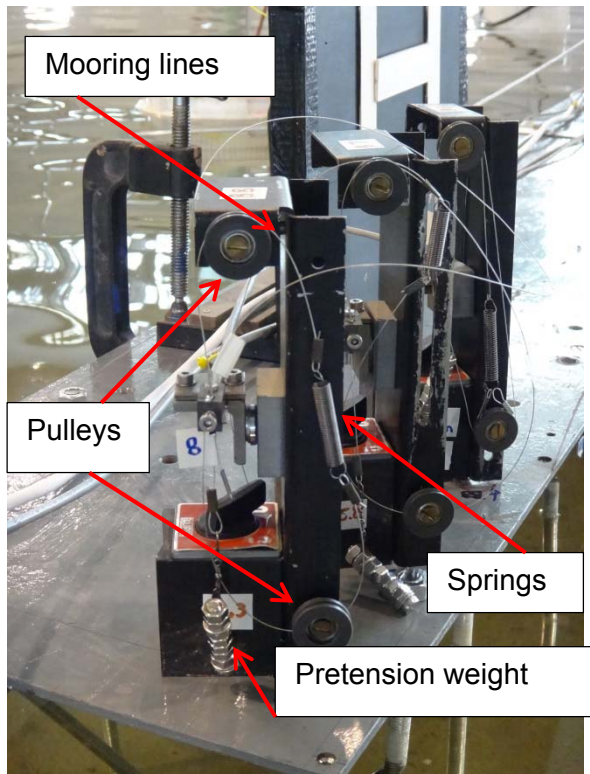


Figure 45: Mooring system

occurring in a small harbour basin. Therefore, it is important to determine the wave period at berth and ascertain whether it is close to the natural period of the moored ship (van der Molen W. , 2006 (a)).

Figure 45 illustrates how the mooring lines are modelled in the physical modelling process. Each mooring line consists of a nylon coated cable connected to a spring and a small pre-tensioning weight. Each spring represents the stiffness of the relevant mooring line. The mooring line runs from the fairlead point on the vessel to a pulley situated at the bottom of the bollard, through to another pulley at the top of the bollard. The spring is positioned between the two pulleys. The weight dangles freely on the other side of the spring to account for the effect

of the natural pre-tension in the mooring lines of a ship at berth, which serves to keep the ship stable.

During the set-up of the mooring lines, the springs need to be chosen/cut/manufactured to fit the prototype stiffness used to represent the mooring line stiffness. Figure 46 illustrates the procedure used to test the spring stiffness. The stiffness is measured by attaching a weight to the spring, noting the displacement and then dividing the specific weight by the displacement the spring produces. This is done for a series of increasing weights and the average is subsequently calculated. This value is compared to the prototype line stiffness and if sufficient, the spring may be used. The stiffness of each mooring line differs because each line has a different length. This is important to take note of. When the mooring lines are modelled numerically, the stiffness in them needs to be represented correctly. Therefore, each spring was calibrated to the relevant prototype mooring line stiffness.

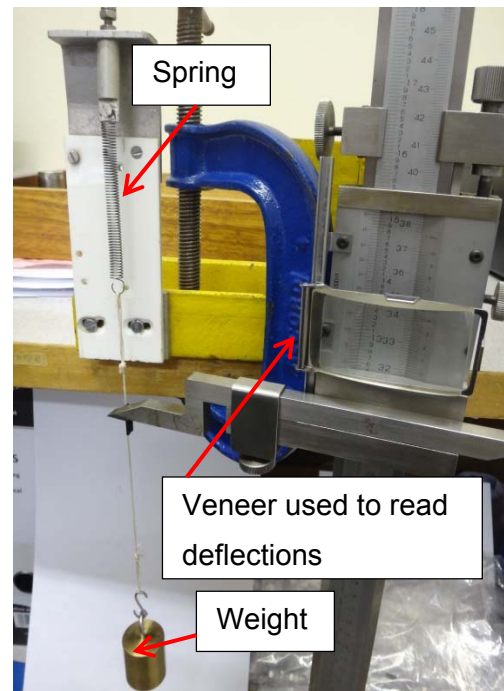


Figure 46: Testing spring stiffness

The object used to connect the pulleys with the mooring line and with a strain gauge is called a “bollard”. The bollard is fixed at its allocated position and keeps the vessel stable by means of mooring lines. Although the bollard in the physical modelling process looks nothing like a real bollard, it serves the same function.



Figure 47: Bollard-pulley-mooring-line system

For the calibration of the bollard, the set-up process needs to be complete. This means that the mooring line, spring, pre-tension weight, and bollards must already be in place. Figure 47 shows the bollard-pulley-mooring-line system. Note the strain gauges and wiring attached to each bollard. The strain gauge needs to be connected to the computer by wiring. It is important to understand that the strain gauges (representing the force in the mooring lines) do not measure force, but voltage. When an external

force is placed on the mooring line, the connected strain gauge measures the voltage. This is done for a series of forces (by applying different weights to deflect the mooring lines) in order to determine the relationship between the voltage and the applied force represented by the weight (force = mass x acceleration). As a result, a force range representing certain voltages is

obtained. Whenever a voltage is measured, a force is available representing that voltage, thus the force is imposed on the mooring lines. The bollards have now been calibrated by means of determining forces from voltage measurements. This bollard calibration procedure accounts for the friction exerted on the pulleys. For explanatory purposes, this paper will henceforth refer to the strain gauges measuring a force, even though they actually measure a voltage.

A fender was represented by a spring steel plate connected to a Teflon bud which presses against the vessel as it moves. As in the case of the bollards, a strain gauge was fixed to the spring steel plate to measure the voltage when it deflects. To calibrate the fenders, more or less the same procedure followed for the bollards applies. The fenders were calibrated to the provided prototype values. The prototype fender used was a specific Super Cone fender. The generic performance of the fenders was obtained from the Fentek Marine Fendering System Manual. Because the fenders are modelled linearly, the linear relationship between the deflection and the reaction force was calculated from the generic performance curve. This linear relationship is later used in QUAYSIM to represent the stiffness of the fenders numerically. Figure 48 shows the linear relationship obtained for the fenders. All fenders were calibrated to the stiffness represented by the linear line.

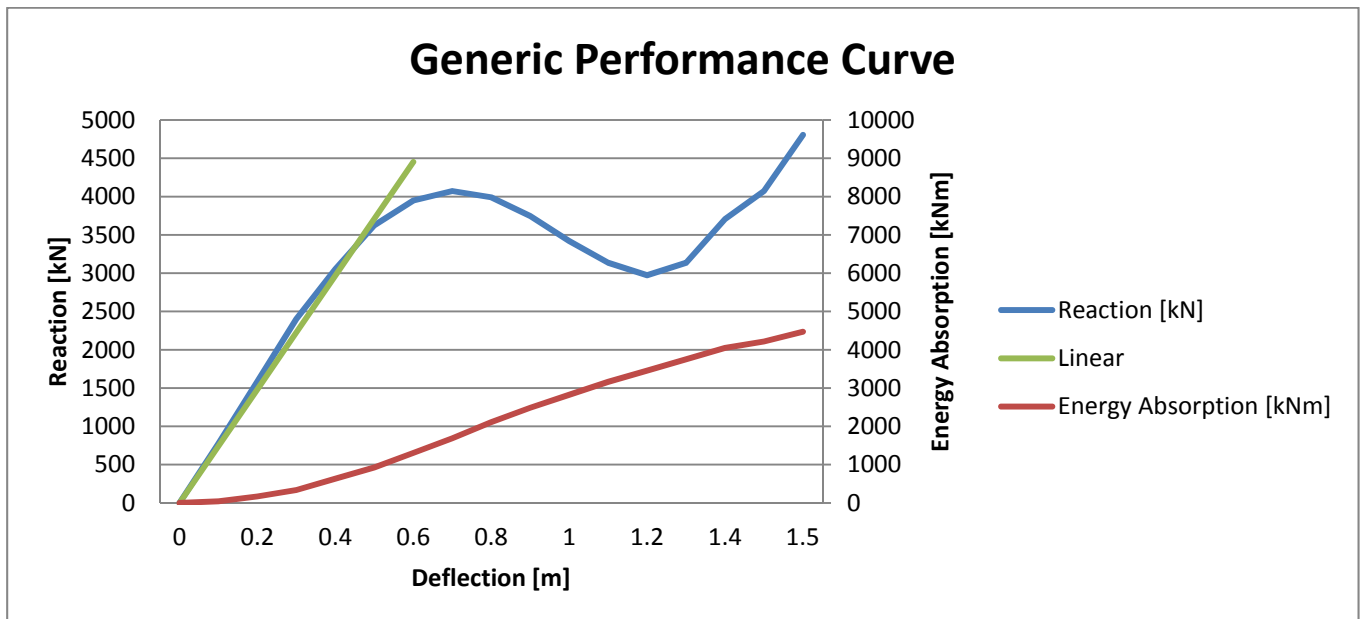


Figure 48: Generic performance curve of a super cone fender

Figure 49 shows how the stiffness was tested in the case of each fender. Firstly, the fender was fixed on the one end of the spring steel plate, with the bud exposed on the other end. A series of weights were connected to the bud, which caused the spring steel plate to deflect. The deflection was measured and the stiffness was calculated by dividing the deflection by the weight. The stiffness was then compared to the prototype stiffness and if sufficient, the fender was used. This was done for eight fenders. Three of the eight fenders were dummy fenders which did not touch the vessel at mid-ships. These fenders were fenders 1, 2, and 8.

The calibration procedure involved connecting the strain gauge to the computer and measuring the voltage readings when weights were placed on the fenders. The same procedure follows for calculating the forces representing the voltages, by obtaining a linear relationship between the voltages and the weights applied to the fenders. For the various different weights applied, a range of voltages were measured. The linear relationship between the voltage and applied weights subsequently provides a range of forces ($F = ma$) available for the respective voltages. Fender stiffness was now calculated by means of dividing the reaction by the deflection. The calibration of the fenders was thus completed by obtaining the same stiffness as the prototype stiffness (i.e. the gradient of the linear relationship on the performance curve).

The data software used to record the mooring line and fender forces is called "CatmanEasy". The data was stored in an ASCII format and was further analysed with Matlab to plot the force readings. The output file was scaled to prototype values.



Figure 49: Fender calibration

Appendix B: Calibrating a Ship

During the first stages, the cradle (cf. Figure 50) needs to be checked and calibrated to determine



Figure 50: Cradle used for calibration procedures

the longitudinal moment of inertia (pitch) and the radius of gyration (k_{yy}). These values (pitch and k_{yy} from the cradle) are required to determine the calibration factors of the ship. These calibration factors are obtained by applying the swinging and displacement test, discussed below. The cradle needs to be levelled, thus care should be taken to place it on level ground (cf. Figure 51). Note how the water meter is not placed on the swing, but on the cradle frame. The swing is always level, because it will automatically be levelled due to gravitational forces. Note how the frame is checked to be level in both directions in Figure 51.



Figure 51: Levelling of the cradle

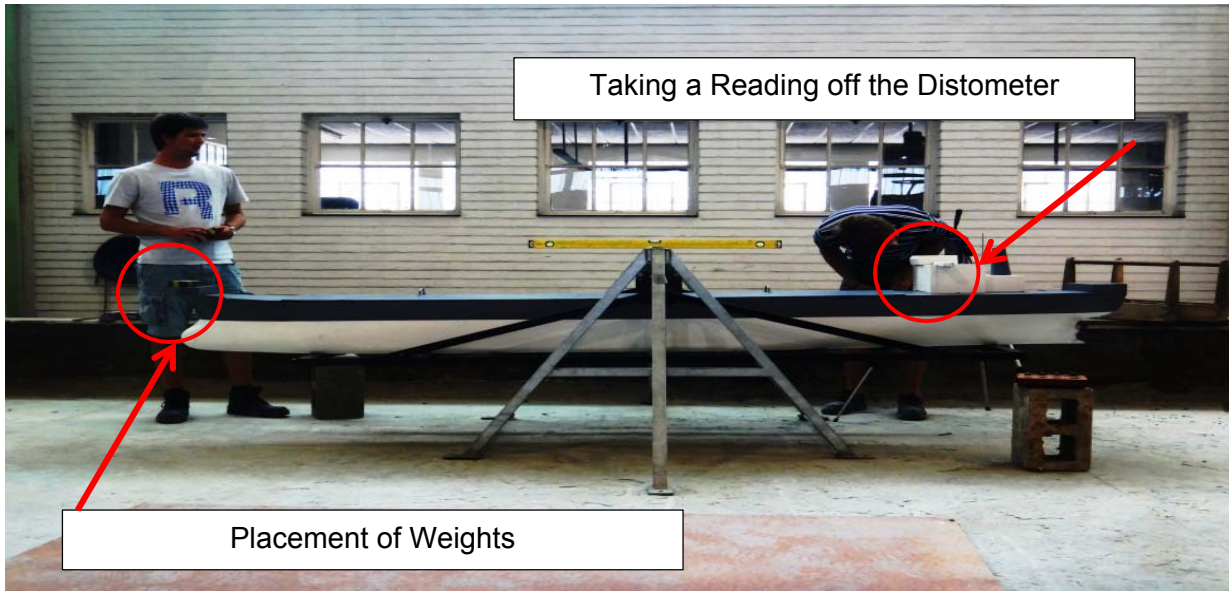


Figure 52: Displacement test

The next step involves placing the ship (an empty vessel) in the cradle. The displacement test (used to determine the centre of gravity) and the swinging test (used to determine the period and radius of gyration used to calculate the longitudinal moment of inertia) are applied. Figure 52 shows the set-up needed to carry out the displacement test, which allows one to obtain the vertical position of the centre of gravity.

For the displacement test, weights are placed at the end of the vessel and the vertical displacements are measured by use of a distometer (cf. Figure 52). The distometer is a device used to read off displacements accurately.



Figure 53: Swinging test

When the swinging test is applied, the period is measured for a fixed number of free oscillations and used to calculate the longitudinal moment of inertia (pitch). The cradle should oscillate through a certain fixed point to effectively count the number of oscillations. A ruler is placed to act as a reference point through which the cradle should oscillate (cf. Figure 53). The swinging test is viable because the vessel (loaded/unloaded) can easily swing with the cradle, with little friction caused as a result.

The same tests done in the case of an empty model ship are applied to the loaded model ship. The model vessel is loaded with small lead blocks to achieve the same DWT as the given prototype. The blocks should be placed in the hull of the ship to obtain the prescribed moment of inertia of the prototype. When the loaded ship is balanced on the cradle, the loaded centre of gravity is determined by shifting the ship horizontally on the

cradle until it is perfectly balanced. These cradle results are subtracted from the loaded vessel results to obtain the proper values for the centre of gravity and longitudinal moment of inertia (pitch). The moment of inertia for yaw is assumed to be equal to the pitch.

To conclude, the four tests used in the calibration of a model ship are:

1. Swinging + displacement test for the cradle
2. Swinging + displacement test for the empty vessel on the cradle
3. Swinging + displacement test for the loaded vessel on the cradle
4. Swinging + displacement test for the loaded vessel in the water

Problems encountered during the third test involved lifting the vertical centre of gravity. The vertical centre of gravity originally obtained was not sufficient when compared to the prototype values. The team had to think of ways in which the vertical centre of gravity could be lifted. The solution was to place lightweight material in the hull of the ship, below the lead blocks. Figure 54 illustrates the ceiling material and hardboard placed in the hull of the ship.



Figure 54: Lifting the centre of gravity

The fourth test used for the calibration of a model ship involves placing the loaded model vessel in a basin filled with water. The water depth should be equal to the water depth in which the vessel will be berthed in the physical model basin. A walkway is needed to operate the tests, as there should be no additional disturbances in the water. This test determines the transverse moment of inertia by measuring the period for a fixed number of free oscillations. This period is used to calculate the transverse moment of inertia (roll) and transverse radius of gyration (K_{xx}).

Appendix C: Physical Modelling, Fender and Mooring Line Force Correlation

C1: Test 01

Table 18: Test 01, mooring line- and fender-force correlation

Mooring Lines			Fender Forces		
	Strain Gauge Output	Keogram Output		Strain Gauge Output	Keogram Output
M1	422	407	F1		
M2	414	423	F2		
M3	487	449	F3	1417	1157
M4	563	566	F4	1083	827
M5	419	425	F5	1864	1360
M6	566	514	F6	1774	1331
M7	519	498	F7	2885	1274
M8	413	436	F8		

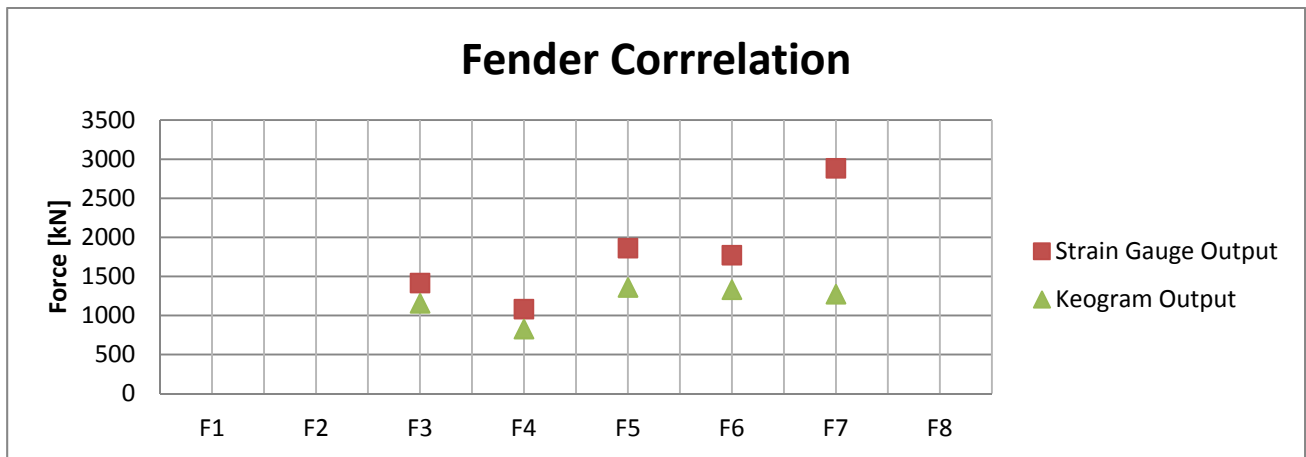


Figure 55: Test 01, graphical representation of fender-force correlation

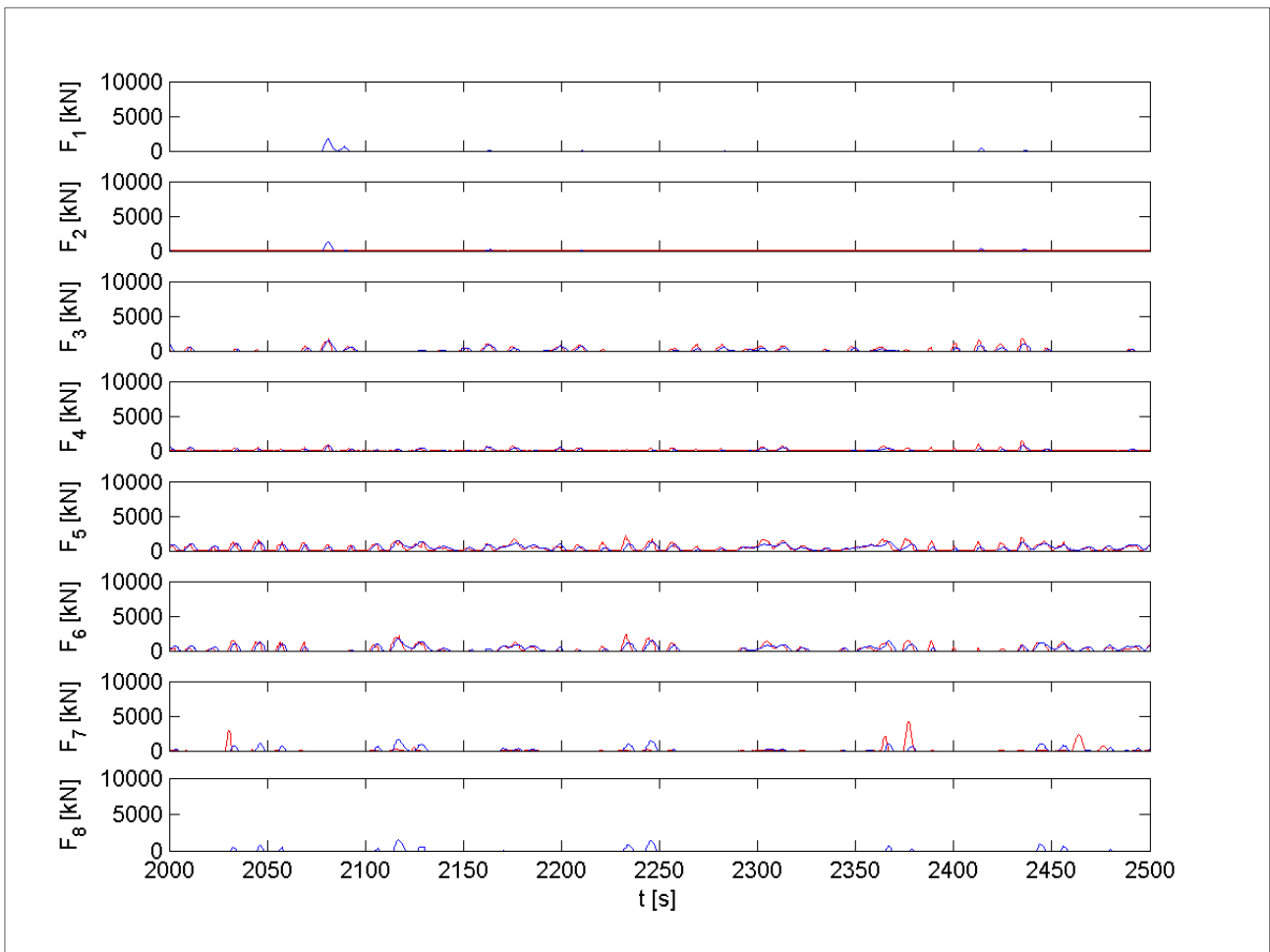


Figure 56: Test 01, strain gauge vs Keogram force measurements, fenders

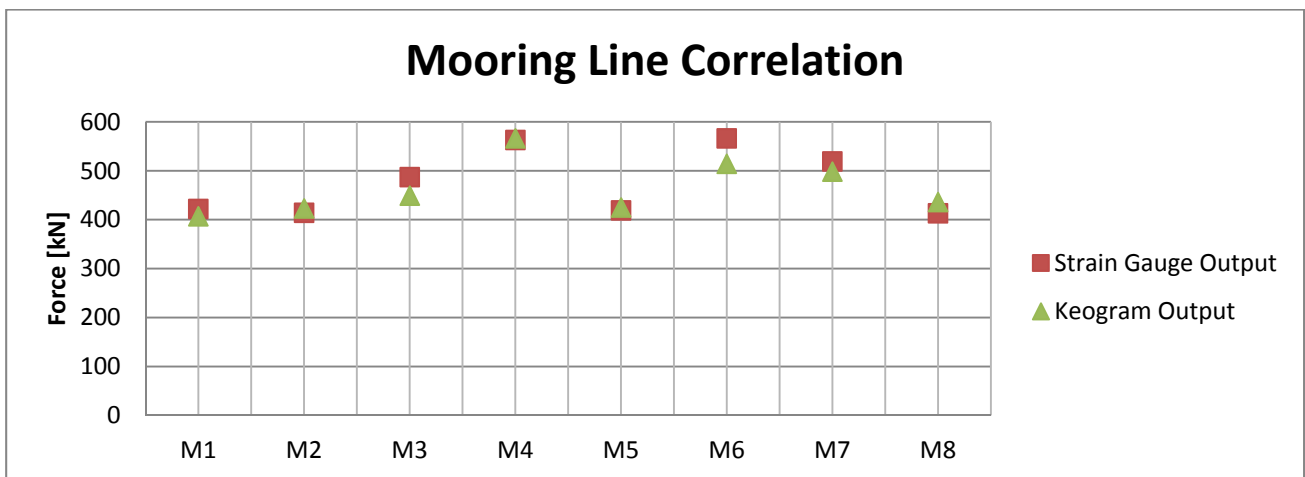


Figure 57: Test 01, graphical representation of mooring-line-force correlation

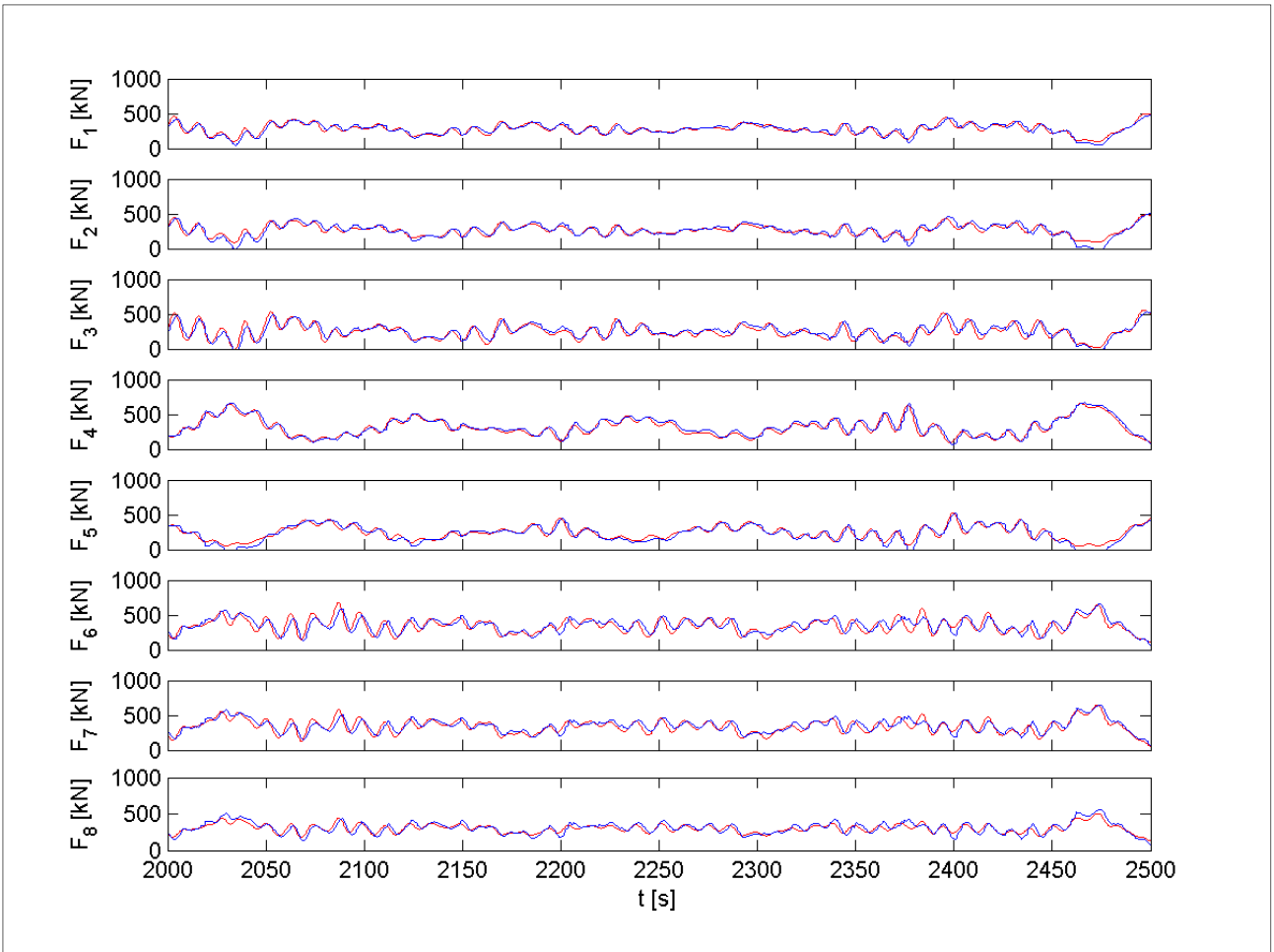


Figure 58: Test 01, strain gauge vs Keogram force measurements, mooring lines

C2: Test 02

Table 19: Test 02, mooring line- and fender-force correlation

Mooring Lines			Fender Forces		
	Strain Gauge Output	Keogram Output		Strain Gauge Output	Keogram Output
M1	363	355	F1		
M2	348	351	F2		
M3	378	367	F3	795	624
M4	418	416	F4	658	452
M5	350	348	F5	1334	898
M6	370	356	F6	1042	726
M7	342	333	F7	79	523
M8	326	336	F8		

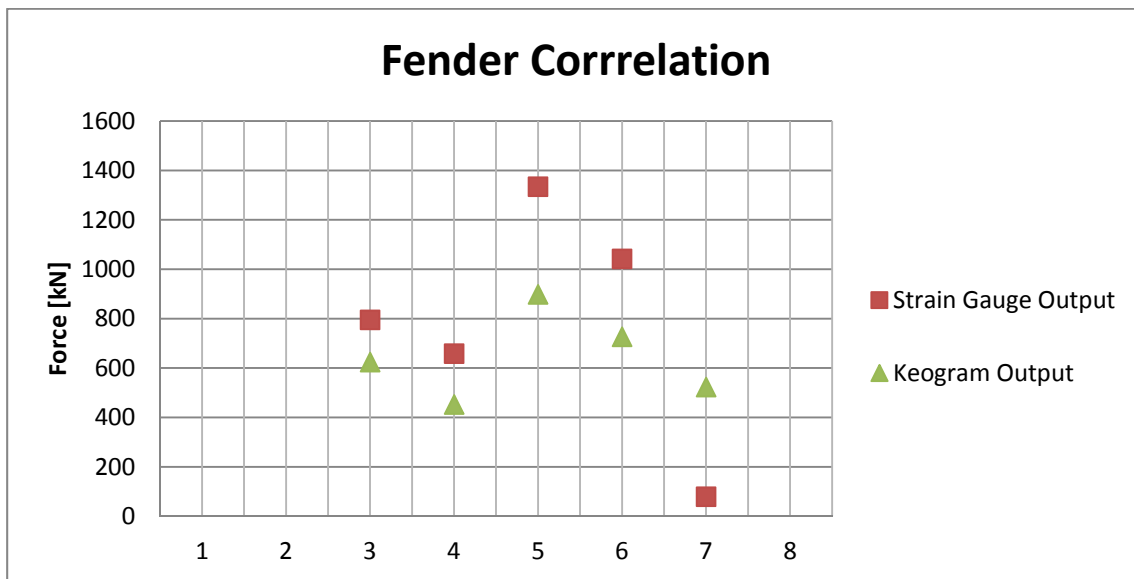


Figure 59: Test 02, graphical representation of fender-force correlation

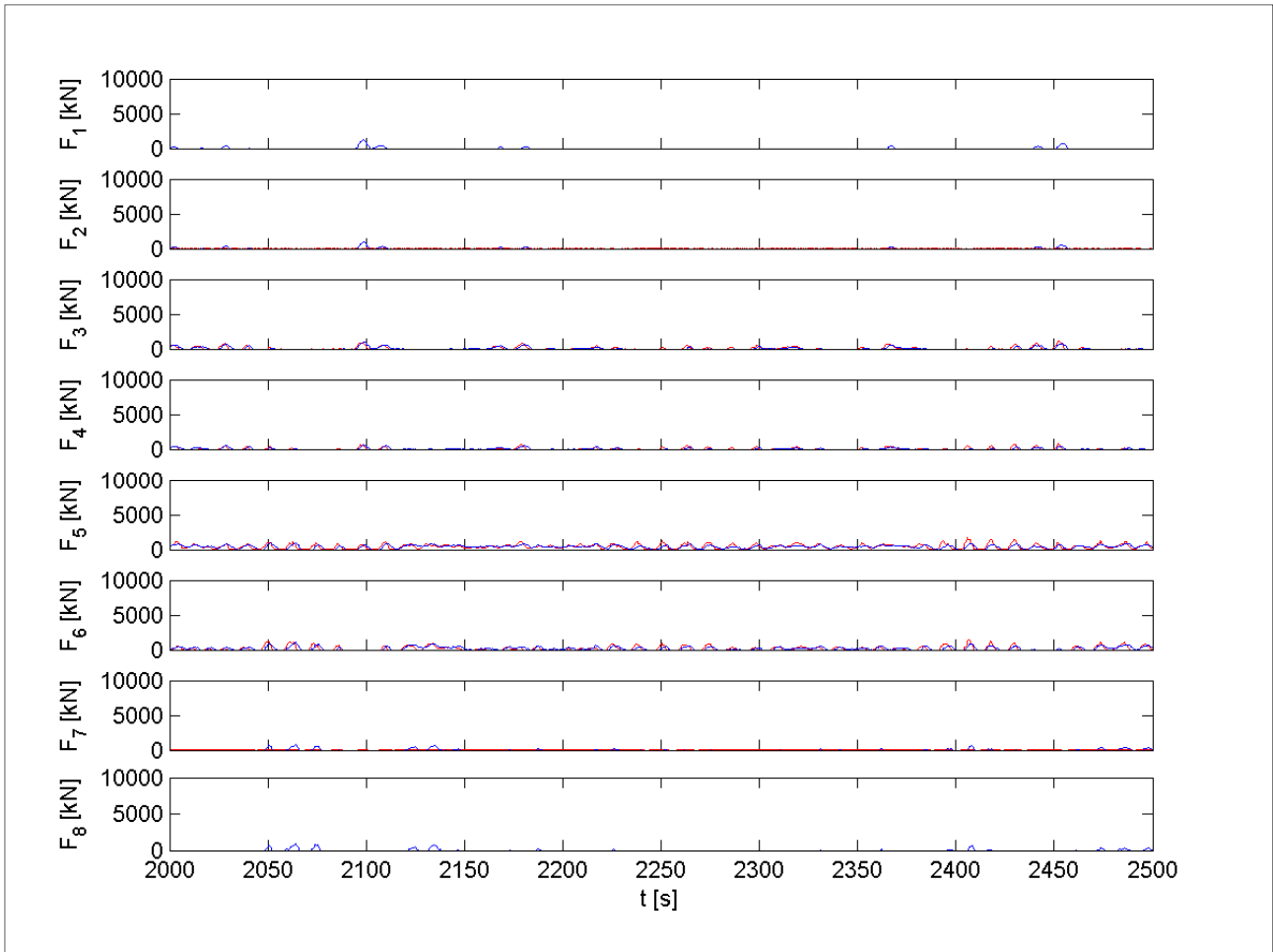


Figure 60: Test 02, strain gauge vs Keogram force measurements, fenders

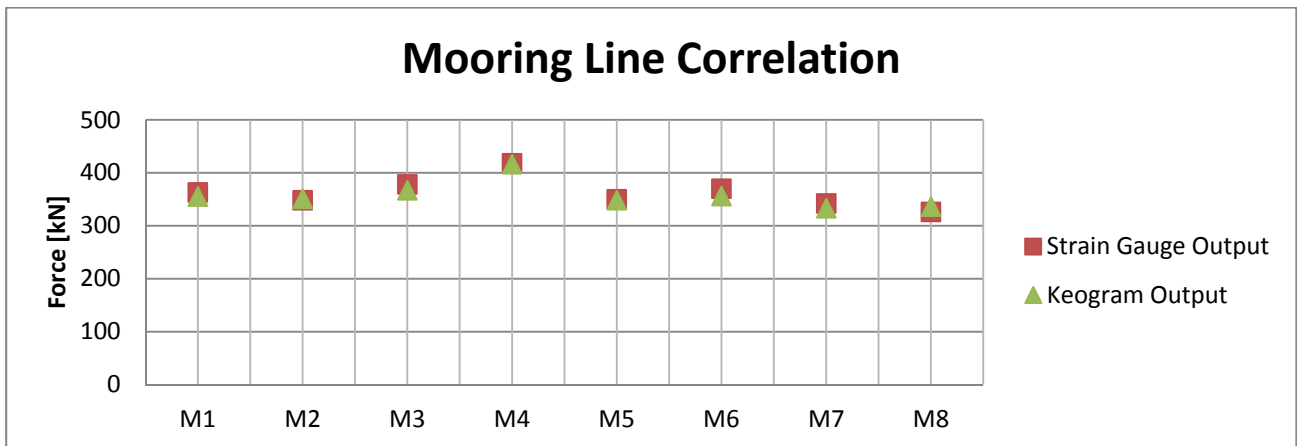


Figure 61: Test 02, graphical representation of mooring-line-force correlation

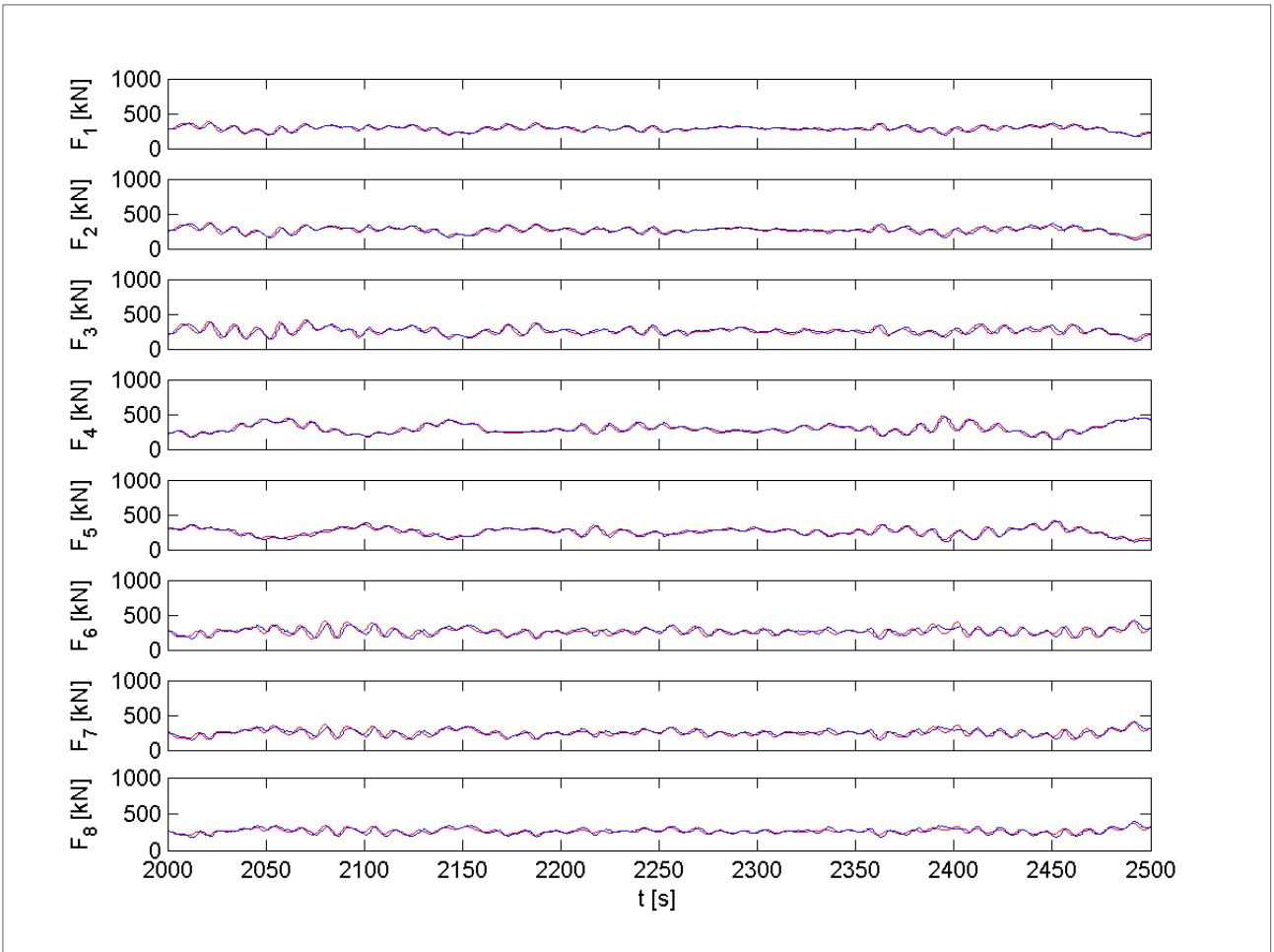


Figure 62: Test 02, strain gauge vs Keogram force measurements, mooring lines

C3: Test 03

Table 20: Test 03, mooring line- and fender-force correlation

Mooring Lines			Fender Forces		
	Strain Gauge Output	Keogram Output		Strain Gauge Output	Keogram Output
M1	529	507	F1		
M2	520	523	F2		
M3	700	647	F3	2209	1922
M4	660	639	F4	1535	1269
M5	470	473	F5	2063	1586
M6	627	606	F6	1922	1528
M7	626	604	F7	1730	1403
M8	437	460	F8		

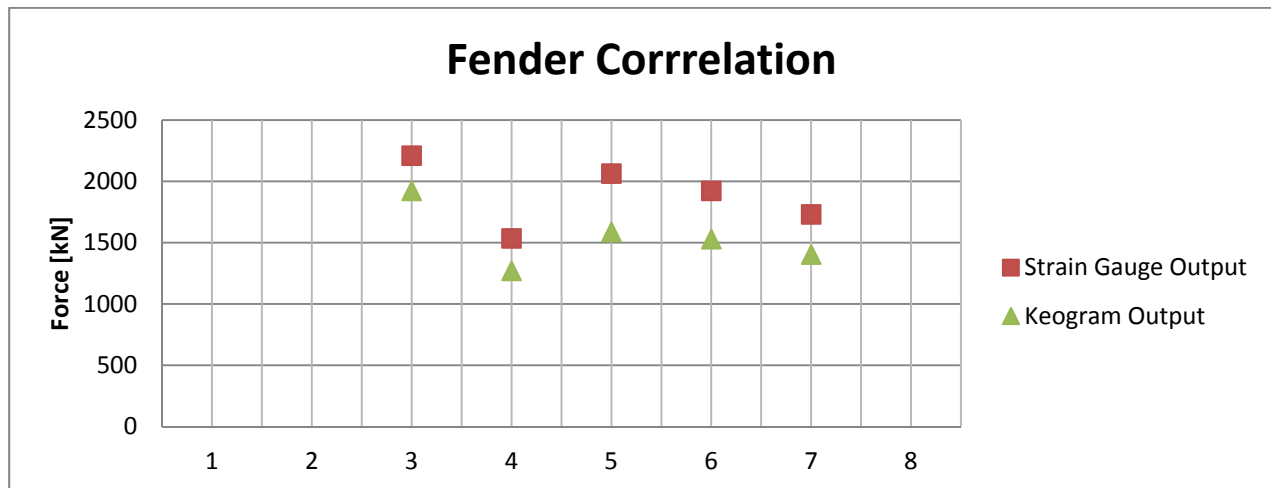


Figure 63: Test 03, graphical representation of fender-force correlation

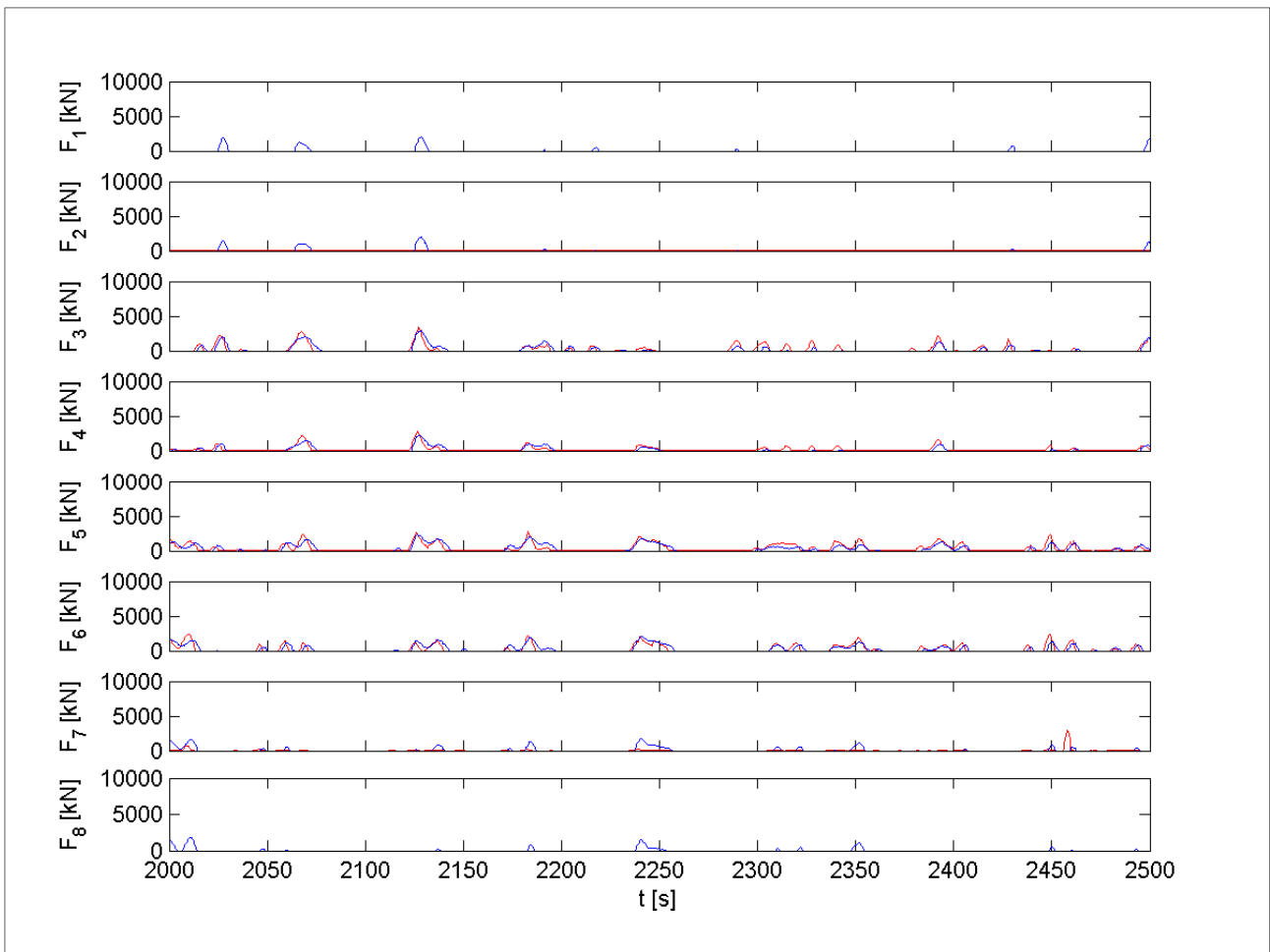


Figure 64: Test 03, strain gauge vs Keogram force measurements, fenders

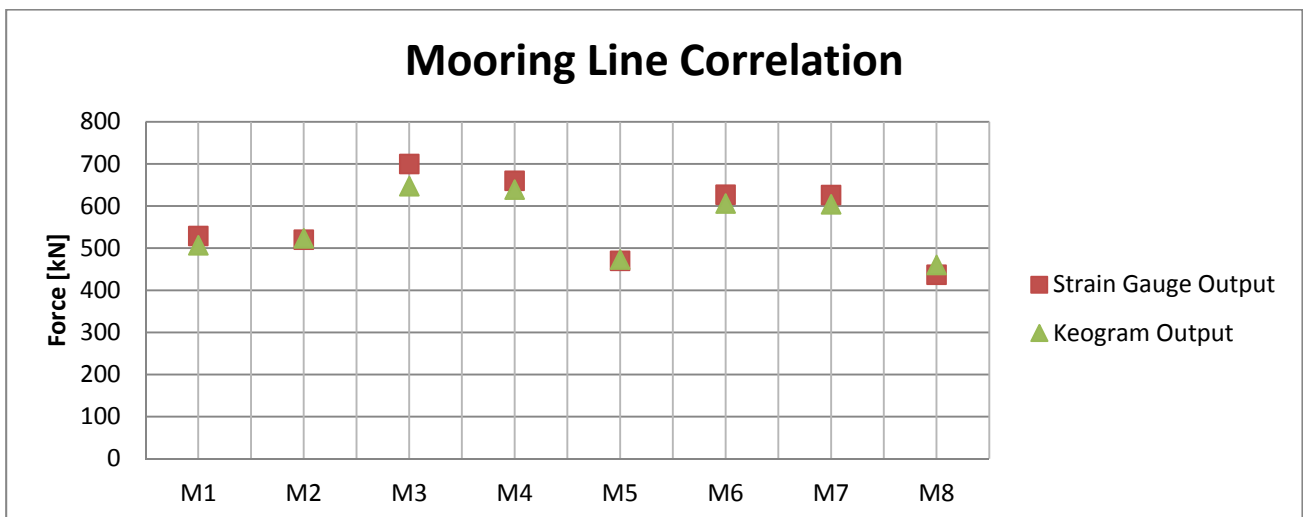


Figure 65: Test 03, graphical representation of mooring-line-force correlation

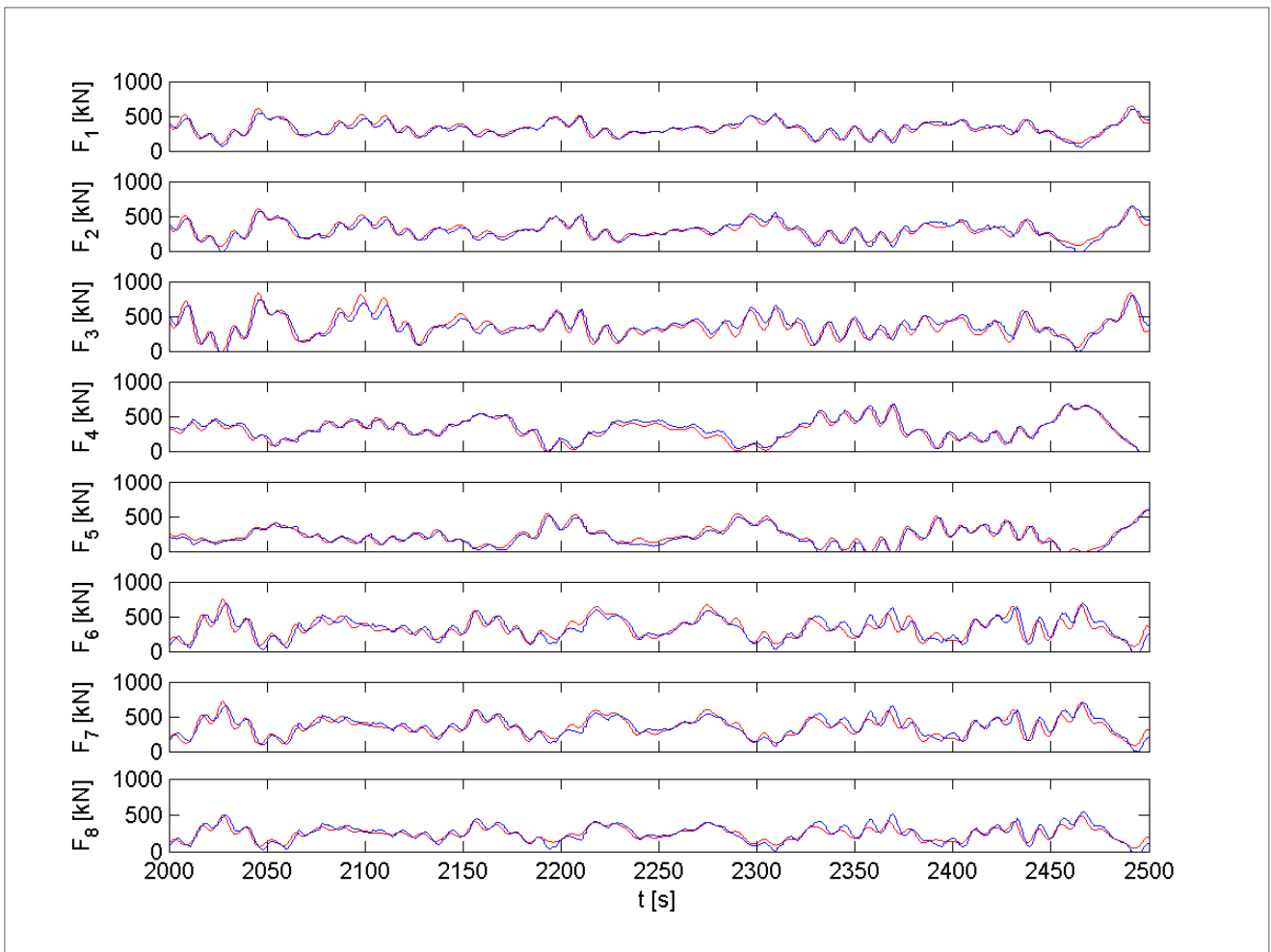


Figure 66: Test 03, strain gauge vs Keogram force measurements, mooring lines

C4: Test 04

Table 21: Test 04, mooring line- and fender-force correlation

Mooring Lines			Fender Forces		
	Strain Gauge Output	Keogram Output		Strain Gauge Output	Keogram Output
M1	361	348	F1		
M2	365	362	F2		
M3	421	401	F3	1118	837
M4	371	370	F4	691	499
M5	315	305	F5	1249	877
M6	389	374	F6	813	619
M7	399	387	F7	72	475
M8	309	319	F8		

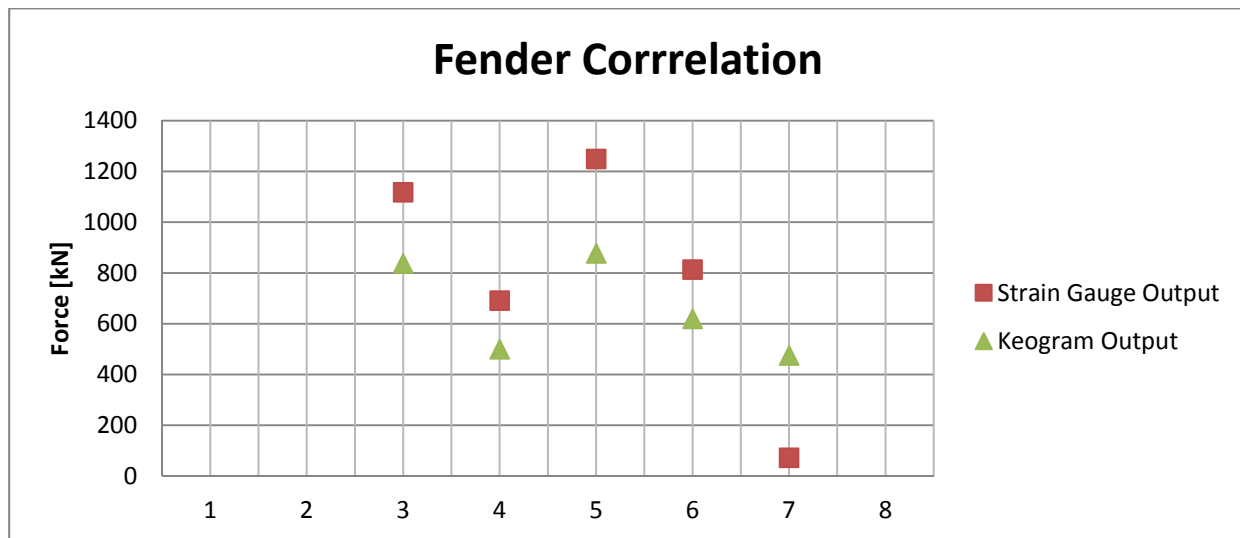


Figure 67: Test 03, graphical representation of fender-force correlation

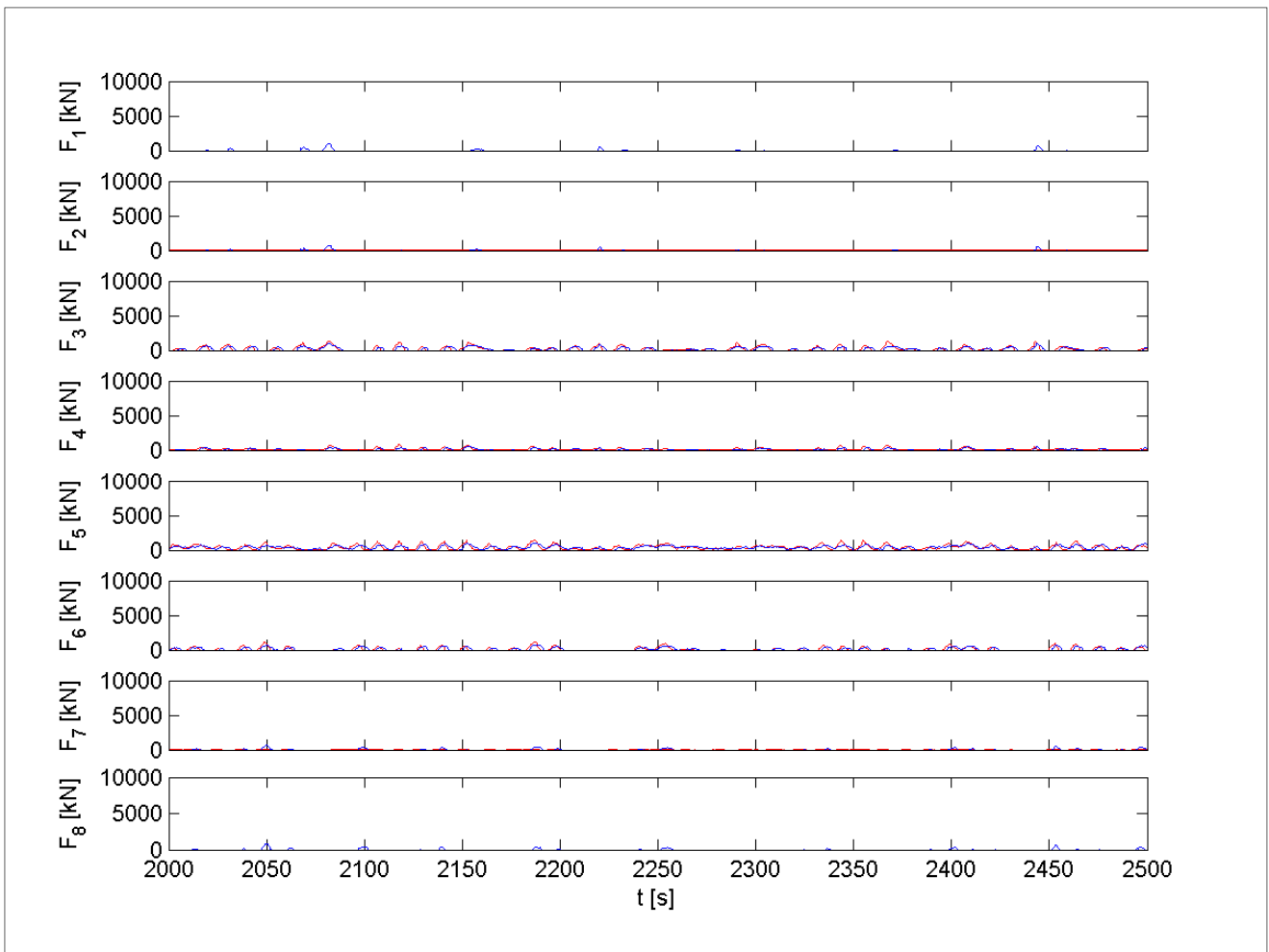


Figure 68: Test 04, strain gauge vs Keogram force measurements, fenders

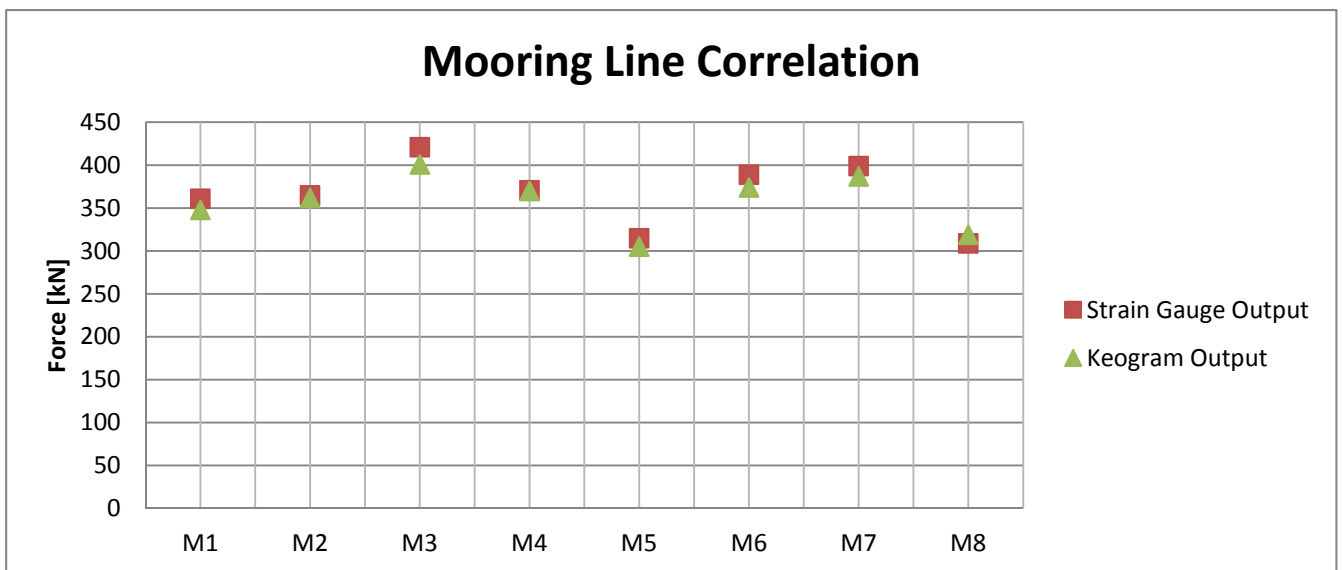


Figure 69: Test 04, graphical representation of mooring-line-force correlation

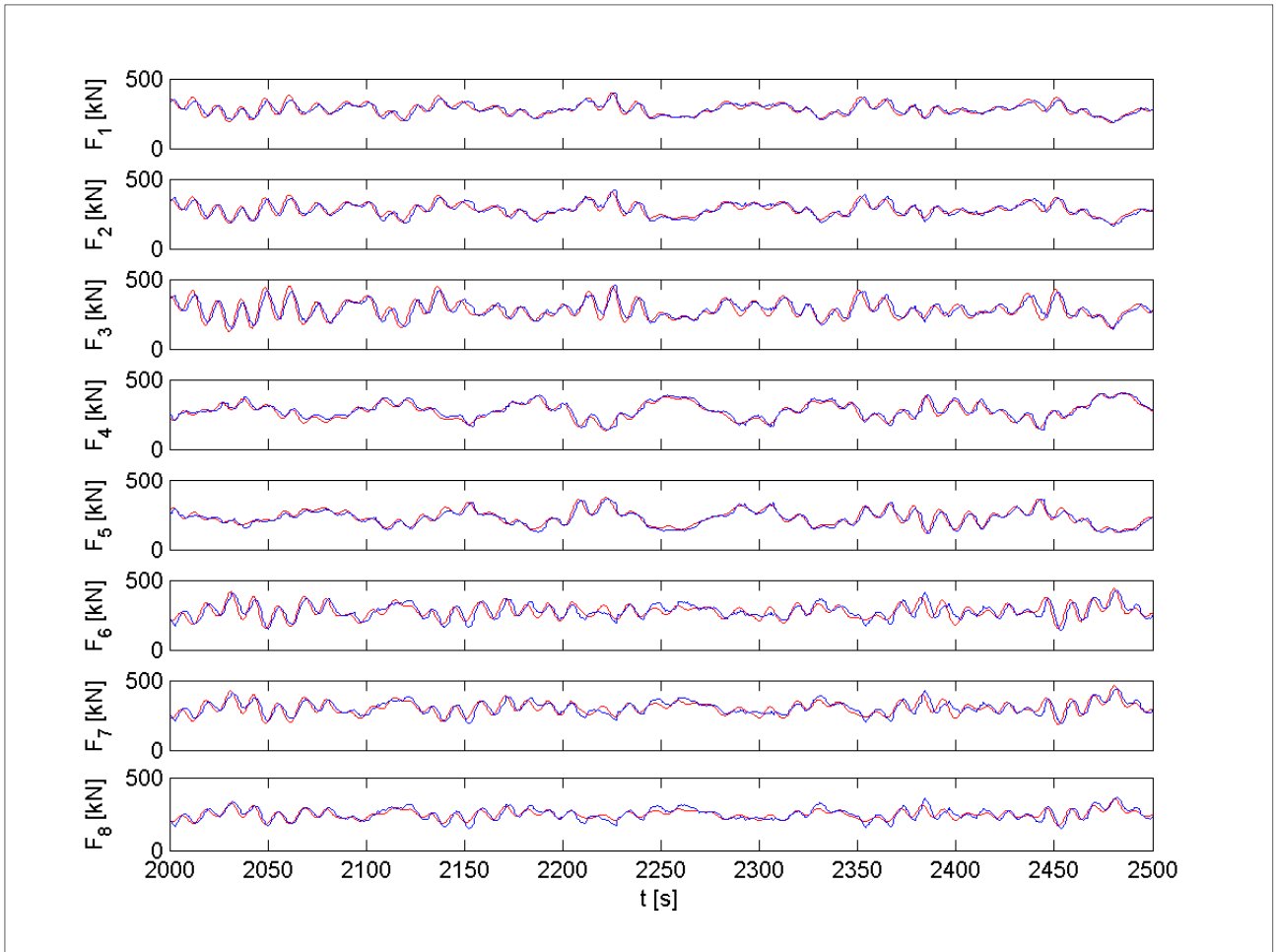


Figure 70: Test 04, strain gauge vs Keogram force measurements, mooring lines

Appendix D: Practical Realities of the Physical Modelling Process

The physical modelling process requires patience and time. A physical model cannot be rushed, as this is where mistakes can occur. In reality, the mistakes that occur are the reason why the modelling process is so time intensive. Having such a large physical model made this thesis even more time intensive, as one is consistently dependent on the physical modelling team. The experience and expertise of each member contributes largely to the project and a given person is not always replaceable. If too many errors occur and the project time was underestimated, the researcher becomes increasingly pressured for time. Nonetheless, the team is only available during working hours and the practice of attempting to run tests throughout the night is not a wise decision as fatigue is likely to negatively impact on the accuracy of the physical modelling process.

By analysing the physical modelling results, one can see in some cases where the equipment might have been off and should have been adjusted. To recognize this, experience in physical modelling is of great significance. Most of the time, different results as to what one might expect were achieved, in which an investigation was required to find the cause of these results.

Experience in the physical modelling process is the key to success. Lack of experience widely contributes to failure and incorrect results. Lack of experience also increases dependence on experienced staff within the laboratory, which in turn again contributes to project and time delays.

Another potential error factor is the influence of humanity. This was a large project with a large number of hands on deck. Humanity is prone to errors such as reading errors from a scale veneer, or pressing the wrong button on the computer. It is difficult to be in control of all of these aspects when having a large team. By reading the physical modelling process chapter and the calibration procedures, one can just imagine the vast effect of the smallest change and the tediousness of the whole procedure.

In a project of this nature and scale, it is standard practice to carry out the numerical modelling process in parallel to the physical modelling process. The learning processes involved in both models are extremely intensive, thus experience in both fields is of immense value. Usually, two different sets of teams are used for the two different modelling processes. In this way, the comparisons can be made quicker and mistakes can also be identified when the models do not compare well. This enables the modeller to fix these mistakes whilst still carrying out the physical modelling process. In cases where the numerical modelling process happens after the physical modelling, it is not always possible to go back to the laboratory as it may be in use for another project or the model may have been deconstructed. Having long waiting periods during which the physical model rests in the basin also risks the accurate calibration of the equipment used for testing. Having to recalibrate all the equipment would waste much time. In this study, the modelling

process was not carried out in parallel with one another. This should be attempted for further studies to eliminate mistakes.

All of these issues need to be mentioned to the modeller in advance before they take on a large project such as this one. Intensive project planning and time management is required, allowing time for mistakes and for modelling both types of models. A set team needs to be assigned to the project until the goals have been reached. This is often not possible, unless the project is funded. To have a large project team available would enable more tests to be run, more experience to be utilised and therefore greater accuracy during both modelling procedures.

Appendix E: Swan Computation Results

E1: Test 01

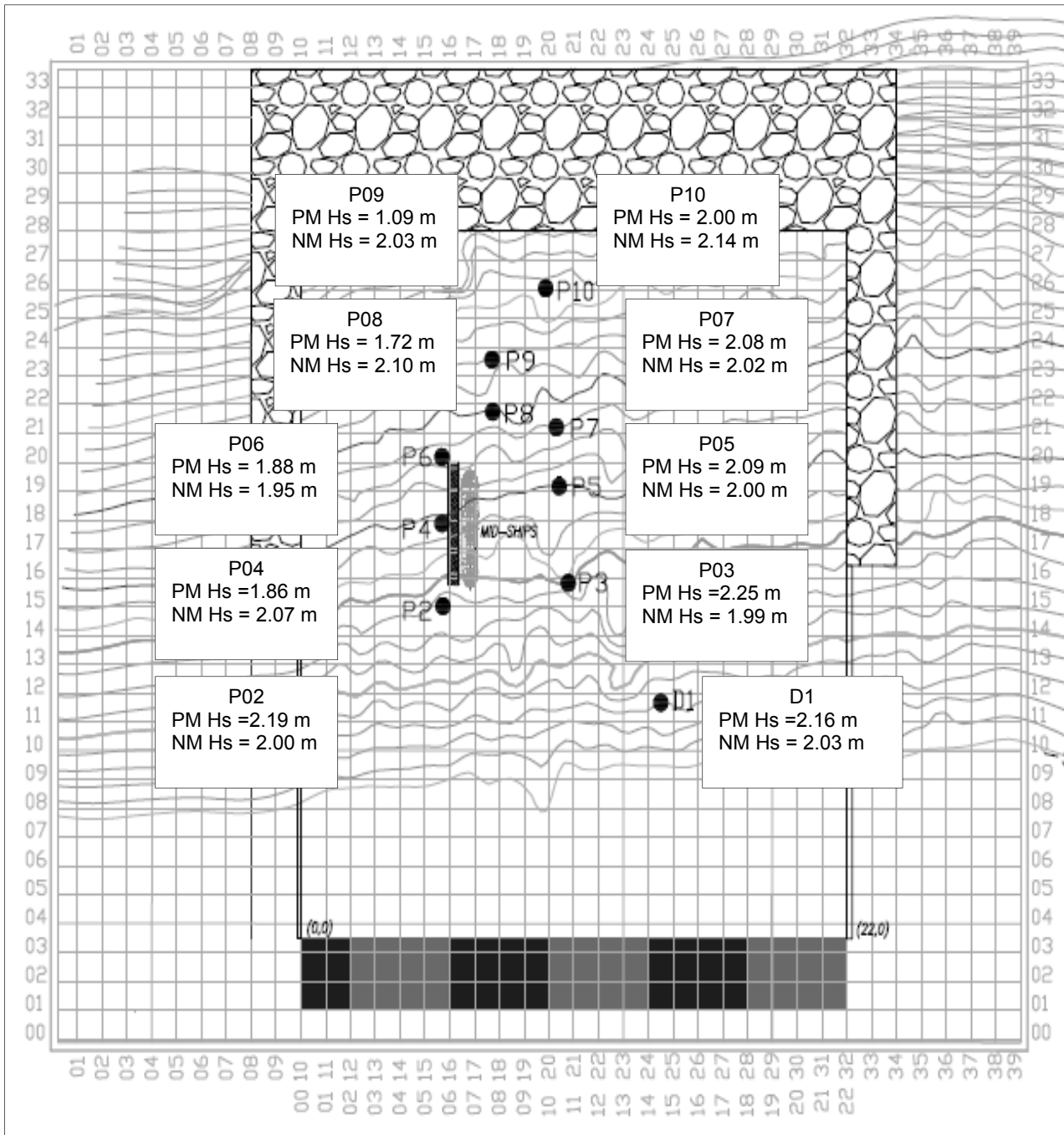


Figure 71: Test 01, physical model high frequency wave heights vs numerical model high frequency wave heights

E2: Test 02

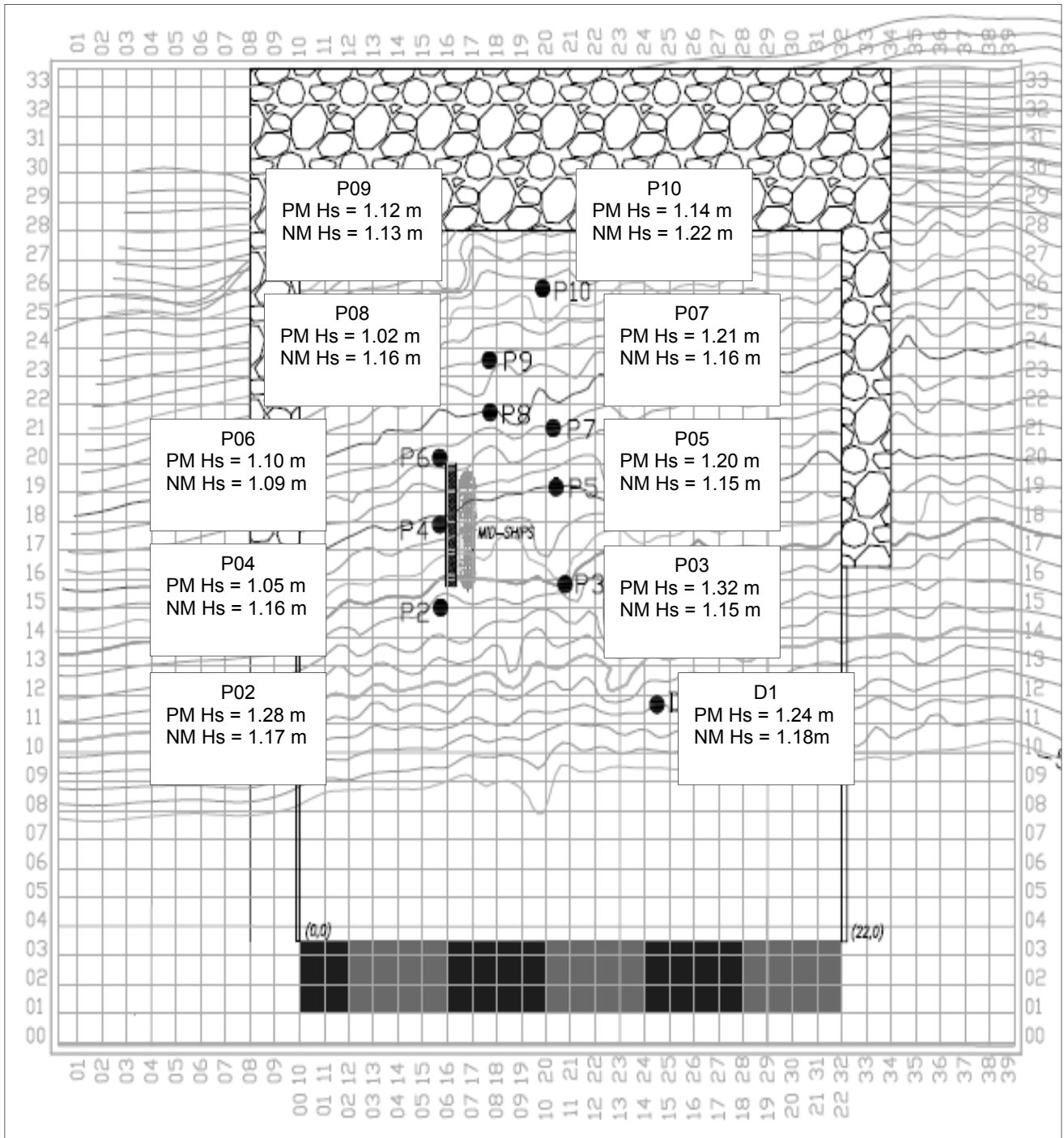


Figure 72: Test 03, physical model high frequency wave heights vs numerical model high frequency wave heights

E3: Test 03

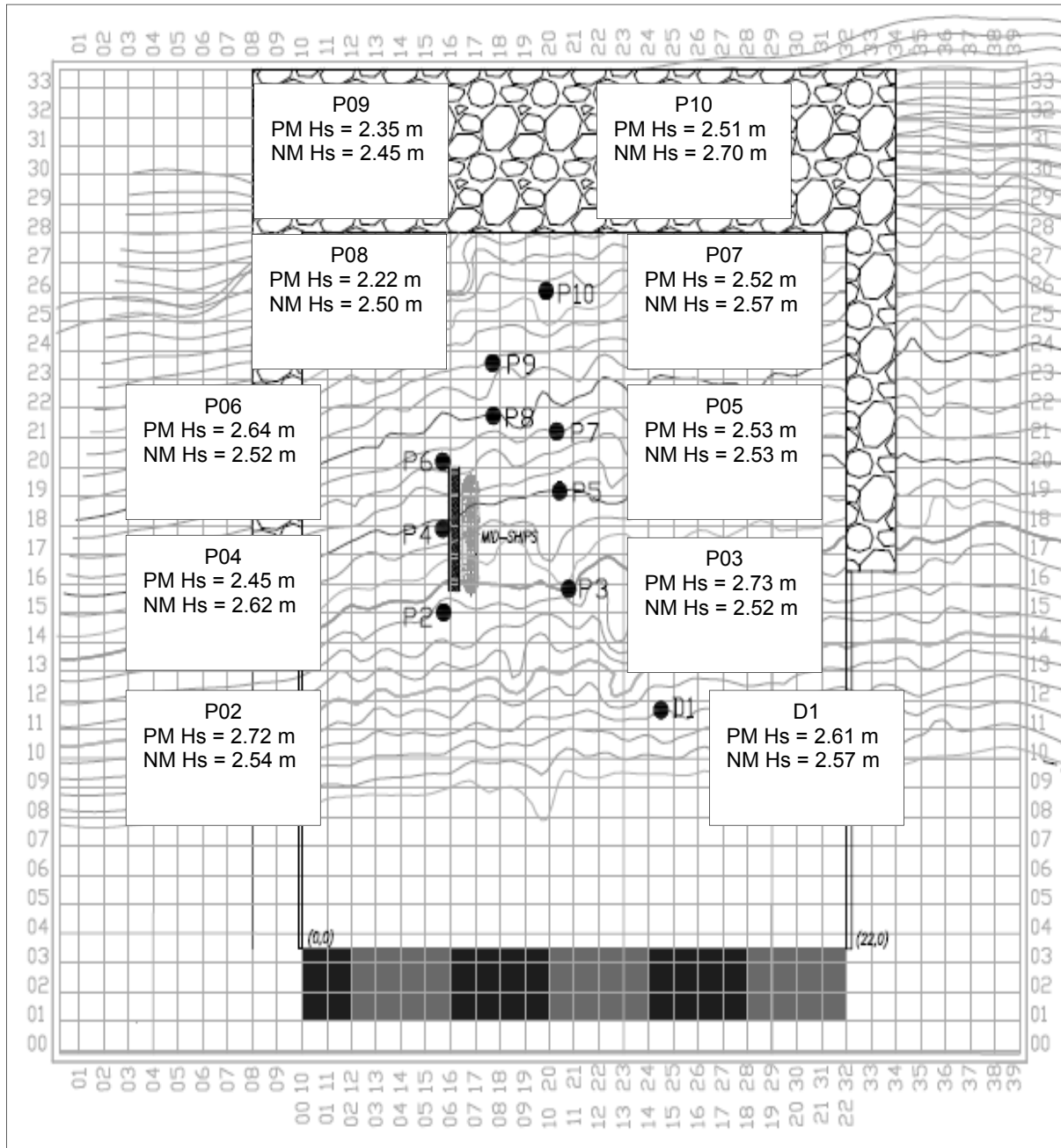


Figure 73: Test 03, physical model high frequency wave heights vs numerical model high frequency wave heights

E4: Test 04

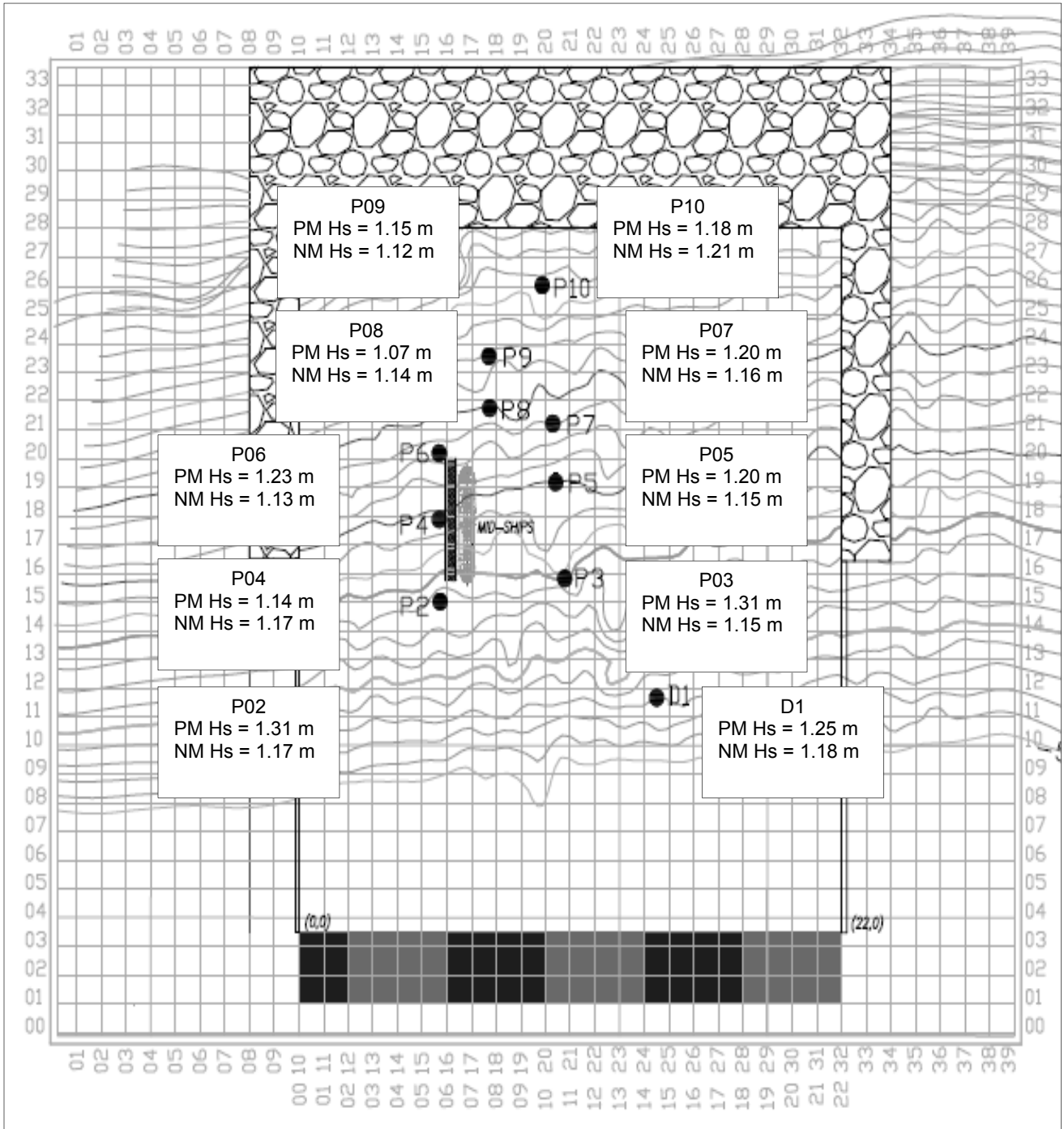


Figure 74: Test 04, physical model high frequency wave heights vs numerical model high frequency wave heights

Appendix F: SURFBEAT Correlation

F1: Test 01

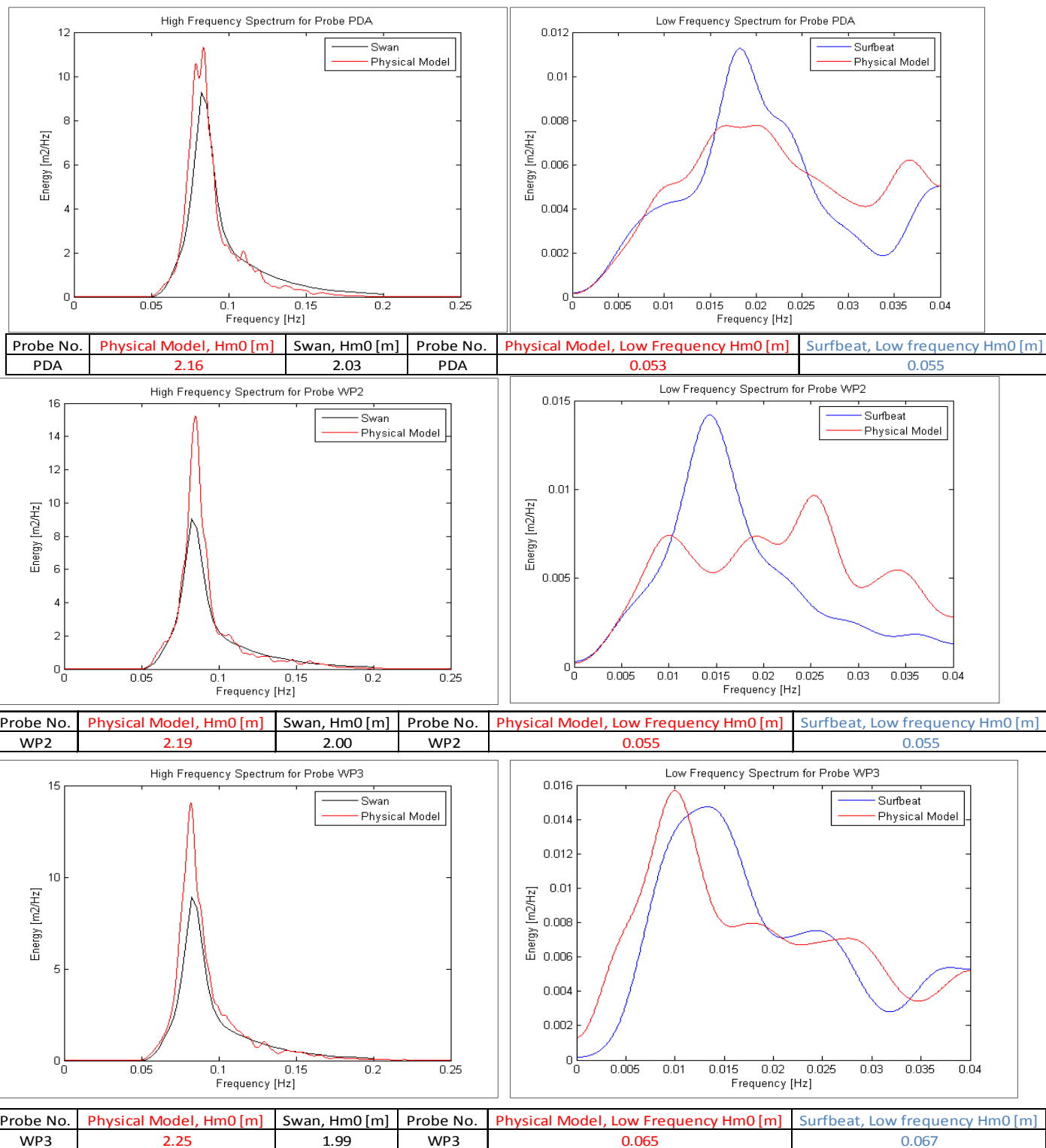
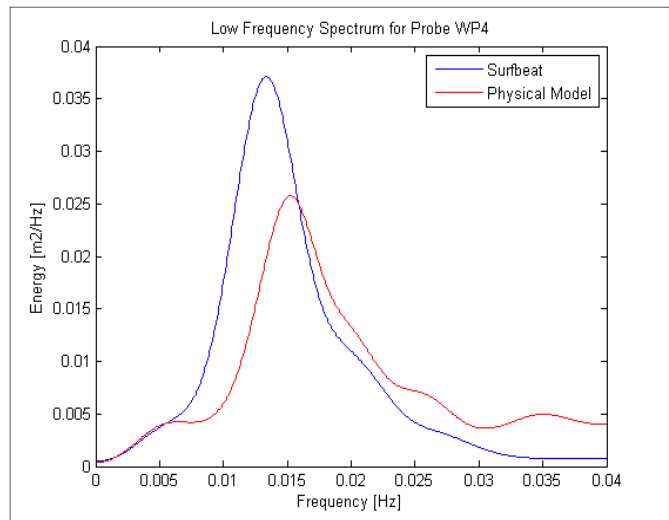
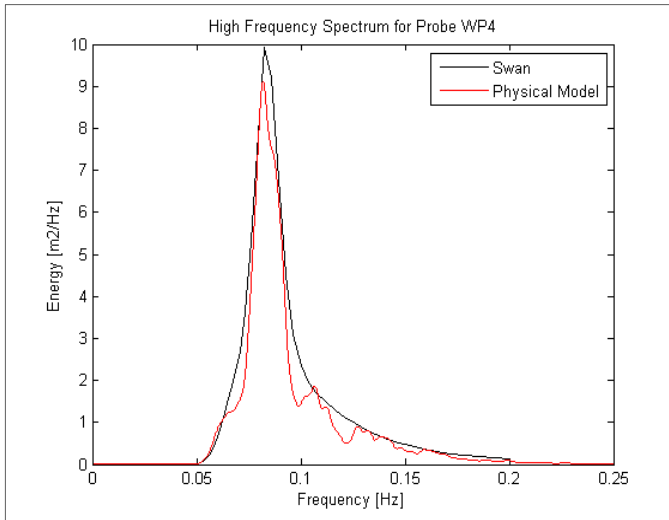
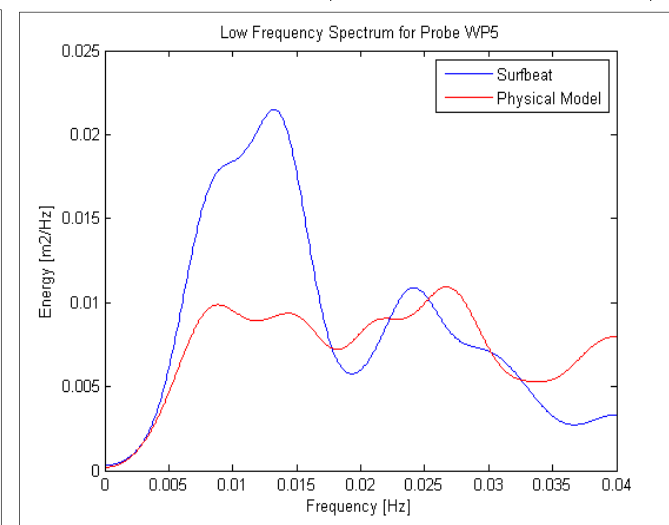
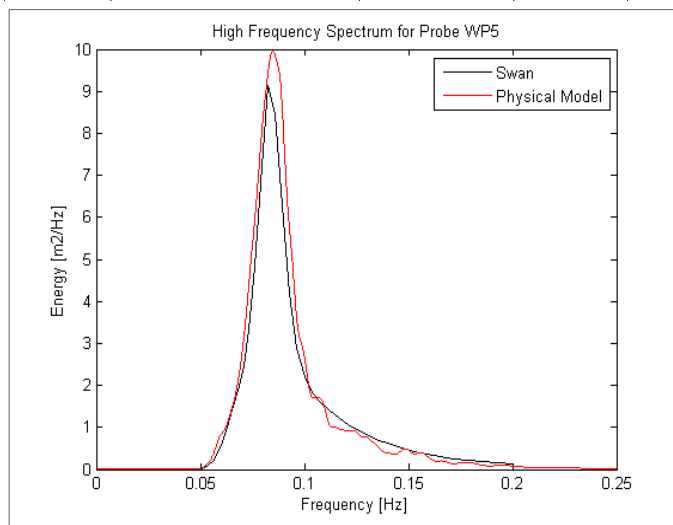


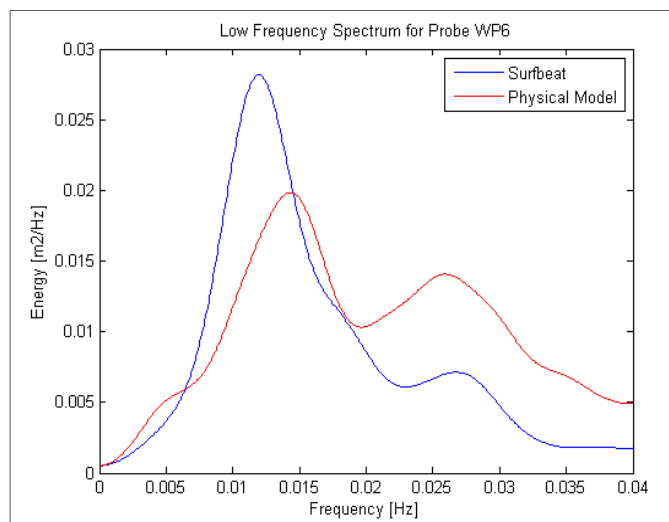
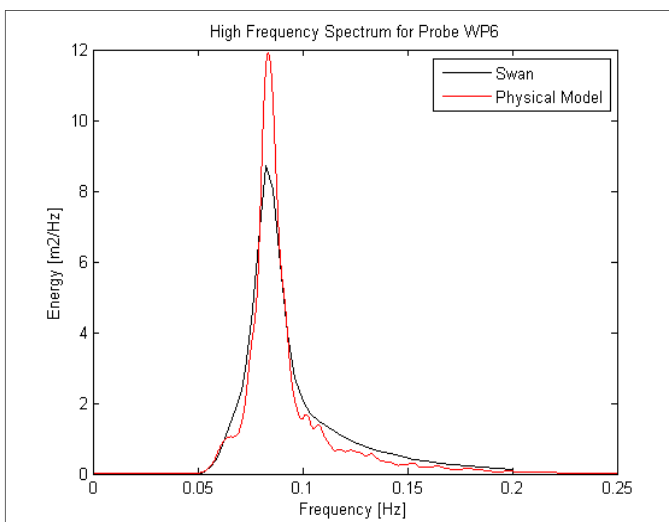
Figure 75: Test 01, long wave and short wave spectra correlation between the physical model, SWAN, and SURFBEAT



Probe No.	Physical Model, Hm0 [m]	Swan, Hm0 [m]	Probe No.	Physical Model, Low Frequency Hm0 [m]	Surfbeat, Low frequency Hm0 [m]
WP4	1.86	2.07	WP4	0.069	0.075

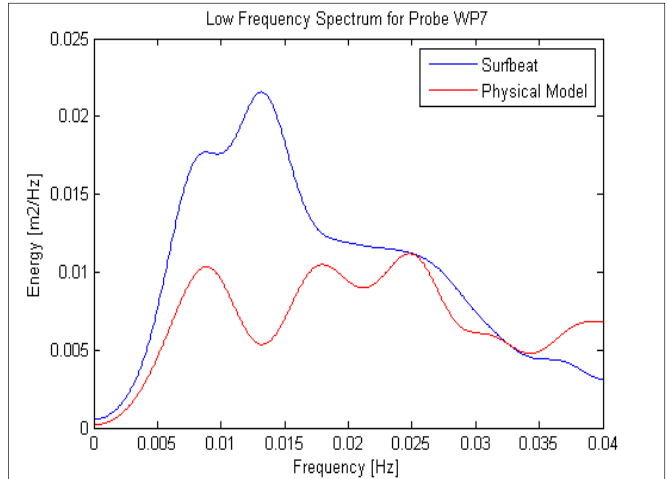
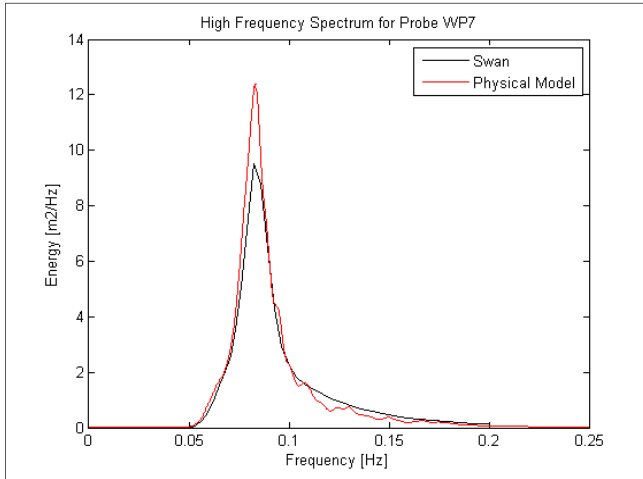


Probe No.	Physical Model, Hm0 [m]	Swan, Hm0 [m]	Probe No.	Physical Model, Low Frequency Hm0 [m]	Surfbeat, Low frequency Hm0 [m]
WP5	2.09	2.00	WP5	0.063	0.075

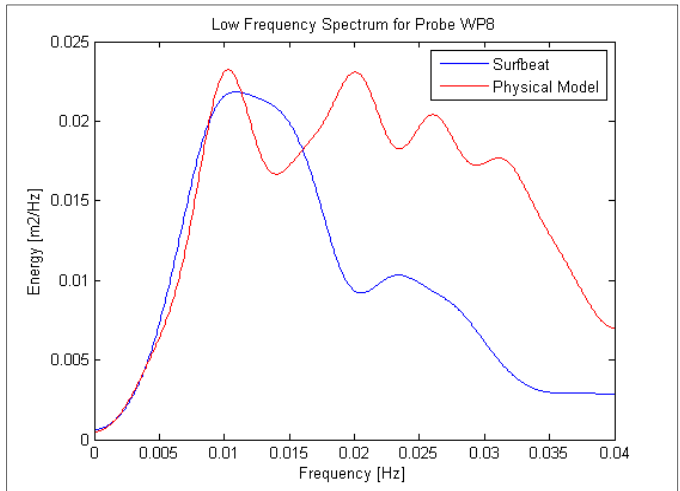
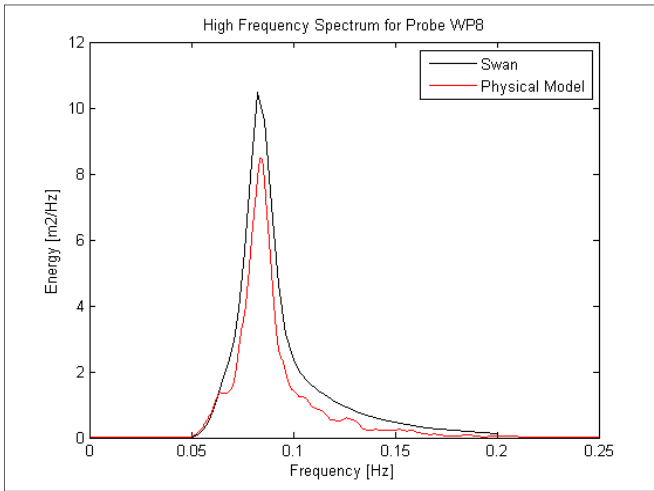


Probe No.	Physical Model, Hm0 [m]	Swan, Hm0 [m]	Probe No.	Physical Model, Low Frequency Hm0 [m]	Surfbeat, Low frequency Hm0 [m]
WP6	1.88	1.95	WP6	0.076	0.073

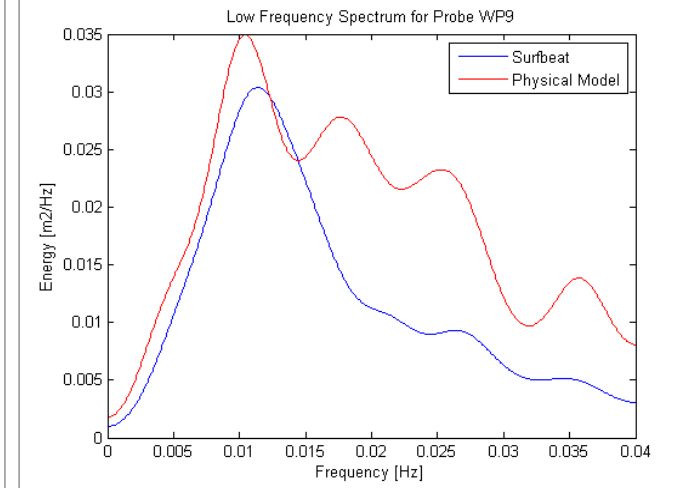
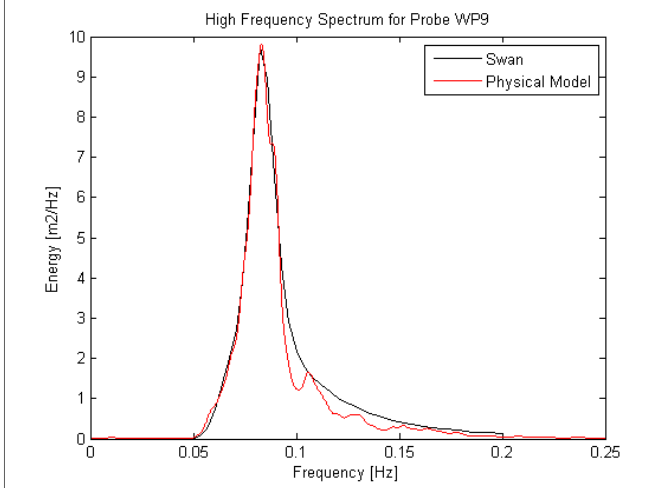
Figure 76: Test 01, long wave and short wave spectra correlation between the physical model, SWAN, and SURFBEAT (contd.)



Probe No.	Physical Model, Hm0 [m]	Swan, Hm0 [m]	Probe No.	Physical Model, Low Frequency Hm0 [m]	Surfbeat, Low frequency Hm0 [m]
WP7	2.08	2.02	WP7	0.062	0.081

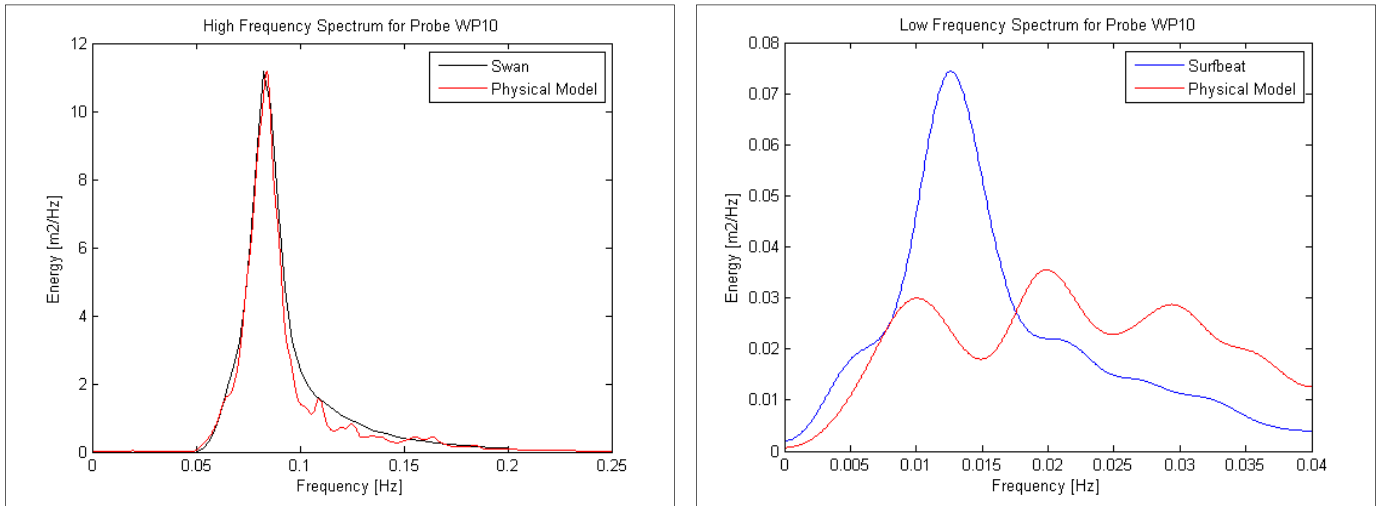


Probe No.	Physical Model, Hm0 [m]	Swan, Hm0 [m]	Probe No.	Physical Model, Low Frequency Hm0 [m]	Surfbeat, Low frequency Hm0 [m]
WP8	1.72	2.10	WP8	0.093	0.080



Probe No.	Physical Model, Hm0 [m]	Swan, Hm0 [m]	Probe No.	Physical Model, Low Frequency Hm0 [m]	Surfbeat, Low frequency Hm0 [m]
WP9	1.90	2.03	WP9	0.104	0.087

Figure 77: Test 01, long wave and short wave spectra correlation between the physical model, SWAN, and SURFBEAT (contd.)



Probe No.	Physical Model, Hm0 [m]	Swan, Hm0 [m]	Probe No.	Physical Model, Low Frequency Hm0 [m]	Surfbeat, Low frequency Hm0 [m]
WP10	2.00	2.14	WP10	0.109	0.119

Figure 78: Test 01, long wave and short wave spectra correlation between the physical model, SWAN, and SURFBEAT (contd.)

F2: Test 02

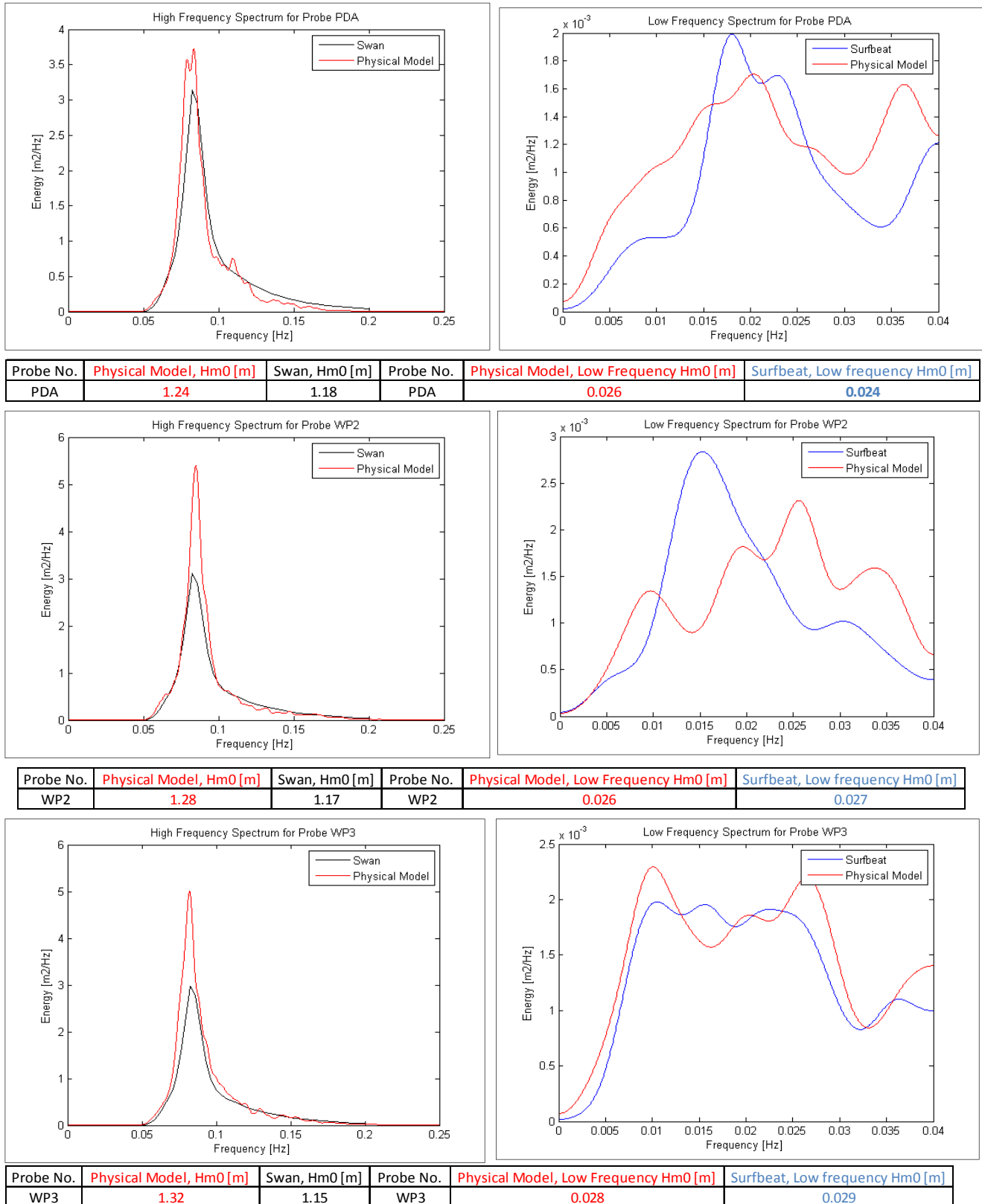
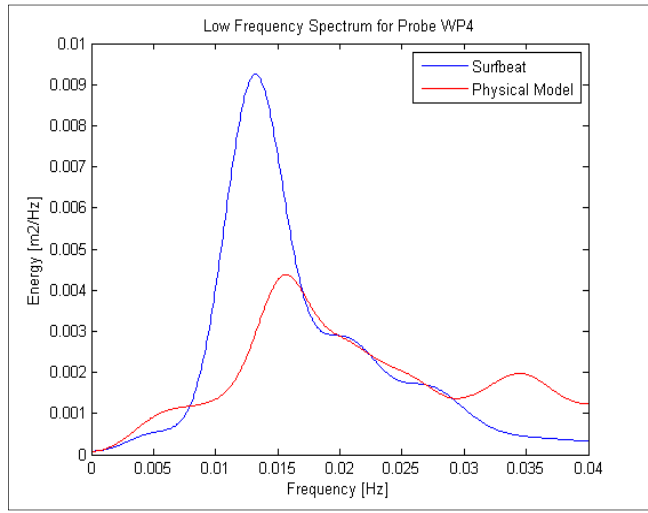
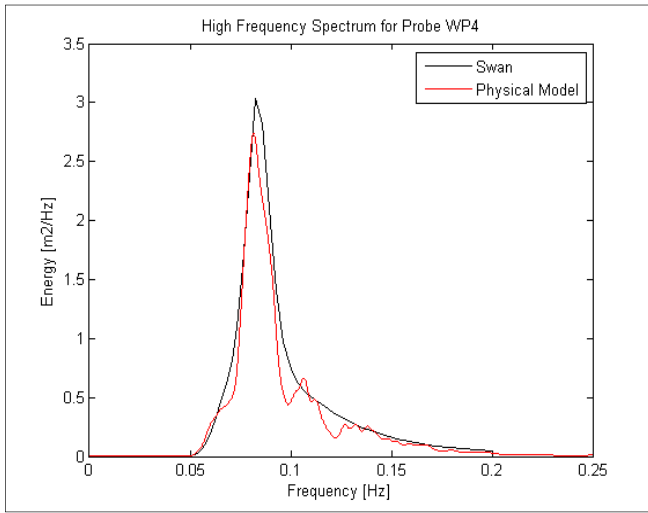
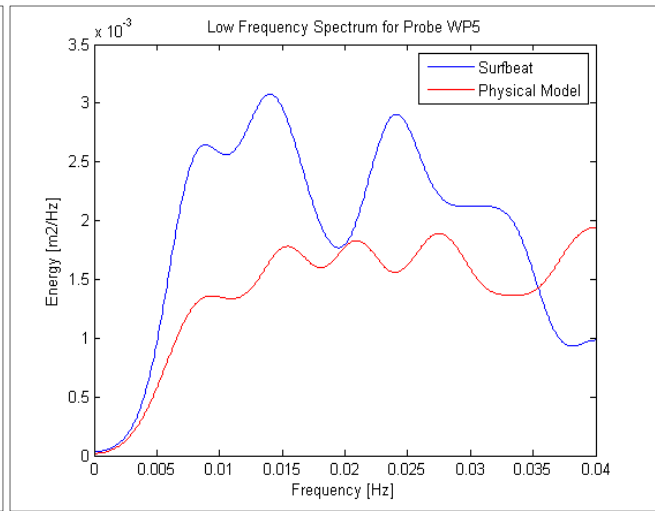
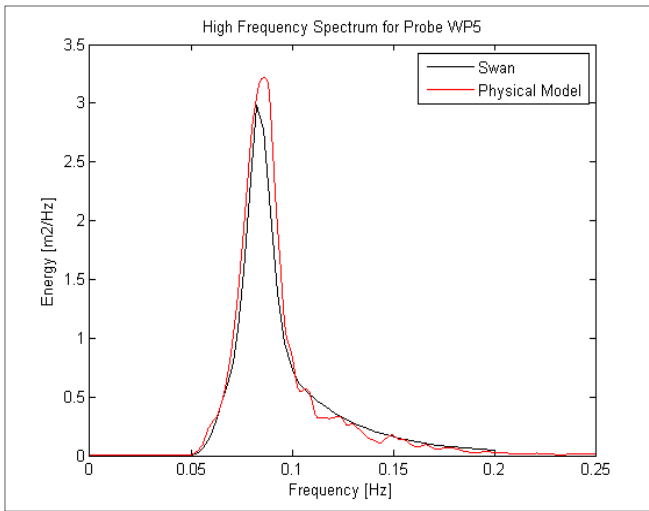


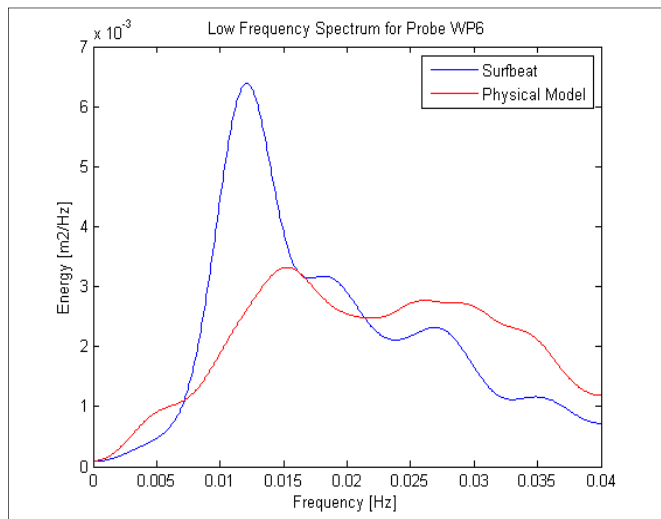
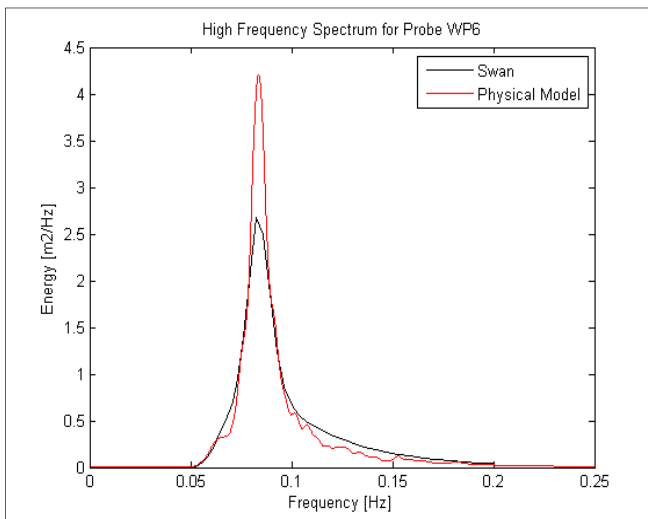
Figure 79: Test 02, long wave and short wave spectra correlation between the physical model, SWAN, and SURFBEAT



Probe No.	Physical Model, Hm0 [m]	Swan, Hm0 [m]	Probe No.	Physical Model, Low Frequency Hm0 [m]	Surfbeat, Low frequency Hm0 [m]
WP4	1.05	1.16	WP4	0.032	0.038

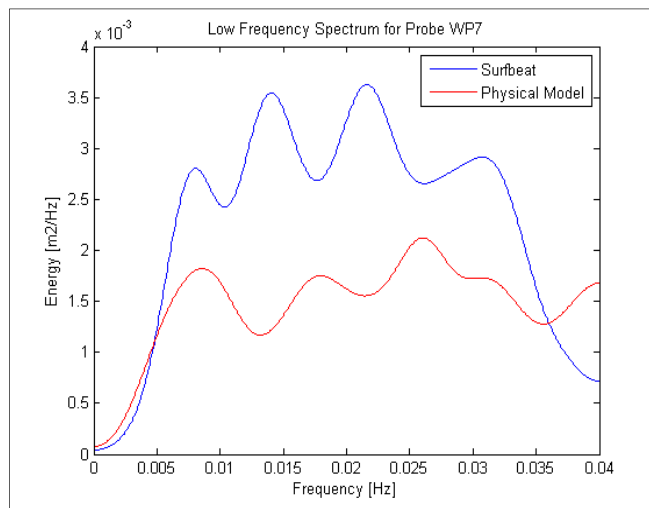
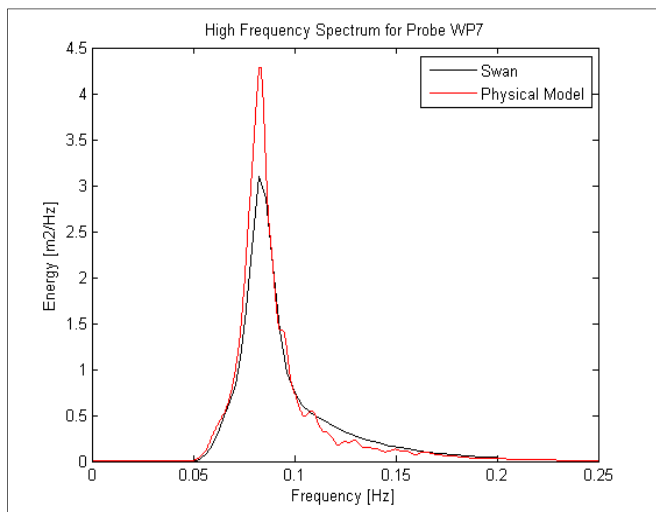


Probe No.	Physical Model, Hm0 [m]	Swan, Hm0 [m]	Probe No.	Physical Model, Low Frequency Hm0 [m]	Surfbeat, Low frequency Hm0 [m]
WP5	1.20	1.15	WP5	0.027	0.035

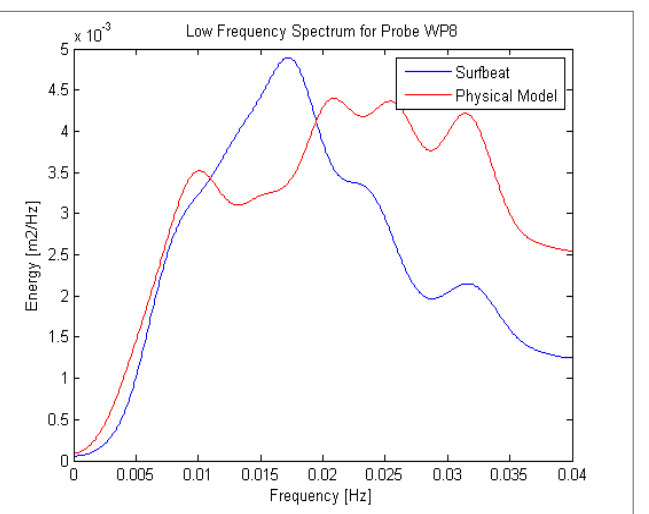
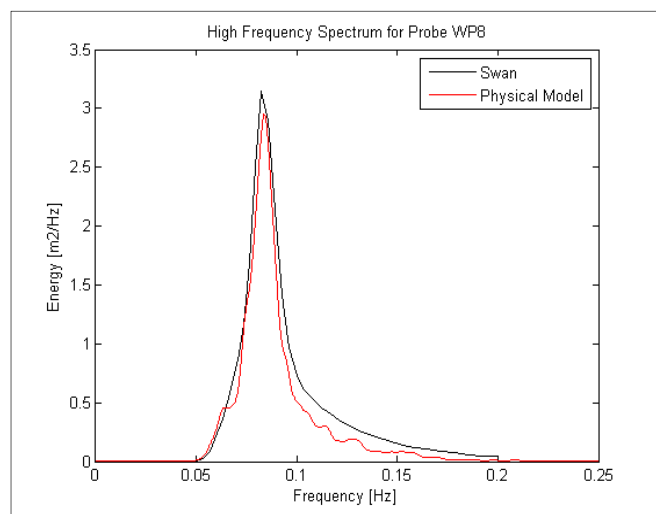


Probe No.	Physical Model, Hm0 [m]	Swan, Hm0 [m]	Probe No.	Physical Model, Low Frequency Hm0 [m]	Surfbeat, Low frequency Hm0 [m]
WP6	1.10	1.09	WP6	0.034	0.037

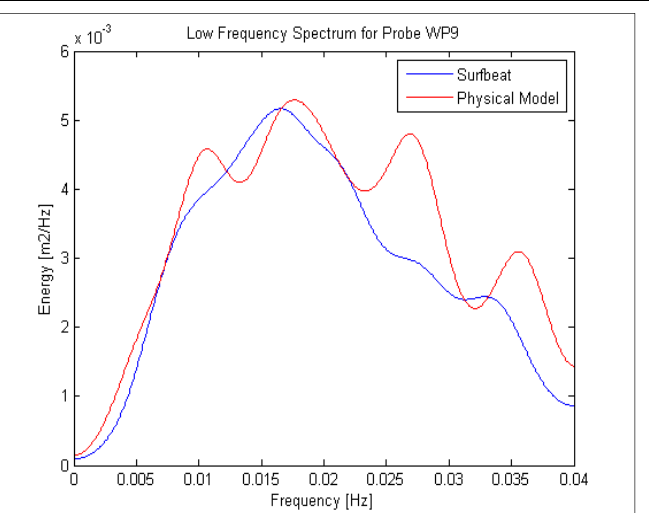
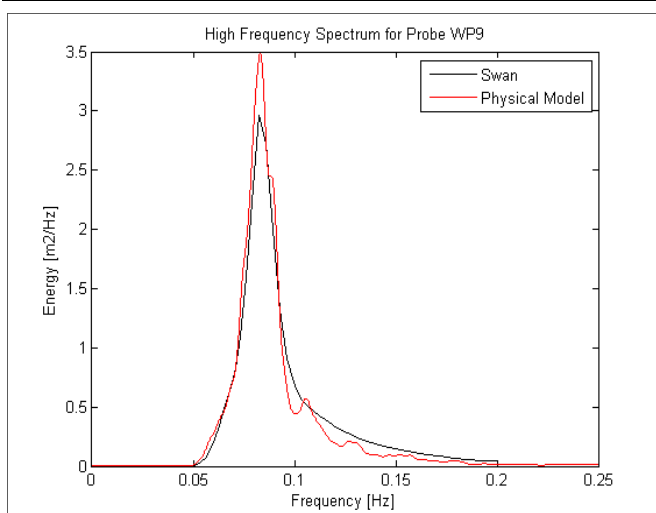
Figure 80: Test 02, long wave and short wave spectra correlation between the physical model, SWAN, and SURFBEAT (contd.)



Probe No.	Physical Model, Hm0 [m]	Swan, Hm0 [m]	Probe No.	Physical Model, Low Frequency Hm0 [m]	Surfbeat, Low frequency Hm0 [m]
WP7	1.21	1.16	WP7	0.028	0.038

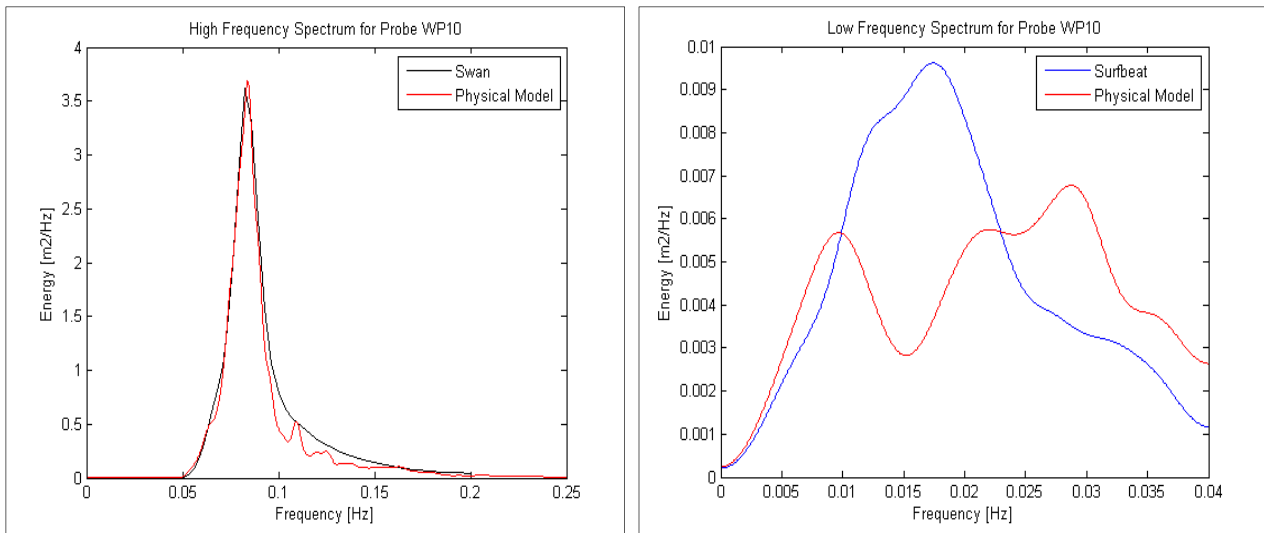


Probe No.	Physical Model, Hm0 [m]	Swan, Hm0 [m]	Probe No.	Physical Model, Low Frequency Hm0 [m]	Surfbeat, Low frequency Hm0 [m]
WP8	1.02	1.16	WP8	0.041	0.040



Probe No.	Physical Model, Hm0 [m]	Swan, Hm0 [m]	Probe No.	Physical Model, Low Frequency Hm0 [m]	Surfbeat, Low frequency Hm0 [m]
WP9	1.12	1.13	WP9	0.043	0.043

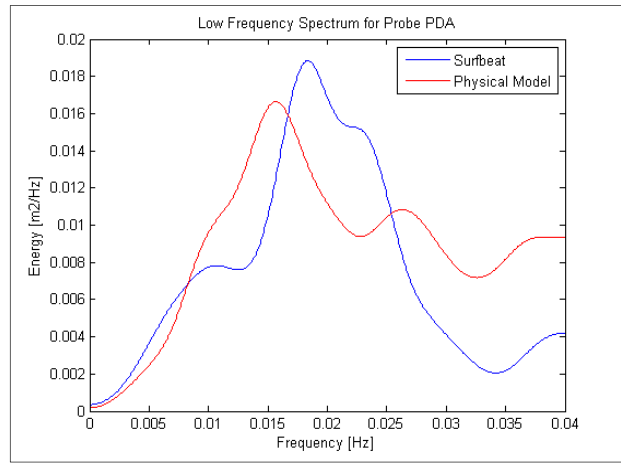
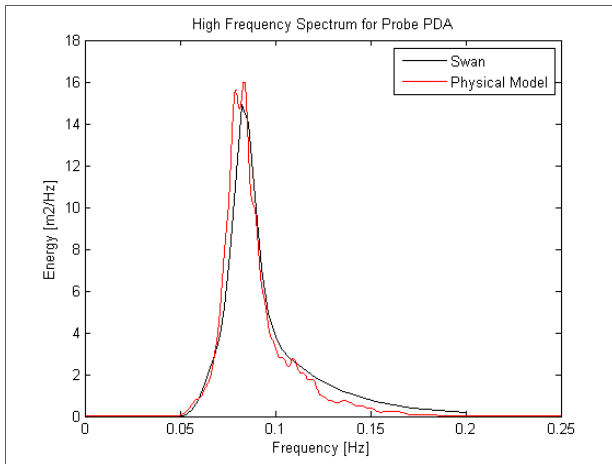
Figure 81: Test 02, long wave and short wave spectra correlation between the physical model, SWAN, and SURFBEAT (contd.)



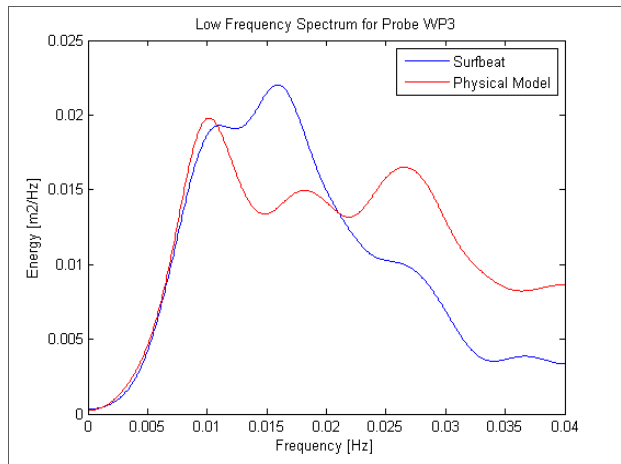
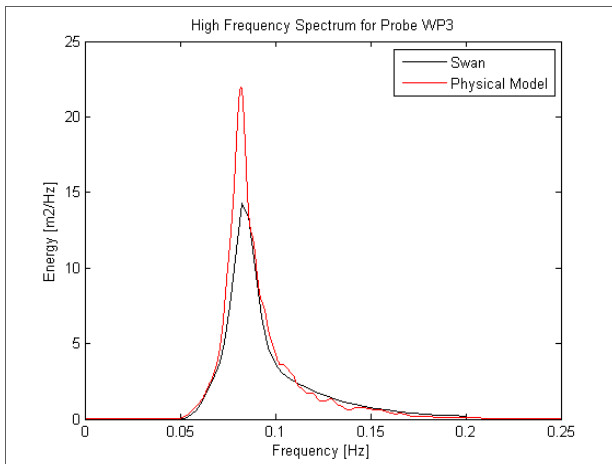
Probe No.	Physical Model, Hm0 [m]	Swan, Hm0 [m]	Probe No.	Physical Model, Low Frequency Hm0 [m]	Surfbeat, Low frequency Hm0 [m]
WP10	1.14	1.22	WP10	0.048	0.054

Figure 82: Test 02, long wave and short wave spectra correlation between the physical model, SWAN, and SURFBEAT (contd.)

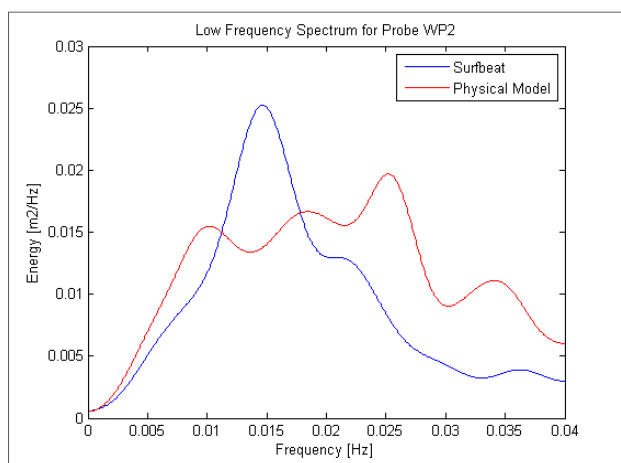
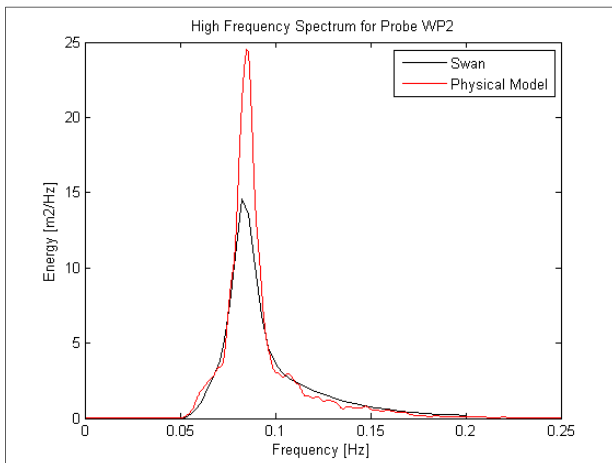
F3: Test 03



Probe No.	Physical Model, Hm0 [m]	Swan, Hm0 [m]	Probe No.	Physical Model, Low Frequency Hm0 [m]	Surfbeat, Low frequency Hm0 [m]
PDA	2.61	2.57	PDA	0.070	0.069

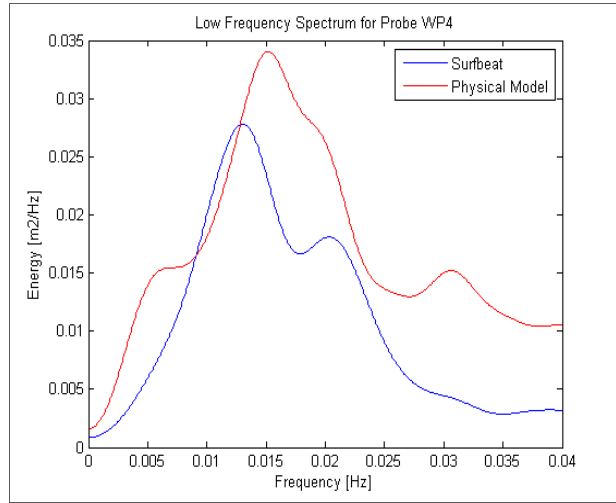
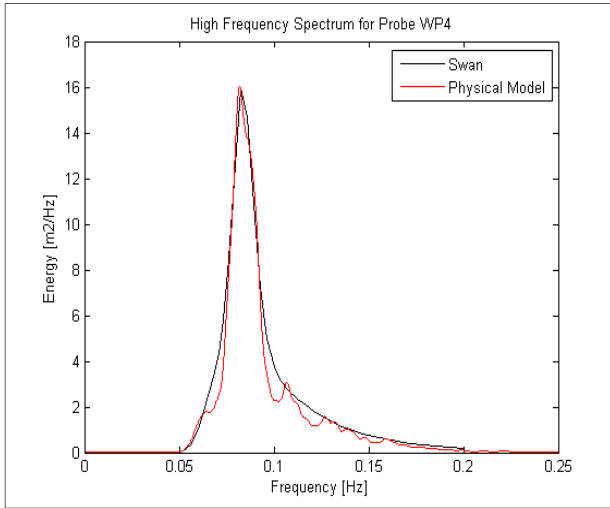


Probe No.	Physical Model, Hm0 [m]	Swan, Hm0 [m]	Probe No.	Physical Model, Low Frequency Hm0 [m]	Surfbeat, Low frequency Hm0 [m]
WP2	2.72	2.54	WP2	0.081	0.076

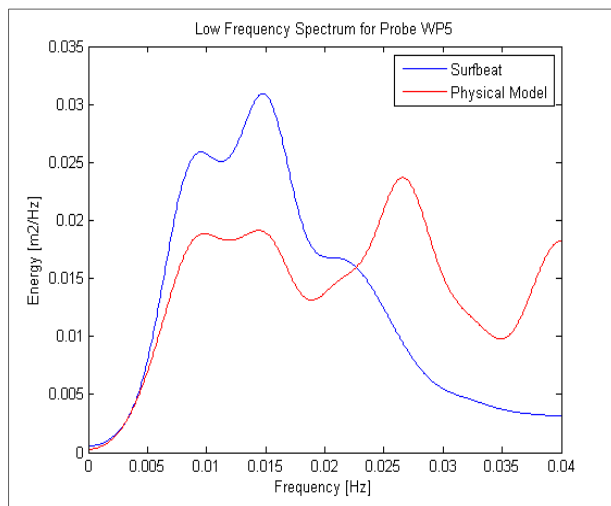
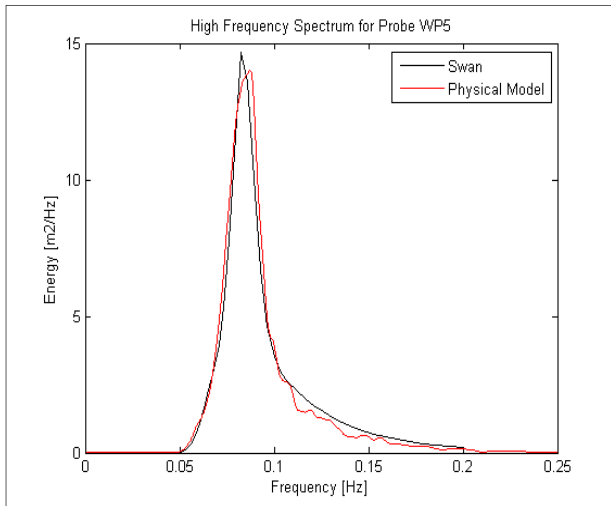


Probe No.	Physical Model, Hm0 [m]	Swan, Hm0 [m]	Probe No.	Physical Model, Low Frequency Hm0 [m]	Surfbeat, Low frequency Hm0 [m]
WP3	2.73	2.52	WP3	0.081	0.081

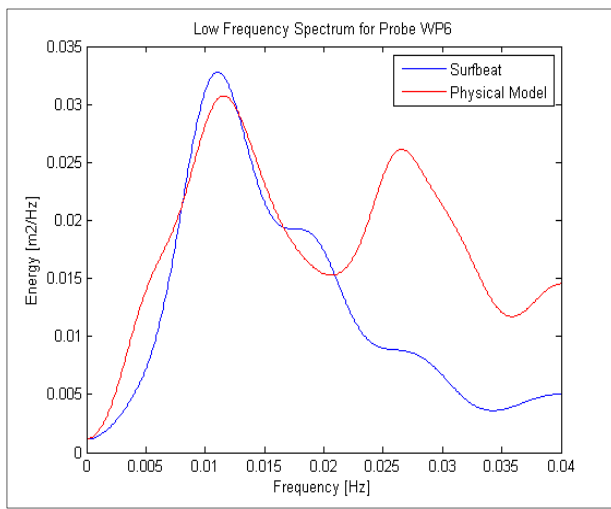
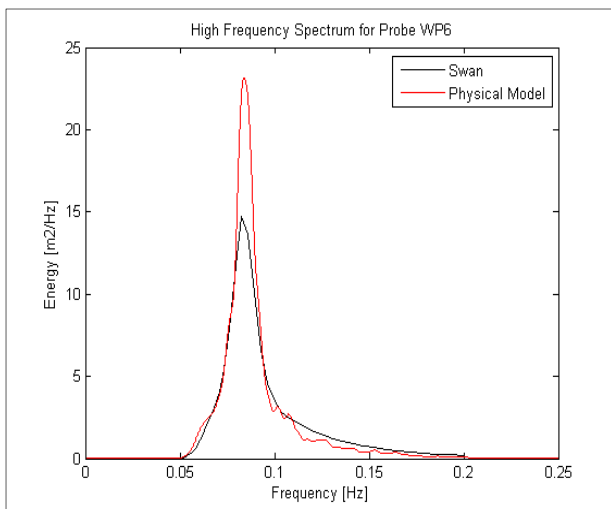
Figure 83: Test 03, long wave and short wave spectra correlation between the physical model, SWAN, and SURFBEAT



Probe No.	Physical Model, Hm0 [m]	Swan, Hm0 [m]	Probe No.	Physical Model, Low Frequency Hm0 [m]	Surfbeat, Low frequency Hm0 [m]
WP4	2.45	2.62	WP4	0.098	0.083

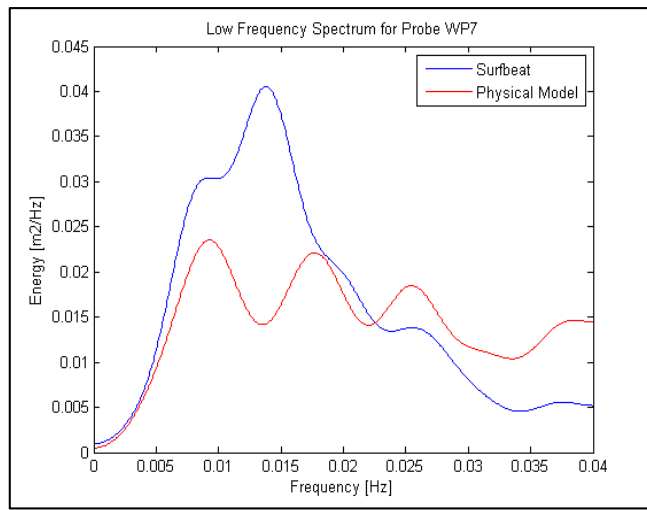
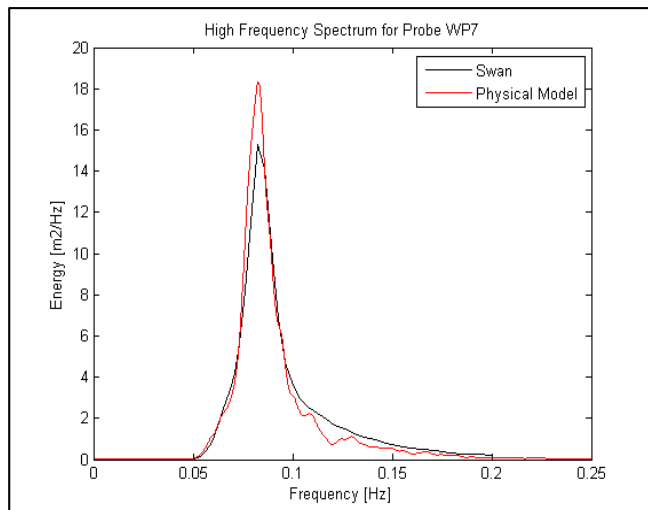


Probe No.	Physical Model, Hm0 [m]	Swan, Hm0 [m]	Probe No.	Physical Model, Low Frequency Hm0 [m]	Surfbeat, Low frequency Hm0 [m]
WP5	2.53	2.53	WP5	0.088	0.091

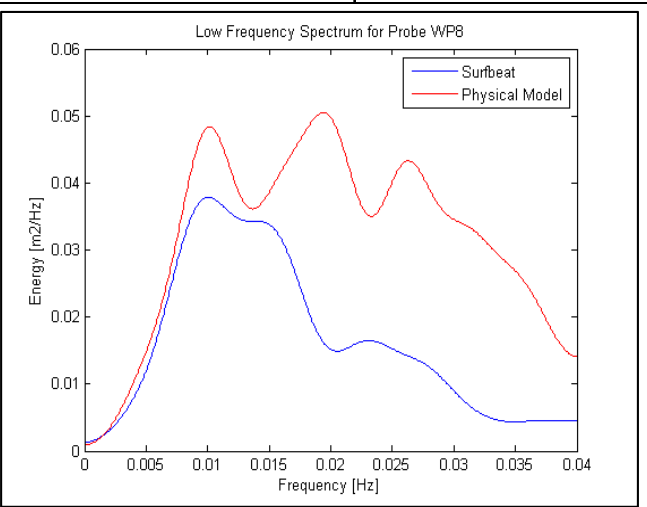
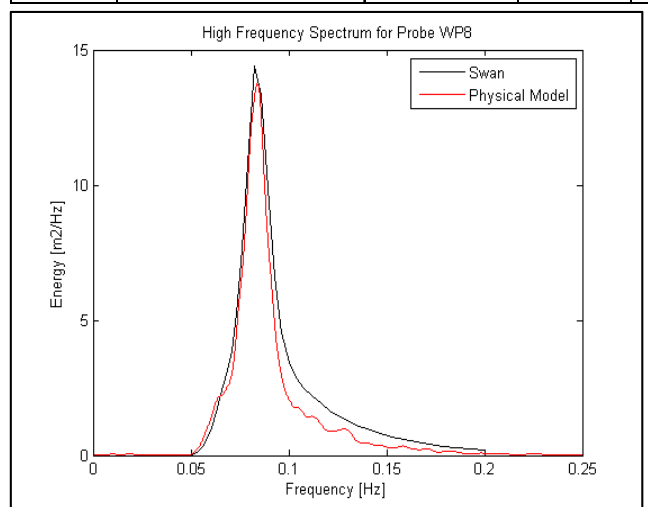


Probe No.	Physical Model, Hm0 [m]	Swan, Hm0 [m]	Probe No.	Physical Model, Low Frequency Hm0 [m]	Surfbeat, Low frequency Hm0 [m]
WP6	2.64	2.52	WP6	0.101	0.089

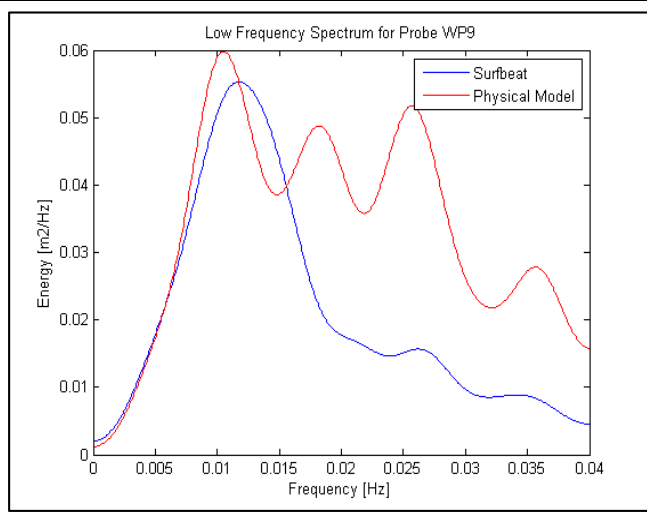
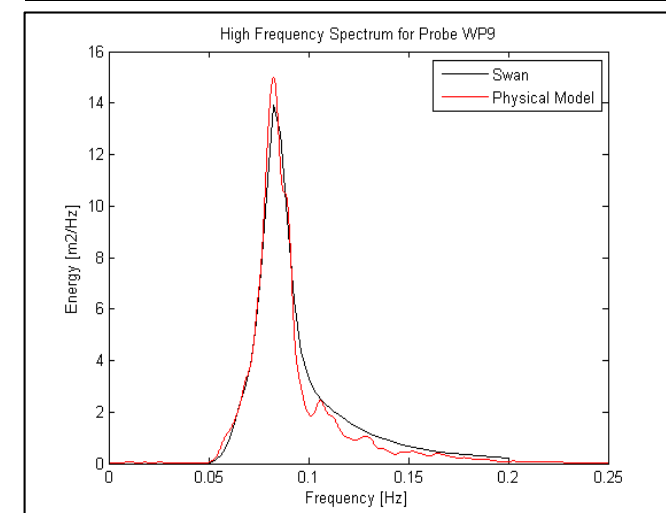
Figure 84: Test 03, long wave and short wave spectra correlation between the physical model, SWAN, and SURFBEAT (contd.)



Probe No.	Physical Model, Hm0 [m]	Swan, Hm0 [m]	Probe No.	Physical Model, Low Frequency Hm0 [m]	Surfbeat, Low frequency Hm0 [m]
WP7	2.52	2.57	WP7	0.088	0.102



Probe No.	Physical Model, Hm0 [m]	Swan, Hm0 [m]	Probe No.	Physical Model, Low Frequency Hm0 [m]	Surfbeat, Low frequency Hm0 [m]
WP8	2.22	2.50	WP8	0.135	0.102



Probe No.	Physical Model, Hm0 [m]	Swan, Hm0 [m]	Probe No.	Physical Model, Low Frequency Hm0 [m]	Surfbeat, Low frequency Hm0 [m]
WP9	2.35	2.45	WP9	0.138	0.115

Figure 85: Test 03, long wave and short wave spectra correlation between the physical model, SWAN, and SURFBEAT (contd.)

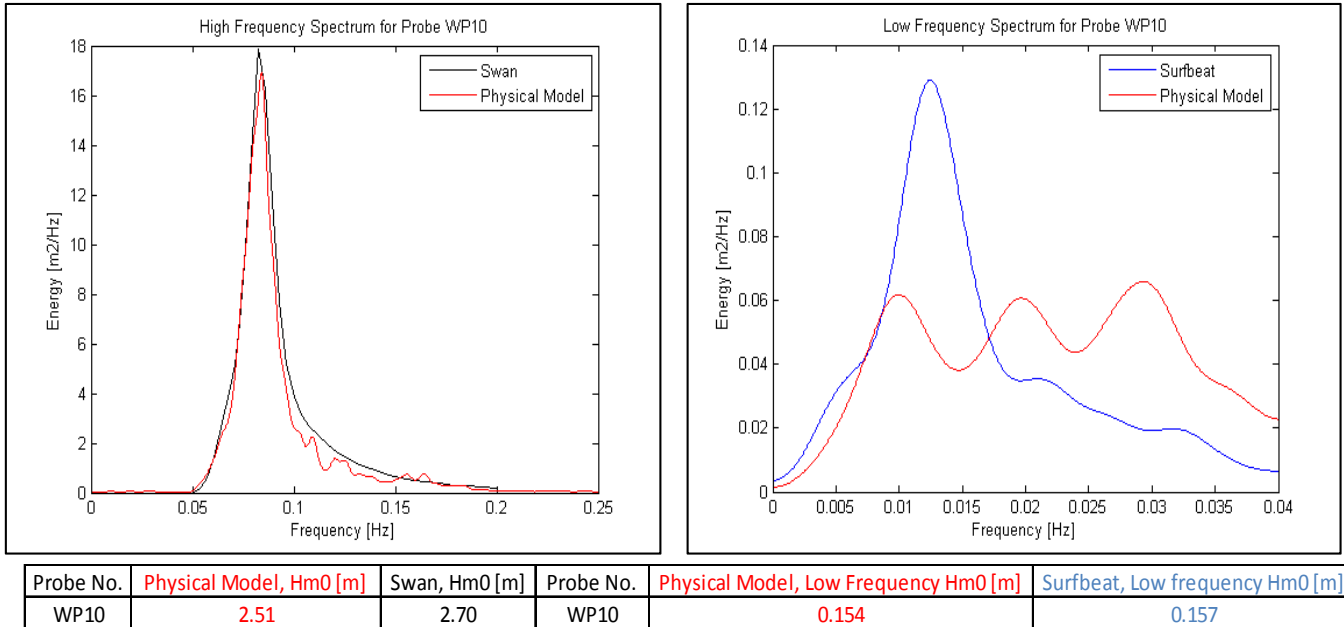


Figure 86: Test 03, long wave and short wave spectra correlation between the physical model, SWAN, and SURFBEAT (contd.)

F4: Test 04

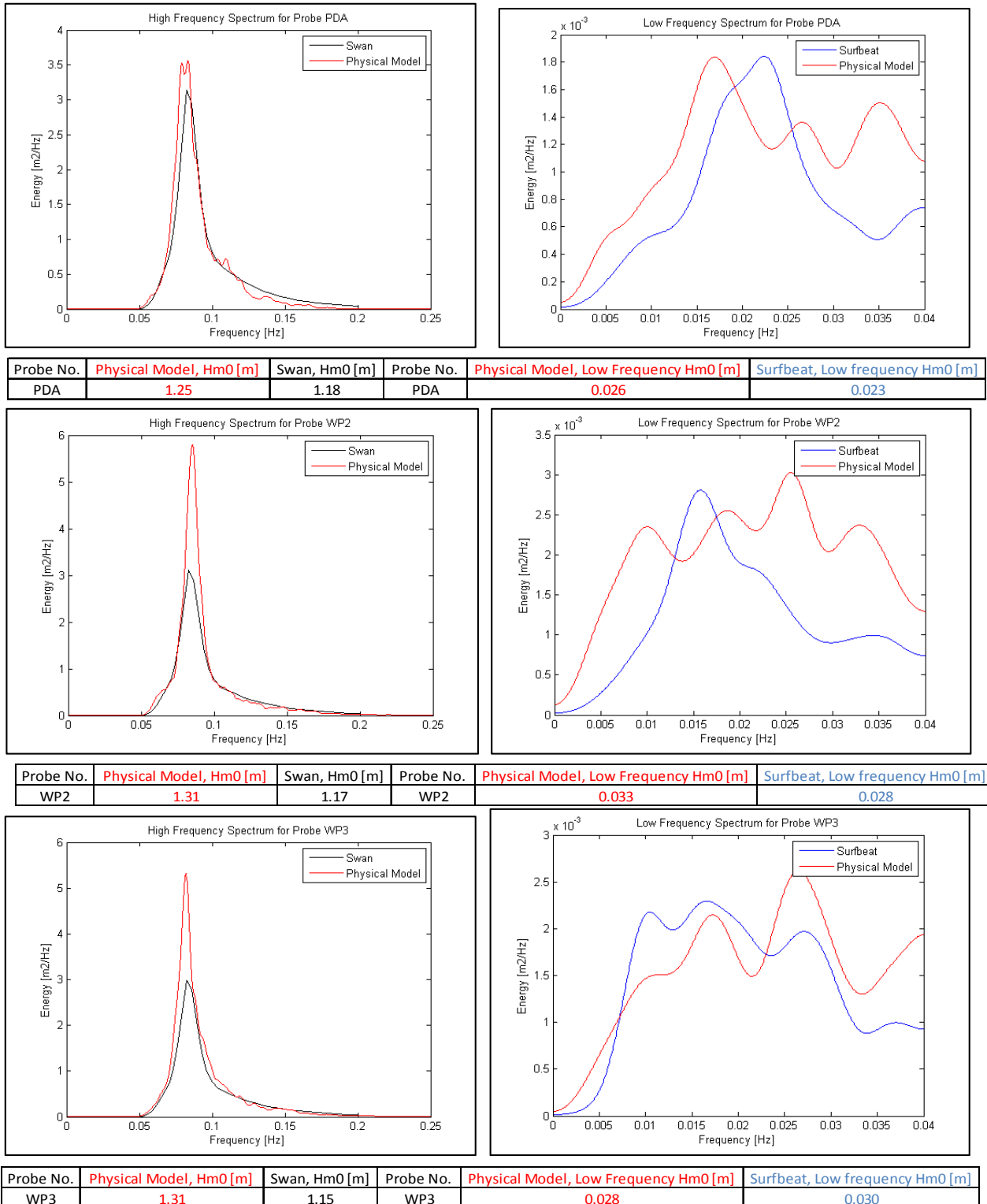


Figure 87: Test 04, long wave and short wave spectra correlation between the physical model, SWAN, and SURFBEAT

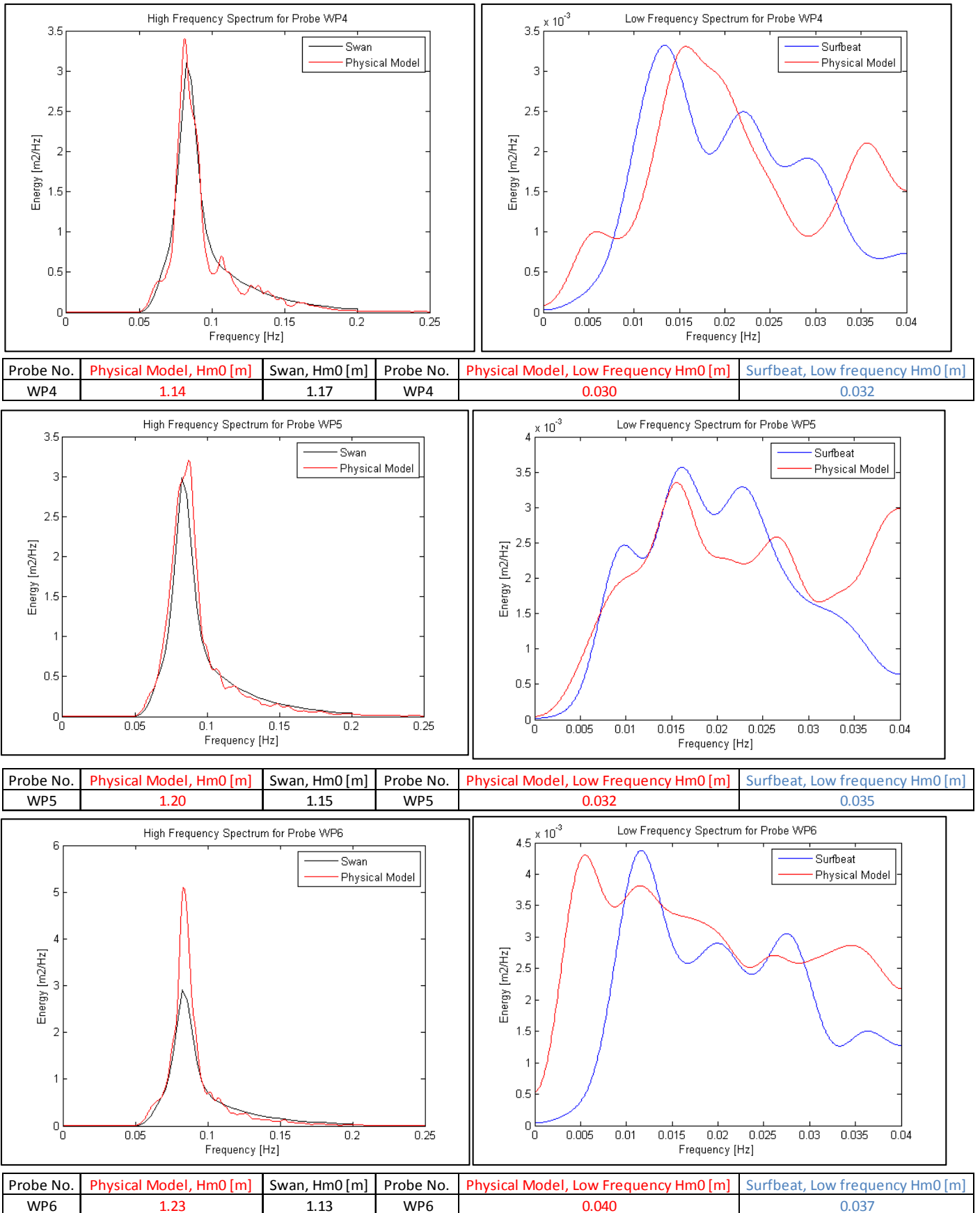


Figure 88: Test 04, long wave and short wave spectra correlation between the physical model, SWAN, and SURFBEAT (contd.)

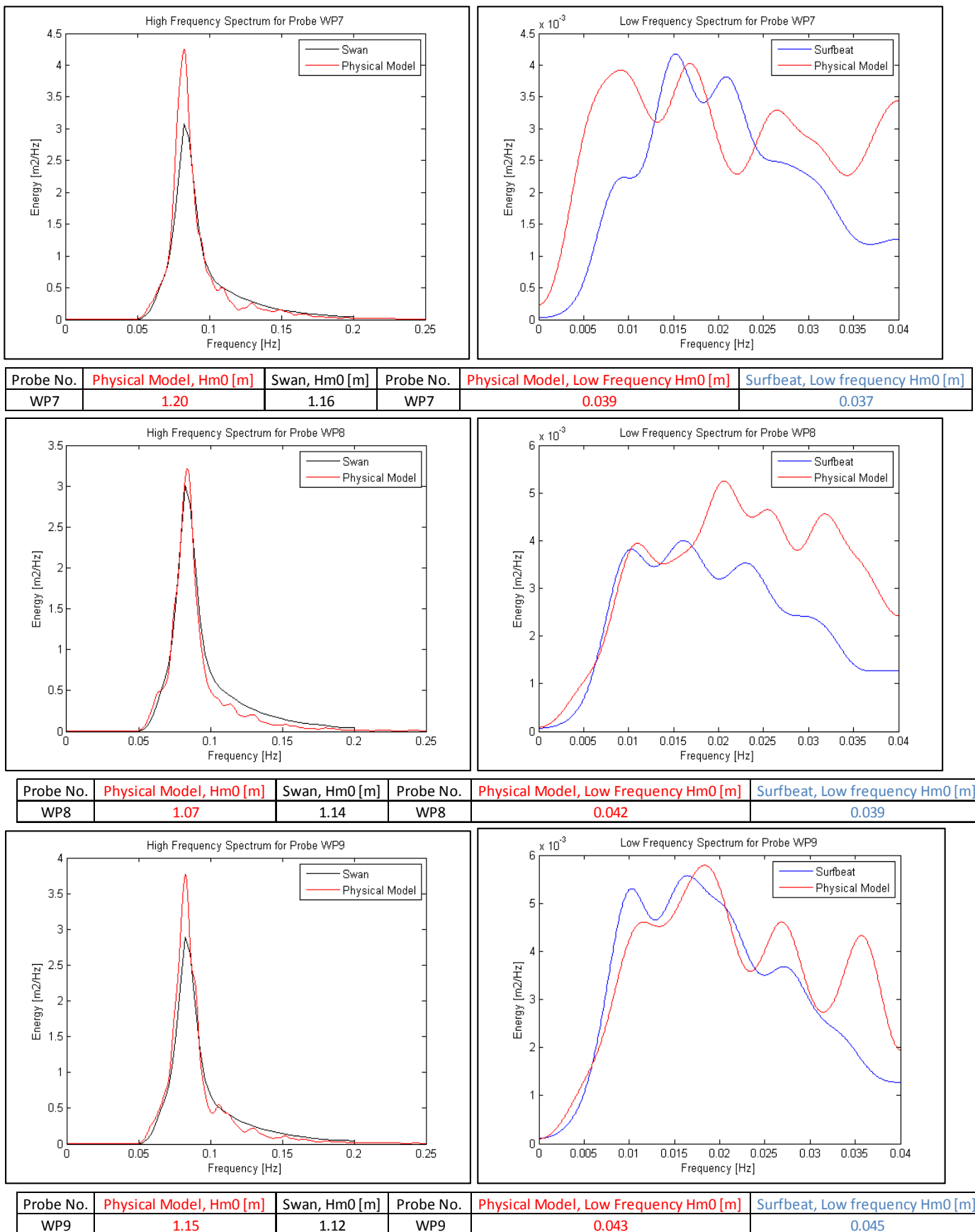
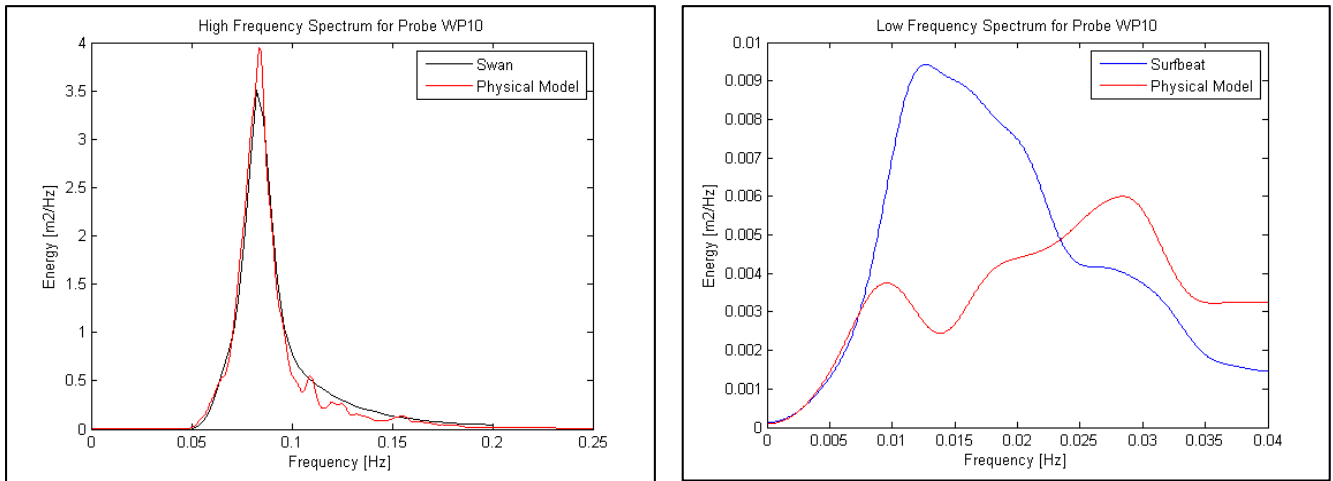


Figure 89: Test 04, long wave and short wave spectra correlation between the physical model, SWAN, and SURFBEAT (contd.)



Probe No.	Physical Model, Hm0 [m]	Swan, Hm0 [m]	Probe No.	Physical Model, Low Frequency Hm0 [m]	Surfbeat, Low frequency Hm0 [m]
WP10	1.18	1.21	WP10	0.044	0.053

Figure 90: Test 04, long wave and short wave spectra correlation between the physical model, SWAN, and SURFBEAT (contd.)

Appendix G: Grid Dependency and Time

Dependency checks

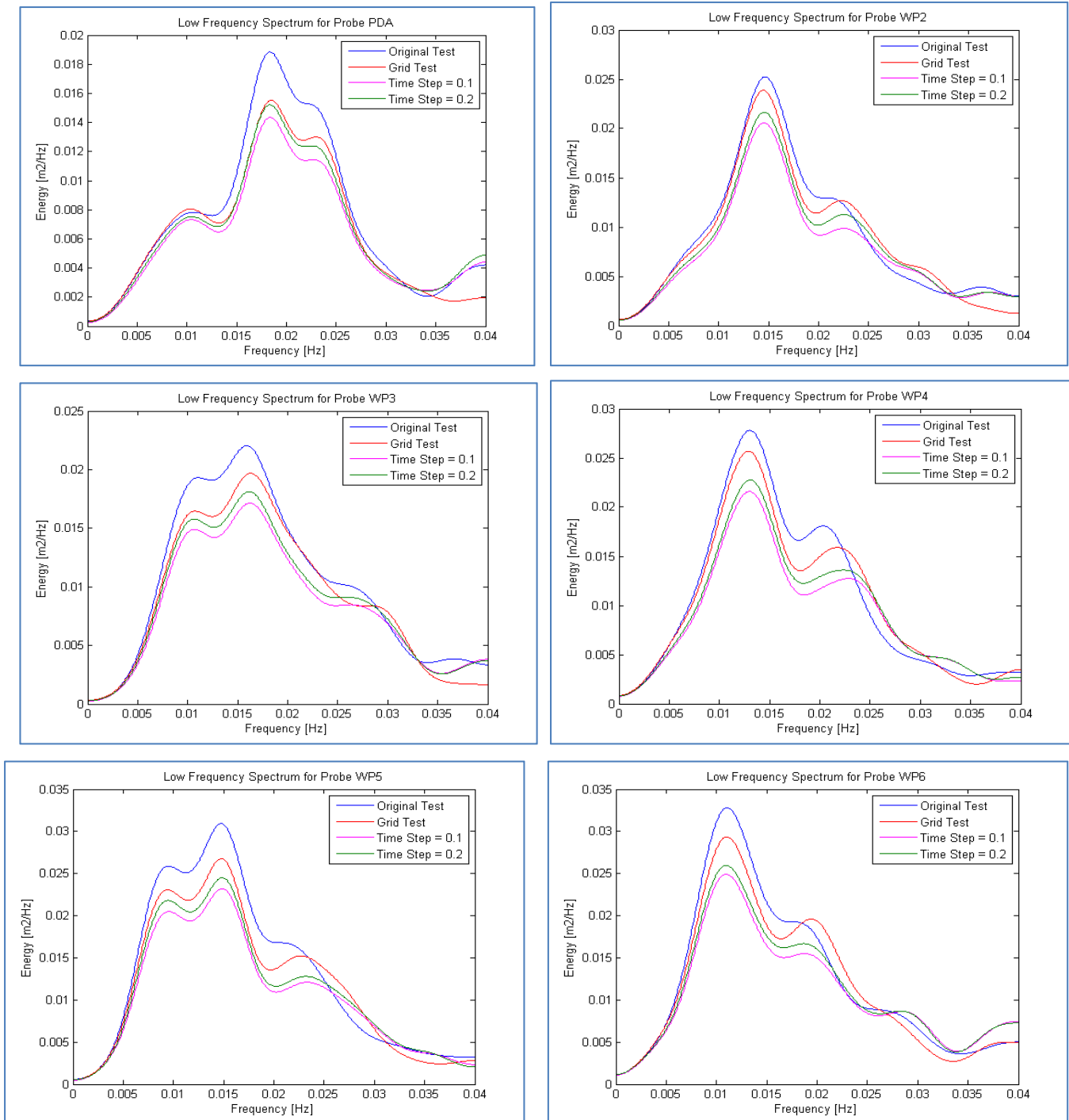


Figure 91: Dependency test results

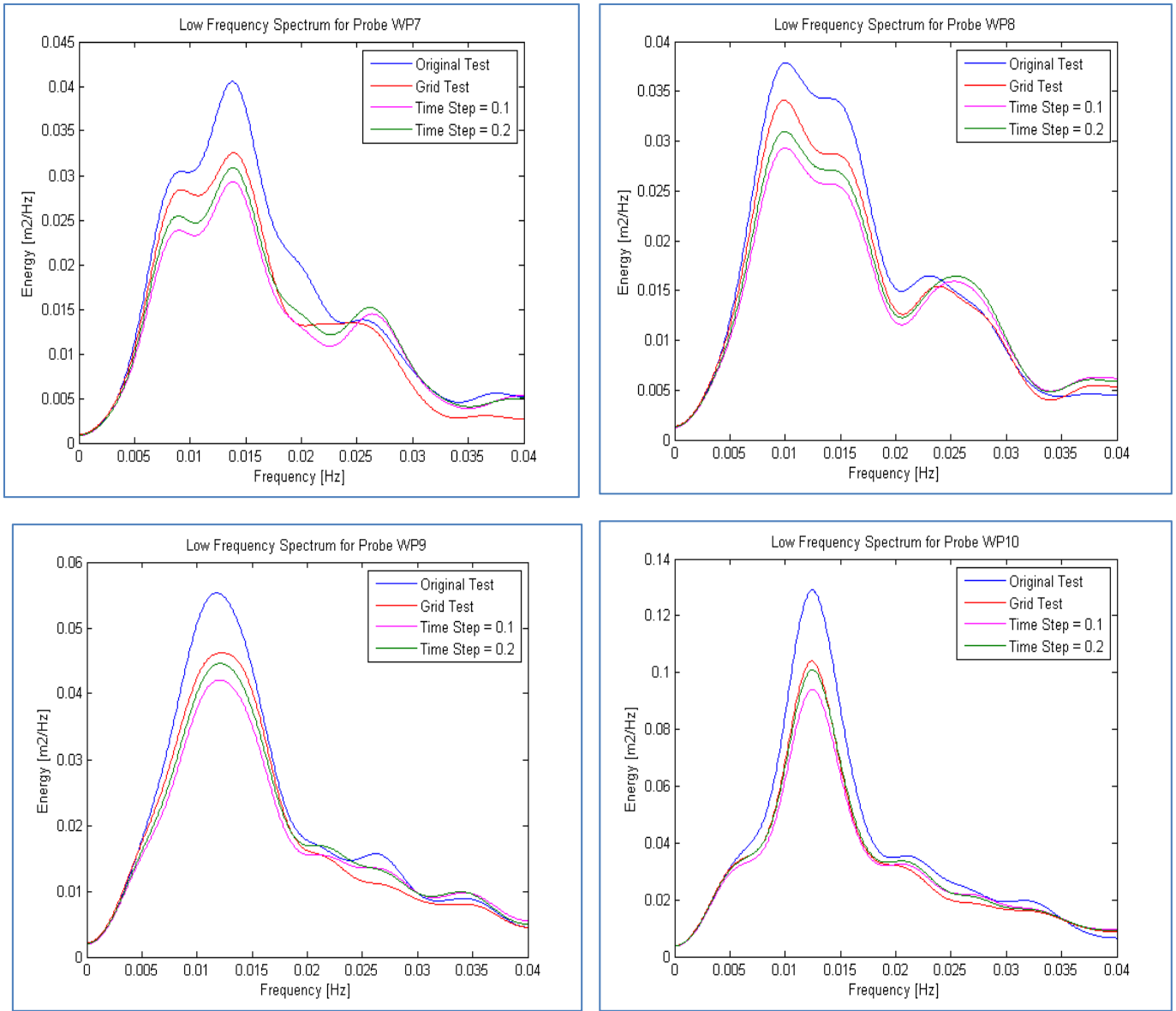


Figure 92: Dependency test results (contd.)

Appendix H: Numerical Modelling Procedure

H1: Hull Form Data

In order to calculate the hydrodynamic coefficients that describe the vessel oscillations, the curvature of the ship's hull needs to be defined. This was done by making use of the SEAWAY manual (Journée, User Manual of Seaway, 2001) to generate a hull form '.hfs' file. This hull form file consists of offset points on the cross-section of a vessel. The offset points can be done manually or by using old files with the same ship dimensions that may be updated by applying a scaling factor.

The hull form file describes the curvature of the hull form and is inspired by ship line drawings. The CSIR has a library of hull form files ('hullform.hfs') based on the available physical model vessels. The 'hullform.hfs' files were edited and scaled to suit the new fully laden vessel employed in the present study. Figure 93 illustrates the strips generated in the 'hullform.hfs' file.

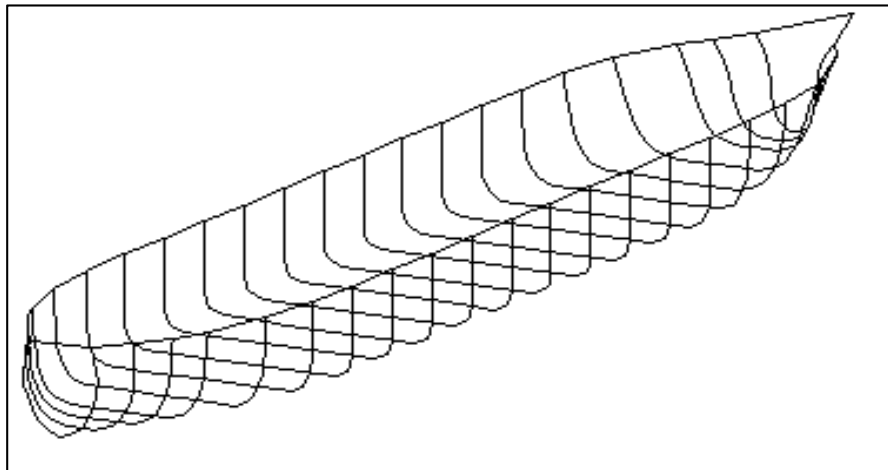


Figure 93: Hull form panels

A 'hullform.hfs' file consist of a series of stations describing the curvature of the hull. The last two stations describe the bow and the stern. As indicated in the next Figure 94, the strips situated near mid-ships are wider than the strips situated near the bow and the stern. The narrower strips are necessary to better describe the curvature at the latter locations. With smaller strips at the bow and stern, the panel sizes will also be smaller. The ship is block-like near the middle, therefore not too many strips are required in this area. This, however, is not true for the areas closest to the bow and the stern.

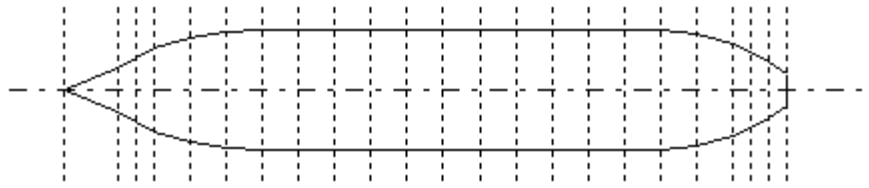


Figure 94: Top view of panel allocation

H2: Mesh Generation

A mesh needs to be applied to the hull form. The mesh file consists of a list of mesh node positions, followed by a list of panel node and line node allocations. In other words, each panel is quadrilateral with four nodes as vertices (van der Molen W. , 2011 (b)). Assigning more panels yields a finer mesh. The panel length, however, should not exceed 1/8 of the smallest wave length occurring in the basin (van der Molen W. , 2011 (b)). Table 22 represents the file structure of a vessel mesh file. This file structure is used to generate the mesh file of the hull form used for LF-STRIP, WAVESCAT and QUAYSIM.

Table 22: Mesh file structure for vessel (van der Molen W. , 2011 (b))

"300 000 DWT container carrier"	Description line used to describe the vessel
Floating	The floating option is used to describe whether the mesh is fixed (in case of a quay wall mesh being used) or floating (in case of a vessel mesh being used)
Symmetry	This option indicates the number of symmetry planes used by the mesh. When the mesh is generated, only half of it is generated and then mirrored to obtain the entire mesh of the vessel. Therefore, in case of a vessel mesh being used, the number of symmetry planes is usually one
LBD	Length between perpendiculars (Lpp), beam, and draft of the vessel
Zcog	Distance of the centre of gravity from the water line (If the centre of gravity is above the water line, a negative value should be inserted.)
Kxi	The transverse radii of gyration, obtained from the vessel calibration procedure
Kyi	Longitudinal radii of gyration, obtained from the vessel calibration procedure
Kzi	Longitudinal radii of gyration, obtained from the vessel calibration procedure
Nodes	Number of nodes in the mesh
Panels	Number of panels in the mesh
Lines	Number of waterline segments in the mesh
Node coordinates	For each node, there are x-, y-, and z-coordinates in the ship-bound coordinate system where the origin is

	situated at the waterline
Panel allocations	Each quadrilateral panel has a panel number and the node numbers of the four vertices. In some cases, the mesh forms a triangular panel which is defined as a quadrilateral panel with two identical vertices
Line segments	Each line segment is defined by the line number and the node numbers of the end points of the line segment

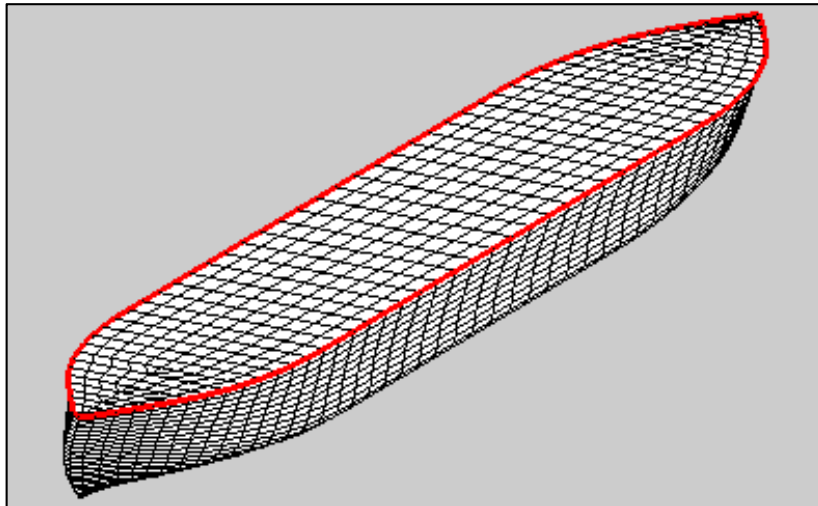


Figure 95: Mesh of the B300 vessel

The node coordinates, panel allocations, and line segments form a large part of the mesh file because this file offers an iterative documentation of all nodes, panels and line segments. In this study, the mesh file was generated by using the Matlab function 'meshgenerator.m', which is based on the hull form of the vessel. Figure 95 illustrates the mesh file obtained using the meshgenerator.m function.

It is important to remember that the physical model tests were carried out with and without a quay wall. Consequently, the numerical model should be analysed in the same way, allowing for both conditions. WAVESCAT has a quay wall option which can be turned on. This option, however, creates an infinitely long quay wall parallel to the vessel, dramatically extending as far as the beach. This is not true for the specific case. In the present study's basin layout, the quay wall had

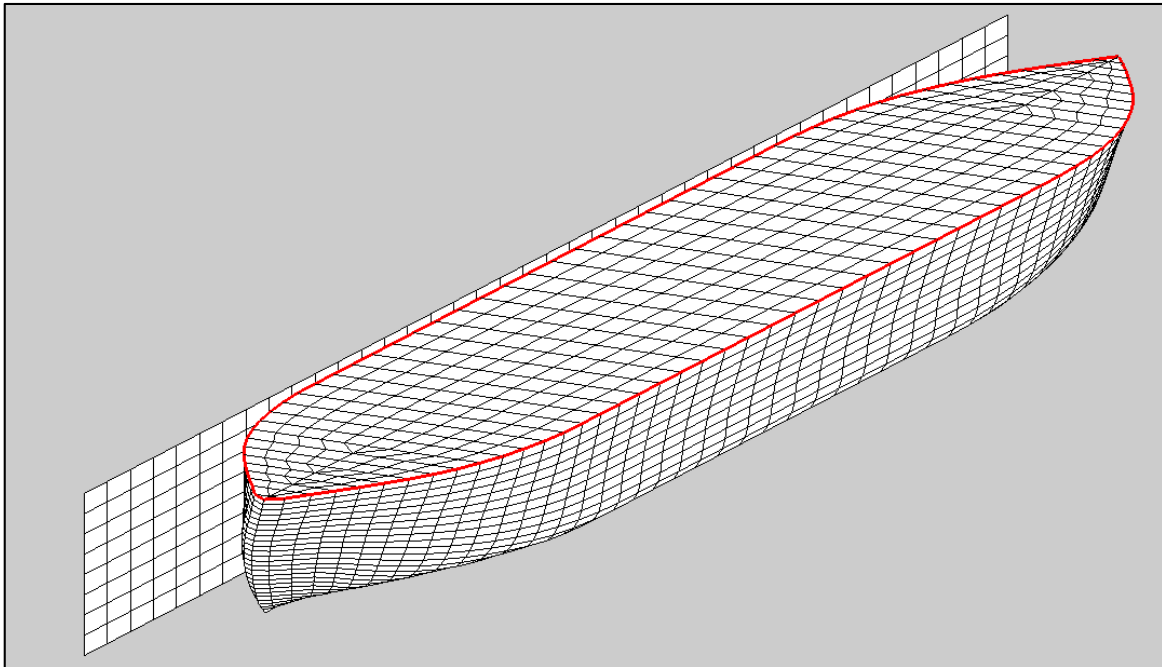


Figure 96: Vessel mesh and quay wall mesh

more or less the same length as the vessel and did not extend to the beach. As such, another mesh needed to be generated by using the Matlab function 'genwall.m', which consists of a function called "genwall (V, Mp, Np, meshfile)". "V" represents a three dimensional array of x-, y-, and z-coordinates of each corner point of the quay wall. "Mp" represents the number of panels in the x-direction (i.e. bow-stern direction) and "Np" represents the number of panels in the z-direction (i.e. keel-deck direction). The last input parameter, "meshfile", refers to the output file name for the wall generated. The mesh created for the vessel together with that created for the quay were plotted to see whether the quay wall dimensions were numerically sufficient in relation to the vessel. Figure 96 illustrates the quay wall mesh plotted alongside the vessel mesh. The wall mesh file has a similar structure to the mesh file used for the vessel, excluding the vessel properties.

Table 23 illustrates the mesh file structure for a quay wall. Note the similarity between this file structure and that of the vessel in the previous Table 22 mentioned earlier. However, in generating the quay wall mesh file, no vessel properties are required for input parameters.

Table 23: Mesh file structure for quay wall (van der Molen W. , 2011 (b))

"My wall"	Description line used to describe the vessel
Floating	The floating option is used to describe whether the mesh is fixed (in case of a quay wall mesh being

	used) or floating (in case of a vessel mesh being used)
Symmetry	This option indicates the number of symmetry planes used by the mesh. When the mesh is generated, only half of it is generated and then mirrored to obtain the entire mesh of the vessel. Therefore, in case of a vessel mesh being used, the number of symmetry planes is usually one
Nodes	Number of nodes in the mesh
Panels	Number of panels in the mesh
Lines	Number of waterline segments in the mesh
Node coordinates	For each node, there are x-, y-, and z-coordinates in the ship-bound coordinate system where the origin is situated at the waterline
Panel allocations	Each quadrilateral panel has a panel number and the node numbers of the four vertices. In some cases, the mesh forms a triangular panel which is defined as a quadrilateral panel with two identical vertices
Line segments	Each line segment is defined by the line number and the node numbers of the end points of the line segment

H3: WAVESCAT

With both the hull form and mesh files having been generated, the WAVESCAT computation could be carried out. Table 24 represents the WAVESCAT file structure required to run the simulation. WAVESCAT uses the generated mesh files to compute the hydrodynamic coefficients caused by the oscillating ship. Pressure and velocity are computed on each mesh panel cell.

Table 24: WAVESCAT file structure (van der Molen W. , 2011 (b))

Acceleration	$g = 9.81 \text{ m/s}^2$
Density of fluid	$\rho = 1025 \text{ kg/m}^3$
Water depth located at mid-ships	31.0 m
Number of viscous roll damping coefficients	1
Viscous roll damping coefficient	0.9
Wave height obtained at vessel position	Probe 3 located closest to vessel
Description line	'300 000 DWT Container Carrier'
Number of mesh bodies	
Mesh filenames (separate line)	'id.msh'
Body number, x- and y-positions (ship-bound with respect to global coordinate systems), heading (angle between global and ship-bound coordinate systems), forward speed (= 0 for moored vessels)	
Number of frequencies, first frequency, frequency step	

Number of wave directions	
Wave direction in global coordinate system	
Drift force option	"far" or "near" method
Hydrodynamic output file name	'id.hyd'
Number of segments where damping is applied on panels	Default = 0
Storing option	Green function / Rankine Green

H4: LF-STRIP

LF-STRIP is a Matlab computation making use of an input file as presented in Table 25. LF-STRIP calls the '.hyd' hydrodynamic file and '.hfs' hull form file and the SURFBEAT simulation to compute the long wave force imposed on the vessel.

Table 25: LF-STRIP input file structure (van der Molen W. , 2011 (c))

runid	Refers to the run ID used to run the SURFBEAT simulation
xship	The x-position of the vessel in the ship-bound coordinate system with respect to the SURFBEAT co-ordinate system
yship	The x-position of the vessel in the ship-bound coordinate system with respect to the SURFBEAT co-ordinate system
KG	The location of the centre of gravity measured from the keel upward
headin	The heading of the vessel in the ship-bound co-ordinate system with respect to the SURFBEAT co-ordinate system
zeta0	Mean water level
tstart	Time in hours when wave force calculation starts
tstop	Time in hours when wave force calculation stops
dtout	Time step
tinit	Initialisation time when wave forces are built up
hydopt	Hydrodynamic option identifier. List of hydrodynamic options are available in the manual (van der Molen W. , 2011 (b))
cof	Cut off frequency of fluid velocities
filhyd	The name of the hydrodynamic '.hyd'file from WAVESCAT
filhul	The name of the hull form '.hfs'file
filfor	The name of the output force files 'id.exf'
descrp	Description text line

The heading of the vessel in the ship-bound coordinate system with respect to the SURFBEAT coordinate system is described in Figure 97. The heading makes use of Cartesian convention measured from the x-axis of the SURFBEAT coordinate system 'going to' the direction of the x-axis of the ship-bound coordinate system.

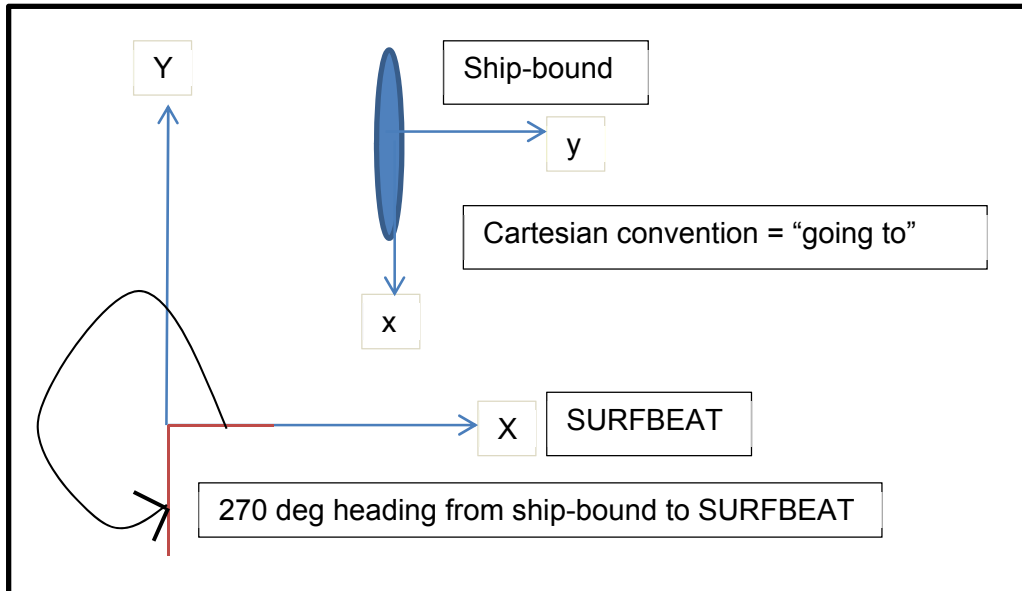


Figure 97: Description for heading of LF-STRIP

H5: QUAYSIM

The program used to convert the hydrodynamic file into wave force file format, is called WAVEFORCES. WAVEFORCES is pre-run to QUAYSIM to create the high frequency wave force file '.exf'. The input structure is similar to QUAYSIM. The input structure of QUAYSIM is well explained referring to Section 2.4.4. Table 26 shows the main input file required for WAVEFORCES.

Table 26: Input file structure for WAVEFORCES

Ship dimensions data file	This option refers to the shipmain.dat file containing all the ship dimensions
Hyd-file	The hydrodynamic file created by WAVESCAT
Wave force file	The output file name produced by WAVEFORCES, '.exf' file created by high frequency wave forces
time step, total time, initialisation time [s]	Inserted in one line, separated by commas
i_wcm = 0 for input of a standard wave spectrum, specify spectral shape: 'JONSWAP' i_wcm = 1 for input of a user-defined wave components file	Option allows the user to make use of a standard Jonswap Spectrum by selecting 0; or making use of the wave component file composed from the SWAN output by selecting 1 and specifying the file name
Drift forces and Set-down option	This option allows the user to include/exclude drift

	forces and set down waves respectively. 0 to exclude set-down waves / drift forces 1 to include set-down waves / drift forces
Significant wave height, H_{m0} [m]	Enter the significant wave height occurring closest to the vessel
Peak period, T_p [s]	
Mean wave direction in the ship bound coordinate system [deg]	
Directional spreading (sigma) [deg]	
Peak enhancement factor, gamma	
Frequency step	Near the (first) peak frequency relative to the peak frequency

The QUASYM main input file makes use of the hydrodynamic file created by WAVESCAT, the two wave force files (LF-STRIP, WAVEFORCES), the mooring data file, and the ship dimension file. Similar patterns can be seen in all tests.

Appendix I: QUAYSIM Results

I1: Test 01

Table 27: Ship motion values for Test 01

	XHmo PM	QUAYSIM
surge [m]	0.86	0.94
sway [m]	0.24	0.59
heave [m]	0.24	0.2
roll [deg]	1.73	0.78
pitch [deg]	0.23	0.15
yaw [deg]	0.19	0.23

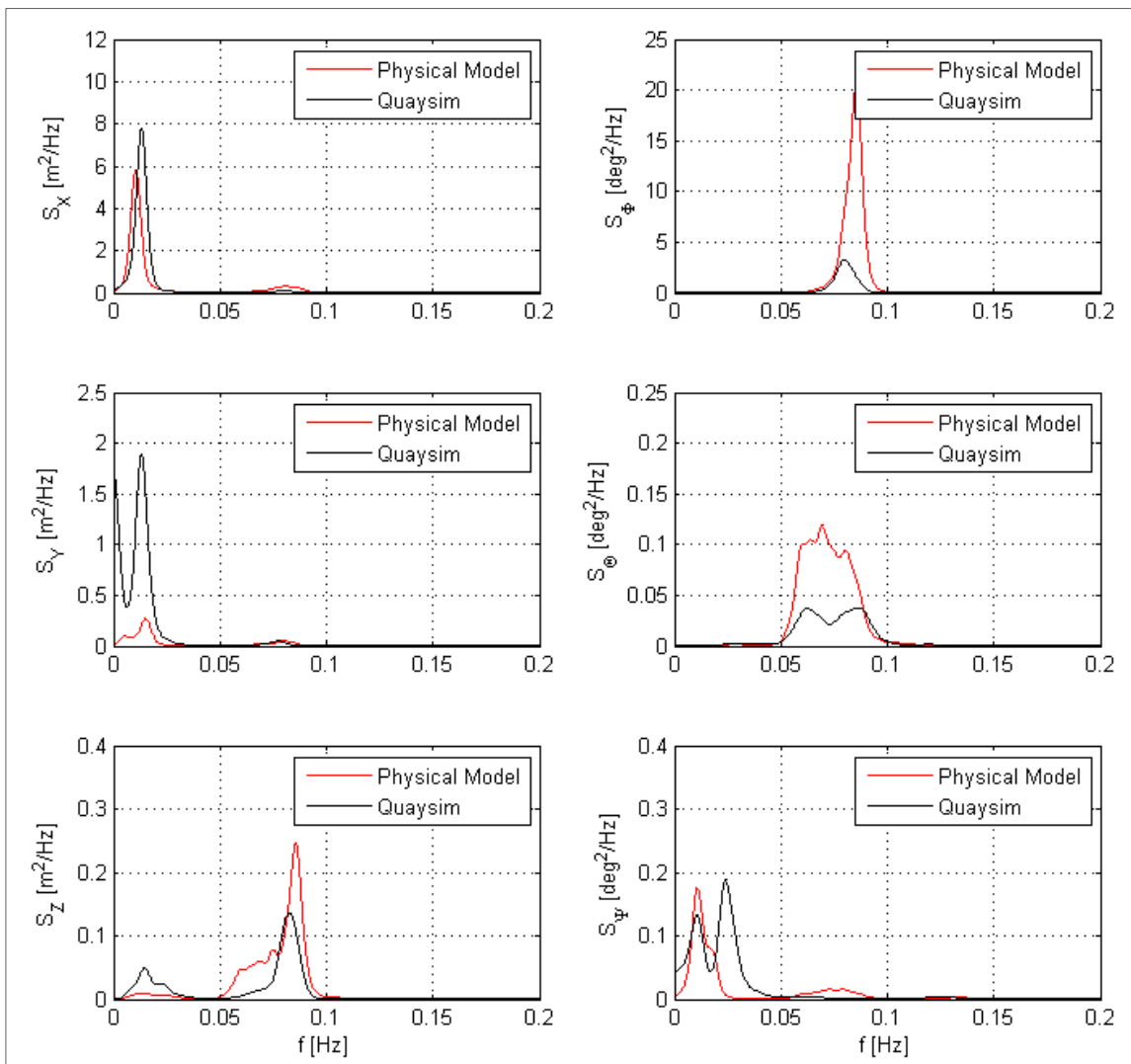


Figure 98: Ship motion spectra for Test 01

Table 28: Fender and mooring line correlation between physical model and QUAYSIM, Test 01

	Physical Model Fender Forces [kN]	QUAYSIM Fender Forces [kN]	Physical Model Mooring Line Forces [kN]	QUAYSIM Mooring Line Forces [kN]
F1			407	433
F2			423	482
F3	1157	946	449	545
F4	827	850	566	561
F5	1360	872	425	525
F6	1331	1031	514	518
F7	1274	1338	498	506
F8			436	436

I2: Test 02

Table 29: Ship motion values for Test 02

	XHmo PM	QUAYSIM
surge [m]	0.39	0.46
sway [m]	0.11	0.26
heave [m]	0.14	0.12
roll [deg]	0.94	0.55
pitch [deg]	0.15	0.1
yaw [deg]	0.09	0.12

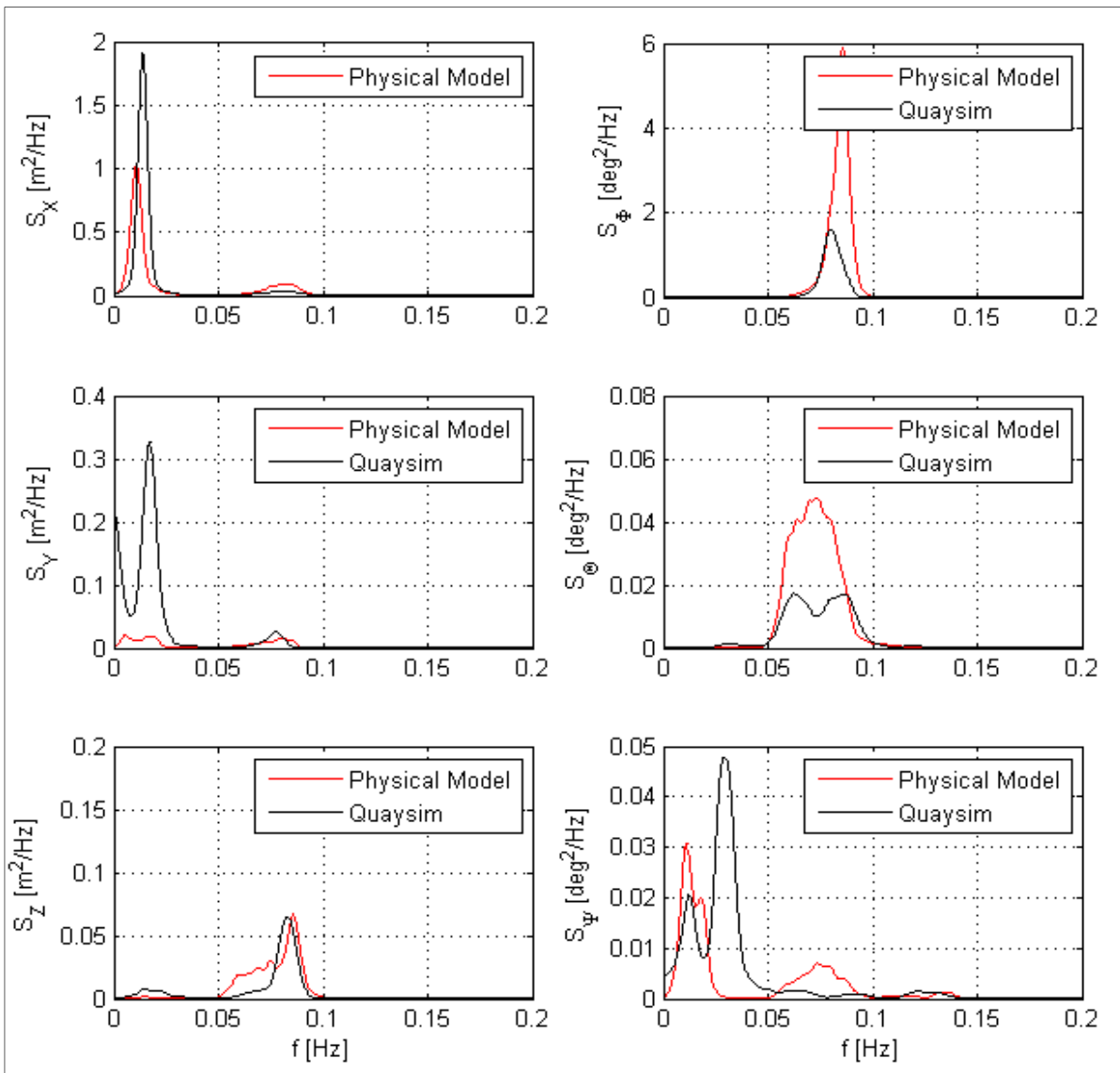


Figure 99: Ship motion spectra for Test 02

Table 30: Fender and mooring line correlation between physical model and QUAYSIM, Test 02

	Physical Model Fender Forces [kN]	QUAYSIM Fender Forces [kN]	Physical Model Mooring Line Forces [kN]	QUAYSIM Mooring Line Forces [kN]
F1			355	339
F2			351	369
F3	624	658	367	396
F4	452	584	416	408
F5	898	602	348	378
F6	726	707	356	384
F7	523	915	333	390
F8			336	334

I3: Test 03

Table 31: Ship motion values for Test 03

	PM	QUAYSIM
surge [m]	1.15	1.16
sway [m]	0.49	0.64
heave [m]	0.38	0.33
roll [deg]	1.20	0.28
pitch [deg]	0.30	0.31
yaw [deg]	0.34	0.23

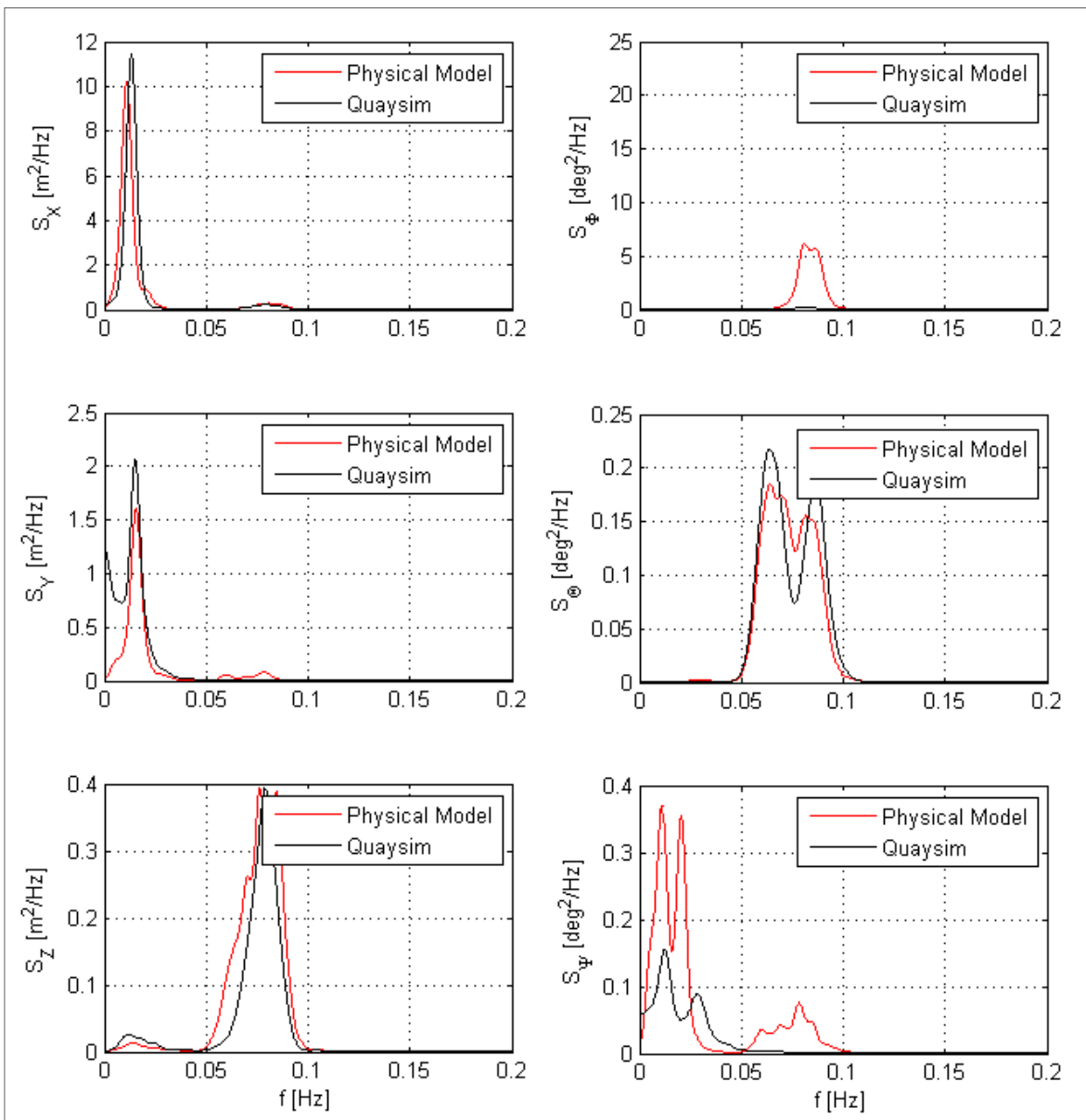


Figure 100: Ship motion spectra for Test 03

Table 32: Fender and mooring line correlation between physical model and QUAYSIM, Test 03

	Physical Model Fender Forces [kN]	QUAYSIM Fender Forces [kN]	Physical Model Mooring Line Forces [kN]	QUAYSIM Mooring Line Forces [kN]
F1			507	436
F2			523	484
F3	1922	1031	647	554
F4	1269	880	639	645
F5	1586	855	473	554
F6	1528	970	606	543
F7	1403	1237	604	545
F8			460	468

I4: Test 04

Table 33: Ship motion values for Test 04

	XHmo PM	QUAYSIM
surge [m]	0.31	0.41
sway [m]	0.12	0.12
heave [m]	0.17	0.19
roll [deg]	0.59	0.13
pitch [deg]	0.16	0.19
yaw [deg]	0.13	0.05

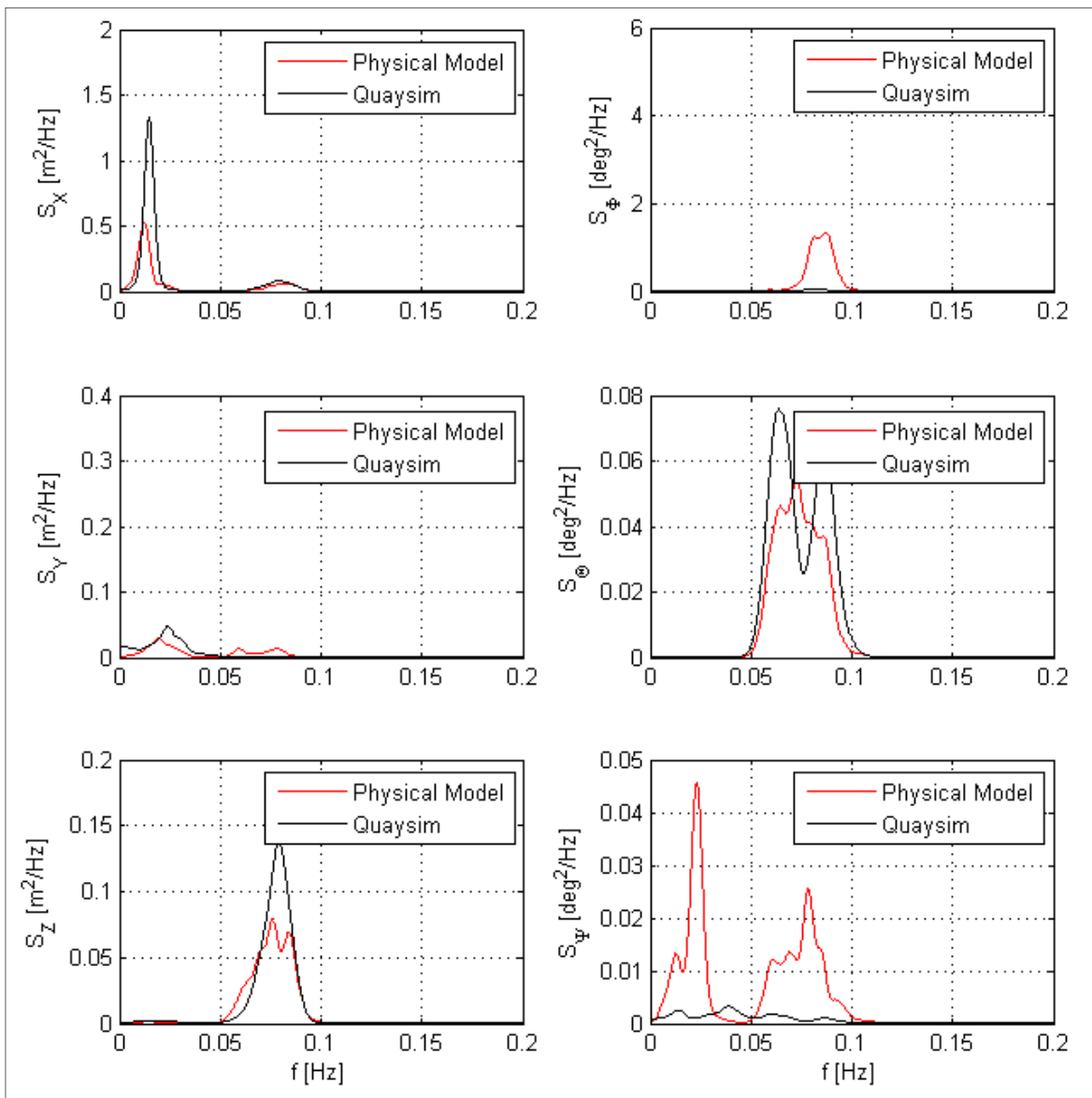


Figure 101: Ship motion spectra for Test 04

Table 34: Fender and mooring line correlation between physical model and QUAYSIM, Test 04

	Physical Model Fender Forces [kN]	QUAYSIM Fender Forces [kN]	Physical Model Mooring Line Forces [kN]	QUAYSIM Mooring Line Forces [kN]
F1			348	313
F2			362	338
F3	837	406	401	341
F4	499	387	370	391
F5	877	412	305	373
F6	619	473	374	333
F7	475	563	387	353
F8			319	304